

Materials and Corrosion Engineering

Exponent[®]

**Effectiveness and
Implementation
Considerations of Covered
Conductors: Testing and
Analysis**





**Effectiveness and Implementation
Considerations of Covered Conductors:
Testing and Analysis**

Prepared for

Southern California Edison Company
1 Innovation Way
Pomona, CA 91768

Applied Technology Services
Pacific Gas & Electric Company
3400 Crown Canyon Rd.
San Ramon, CA 94583

San Diego Gas & Electric
8316 Century Park Ct
San Diego, CA 92123

Prepared by

Exponent
149 Commonwealth Drive
Menlo Park, CA 94025

December 22, 2022

© Exponent, Inc.

Contents

	<u>Page</u>
Acronyms and Abbreviations	v
Executive Summary	vi
Introduction	1
Background and Motivation	1
Scope	2
Phase-to-Phase Contact Testing	2
Wire-Down Ignition Testing	3
Corrosion Susceptibility	3
Flammability Testing	3
System Strength	3
Conductor Specifications	4
Phase-to-Phase Contact Testing	6
Scope	6
Experimental Setup	7
Test Setup and Equipment	7
Testing Procedure	8
Foreign Objects and Vegetation	9
Ambient Conditions	10
Results	11
Phase-to-Phase Contact Testing—Bare Conductors	14
Phase-to-Phase Contact Testing with CCs—Rated Voltage	15
Extended Phase-to-Phase Contact Testing—Rated Voltage	21
Phase-to-Phase Contact Testing with CCs—Extreme Voltage	24
Sequential Breakdown Testing	31
Discussion and Conclusions: Phase-to-Phase Contact Testing	33
Simulated Wire-Down	35
Scope	35
Experimental Setup	35

Results	37
Discussion and Conclusions: Simulated Wire-Down	40
Corrosion Testing	42
Motivation and Scope	42
Water Ingress Testing	45
Experimental Setup	46
Results	47
Salt Spray Testing	51
Experimental Setup	51
Results	53
Cyclic Polarization Testing	71
Experimental Setup	71
Results	73
Discussion and Conclusions: Corrosion Testing	79
Flammability Testing	80
Motivation and Scope	80
Experimental Setup	81
Results	83
Discussion and Conclusions: Flammability Testing	83
System Strength Testing	87
Scope	87
Experimental Setup	87
Splice Maximum Load Test	87
Insulator Slip Test	90
Full System Tree-Fall Test	92
Results	94
Splice Maximum Load Test	94
Insulator Slip Test	97
Full-System Tree-Fall Test	101
Discussion and Conclusions: System Strength	106
Limitations	107

Appendix A	Methods
Appendix B	Simulated Wire-Down Tests: Additional Figures
Appendix C	Standards and Guidelines
Appendix D	Literature References
Appendix E	SCE Covered Conductor Dead-End Strength Testing
Appendix F	Kinectrics Mechanical Testing Reports

Acronyms and Abbreviations

AAC	all aluminum conductor
AC	alternating current
ACSR	aluminum conductor, steel reinforced
ASTM	ASTM International (formerly American Society for Testing and Materials)
CC	covered conductor
CPUC	California Public Utilities Commission
GO	General Order
ICEA	Insulated Cable Engineers Association
IEEE	Institute of Electrical and Electronics Engineers
IOU	investor-owned utility
IPC	insulation-piercing connector
kcmil	one thousand circular mils (a unit of wire gauge)
kN	kilonewton
kV	kilovolt
mA	milliamp (a unit of current equal to one-thousandth of an ampere)
ms	millisecond
NaCl	sodium chloride
PE	polyethylene
PG&E	Pacific Gas & Electric
RTS	rated tensile strength
SCE	Southern California Edison
SDG&E	San Diego Gas & Electric
UTM	universal testing machine
UTS	ultimate tensile strength
XL-HDPE	cross-linked high-density polyethylene
XL-LDPE	cross-linked low-density polyethylene

Executive Summary

Exponent, Inc. (Exponent) was retained by Southern California Edison as part of a joint effort with investor-owned utilities to independently investigate the effectiveness of covered conductors (CCs) for overhead distribution systems. Our investigation included lab-based testing of 15-kV rated 1/0 aluminum conductor, steel reinforced (ACSR) CC provided by SDG&E, 17-kV and 35-kV rated 1/0 ACSR provided by SCE, 22-kV rated 397.5 kcmil all aluminum conductor (AAC) provided by PG&E, and 17-kV rated 2/0 copper CC provided by SCE (corrosion testing only). Based on our investigation, we have come to the following conclusions:

1. CC effectiveness was evaluated by phase-to-phase contact and simulated wire-down testing. CCs were 100% effective at preventing arcing and ignition in tested scenarios at rated voltages. This is consistent with documented field experience as reported in Exponent's Phase I report.
2. CCs prevented arcing and ignition and limited current flow to less than 2.5 mA in 100% of tested phase-to-phase contact scenarios at rated conductor voltages, which included different types of vegetation, balloons, simulated animals, and conductor slapping.
3. CCs prevented arcing and ignition in 100% of simulated wire-down events in dry brush. Broken conductors and conductors with damage that exposed the underlying metal showed potential for ignition.
4. Thermal testing was performed to understand the impact of a nearby wildfire on CC installations. Results suggested that the heat fluxes and times required for auto-ignition of the polyethylene sheaths were unlikely to be encountered during a surface or low-lying brush fire; however, a canopy fire may be sufficient to cause conductor sheath ignition.
5. Water ingress testing was performed to understand if implementation of CCs introduces a unique corrosion risk relative to bare conductors. Stripped ends of CCs and CCs with insulation-piercing connectors (IPCs) were found to be susceptible to water ingress. While the test conditions were extreme relative to typical service conditions and did not account for potential heating/evaporation in service, water may percolate down the conductor length from a stripped end in some scenarios.
6. Corrosion was observed under the CC sheath near the stripped ends but was not observed under IPCs following salt spray testing. While this indicates that subsurface corrosion is possible near a stripped CC end, subsequent tensile testing showed minimal reduction in total strength of the conductor. Potential water-ingress mitigation measures may help to prevent corrosion in areas where precipitation is likely to collect on the conductor.
7. Mechanical testing was performed to assess the strength of CCs and their associated hardware. Strength testing of splices met or exceeded the rated strengths of the

conductors. In simulated tree-fall conditions and insulator slip tests, vise-top pin insulators exhibited deformation of the metal pin. Clamp-top post insulators exhibited conductor slippage with no apparent signs of damage to the hardware.

Note that this Executive Summary does not contain all of Exponent's technical evaluations, analyses, conclusions, and recommendations. Hence, the main body of this report is at all times the controlling document.

Introduction

Background and Motivation

In 2021, California investor-owned utilities (IOUs) Pacific Gas & Electric (PG&E), Southern California Edison (SCE), and San Diego Gas & Electric (SDG&E) engaged Exponent to investigate the effectiveness of covered connectors (CCs) for hardening of overhead distribution electric lines. During the project, three additional California IOUs joined the effort: Liberty, PacifiCorp, and Bear Valley Electric Service. CCs have gained industry attention due to their potential for mitigating risks associated with public safety, reliability, and wildfire ignition. The initial phase of this investigation (“Phase I”) was a literature-based study of CC performance to better understand the advantages, operative failure modes, and current state of knowledge regarding CCs. The Phase I study included a review of publicly available literature, utility-provided data, and manufacturer information. Additionally, a high-level failure mode identification workshop was conducted to identify any gaps between the current state of knowledge and operative failure modes.¹

The Phase I analysis concluded that CCs are a mature technology and have the potential to mitigate several safety, reliability, and wildfire risks inherent to bare conductors.¹ One of the most common bare conductor failure modes is arcing due to external contact (from a foreign object or conductor slapping), a failure mode shown by field applications to be mitigated by CC use. Field studies from around the world have demonstrated increases in safety and reliability with adoption of CCs. However, those studies do not provide quantitative, lab-based data assessing the degree to which individual bare conductor failure modes are remediated (or accelerated) by CC adoption. Based on the relative scarcity of laboratory analyses offering this type of information, Exponent proposed additional CC testing to target specific knowledge gaps identified in Phase I. SCE independently retained Exponent to perform follow-up testing to address these gaps. The high-level recommendations from Phase I and the testing performed for the current study (“Phase II”) are outlined in Table 1.

¹ “Effectiveness of Covered Conductors: Failure Mode Identification and Literature Review,” Exponent Report No. 2103590.000 – 6880, December 22, 2021.

Table 1. Exponent proposed testing based on Phase I recommendations.

Phase I Recommendations	Phase II Testing	Notes
Characterize CC susceptibility to certain mechanical failure modes (Aeolian vibration, galloping, etc.).	System strength testing.	An analytical study of appropriate line tension considering CC size/weight is recommended but outside the current testing scope. System strength tests will inform analytical studies.
Characterize key understudied contact-mediated fault scenarios (e.g., foreign object contact).	Phase-to-phase contact testing, wire-down ignition testing.	
Characterize CC-specific failure modes.	Moisture ingress testing, flammability testing, corrosion testing, system strength testing.	
Research early fault detection technologies.	N/A	Subject of current research. Additional literature investigation is recommended but outside the current testing scope.

Scope

Exponent designed a testing program to address the various knowledge gaps identified in the Phase I study, and as outlined in Table 1. This program sought to quantify the performance of CCs relative to bare conductors in terms of contact-mediated faults, fire ignition risk, corrosion susceptibility, and physical system strength. This testing program focused on performance of covered conductors in the as-installed condition, and did not investigate aging or potential material degradation. While the testing presented here is unique and sought to replicate specific field scenarios, tests were designed and performed according to relevant industry guidance, testing standards (Appendix C), and literature sources (Appendix D) where possible. The five primary categories of CC testing are described below.

Phase-to-Phase Contact Testing

Electric distribution lines are subject to contact with a variety of foreign objects, including vegetation (branches, sticks, palm fronds, etc.), birds and small animals, helium balloons, and other wind-blown objects. Additionally, windy conditions can induce a phenomenon known as conductor slapping, in which adjacent phases intermittently contact one another. Traditional bare conductors are susceptible to arcing in these scenarios, which can lead to potential fire ignition and/or service outages. This group of tests was conducted to understand the effectiveness of CCs at mitigating phase-to-phase arcing in simulated contact scenarios.

Wire-Down Ignition Testing

Energized downed conductors are a major risk for fire ignition, especially in dry/windy wildfire-prone conditions. A wire-down event may occur due to tree fall, third-party damage, conductor breakage, or other hardware/structure failure. Downed bare conductors can result in direct contact between the energized conductor and any underlying fuel source such as dry brush, leading to fire ignition. This group of tests evaluated the performance of CCs relative to bare conductors in a simulated wire-down event.

Corrosion Susceptibility

Electric distribution lines are perpetually exposed to the environment and are thus susceptible to corrosion from prolonged moisture exposure and deposition of various environmental, agricultural, and industrial contaminants. CCs are, by design, largely protected from environmental ingress. In this way, use of CCs mitigates a large portion of the corrosion risk. However, scenarios exist that require stripping of the CC sheath (e.g., dead-end terminations, midspan splicing, etc.), which can create the potential for corrosion and water ingress at these locations.

First, water ingress testing was performed on CC samples to understand the propensity for water to enter a covered section from a nearby stripped end. This is important for evaluating the likelihood of prolonged moisture contact. Second, accelerated salt fog corrosion testing was performed on sections of CC stripped ends to understand potential effects of water pooling at these locations and/or potential crevice corrosion effects relative to bare conductors. Lastly, the copper and aluminum conductor, steel reinforced (ACSR) CCs were subject to electrochemical testing to evaluate the resistance of the conductors to localized corrosion.

Flammability Testing

CCs are unique in that they incorporate a polyethylene (PE) sheath along the entire length of the conductor. It is important to understand the propensity of the PE sheath to ignite in the event of a nearby wildfire. This group of tests systematically measured the time and heat flux required for auto-ignition to better understand the limits of the CC sheath relative to the conditions expected under different wildfire scenarios (e.g., low-lying brush fire, canopy fire, etc.).

System Strength

CCs are physically different from bare conductors in weight, diameter, and stiffness. Further, specified hardware in a CC installation may differ from that of a bare conductor installation. Therefore, the system response to external stimuli such as wind, tree fall, or ice accretion may be modified by using CCs. Understanding these differences is critical for evaluating the relative risk of these scenarios to CC installations. Both component-level and system-level mechanical strength tests were conducted to assess the performance of CCs and their associated hardware. The results of these tests, which include the strength of CC-specific splices, the slip strength of

post insulator clamps, and the mechanical response of the pole/cross-arm/hardware assembly, may inform risk calculations and subsequent finite element modeling efforts.

Conductor Specifications

The IOUs requested that Exponent perform testing on five conductor types: 15-kV rated 1/0 ACSR CC provided by SDG&E, 17-kV and 35-kV rated 1/0 ACSR provided by SCE, 22-kV rated 397.5 kcmil all aluminum conductor (AAC) provided by PG&E, and a 17-kV rated 2/0 copper CC provided by SCE. The copper conductor was also used for corrosion testing only, as the electrical and physical characteristics of the polymer sheath is the same as the 17-kV ACSR CC. All conductor types incorporate a three-layer design, which includes:

- A semiconducting shield layer, which reduces voltage stress concentrations caused by flux lines from individual strands.
- A cross-linked low-density polyethylene (XL-LDPE) insulating layer for impulse strength.
- A cross-linked high-density polyethylene (XL-HDPE) insulating layer for impulse strength and abrasion/impact resistance.

The 15-kV, 17-kV, and 35-kV 1/0 ACSR conductors have the same underlying conductor construction (six aluminum strands and one steel wire at the core) and polymer sheath stack-up. The 15-kV and 17-kV conductors have similar polymer sheath layer thicknesses while the 35-kV conductor layers are slightly thicker, as shown in Table 2. The 22-kV 397.5 kcmil AAC contains 19 aluminum strands but has a similar polymer sheath layer stack-up to the 1/0 ACSR covered conductors. Representative cross-section images of each conductor type are shown in Figure 1. Additional specifications are shown in Table 3.

Table 2. CC sheath dimensions.

Layer	Specified Thickness / Measured Thickness ²			
	15-kV ACSR (SDG&E)	17-kV ACSR (SCE)	35-kV ACSR (SCE)	22-kV AAC (PG&E)
Conductor Shield Layer	0.38 mm / 0.60 mm	0.38–0.64 mm / 0.58 mm	0.38–0.64 mm / 0.58 mm	0.64 mm / 0.50 mm
XL-LDPE Inner Layer	1.91 mm / 1.91 mm	1.91 mm / 1.91 mm	4.45 mm / 4.11 mm	1.91 mm / 2.10 mm
XL-HDPE Outer Layer	1.91 mm / 1.80 mm	1.91 mm / 1.83 mm	3.18 mm / 3.33 mm	1.91 mm / 1.82 mm

² Reported thickness measurements are the average of eight individual measurements taken around the circumference of a single conductor cross section.

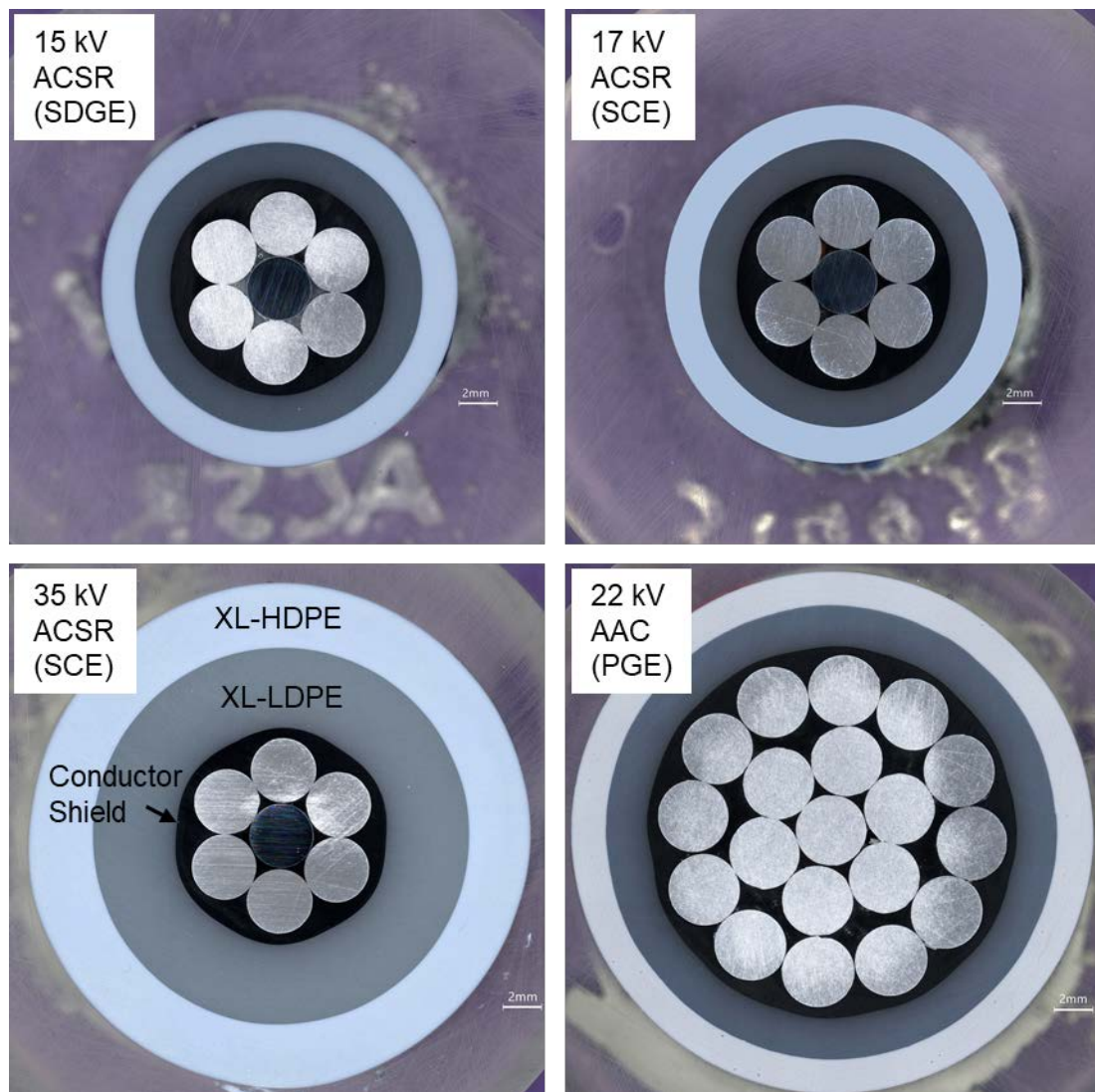


Figure 1. Cross-sectional images of all four CC types used in the present study. The measured layer thicknesses are compared to their nominal values in Table 2.

Table 3. Conductor specifications.

Rated Voltage	Size/Type	Max. Nominal Overall Dia.	Max. Rated Strength (lb.)	Ampacity per Conductor (A)
15-kV	1/0 ACSR (6x1)	18.5 mm	4,160	*
17-kV	1/0 ACSR (6x1)	19.0 mm	4,160	271
22-kV	397.5 kcmil AAC	27.3 mm	6,754	*
35-kV	1/0 ACSR (6x1)	26.6 mm	4,160	255

* Not specified.

Phase-to-Phase Contact Testing

Scope

Phase-to-phase contact testing was conducted to understand the effectiveness of CCs in mitigating current flow, arcing, and/or ignition in various contact scenarios. To simulate the potential difference across two phases of a three-phase distribution system, one conductor span was energized to the phase-to-phase voltage while the other conductor was grounded. The two conductors were bridged by a foreign object or tied together to simulate conductor slapping.

Tests consisted of several permutations of standard CCs, CCs with artificially induced sheath damage, and equivalent bare conductors (Table 4). The first stage of testing assessed the conductor performance at rated operating voltages for each respective conductor type. The second stage of testing investigated the conductor behavior in extreme conditions above their rated voltages (up to ~6x rated voltage).

Table 4. Phase-to-phase contact tests.

Side A (Energized)	Foreign Object	Side B (Grounded)	Conditions
Bare	Leafy Branch	Bare	Dry
CC	Leafy Branch	CC	Dry/Wet
CC	Conductor Slapping	CC	Dry
CC	Bare Conductor	CC	Wet
CC	Stick	CC	Dry/Wet
CC	Palm Frond	CC	Dry/Wet
CC	Mylar Balloon	CC	Dry
CC w/ splice	Palm Frond	CC	Dry
Bare	Leafy Branch	CC	Dry
Bare	Conductor Slapping	CC	Dry
CC	Messenger Wire	Bare	Dry
CC, full-thickness flaw	Leafy Branch	CC	Dry/Wet
CC, half-thickness flaw	Leafy Branch	CC	Dry/Wet
CC, pinhole flaw	Leafy Branch	CC	Dry
CC w/ wildlife guard*	Leafy Branch	CC w/ wildlife guard*	Dry/Wet
CC w/ wildlife guard*	Simulated Animal	CC w/ wildlife guard*	Dry
CC w/ wildlife guard*	Simulated Animal	CC, 1 ft stripped	Dry
CC	Control Test	CC	Dry

A total of 264 tests were performed on the various CC types (15-kV, 17-kV, and 35-kV 1/0 ACSR as well as 22-kV 397.5 kcmil AAC). Foreign objects included fresh leafy eucalyptus

branches, large eucalyptus branches without leaves or secondary branches, palm fronds, Mylar balloons, and simulated small animals (simulated by raw meat procured from a butcher). Additional tests were also performed to assess the impact of installing a wildlife guard over a one-foot stripped segment of conductor at a dead-end connection. Selected tests were carried out in both wet and dry conditions to assess the impact of precipitation on CC performance in the field. An extended (seven-day) contact study was conducted to better understand the potential effects of long-term phase-to-phase contact. Finally, testing was performed to evaluate the performance of CCs after a high-fault event such as a lightning strike; these tests were termed “sequential” tests. To ensure test reproducibility, tests were conducted in triplicate.

Experimental Setup

Test Setup and Equipment

One energized conductor and one grounded conductor were physically arranged in parallel with a spacing of 18 inches to 24 inches to simulate two phases of a three-phase distribution line (Figure 2). The two conductors were bridged by a foreign object or tied tightly together to simulate conductor slapping according to the scenarios outlined in Table 4. The potential on the energized side was set to the rated phase-to-phase voltage for the conductor type while the remaining conductor was kept at 0V potential via a high-voltage insulated cable connected to ground.

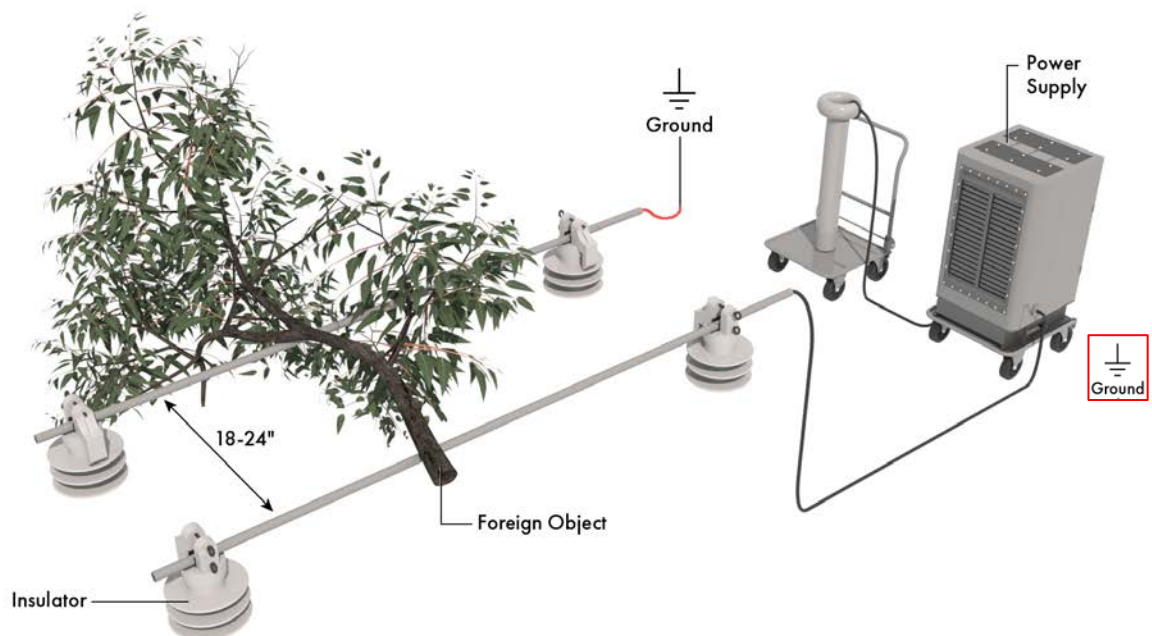


Figure 2. Schematic of experimental test setup for simulated contact testing.

The span length generally ranged from six to twelve feet, though longer spans were used for some tests in which a potential risk of damage to the equipment was identified. The conductors were secured using four polymer vise-top insulators. The phase separation for each conductor type was set according to California Public Utilities Commission (CPUC) General Order (GO) 95 specified minimum separations³ and is shown in Table 5. Approximately 1.5 inches of insulation were stripped from one end of each conductor to provide the connection to power and to ground. The leakage current through the circuit was measured with a current transducer placed around the grounded conductor cable.

Table 5. GO-95⁴ standard phase spacings.

Rated Voltage	Size/Type	Phase Separation
15-kV	1/0 ACSR (6x1)	17.5 inches
17-kV	1/0 ACSR (6x1)	
22-kV	397.5 kcmil AAC	24 inches
35-kV	1/0 ACSR (6x1)	

The CC contact tests were performed using an 800 kV, 3 amps alternating current (AC) resonant power supply, while the extended (seven-day) tests were performed using a 30 kV, 1 amp transformer. Differences in power supply did not affect results for tests with at least one CC due to the high system impedance and very limited observed current flow. Phase-to-phase contact tests involving two bare conductors utilized a third power supply rated at 7.1 kV, 2 amps.

Testing Procedure

For the first stage of testing, the voltage was increased to the rated voltage and held for five minutes. The leakage current was measured at the beginning and end of the five-minute hold. For the second stage, the voltage was increased by approximately 1 kV/sec to ~90 kV and the leakage currents were recorded as a function of applied voltage. A limited number of tests experienced a setup-related arcing event at voltages above the conductor rating. In these cases, the maximum voltage and leakage current were recorded and the test was concluded to protect the equipment. For tests that involved two bare conductors bridged by a foreign object, the full voltage could not be achieved due to low system impedance, high leakage currents, and power supply limitations. However, these tests consistently resulted in ignition of vegetation (the expected outcome) and were considered successful for their intended purpose.

Full-thickness and half-thickness coating flaws were introduced with an adjustable cable midspan stripping tool. These flaws were designed to simulate abrasion from vegetation or other third-party objects, or from animal chewing.

³ California Public Utilities Commission (CPUC) General Order (GO) 95. Section III. Requirements for All Lines. Table 2.

⁴ Ibid.

Wildlife guards are used near dead-end structures to mitigate the risk of animal contact to exposed bare conductor sections. Two scenarios were designed to test the effectiveness of wildlife guards in preventing current flow. In the first scenario, two wildlife guards covering approximately one-foot sections of exposed bare conductor were bridged by a leafy eucalyptus branch or a simulated animal (using raw meat from a local butcher). In the second scenario, one of these wildlife guards was removed to expose the bare conductor and to simulate the loss of a wildlife guard. One-foot sections of insulation were removed with an adjustable cable midspan stripping tool.

Extended (seven-day) tests were performed to simulate prolonged foreign object contact. This is especially important with CC systems since the contact results in little to no current flow and is unlikely to trip protection relays. One CC was energized to the rated voltage and was subjected to a loop current of 270 amps, the maximum ampacity determined by the ACSR technical datasheets.⁵ The loop current was intended to cause resistive heating of the conductor to simulate a loaded distribution line.

Sequential tests were performed to evaluate the performance of CCs after a fault event such as a lightning strike. The CCs were wrapped in a grounded metal braid at midspan, and the voltage was increased until the electric field was strong enough to induce breakdown in the insulation. Following breakdown, the CCs were exposed to high voltage a second time to effectively “grow” the flaw. The CCs were then phase-to-phase contact tested at rated and extreme voltages.

Foreign Objects and Vegetation

A variety of foreign objects previously identified as potential risks to distribution lines were used for the phase-to-phase contact tests. Foreign objects included leafy eucalyptus branches, eucalyptus branches without leaves or secondary branches (i.e., sticks), palm fronds, Mylar balloons, and simulated small animals (raw meat procured from a butcher).

Eucalyptus trees, non-native and invasive species in southern California, present a risk to power distribution systems because of their ability to grow quickly at high densities (eight-foot spacing on average between trees)⁶ and because of their high flammability potential.⁷ Oily eucalyptus resins reportedly have a lower activation energy for ignition compared to other species.⁸

Three mature eucalyptus cinerea trees were sourced from Gilroy, California, for use in phase-to-phase contact testing. The trees were consistently watered to maintain their freshness and

⁵ Southern California Edison Covered Conductor Data Sheet for 17 kV and 35 kV. 2020.

⁶ McBride, J.R. (2014) The History, Ecology and Future of Eucalyptus Plantations in the Bay Area: A lecture at the Commonwealth Club of San Francisco Understanding Eucalyptus in the Bay Area. San Francisco Forest Alliance.

⁷ Nance, A. (2014). The Plight of the Eucalyptus Trees in San Francisco: A Case Study on the Values and Considerations Involved in a Decision that Requires Comparative Valuation of Species. *Hastings W.-Nw. J. Env'tl L. & Pol'y*, 20, 429.

⁸ Dickinson, K. J. M., and J. B. Kirkpatrick. 1985. The flammability and energy content of some important plant species and fuel components in the forests of southeastern Tasmania. *Journal of Biogeography* 12:121-134.

moisture. Branches were cut into 4.5-foot sections and labeled according to their original position on the tree. Diameter and moisture measurements were made at the cut end and center of each branch. Immediately after cutting, the ends were sealed and the branches were packaged in thick plastic bags under vacuum. Additional information regarding branch preparation, quality control, and moisture content is referenced in Appendix A. The palm fronds (*ravenea rivularis*), Mylar balloons, and raw meats were locally sourced at the testing lab, and the bare conductor was provided by SCE, as shown in Table 6.

Table 6. Sourcing of foreign object for phase-to-phase contact tests.

<u>Foreign Object</u>	<u>Source</u>
Leafy Eucalyptus Branch	Eucalyptus cinerea from Gilroy, CA
Bare Conductor	Bare conductor provided by SCE
Eucalyptus Stick	Eucalyptus cinerea from Gilroy, CA
Palm Frond	Ravenea rivularis (majesty palm)
Mylar Balloon	34" mylar balloon
Messenger Wire Contact	Bare conductor provided by SCE
Raw Meat	Rabbit and pork ribs from Ontario

Ambient Conditions

Since high-voltage tests are known to be sensitive to environmental conditions,⁹ the temperature and relative humidity in the lab were recorded for each test. The ambient temperature in the facility averaged 72.7°F while the relative humidity averaged 25.5%. The approximate elevation of the testing lab was 120 m above sea level. All testing conditions fell within the range specified by IEEE Standard 4-2013 (Table 7).¹⁰

Table 7. Normal environmental conditions for high-voltage tests and measurements specified by IEEE Standard 4.

	<u>IEEE Standard4</u>	<u>Test Conditions</u>
Temperature	50°F to 104°F	58.1°F to 84.4°F
Relative Humidity	< 95%	9.7% to 45.0%
Elevation	< 1000 m	120 m

While dry environmental conditions are thought to be “worst case” from a fire ignition perspective, wet conditions may improve conduction and may affect the propensity for current

⁹ Yousefpour, K. “Effect of Ambient Conditions on Insulation Strength of High Voltage Protection Devices.” HAL Open Science. 2020.

¹⁰ IEEE Std. 4™-2013 “IEEE Standard for High Voltage Testing Techniques,” Institute of Electrical and Electronics Engineers, 2013.

flow. Wet tests were performed to evaluate the performance of CCs under specified precipitation conditions. The vertical and horizontal components of the precipitation rate as well as the water temperature and conductivity were controlled using a purpose-built rain system. All wet test and precipitation parameters were in accordance IEEE Standard 4-2013 specifications.¹¹ Additional information regarding the wet testing is referenced in Appendix A.

Results

CCs prevented arcing/ignition and limited current flows to less than 2.5 mA under all tested conditions at rated voltages. The results of the phase-to-phase contact testing are summarized in Table 8.

In stark contrast to the low current flows (<2.5 mA) detected at rated voltages for tests with CCs, much higher currents were detected (>2000 mA) in tests with two bare conductors. Energized bare conductors bridged by leafy branches consistently resulted in rapid expulsion of moisture, smoking, and ignition of the vegetation.

For CC phase-to-phase contact testing at rated voltages, no arcing event or ignition was observed in any test. The conductors were energized to their rated voltages and held for five minutes. No arcing, insulation breakdown, or visual damage to the energized and/or grounded conductors was observed. Leakage currents were low (less than 2.5 mA) and likely influenced by coupling effects rather than current flow through the insulation.

For CC contact testing at extreme voltages (1 kV/sec ramp rate from rated voltage), the results were as follows:

- **No arcing event or ignition:** Test was energized to approximately 90 kV with no insulation breakdown, pinhole formation, or phase-to-phase arcing. Minor charring was observed on the eucalyptus branches when direct contact was made with exposed bare conductor at extreme voltages.
- **Setup-related arcing:** In the range of 60 kV to 90 kV (well above the rated voltages), some early tests with a six-foot span length experienced setup-related arcing. Under these voltage conditions, arcing sometimes occurred due to surface tracking and/or breakdown through the air. This was mitigated in later tests by using longer (10 feet) conductor spans.
- **Insulation breakdown:** Test experienced a breakdown of the insulation, resulting in pinhole formation well above the rated voltage. This occurred in the range of 55 kV to 85 kV for the 15-kV and 17-kV ACSR CCs and 22-kV AAC CCs when an artificial half-thickness coating flaw was introduced. Insulation breakdown did not occur for the 35-kV ACSR CC with a half-thickness flaw up to 90 kV.

¹¹ IEEE Std. 4™-2013 “IEEE Standard for High Voltage Testing Techniques,” Institute of Electrical and Electronics Engineers, 2013.

There were no significant differences in leakage current observed between dry and wet tests at rated or extreme voltages. This suggests that CCs are effective at preventing current flow in both dry and wet conditions. For tests in which direct contact was made at high voltage with exposed bare conductor, the rain suppressed charring of the branch.

Table 8. Results of phase-to-phase contact testing at rated voltages.

Test Configuration			Maximum Leakage Current at Rated Voltage (mA)					Negligible Detected Current at Rated Voltage? (<2.5 mA)
Side A (Energized)	Foreign Object	Side B (Grounded)	Conditions	15 kV ACSR	17 kV ACSR	35 kV ACSR	22 kV AAC	
Bare	Leafy Branch	Bare	Dry	>2000**	>2000**	>2000**	>2000**	No
CC	Leafy Branch	CC	Dry/Wet	0.1 / 0.1	0.8 / 0.3	0.8 / 0.7	0.2 / 1.0	Yes
CC	Conductor Slapping	CC	Dry	0.2	0.9	0.8	0.2	Yes
CC	Bare Conductor	CC	Wet	0.2	0.1	0.5	0.8	Yes
CC	Stick	CC	Dry/Wet	0.1 / 0.1	0.7 / 0.3	0.7 / 0.4	0.1 / 0.5	Yes
CC	Palm Frond	CC	Dry/Wet	0.1 / 0.4	0.7 / 0.5	0.2 / 0.5	0.2 / 0.7	Yes
CC	Mylar Balloon	CC	Dry	0.1	0.1	0.2	0.1	Yes
CC w/ splice	Palm Frond	CC	Dry	0.2	0.2	0.3	0.2	Yes
Bare	Leafy Branch	CC	Dry	0.2	0.9	0.8	0.5	Yes
Bare	Conductor Slapping	CC	Dry	0.4	0.9	0.8	0.6	Yes
CC	Conductor Slapping	Bare	Dry	0.5	0.4	0.4	0.7	Yes
CC, full-thickness flaw	Leafy Branch	CC	Dry/Wet	0.2 / 0.4	0.5 / 0.1	0.5 / 0.2	1.0 / 2.4	Yes
CC, half-thickness flaw	Leafy Branch	CC	Dry/Wet	0.1 / 0.2	0.2 / 0.1	0.2 / 0.5	0.1 / 0.5	Yes
CC, pinhole flaw	Leafy Branch	CC	Dry	-	0.4	1.0	0.3	Yes
CC w/ animal guard*	Leafy Branch	CC w/ animal guard*	Dry/Wet	0.1 / 0.1	0.4 / 0.8	0.2 / 0.2	0.1 / 0.2	Yes
CC w/ animal guard*	Simulated Animal	CC w/ animal guard*	Dry	0.1	0.1	0.2	0.1	Yes
CC w/ animal guard*	Simulated Animal	CC, 1 ft stripped	Dry	0.1	0.1	0.2	0.1	Yes
CC	Control Test	CC	Dry	-	0.1	0.2	-	-

*Animal guards were placed over 1ft a section of exposed bare conductor.

**Tests with two bare conductors could not reach full voltage due to high leakage currents and power supply limitations. Current limited to 2 A.

Phase-to-Phase Contact Testing—Bare Conductors

Control tests were performed with traditional bare conductors (Figure 3) to provide a point of reference that can be used to compare to CC performance. Two bare conductors of equivalent size to their CC counterpart were bridged by a leafy eucalyptus branch. Three tests were performed for each bare conductor type.

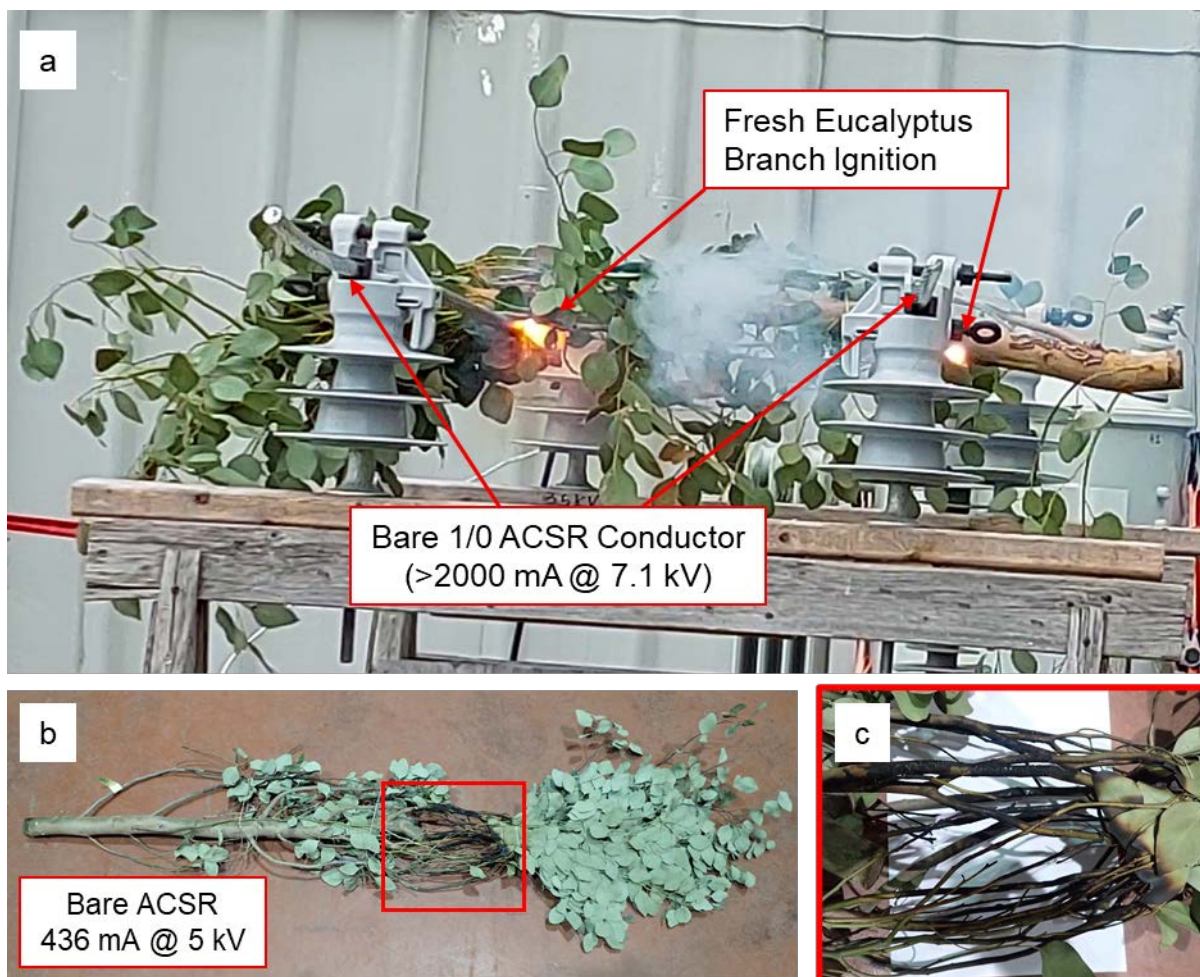


Figure 3. Phase-to-phase contact tests with two bare conductors. (a) Leafy eucalyptus branch spanning two bare 1/0 ACSR conductors with a 7.1-kV voltage drop. (b) Post-test inspection of the points of contact between the branch and conductors identified evidence of ignition. (c) Close-up view of (b).

Immediately after energizing, a loud, high-pitched noise was clearly audible, consistent with rapid evaporation of branch moisture. After three seconds, smoking and ignition were observed at both points of contact between the branch and the bare conductors (Figure 3a). Upon inspection of the branch post-test, clear evidence of ignition, burning, and tracking along the surface of the branch were observed (Figure 3b,c). The highest attainable voltage for these tests

was 7.1 kV (using a 7.1-kV, 2 amp power supply) due to low system impedance, high leakage current, and equipment power limitations.

Across the six bare conductor tests, three different power supplies were used. Applied voltages ranged from 3 kV to 7.1 kV and leakage currents ranged from 200 mA to 2,000 mA. In all tests, the power supply limit was reached. It is likely that significantly higher currents could have been attained at full voltage with sufficient power supply capacity, as would be available in an actual distribution system. Leakage currents increased with voltage and depended strongly upon the diameter and moisture of the branch. Larger branches resulted in greater leakage current, consistent with literature sources that the electrical impedance of live branches is variable and depends on diameter and moisture content.¹²

Phase-to-Phase Contact Testing with CCs—Rated Voltage

CC phase-to-phase contact tests were broken up into four sub-groups:

- Two standard CCs (Figure 4).
- One spliced CC and one standard CC (Figure 5).
- One CC with an artificially induced insulation flaw and one standard CC (Figure 6).
- One bare conductor and one standard CC (Figure 7).
- Simulated dead-end configuration with (a) two wildlife guards, each covering one foot of bare conductor (simulated dead-end connection), and (b) one wildlife guard covering one foot of exposed conductor and one CC with one foot of exposed conductor (Figure 8).

Selected tests were carried out in both wet and dry conditions to assess whether precipitation might impact CC performance in the field.

Two Standard CCs at Rated Voltage

Leakage currents for all tests with two standard CCs were below 2.5 mA and were stable at rated voltages for the duration of the five-minute hold. No insulation breakdown, phase-to-phase arcing, damage to the insulation, or damage to the foreign objects was observed in any scenarios at rated voltages with two CCs. Minor corona discharge was observed near the surface of the energized CCs at the point of contact with the foreign object. This occurs because the presence of the foreign object causes a sharp potential gradient and strong electric field, resulting in local dielectric breakdown and ionization of the surrounding air, observed visually as corona discharge.

The dry tests simulating CC slapping (Figure 4c) and wet tests with two CC bridged by a bare conductor (Figure 4d) were designed to represent the two worst-case scenarios, as these lowest impedance configurations should lead to the highest likelihood of energy transfer between the two conductors. There was no evidence of significant current flow for either of these tests, nor for any other scenarios tested with two CCs.

¹² Goodfellow and Appelt. “How Trees Cause Outages.” Environmental Consultants, Inc.

There were no significant differences in leakage current observed between dry and wet tests at rated voltages, as is evident from Table 8. This suggests that the CCs are effective at preventing current flow in both dry and wet conditions.

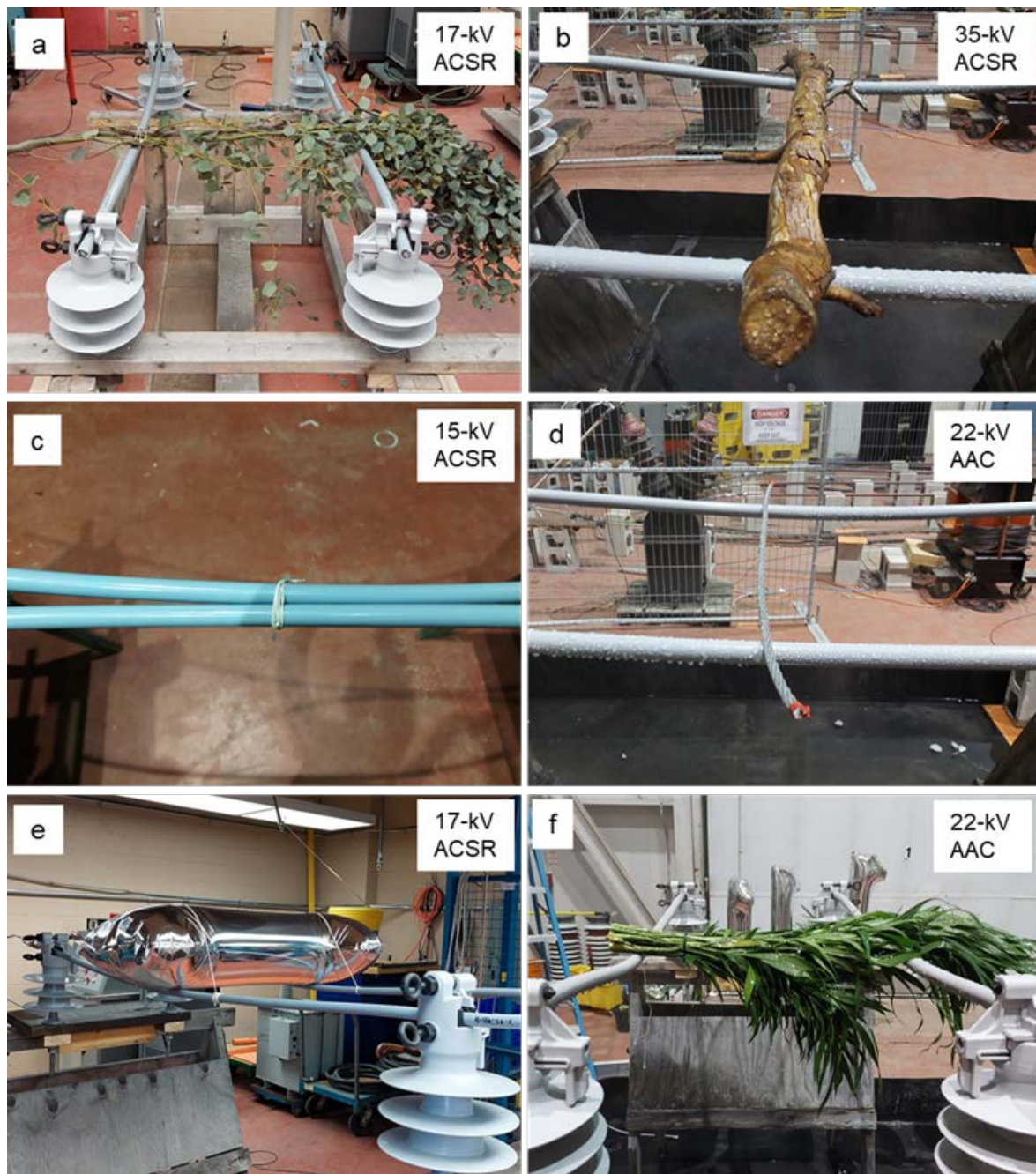


Figure 4. Rated voltage testing of two standard covered conductors with various bridging objects: (a) Leafy eucalyptus branch. (b) Large eucalyptus stick (wet test). (c) Conductor slapping of two CCs. (d) Bare ACSR conductor (wet test). (e) Mylar balloon. (f) Palm frond (wet test).

One Spliced CC at Rated Voltage

In this scenario, the energized CC was spliced with the splice hardware specified in Table 9 and cold shrink insulation. The spliced CC was bridged to a standard CC with a palm frond to simulate vegetation contact, as shown in Figure 5. Splice test leakage currents were 0.34 mA or lower and were stable at rated voltages for the duration of the five-minute hold.

Table 9. Splices used for phase-to-phase testing.

Rated Voltage	Size/Type	Splice
15-kV	1/0 ACSR (6x1)	Splice A
17-kV	1/0 ACSR (6x1)	Splice B
22-kV	397.5 kcmil AAC	Splice C
35-kV	1/0 ACSR (6x1)	Splice B

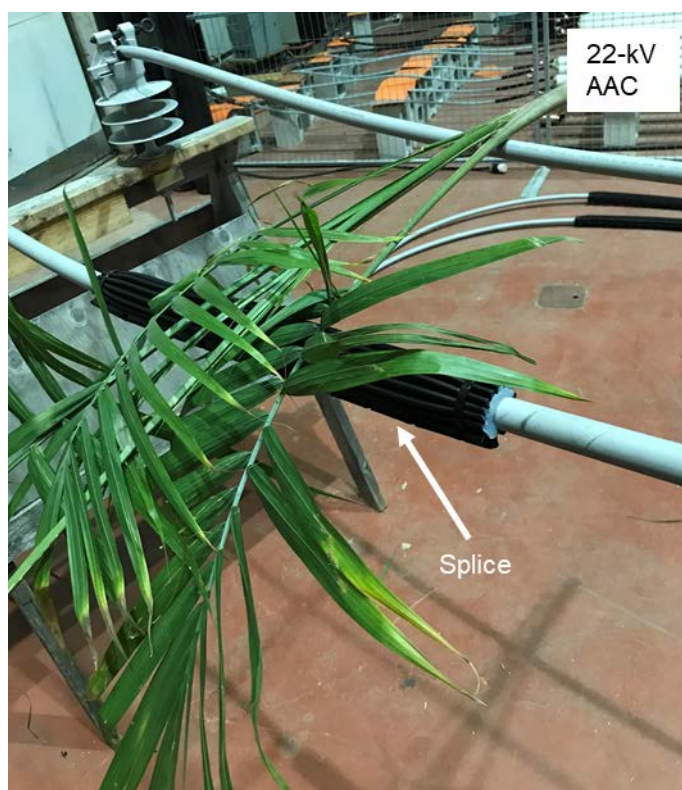


Figure 5. Rated voltage testing of a spliced CC and a standard CC bridged by a palm frond (22-kV AAC pictured).

One CC with a Simulated Flaw at Rated Voltage

One-inch full-thickness (Figure 6a) and one-inch half-thickness (Figure 6b) insulation flaws were artificially introduced to CCs on the energized side of the setup to simulate abrasion from vegetation contact or animal chewing. Full-thickness flaws exposed the underlying conductor, while half-thickness flaws removed roughly half of the polymer sheath thickness. A standard CC was used on the grounded side of the system. A leafy eucalyptus branch was used to bridge the two conductors and was tightly secured against the flaws (Figure 6c,d). The leakage currents for both tests with insulation flaws were below 1 mA and were stable at rated voltages for the duration of the five-minute hold.

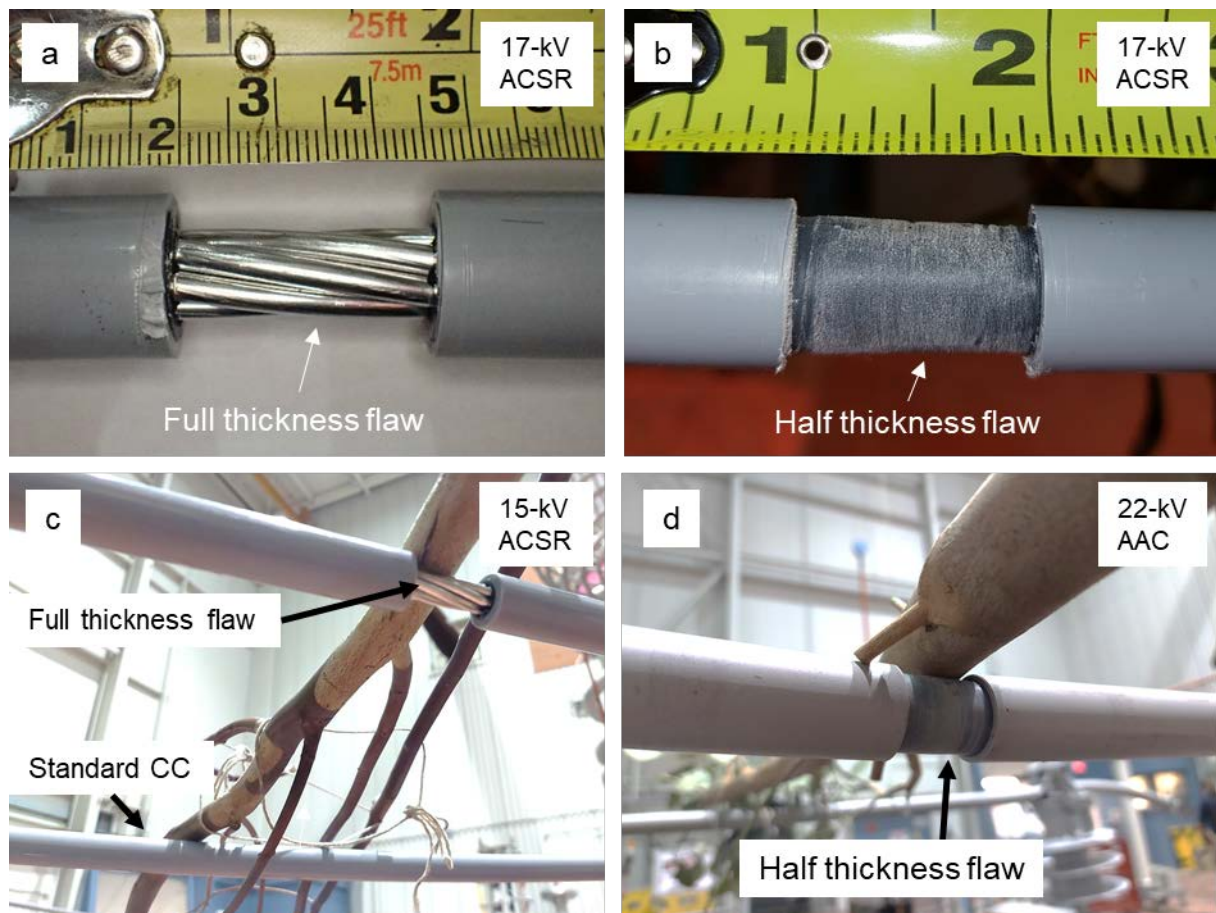


Figure 6. Simulated full- and half-thickness defects at rated voltages. (a) 17-kV ACSR CC with a through-thickness flaw. (b) 17-kV ACSR CC with a half-thickness flaw. (c) 22-kV AAC CC with a through-thickness flaw. (d) 22-kV AAC CC with a half-thickness flaw.

One CC and One Bare Conductor at Rated Voltage

In mixed systems (i.e., one bare conductor and one standard CC, shown in Figure 7a-d), leakage currents at rated voltages were comparable to systems with two CCs. All leakage current values remained below 1 mA for all classes of covered conductors and were stable for the duration of the five-minute hold. No insulation breakdown, phase-to-phase arcing, or damage to the CC was observed for any tests. As with two CCs, direct physical contact between one CC and one bare conductor did not result in significant current flow. This suggests that damage to the covering that exposes the underlying conductor on a single phase does not significantly increase the risk of arcing or ignition at rated voltages.

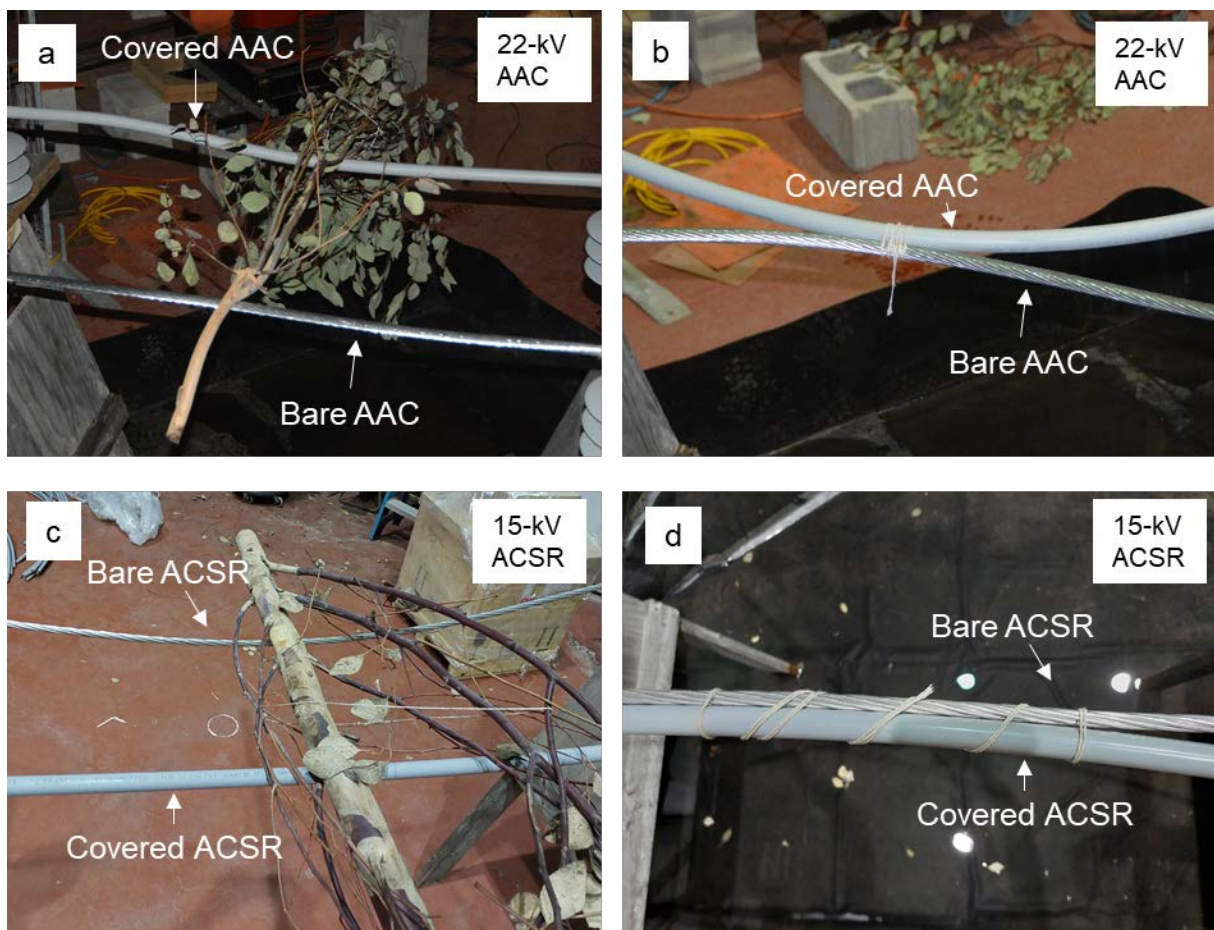


Figure 7. Mixed systems (one CC and one bare conductor) at rated voltages. (a) One bare conductor and one 22-kV AAC CC bridged by a leafy eucalyptus branch. (b) Simulated conductor slapping between a bare conductor and a 22-kV AAC CC. (c) One bare conductor and one standard 15-kV ACSR CC bridged by a large eucalyptus branch. (d) Simulated conductor slapping between a bare conductor and a 15-kV ACSR CC.

Wildlife Guard Tests at Rated Voltage

Wildlife guards are used near dead-end structures to mitigate the risk of animal contact to exposed bare conductor sections. Two scenarios were designed that involved testing wildlife guards at rated voltages. In the first scenario, two wildlife guards covering approximately one-foot sections of exposed bare conductor were bridged by a leafy eucalyptus branch or a simulated animal (using raw meat from a local butcher; see Figure 8a,c,d). The second scenario was similar, though one phase had a wildlife guard whereas the other conductor was exposed to simulate the loss of a wildlife guard (Figure 8b). Leakage currents were low (< 1 mA) in all tests with all four CC types, and no activity was observed for any of the tests at the rated voltages.

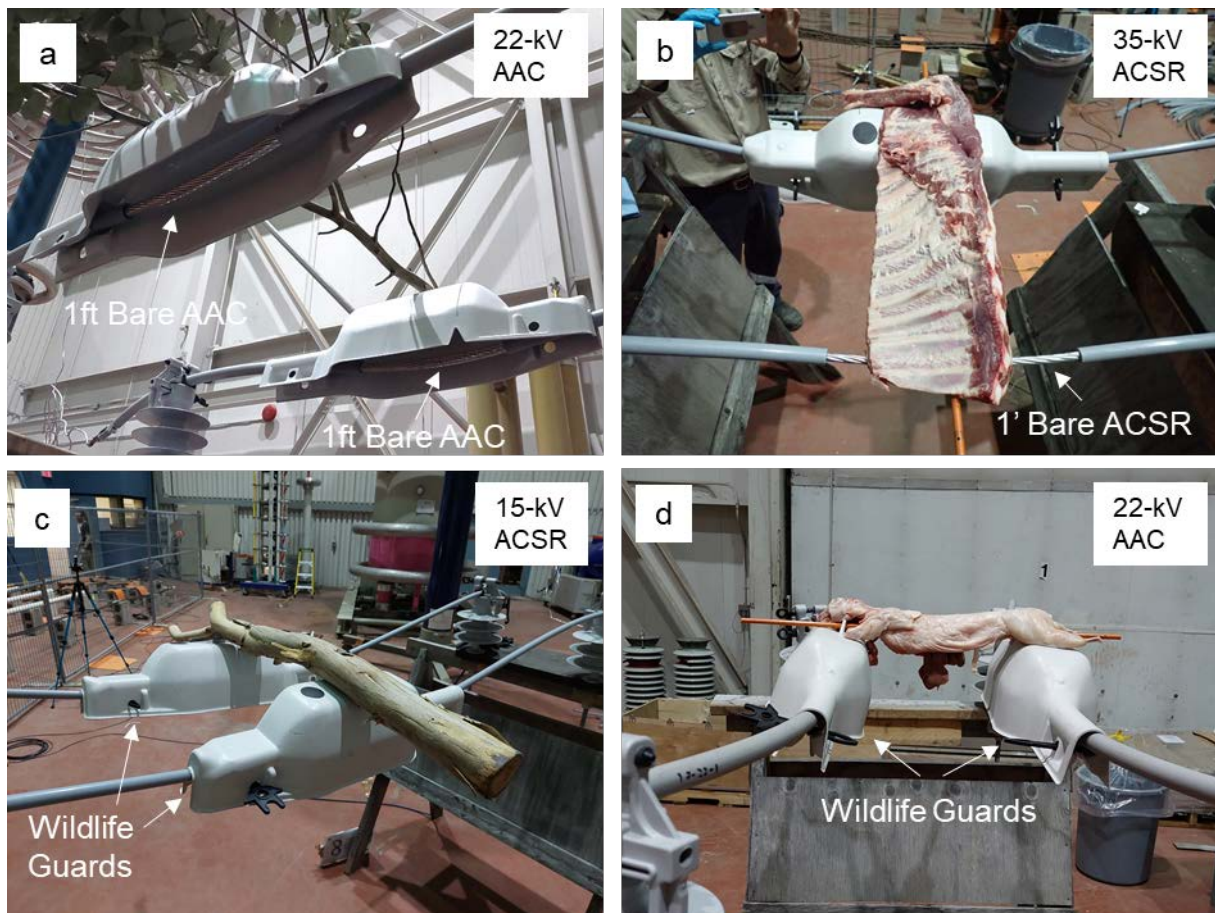


Figure 8. Wildlife guard tests in various configurations at rated voltages. (a) Leafy branches bridging two 22-kV AAC CCs with wildlife guards covering one foot of bare conductor on either side. (b) Simulated animal bridging one 35-kV ACSR CC with a wildlife guard and one 35-kV ACSR CC with one foot of bare conductor exposed. (c) Large eucalyptus stick bridging two 15-kV ACSR CCs with wildlife guards covering one foot of bare conductor on either side. (d) Simulated animal bridging one 22-kV AAC CC with wildlife guards covering one foot of bare conductor on either side.

Extended Phase-to-Phase Contact Testing—Rated Voltage

During the Phase I literature study, subject matter experts identified the potential risk of long-term foreign object contact.¹³ In addition to the relatively short-term contact scenarios discussed previously, extended contact tests were performed to investigate the time-dependent effects of foreign object contact, such as what might be experienced if a tree branch grew into a CC line but did not immediately cause an outage. While month-long tests (or longer) were out of scope for the current study, tests were designed to explore this concept within the constraints of the project timeline.

Two CCs were bridged by a leafy eucalyptus branch for seven days, as shown in Figure 9. One CC was energized to the rated voltage while the other CC was grounded. The energized conductor was also subjected to a loop current of 270 amps, the maximum ampacity determined by the technical datasheet.¹⁴ The loop current was intended to cause resistive heating of the conductor to simulate a loaded distribution line.

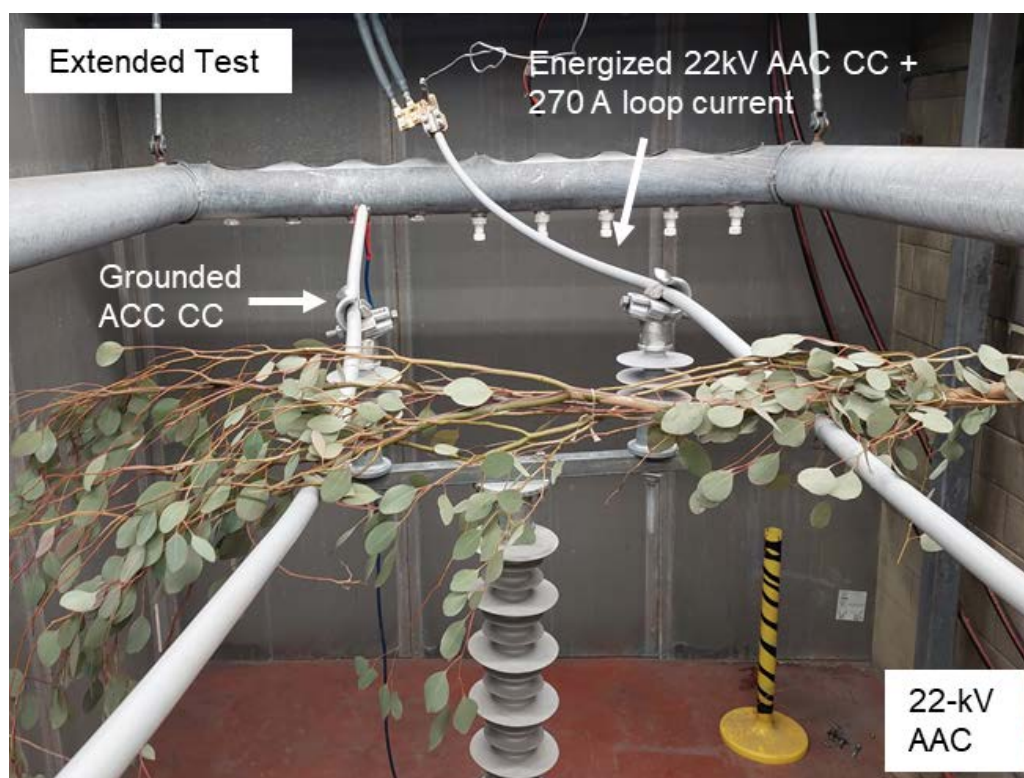


Figure 9. Test setup for 22-kV AAC CC one-week extended hold test at rated voltage and 270 amp loop current.

¹³ “Effectiveness of Covered Conductors: Failure Mode Identification and Literature Review,” Exponent Report No. 2103590.000 – 6880, December 22, 2021.

¹⁴ Southern California Edison. Covered Conductor Data Sheet for 17 kV and 35 kV. 2020.

No insulation breakdown, phase-to-phase arcing, or damage to the leafy branches (except for natural drying over time) was observed in these tests. Figure 10 and Figure 11 show images of the surface of the energized CCs after the one-week hold. The surface of the polymer sheaths on both the ACSR and AAC CCs were discolored at the point of contact with the branch at the conclusion of the test. The surface of the 35-kV CC also showed signs of minor insulation damage.

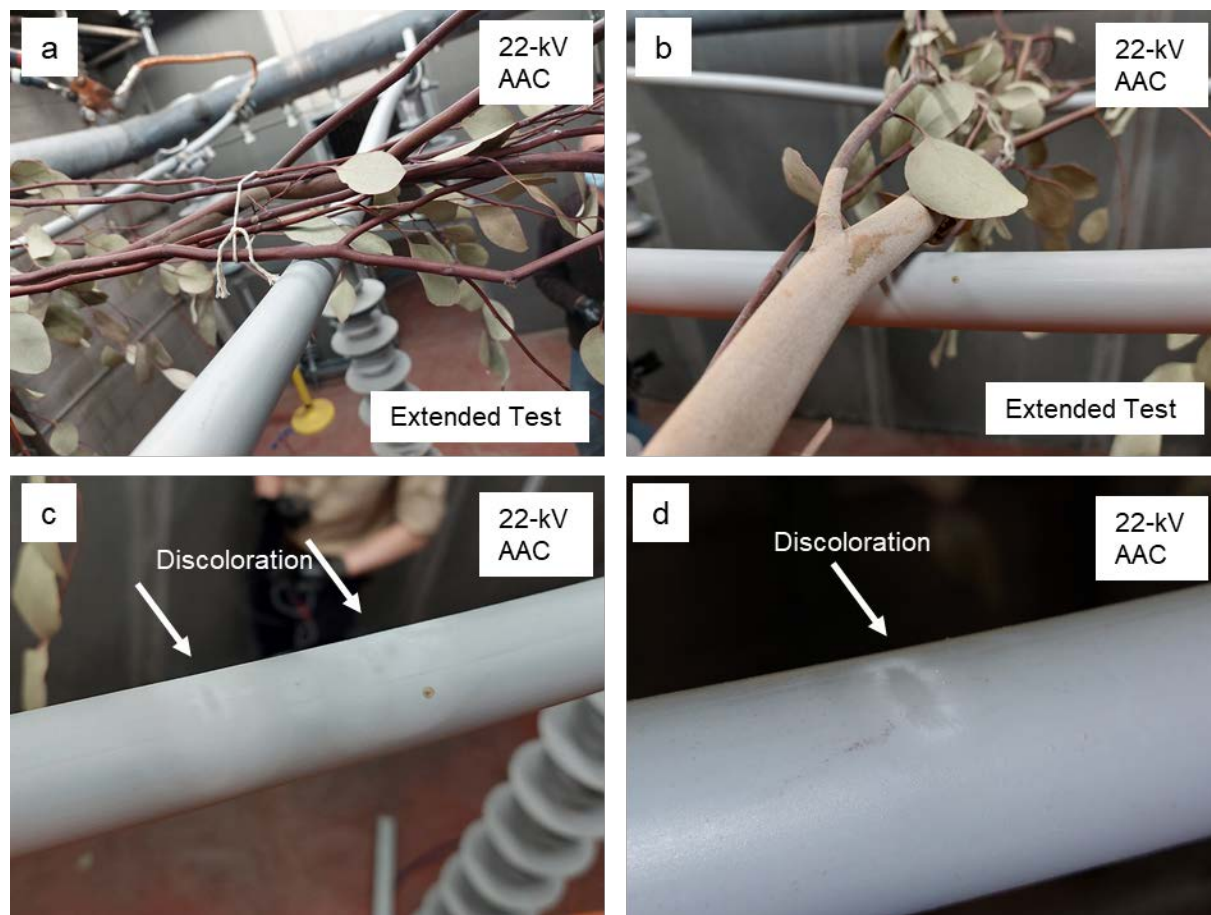


Figure 10. (a,b) Test setup for one-week extended test at rated voltage (22-kV AAC pictured). (c,d) Discoloration on the surface of 22-kV AAC after one week.

For all four conductor types, evidence of corona discharge was observed in the vicinity of the point of contact between the energized conductor and the leafy branch. Corona discharge refers to the ionization of surrounding air due to a sharp local potential gradient resulting in the formation of a plasma. The plasma facilitates the formation of ozone gas. The discoloration/damage observed may be consistent with oxidation of the PE sheath due to extended exposure to a plasma and/or ozone. In situations where the potential for extended contact exists, it may be prudent to perform additional long-term studies to identify the potential impact of extended exposure to corona discharge on the material properties of the insulation.

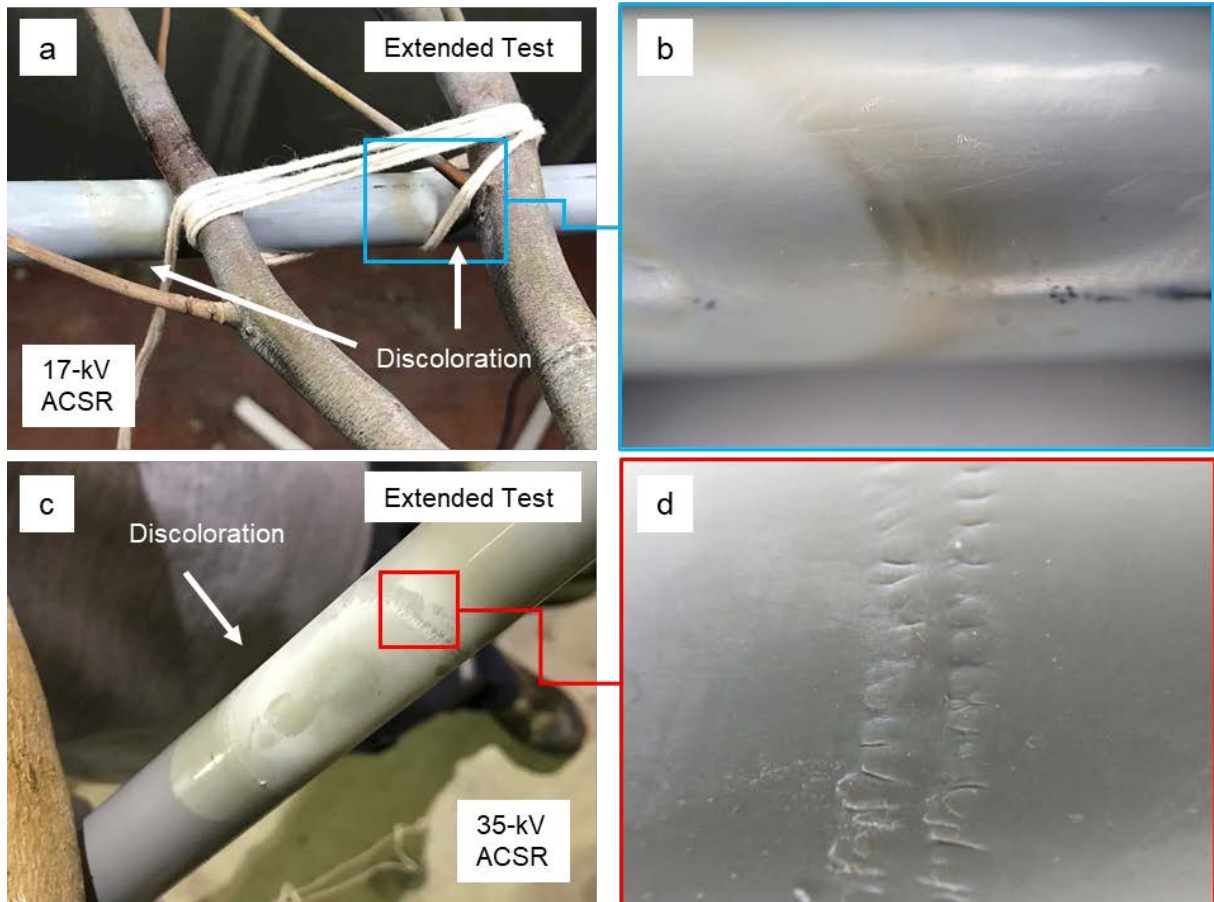


Figure 11. Results of one-week extended contact test at rated voltages. (a) Discoloration on the surface of 17-kV ACSR CC after one week and (b) higher-magnification image of the indicated area in (a). (c) Discoloration and damage on the surface of a 35-kV ACSR after one week, and (d) higher-magnification image of the indicated area in (c).

Phase-to-Phase Contact Testing with CCs—Extreme Voltage

For all phase-to-phase contact tests, the voltage was increased at a rate of 1 kV/sec to approximately 90 kV after the five-minute hold at rated voltages. Most tests were energized to ~90 kV with no observed insulation breakdown, pinhole formation, or phase-to-phase arcing. Some early tests with shorter (six-foot) conductor span lengths suffered from setup-related arcing events in the range of 60 kV to 90 kV. At these voltage levels, arcing sometimes occurred due to surface tracking and/or breakdown through the air. This effect was mitigated in later tests by increasing the conductor span length to 10 feet.

Insulation breakdown was observed in the 15-kV and 17-kV ACSR CC as well as the 22-kV AAC CC, but only when an artificial half-thickness coating flaw was introduced and the voltage was increased to greater than three times the rated voltage. Insulation breakdown was never observed in the 35-kV ACSR CC, even when the half-thickness coating flaw was introduced.

Two Standard CCs at Extreme Voltage

For tests with two CCs, the leakage current increased with applied voltage (Figure 12). Leakage current magnitudes at 90 kV were below 10 mA for all tested conductor types. The conductor slapping tests exhibited the highest leakage currents for this group, likely due to facilitated surface tracking and increased coupling effects because the conductors were physically fixed together.

It should be considered, however, that conductor slapping is a dynamic process with incidental contact; therefore, the static fixation used in this scenario represents an extreme (i.e., conservative) case. Interpretation of the leakage data requires an understanding of the possible current paths to ground:

- Tracking along the surface of the conductors and foreign object
- Coupling through the air
- Through the CC insulation (small component)
- Through the grips and insulating supports (small component)

Control tests were performed on the 17-kV and 35-kV ACSR CCs to better understand the effects of coupling on the measured current at ground. The setup for the control tests was identical to the foreign object contact tests, but no foreign object was used to bridge the two phases. The measured leakage currents at the rated voltages were approximately 0.1 mA and 0.2 mA for the 17-kV and 35-kV ACSR CCs, respectively. The measured leakage current at 90 kV was approximately 0.4 mA for both conductor classes (Figure 12).

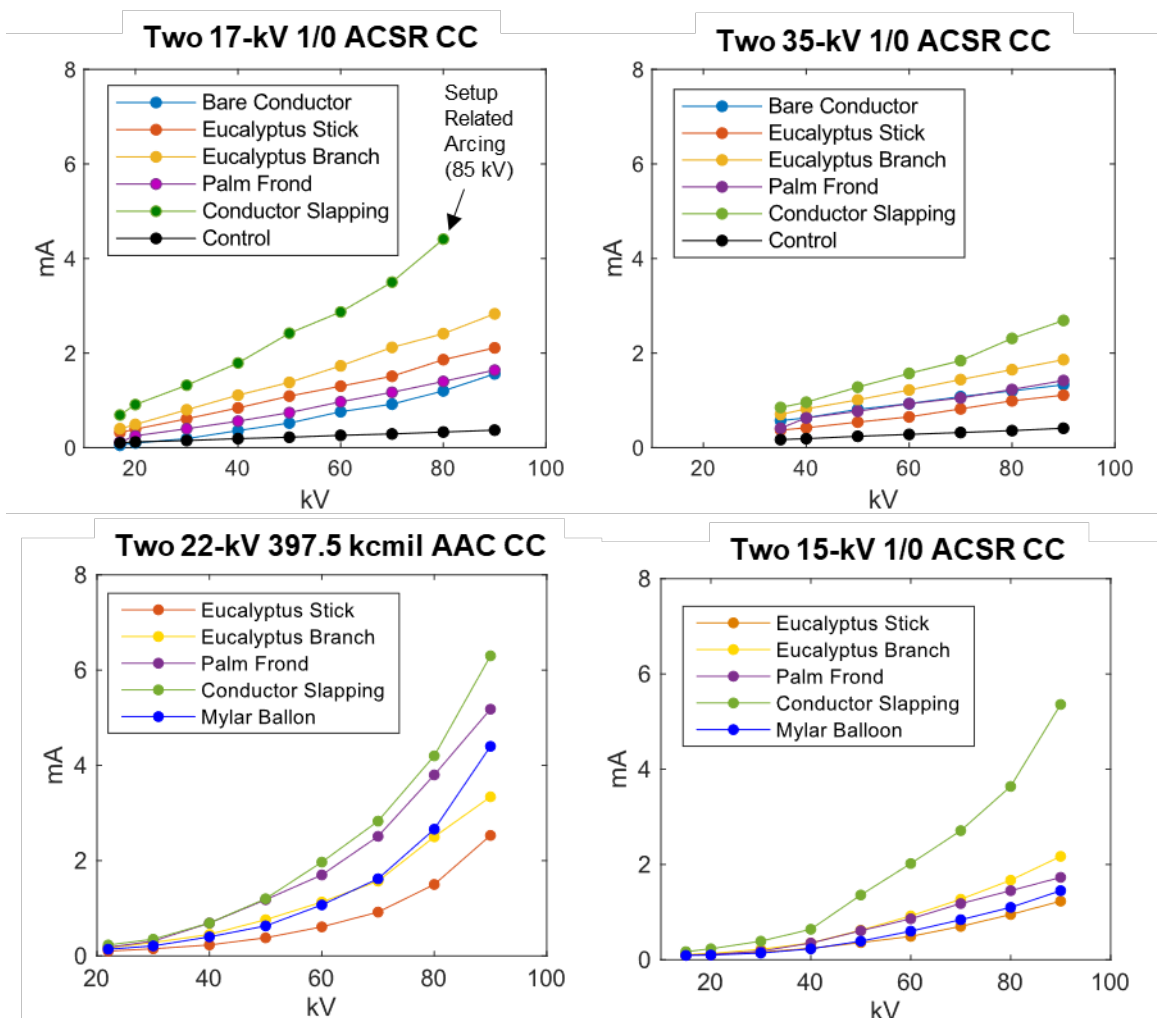


Figure 12. Leakage current as a function of voltage for two 17-kV ACSR CCs (top left), two 35-kV ACSR CCs (top right), two 22-kV AAC CCs (bottom left), and two 15-kV ACSR CCs (bottom right) with various bridging objects.

Above 60 kV, the development of corona discharge and surface tracking was evident for all conductor classes. For tests with two standard CCs bridged by a foreign object, the corona discharge and surface tracking were observed on both the energized and grounded CCs, concentrated near the points of contact with the foreign object.

One Spliced CC at Extreme Voltage

Spliced CCs exhibited similar leakage currents to standard CCs in the extreme voltage regime. Leakage current magnitudes at 90 kV were below 4.0 mA for all tested conductor/splice configurations.

One CC with a Simulated Flaw at Extreme Voltage

For CC tests with a full-thickness insulation flaw bridged to a standard CC by a leafy eucalyptus branch, minor charring was observed at the point of contact between the branch and flaw after 90 kV exposure (Figure 13). A distinct odor of eucalyptus could also be identified post-test, consistent with expulsion of moisture from the branch. The branch was also slightly warm to the touch, consistent with resistive heating due to the passage of current. Despite observing minor charring on the outer surface of the branch following high-voltage exposure, there was no evidence of ignition or flame spreading to other parts of the branch.

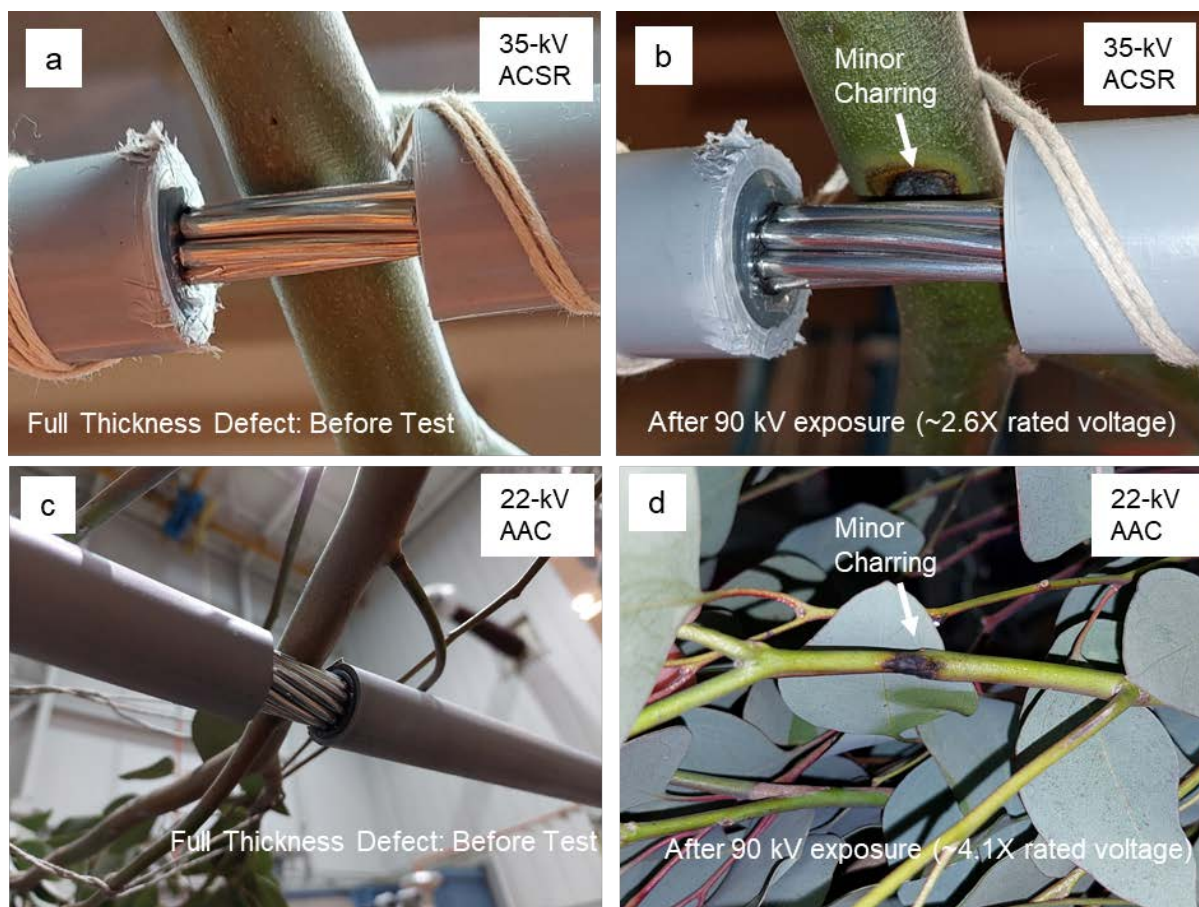


Figure 13. Full-thickness defect tests at rated voltages and extreme voltages. (a) One 17-kV ACSR CC with a full-thickness flaw and a standard CC. (b) Charring was observed at the point of contact between the branch and exposed conductor after high-voltage exposure at 90 kV (~2.6X rated voltage). (c) One 22-kV AAC CC with a full-thickness flaw and a standard CC. (d) Charring was observed at the point of contact between the branch and exposed conductor after high-voltage exposure at 90 kV (~4.1X rated voltage).

After exposure to extreme voltages, breakdown and pinhole formation were observed in all covered conductor tests with a half-thickness coating flaw (Figure 14) except for the 35-kV ACSR CC, likely due to increased sheath layer thicknesses. The statistics and breakdown voltages are presented in Table 10. In dry tests, minor charring was observed on the eucalyptus

branch at the point of contact with the flaw following breakdown and pinhole formation. Despite minor charring on the outer surface, there was no evidence of ignition or flame spreading to other parts of the branch. Charring was suppressed in the wet tests.

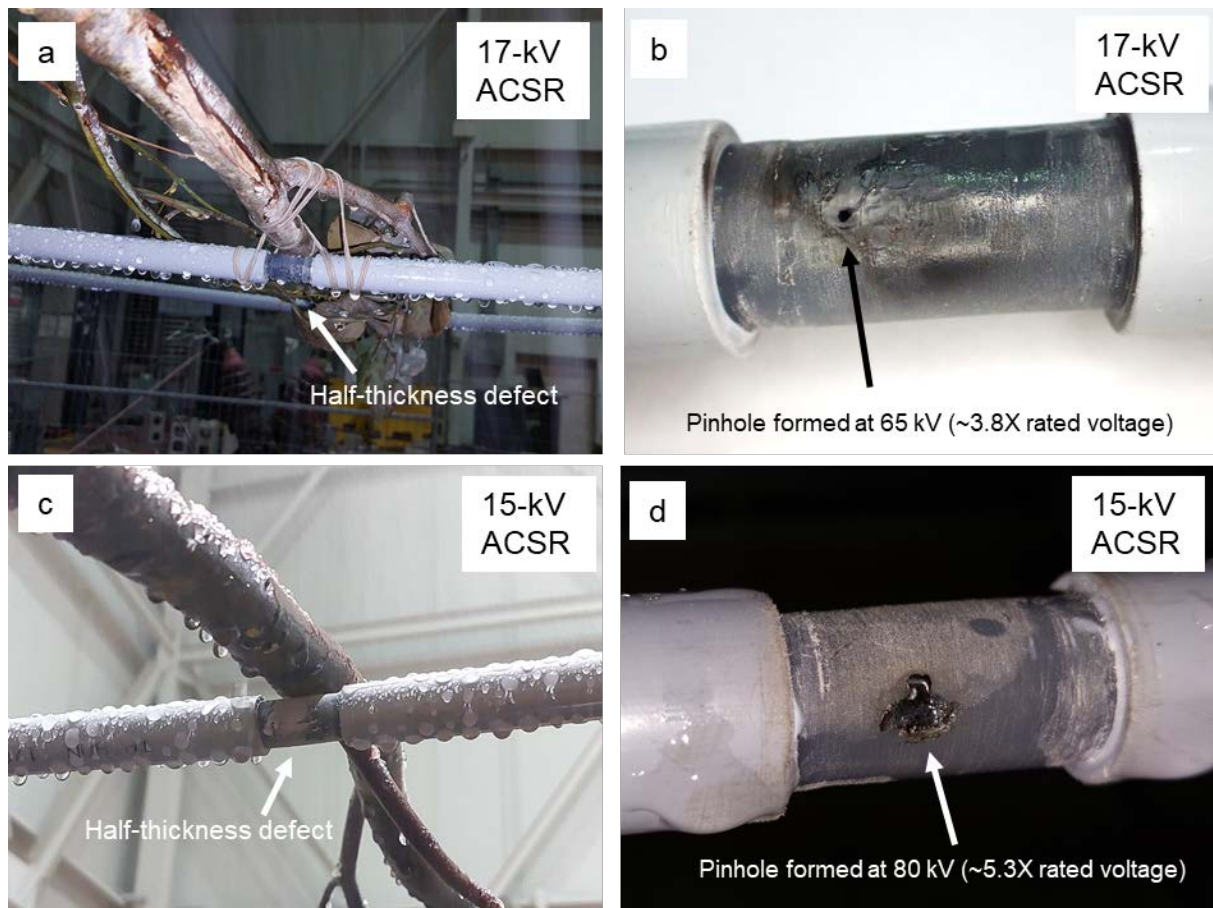


Figure 14. One CC with a simulated flaw at extreme voltages. (a) Wet 17-kV ACSR CC with a half-thickness flaw and a standard CC bridged by a eucalyptus branch. (b) Insulation breakdown and pinhole formation at 65 kV (~3.8X rated voltage). (c) Wet 15-kV ACSR CC with a half-thickness flaw and a standard CC bridged by a eucalyptus branch. (d) Insulation breakdown and pinhole formation at 80 kV (~5.3X rated voltage).

Table 10. Summary of pinhole formation in phase-to-phase contact tests at extreme voltages where one CC contains a half-thickness defect

Covered Conductor Type	Total # of Half-Thickness Defect Tests (wet + dry)	Fraction of Tests with Pinhole Observed Up to 90 kV	Average Voltage at Breakdown (kV) (times rated voltage)
15-kV ACSR CC	6	2 out of 6	65 (4.3X)
17-kV ACSR CC	6	5 out of 6	67 (3.9X)
22-kV AAC CC	6	2 out of 6	83 (3.8X)
35-kV ACSR CC	6	0 out of 6	N/A

The plots in Figure 15 present leakage currents as a function of applied voltage for the four conductor classes. Prior to breakdown, leakage currents for the half-thickness insulation flaw tests were similar to those of the standard CCs. Following the formation of the pinhole, leakage currents for the half-thickness flaw were elevated and were similar to those of the full-thickness flaw. No insulation breakdown or current increase was observed for the 35-kV ACSR CC.

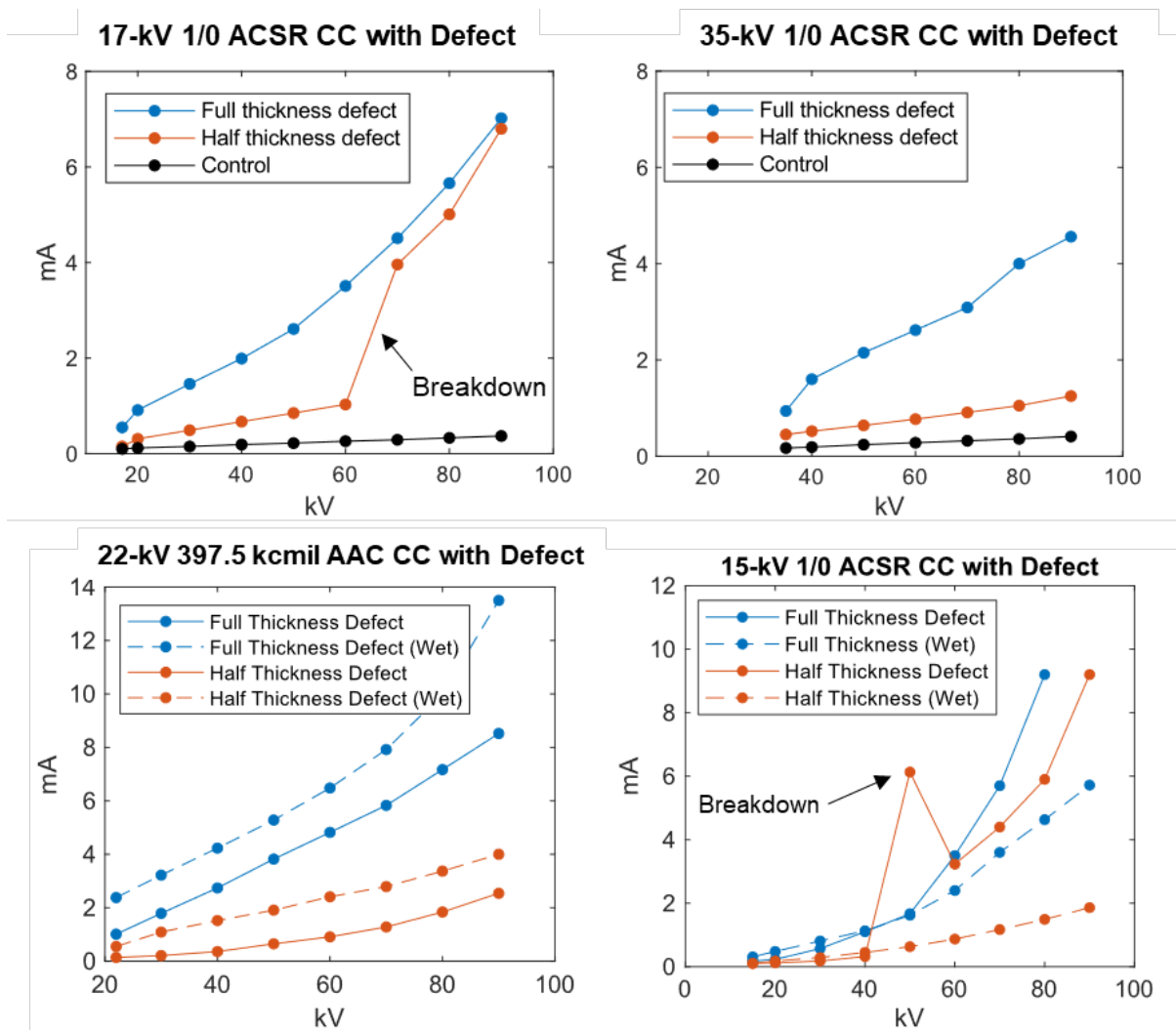


Figure 15. Leakage current as a function of voltage for one CC with a flaw and one standard CC for 17-kV ACSR (top left), 35-kV ACSR (top right), 22-kV AAC (bottom left), and 15-kV ACSR (bottom right).

One CC and One Bare Conductor at Extreme Voltage

When the bare conductor was exposed on the energized side of a mixed system, corona discharge and surface tracking were frequently observed on the grounded CC above 60 kV. Again, this was concentrated near the point of contact with the foreign object. In these cases, tracking along the insulation of the grounded conductor to the ground wire resulted in conclusion of the test prior to reaching 90 kV. Tracking to ground could be mitigated by increasing the span length of conductor.

Wildlife Guard Tests at Extreme Voltage

The wildlife guard tests were unique in that they consisted of exposed sections of bare conductor on both sides. For tests with two wildlife guards covering one-foot sections of exposed bare conductor bridged by a leafy eucalyptus branch (Figure 16a,c), breakdown through the air and around the wildlife guard occurred for three out of six tests in the range of 82 kV to 90 kV. These occurred due to branch extremities extending around the wildlife guard and near the exposed conductor. No breakdown through the air was observed when two wildlife guards were used and the bridging object was an animal simulated by raw meat.

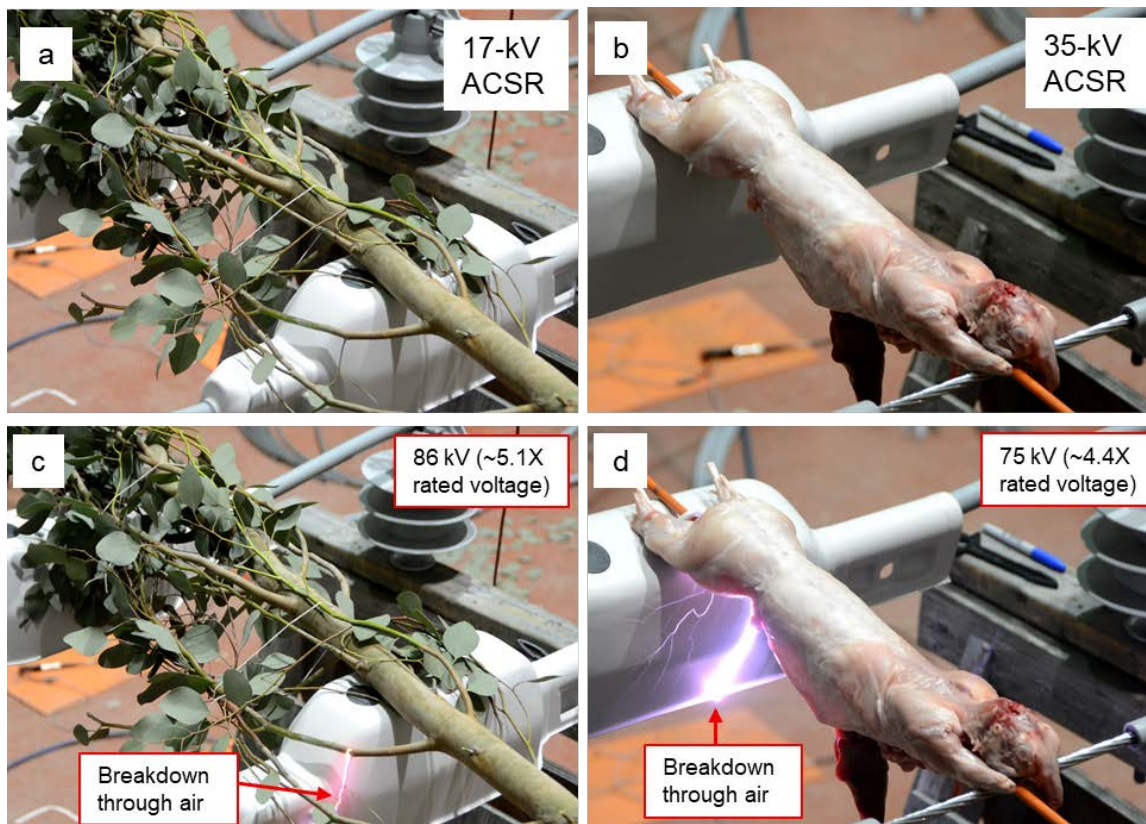


Figure 16. Wildlife guard tests. (a) Leafy eucalyptus branch test at rated voltage bridging two 17-kV ACSR CCs with animal guards covering one foot of bare conductor on either side. (b) Animal simulated by raw meat test at rated voltage bridging one 17-kV ACSR CC with an animal guard and one CC with one foot of bare conductor exposed. (c) Breakdown through the air around the animal guard observed at 86 kV (~5.1X rated voltage). (d) Breakdown through the air around the animal guard observed at 75 kV (~4.4X rated voltage).

For tests with one missing wildlife guard (Figure 16b,d), breakdown through the air occurred for all six tests between 60 kV and 75 kV. The arcs tracked around the animal guard on the grounded side. This is notably an aggressive scenario since the voltages are extreme and the foreign object is in direct contact with the bare conductor. This scenario would have a low probability of occurrence in the field.

Sequential Breakdown Testing

The purpose of the sequential test was to better understand performance of CCs following a significant overvoltage or fault, such as a lightning strike. To force breakdown, the CCs were wrapped in a grounded metal braid at midspan and were exposed to high voltage, up to 150 kV (Figure 17a,b). The large potential difference between the conductor and metal braid resulted in a strong electric field, capable of inducing a breakdown in the insulation (Figure 17c,d). Several breakdown tests were performed on 40-foot segments of covered conductor. For the first test on 17-kV ACSR CC, breakdown occurred around 95 kV. For the second test on 17-kV ACSR CC, breakdown occurred around 85 kV. Following breakdown, each conductor was exposed to high voltage a second time to effectively “grow” the flaw.

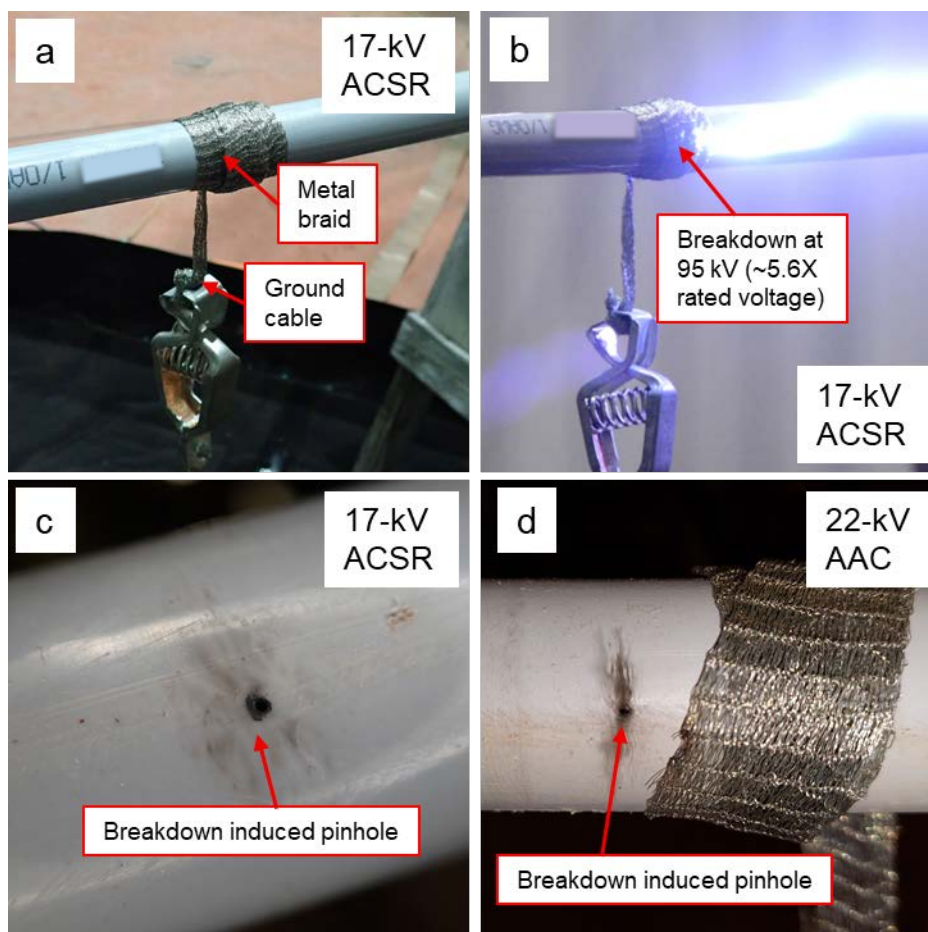


Figure 17. Breakdown test setup. (a) 17-kV ACSR CC was wrapped in a grounded metal braid and was exposed to voltage until (b) breakdown of the insulation at 95 kV resulted in (c) pinhole formation. (d) Pinhole formation in 22-kV AAC after high-voltage breakdown test.

Since the thickness of the polymer sheath was 4.31 mm, this corresponded to an approximate minimum breakdown strength between 20 kV/mm and 22 kV/mm. It should be noted that this was not an ASTM standard breakdown strength procedure, so these values are expected to differ

from values determined from standardized tests. The voltage for the 35-kV ACSR CC could not be increased above 150 kV due to high power losses from surface tracking. Given an insulation thickness of 8.02 mm, the breakdown strength of the 35-kV ACSR CC exceeded 18.7 kV/mm.

Surface tracking was a significant concern at high voltage for both conductor classes, so 40-foot spans were used to prevent damage to the equipment (Figure 18a). The presence of sustained high-voltage corona and surface tracking resulted in arc-tracking damage to the surface of the CC (Figure 18b).

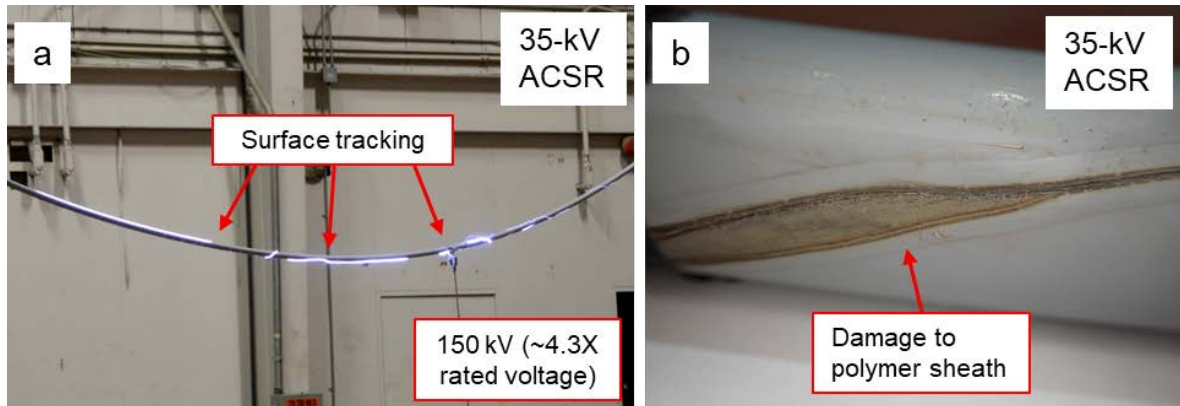


Figure 18. (a) Surface tracking during breakdown test at 150 kV in the 35-kV ACSR CC. (b) Damage to the surface of the CC due to sustained exposure to high-voltage corona and surface tracking.

The CCs with induced pinhole flaws were bridged by a leafy eucalyptus branch to one standard CC for contact testing at rated and extreme voltages (Figure 19a). The branches were tied down tightly with electrical tape to ensure good contact with the pinhole flaw. The leakage currents were stable and below 1 mA during the five-minute hold at rated voltages. Following high-voltage exposure, the defect in the covering grew in size and minor charring was observed at the point of contact with the branch (Figure 19b-d). There was no evidence of ignition or flames, and charring did not spread to other parts of the branch. Note that this represented the second extreme voltage exposure for these conductors, as the first exposure was used to induce the pinhole.

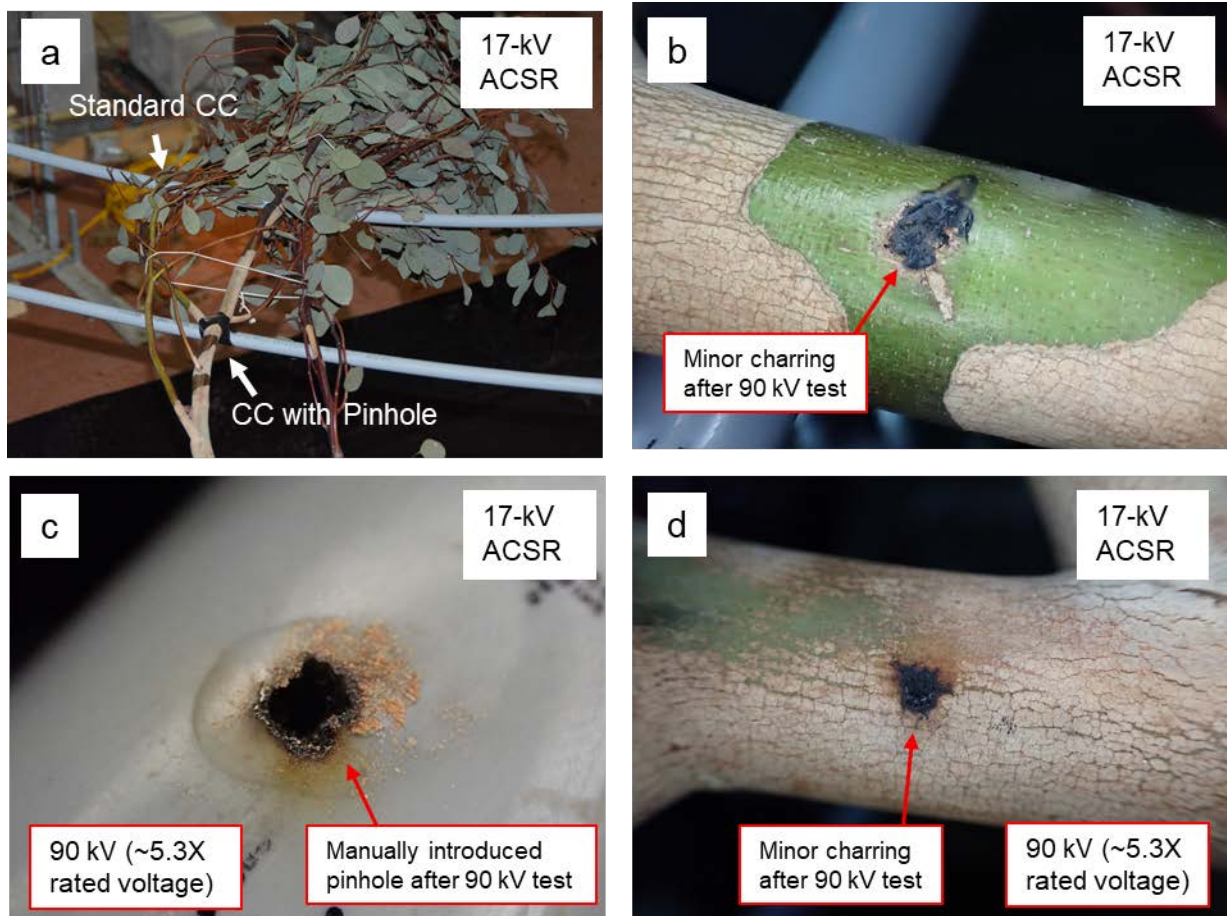


Figure 19. (a) Sequential phase-to-phase contact testing after induced breakdown. (b) Contact point showing minor charring on leafy eucalyptus branch after exposure to 90 kV. (c) Manually introduced pinhole flaw in 35-kV ACSR CC after contact testing at 90 kV. (d) Contact point showing minor charring on leafy eucalyptus branch after exposure to 90 kV.

Discussion and Conclusions: Phase-to-Phase Contact Testing

Tests with two bare conductors demonstrated the clear ignition risks associated with contact by leafy branches or other potential foreign objects. Immediately after applying voltage, the branches started screeching, consistent with the rapid expulsion of moisture, and smoking at both points of contact with the bare conductors. Leakage currents reached the maximum allowed by the test setup (2000 mA), suggesting that current was able to pass freely through the branch. Three seconds after applying voltage, ignition of the branch was clearly observed at both points of contact.

However, for tests in which at least one CC was present, no current transfer greater than 2.5 mA was detected in any scenario at rated voltages involving contact of a foreign object, splice, or conductor slapping. These results demonstrate that the insulation of the tested CCs is highly

effective at preventing current flow, arcing across phases, and ignition at rated voltages regardless of environmental condition (wet or dry), or the nature of the object between phases. The only time when significant current transfer was observed was when sections of bare conductor were exposed on *both* sides of the system.

Extended contact of a eucalyptus branch across two CCs at rated voltages for one week resulted in discoloration of the polymer sheath in all four conductor classes. The 35-kV CC suffered minor damage to the surface of the sheath in addition to discoloration. The yellowing and damage were likely due to the sustained presence of corona discharge at the point of contact with the branch. The corona effect was more significant at higher voltages. For situations in which extended foreign object contact is of particular concern, further long-term testing is recommended to investigate the impact of longer times and the effect on the insulating strength of the sheath.

CCs were also effective at preventing current flow, phase-to-phase arcing, and ignition well above their rated voltages and up to 90 kV. Leakage current magnitudes at 90 kV with two CCs present were below 9 mA for all four conductor classes. In tests with one bare conductor, and only after exposure to 90 kV, minor charring was observed on the leafy eucalyptus branches. However, there was no evidence of ignition, flame, or spreading of charring to other parts of the branch. When a half-thickness insulation flaw was manually introduced on the energized conductor, insulation breakdown occurred in the 15-kV ACSR, 17-kV ACSR, and 22-kV AAC at an average voltage of 65 kV, 67 kV, and 83 kV, respectively. No breakdown was observed up to 90 kV in the 35-kV ACSR.

Simulated Wire-Down

Scope

The Phase I literature study identified the need for additional testing to investigate the effectiveness of CCs at mitigating fire ignition risks during a wire-down event. A 2015 study commissioned by the Australian State of Victoria’s Powerline Bushfire Safety Program concluded that intact CCs effectively mitigate the ignition risks posed by wire-down events.¹⁵ However, the same study also concluded that CCs with full-thickness insulation flaws may pose an ignition risk, in addition to bare conductors. The present testing investigated this scenario as well as others such as partial (half-thickness) insulation removal and a severed conductor end, as outlined in Table 11. Three flaw types were investigated for CCs: full-thickness insulation flaws, half-thickness insulation flaws, and a broken end.

Table 11. Simulated wire-down ignition risk scenarios.

Conductor Type	Flaw Type
Bare 1/0 ACSR and 397.5 kcmil AAC	N/A
CC – all four types	Standard CC (No flaw)
CC – all four types	1” full thickness sheath removed
CC – all four types	1” half thickness sheath removed
CC – all four types	Broken end

Experimental Setup

A schematic representation of the experimental setup used to conduct the simulated wire-down testing is shown in Figure 20. A 460 V AC variable power supply was “stepped up” to 7.1 kV with a transformer. The power supply was capable of producing greater than 40 amps of current depending on the overall system impedance. The conductor was suspended, energized, and abruptly dropped into the fuel bed to simulate the dynamics of a wire-down event. A high-speed control unit continuously monitored the voltage and current waveforms. Fault currents generally ranged from 6 amps to 15 amps. If a fault was generated, the control unit would trip, and the power would shut off after a set amount of time governed by an adjustable delay switch (0-1000 ms).

¹⁵ Marxsen, T. “Powerline Bushfire Safety Program, Vegetation Conduction Ignition Test Report-Final.” 2015.

The expected outcome of dropping a bare conductor into the soil was the generation of a power arc with sufficient energy to cause ignition of the nearby dry grass fuel. If no fault was detected, the wire was dropped into the fuel bed two more times to confirm the result.

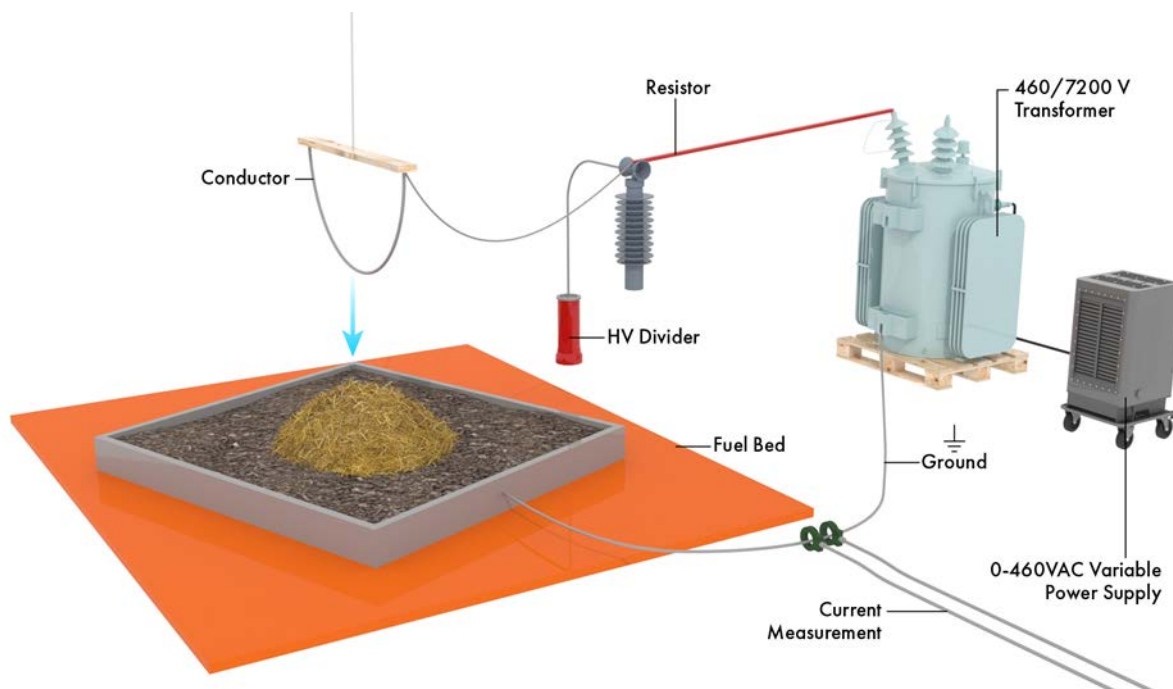


Figure 20. Schematic representation of experimental setup used in simulated wire-down testing. The conductor was energized to 7.1 kV and dropped abruptly into the fuel bed. Fault currents ranged from 6 amps to 15 amps. If no fault was observed, the conductor was dropped two more times to confirm the result.

Test development trials were performed with the bare conductor to tune the equipment and to better understand the impact of voltage, current, and fault duration on the ignition probability. These trials demonstrated that dropping a bare conductor into the fuel bed could produce a power arc at voltages as low as 1.5 kV up to 7.1 kV. This analysis also showed that the probability of ignition for a downed bare conductor depended strongly on the fault current. In these preliminary tests, fault currents ranged from 0.9 amps to 40 amps. Ignition did not occur for tests with a peak leakage current of less than 4 amps. However, ignition occurred in most tests with a peak leakage current greater than 5 amps. In later trials, a 500-ohm resistor was employed to maintain more consistent fault currents. Fault durations in development trials ranged from 17 ms to 272 ms. Trials with low current did not result in ignition regardless of fault duration whereas trials with sufficiently high current (>5 amps) resulted in ignition regardless of fault duration.

Following the development phase, equipment parameters were held constant to ensure direct comparison across the tested scenarios. The applied voltage for all “real” tests was 7.1 kV and the fault duration was 125 ms. The leakage currents remained sensitive to system impedance, but all fell within the range of 6 amps to 15 amps.

The fuel bed was composed of a soil mixture and conditioned dry excelsior in a grounded steel pan. Excelsior is a wood wool product made of fine wooden slivers cut from logs. The soil mixture, which simulated the topsoil composition from Southern California's rolling uplands, was modeled after data obtained from the University of California, Berkeley College of Agriculture's Generalized Soil Map of California.¹⁶ The soil consisted of a granular sandy loam with relatively high clay content. The soil mixture was composed of four parts organic loamy topsoil, two parts coarse deco sand, and one part natural clay by mass.

Prior to assembly of the fuel bed and testing, the excelsior was conditioned in accordance with ASTM D4933 in an environmental chamber at 104° F and 20% relative humidity for 24 hours. The approximate moisture content of the excelsior was 5% following conditioning, consistent with CAL FIRE's Powerline Fire Prevention Field Guide guidelines for simulating dry grass fuel.¹⁷ Finally, the fuel bed was assembled by placing approximately two inches of the topsoil mixture in a rectangular steel container and partially embedding the conditioned excelsior into the soil. Figure 21 shows a photograph of a representative fuel bed assembled.



Figure 21. Example of simulated California soil and fuel bed used in wire-down testing.

Electrical equipment operation and measurements were informed by IEEE4: High Voltage Testing Techniques. The soil was nominally dry during the initial testing trials. However, initial results suggested that the high resistance of the fuel bed prevented current from making it to ground. Thus, for subsequent testing, a small amount of water was added to the soil prior to each test to improve its conductivity.

Results

The results of the five tested scenarios are shown in Table 12. No arcing events were observed when standard CCs or CCs with half-thickness insulation flaws were energized to the phase-to-ground voltage and dropped into the fuel bed (Figure 22). In contrast, the bare conductor tests demonstrated a propensity for arcing and fire ignition even at voltage and current conditions

¹⁶ R. Storie and W. Weir. "Generalized Soil Map of California." California Agricultural Experiment Station Extension Service.

¹⁷ Powerline Fire Prevention Field Guide: 2008 Edition. CAL FIRE, 2008.

lower than would be expected from a real distribution system (Figure 23). Tests involving CCs in which the underlying conductor was directly exposed to the fuel bed, i.e., in the case of a full-thickness flaw or a severed conductor end, also showed propensity for arcing and ignition (Figure 24 and Figure 25). The body of this report shows representative images for the 17-kV and 35-kV ACSR CC wire-down tests. The results for the 22-kV AAC CC and 15-kV ACSR CC are presented in Appendix B.

Table 12. Results for simulated wire-down tests.

Test	Result			
	15 kV ACSR	17 kV ACSR	35 kV ACSR	22 kV AAC
Standard CC	No arcing observed	No arcing observed	No arcing observed	No arcing observed
CC w/ half-thickness flaw	No arcing observed	No arcing observed	No arcing observed	No arcing observed
Bare conductor	Arcing / ignition	Arcing / ignition	Arcing / ignition	Arcing / ignition
CC w/ full-thickness flaw	Arcing / ignition	Arcing / ignition	Arcing / ignition	Arcing / ignition
Broken CC w/ exposed end	Arcing / ignition	Arcing / ignition	Arcing / ignition	Arcing / ignition

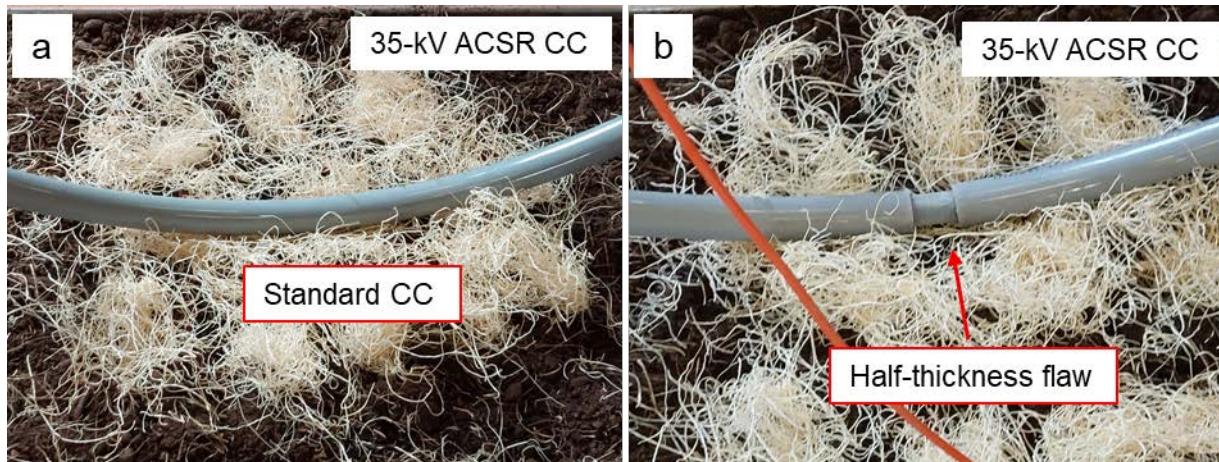


Figure 22. (a) Simulated wire-down test of a 35-kV ACSR CC. No ignition was observed after three tests. (b) Simulated wire-down test of a 35-kV ACSR CC with a half-thickness flaw. No ignition was observed after three tests.

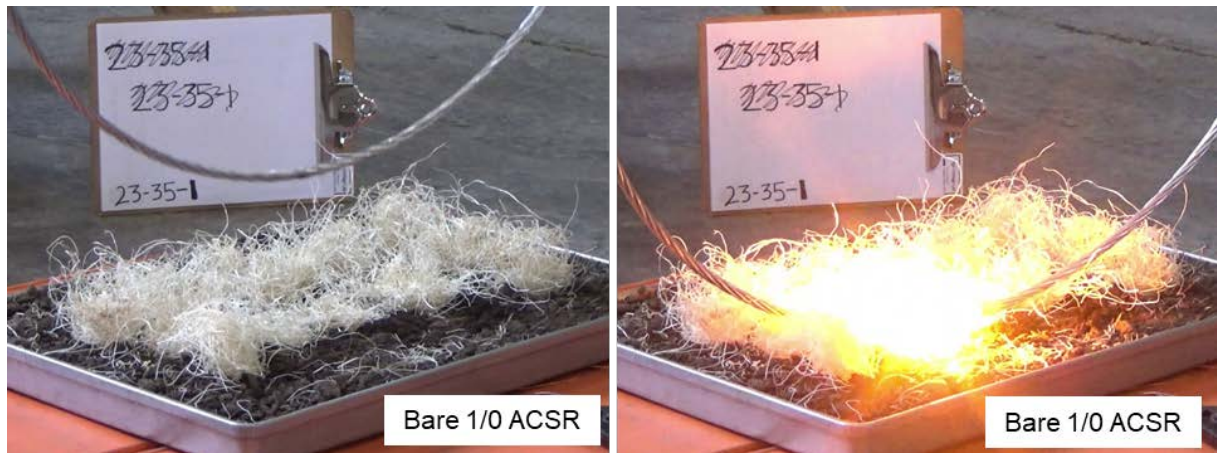


Figure 23. Simulated wire-down test of a bare ACSR conductor demonstrating the potential for ignition of the dry brush.

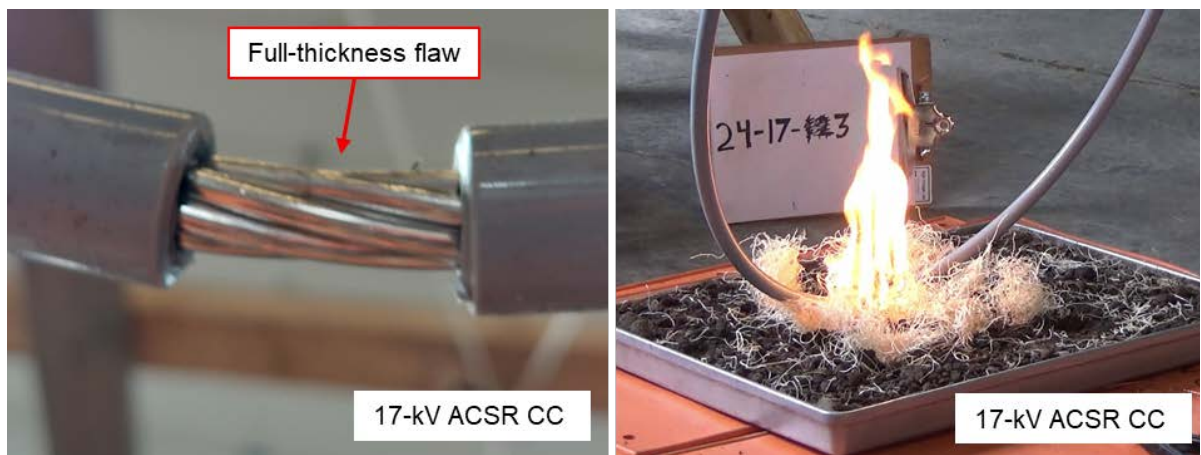


Figure 24. Simulated wire-down test of a 17-kV ACSR CC with a full-thickness flaw demonstrating the potential for ignition of the dry brush.

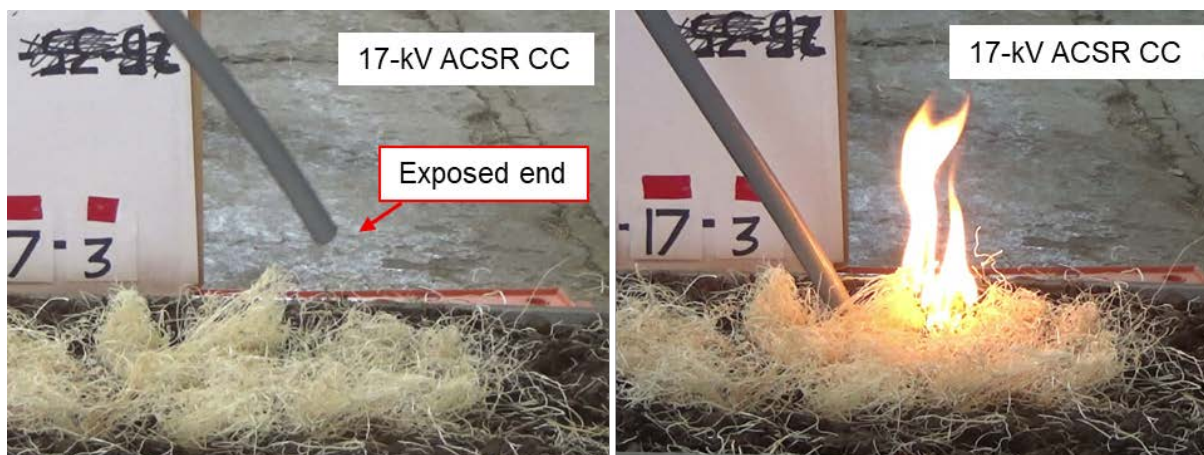


Figure 25. Simulated wire-down test of a 17-kV ACSR CC with a broken end demonstrating the potential for ignition of the dry brush.

Since arcing was not observed with the given test setup for any standard CCs or CCs with a half-thickness flaw, it was necessary to confirm that application of the full phase-to-ground voltage would also not result in arcing or insulation breakdown. Separate simulated wire-down tests were performed with a hi-pot 800 kV power supply. The CCs and CCs with a half-thickness flaw were energized to the appropriate phase-to-ground voltage and dropped into the fuel bed. No breakdown was observed for the standard CC or CC with a half-thickness flaw. This result was consistent with phase-to-phase contact tests discussed in the previous section.

Discussion and Conclusions: Simulated Wire-Down

This testing showed that CCs in a wire-down event are not likely to pose an ignition risk unless they are sufficiently damaged such that the bare wire beneath the coating is exposed and can arc to ground.

In each simulated wire-down test, one of three outcomes was observed:

1. An arc was generated, resulting in ignition of the dry fuel. The conductor impacted the soil and drew a current arc between it and the earth. The electric arc heated the nearby dry grass, generating pyrolysis gases such as methane, hydrogen, and carbon monoxide. The gases accumulated near the arc and ignited. The resultant flame heated more neighboring dry grass, generating more gases, and created a sustained fire.¹⁸ No ignition of the CC polymer sheath was observed for the test duration.
2. An arc was generated upon impact with the soil, but no sustained fire was observed. This could have occurred for a number of reasons. The arc may have been too far away from the grass to cause enough pyrolysis gases to be generated. The gases may also have dispersed and never reached the minimum concentration necessary for ignition. If an

¹⁸ Tony Marxsen. "Ignition Tests – lo-sag conductor." Powerline Bushfire Safety Program. 2015.

initial small flame did form, it may have been extinguished by windy conditions or may not have been close enough to other grasses to create sufficient pyrolysis gases required for a sustained fire. Finally, the conductor itself may have covered and extinguished the initial flame.¹⁹ Since the formation of an arc had the potential to ignite nearby fuel, regardless of whether ignition was observed in each individual test, these outcomes were categorized as a potential ignition event.

3. No arcing event or current flow was observed despite good contact between the wire and the fuel bed.

As there is a wide variety of conductor-falling velocities and angles in the field, tests were similarly varied in the velocity and incident angle of the dropping conductor. Although steps were taken to ensure consistency and conservatism in this testing, the probability of ignition was nevertheless still a function of the proximity of the generated arc to the nearest vegetation.

¹⁹ Tony Marxsen. "Ignition Tests – lo-sag conductor." Powerline Bushfire Safety Program. 2015.

Corrosion Testing

Motivation and Scope

As discussed in the introduction, the Phase I literature review recommended better understanding of failure modes specific to CCs that would not be present in bare conductor use cases. The Phase I work identified localized corrosion of CCs near stripped ends as a potential failure mode unique to CCs. While, for the most part, the polymer sheath of CCs acts to *improve* the corrosion resistance of conductors, in some cases the sheath is removed or pierced to expose or make contact to the bare conductor (e.g., at dead-end structures and connectors). Crevices may form at polymer sheath removal sites between the sheath and the conductor, and water ingress into these crevices may facilitate localized corrosion processes.

Exponent used three methods to evaluate the corrosion resistance of CCs relative to bare conductors; these tests are summarized in Table 13. These analyses probed the potential for water ingress and corrosion at the interface between the exposed conductor and the polymer sheath as well as further underneath the polymer sheath. First, water ingress testing probed how, and to what degree, liquids may enter and pass along CCs at stripped ends or connection points. Next, salt spray testing evaluated whether CCs showed accelerated corrosion relative to bare conductors under harsh environmental conditions. By artificially damaging some CCs at the stripped ends and at midspan sections, this testing evaluated whether polymer sheath damage may lead to localized corrosion acceleration. Finally, cyclic polarization testing characterized the localized corrosion resistance of CC stripped ends relative to bare conductors for both as-received samples and samples that were artificially aged in a highly aggressive environment.

Initial testing assessed the corrosion susceptibility of 17-kV ACSR and 17-kV copper CCs using all three test methods (water ingress, salt spray, and cyclic polarization) and two different stripping methods (manual stripping versus a dedicated Ripley WS5A end stripper tool). Corrosion susceptibility of the 22-kV AAC and 15-kV ACSR CCs was assessed using only water ingress and salt spray testing, as results from the cyclic polarization testing of the 17-kV CCs were not conclusive. In addition, the 22-kV AAC CC was limited to a single stripping method (using a dedicated Ripley WS64-U-EM tool), as different stripping methods were not observed to significantly affect the corrosion susceptibility of the 17-kV CCs. Finally, the 15-kV ACSR CC testing was primarily focused on the use of insulation-piercing connectors (IPCs) rather than stripping lengths of polymer sheath, as this is the implementation method reportedly used by SDG&E in the field. The 35-kV ACSR CC was not tested, as the underlying metal conductor is the same as in the 17-kV ACSR CC case.

Table 13. Detailed test matrix for evaluating corrosion resistance of CCs relative to bare conductors.

Test Method	Conductor Type	Stripping Method	Strip/Damage Type
Water Ingress	17 kV ACSR CC	Ripley ¹	End Strip
		Manual	End Strip
	17 kV Cu CC	Ripley ¹	End Strip
		Manual	End Strip
	22 kV AAC CC	Ripley ²	Midspan Strip
15 kV ACSR CC	-	IPC	
Salt Spray	17 kV ACSR CC	Ripley ¹	End Strip
			Midspan Damage
			Artificial Crevice
		Manual	End Strip
			Midspan Damage
			Artificial Crevice
	17 kV Cu CC	Ripley ¹	End Strip
		Manual	Midspan Damage
			End Strip
	17 kV Bare ACSR	-	-
	17 kV Bare Cu	-	-
	22 kV AAC CC	Ripley ²	End Strip
			Midspan Damage
			Artificial Crevice
22 kV Bare AAC		-	-
15 kV ACSR CC		-	IPC
15 kV Bare ACSR	Ripley ²	Midspan Damage	
15 kV Bare ACSR	-	-	
	Ripley ¹	End Strip	
		Artificial Crevice	
	Manual	End Strip	
		Artificial Crevice	
	Cyclic Polarization: (as-received and after 1 week immersion testing)	17 kV ACSR CC	Ripley ¹
Manual			Artificial Crevice
17 kV Cu CC		Ripley ¹	End Strip
		Manual	End Strip
17 kV Bare ACSR	-	-	
17 kV Bare Cu	-	-	

¹ Ripley WS5A End Stripper Tool

² Ripley WS64-U-EM Cable Stripper Tool

Different polymer sheath stripping techniques generate different sheath/conductor interfaces, as illustrated in Figure 26. For some samples, Exponent used a dedicated and assumed representative cable stripping tool (Ripley) to remove the sheath from the CCs. Although this tool easily removed the polymer sheath, it left a visible gap between the sheath and the conductor at the stripped interface (Figure 26a). The presence of such gaps may allow for water ingress and thus may enhance localized corrosion of the conductor. To assess differences, a “manual” stripping method was also investigated. This consisted of cutting into the polymer sheath with a razor blade and then manually removing it. This technique generally resulted in smaller gaps between the polymer sheath and the conductor but resulted in minor damage to the conductor at the stripped interface due to razor blade contact with the conductor strands (Figure 26b). Further, some variability in workmanship (i.e., damage) is expected to occur occasionally in the field during sheath removal and may affect the corrosion susceptibility of the conductor. To model an example of poor workmanship, Exponent induced “artificial crevices” at the stripped ends by cutting into the polymer sheath and removing a small area of the PE. Electrical tape was then applied to cover the cut-away area and form an occluded area at the sheath/conductor interface (Figure 26c). In addition, artificial damage on “midspan” areas of the conductor was used to mimic abrasion of CCs. A small area of the polymer sheath was cut away using a razor blade and the area was then left exposed during testing (Figure 26d). For the 15-kV ACSR CCs, IPCs installed on CCs (Figure 26e) were tested as received.

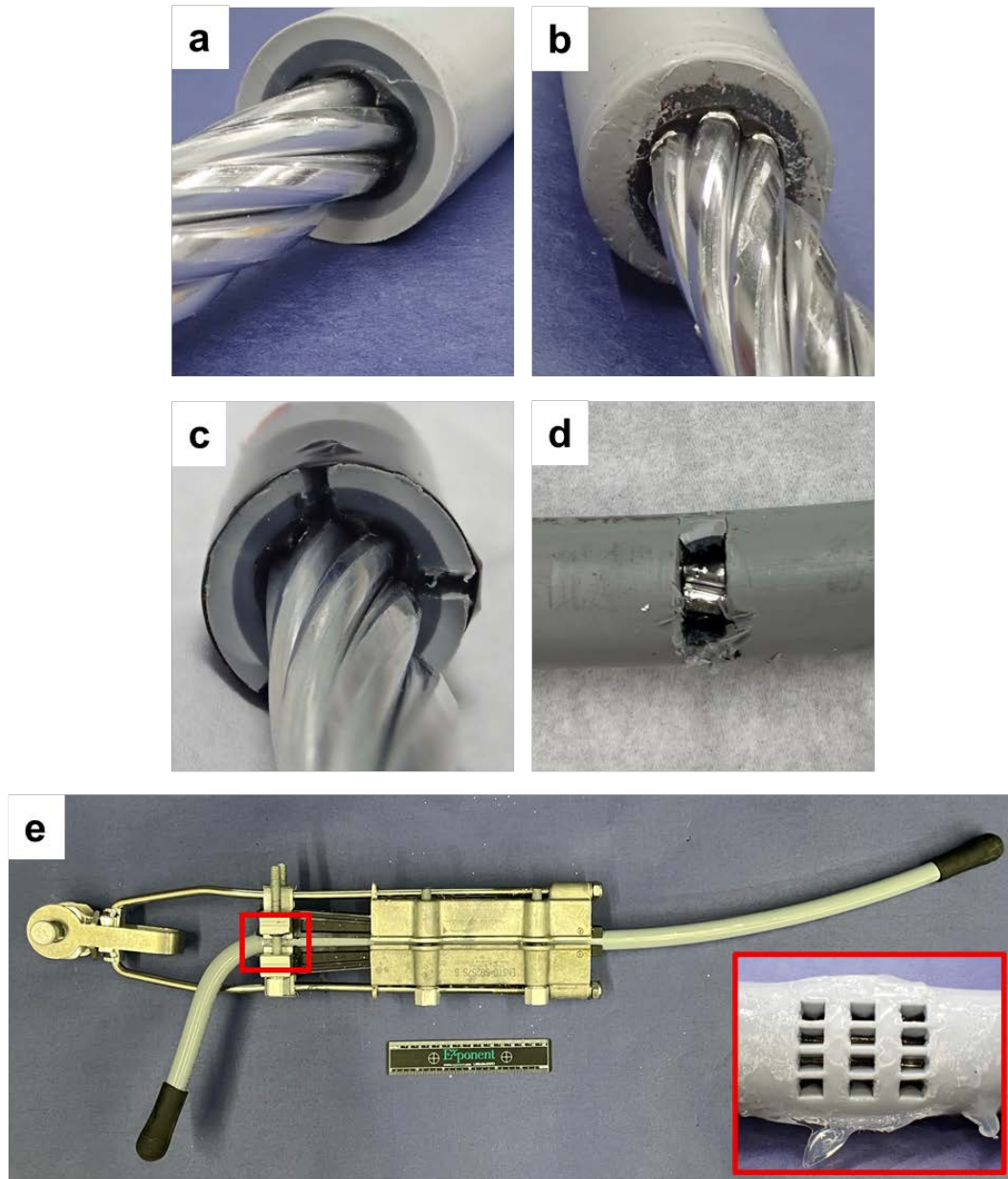


Figure 26. Representative images showing (a) Ripley and (b) manual stripping techniques and (c) creviced end (intended to mimic poor workmanship), (d) midspan artificial damage (to simulate abrasion), and (e) IPCs (inset shows pierced CC area after IPC is removed) used throughout testing.

Water Ingress Testing

Water ingress testing evaluated the ability of water to enter a CC at a stripped or exposed area and to percolate down the length of the conductor once inside.

Experimental Setup

Water ingress testing procedures were adapted from ANSI/ICEA T-31-610-2018 Section 4.²⁰ A schematic of the test setup is provided in Figure 27. For the 17-kV CCs, Exponent removed a ~2.5-inch section of the polymer sheath from one end of a length of CC. The remaining length was cut such that the covered section measured ~36 inches in length. Exponent tested six samples each of 17-kV ACSR CC and 17-kV copper CC. Of each of these six, three were stripped using the Ripley WS5A tool and three were stripped manually. The prepared conductors were then vertically mounted with the stripped end at the top. A watertight upper reservoir was attached such that the top of the reservoir was above the top of the stripped end and the bottom of the reservoir was below the bottom of the stripped end. Subsequently, a mixture of water and fluorescent dye was introduced to the reservoir such that the liquid level covered a portion of the stripped section, not including the bare conductor end. The far end of the conductor was monitored for leakage. If liquid was observed at the far end, the polymer sheath was removed, and the conductor and polymer sheath were visually inspected to identify the ingress pathway.

Similar testing was performed with the 22-kV AAC CCs and 15-kV ACSR CC; each of these conductor types was tested in duplicate. For the 22-kV AAC CC, the test procedure was similar to that used for the 17-kV CCs except that a ~2.5-inch section of the polymer sheath was removed using a Ripley tool from a midspan area near the end of the conductor wire. This method was used to prevent spreading of individual aluminum strands when cut at a free end, which could potentially introduce additional water ingress pathways. For the 15-kV ACSR CC, the entire IPC assembly was submerged in a container of water with the cable ends sticking out so they were isolated from liquid contact. The ends of the cable were monitored for liquid output. These tests were performed with pure water, as, in the event of liquid ingress, the longitudinal ingress pathway is expected to be similar to that observed with the 17-kV CCs.

The conditions in this test are far more aggressive than those encountered in the field (i.e., conductors in the field would not be mounted vertically and/or fully immersed in liquid, and resistive heating may reduce liquid ingress on live lines). However, these conditions were modeled after the ICEA T-31-610-2018 standard and conservatively identify potential ingress paths.

²⁰ ICEA T-31-610-2018 “Test Method for Conducting Longitudinal Water Penetration Resistance Tests on Blocked Conductors,” Insulated Cable Engineers Association, 2018.

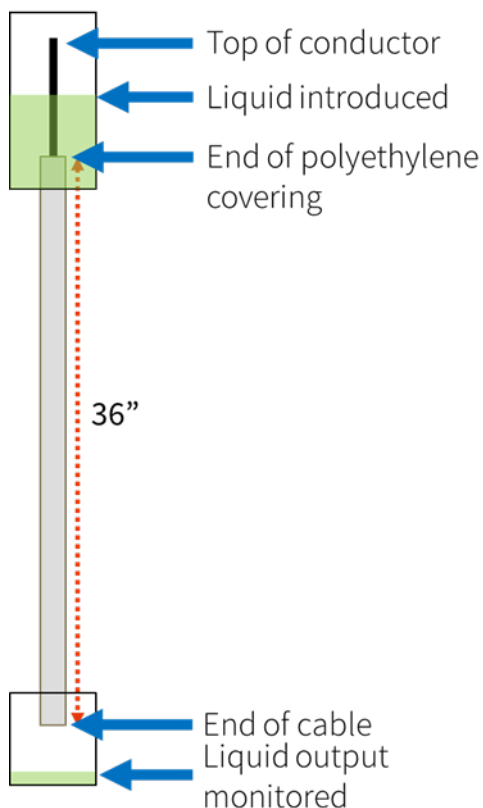


Figure 27. Schematic of water ingress test configuration. Liquid was introduced to the stripped end of a CC 36 inches in length, and the far end was monitored for liquid output.

Results

- Liquid easily passed through the length of the CCs without externally applied pressure for all CC types. Liquid ingress and flow seemed to occur primarily between the individual conductor strands, although some minor liquid flow was also observed between the conductor and the polymer sheath for 17-kV ACSR CCs.
- Although IPCs do not require stripping of the covering, liquid was still found to pass through the cover-piercing location to the metal conductor under full immersion.
- Liquid ingress did not appear to be significantly affected by the stripping method used.
- Although these conditions are extreme relative to what would be encountered during normal use conditions in the field, the results indicate that it is possible for liquid to enter beneath the polymer sheath of a CC and to traverse distances and possibly collect at low spots.

In all cases, liquid passed through the full sample length without externally applied pressure. Representative photographs of liquid ingress testing for 17-kV ACSR, 17-kV copper CCs, and 15-kV ACSR CCs with IPC hardware are presented in Figure 28, Figure 29, and Figure 30, respectively.

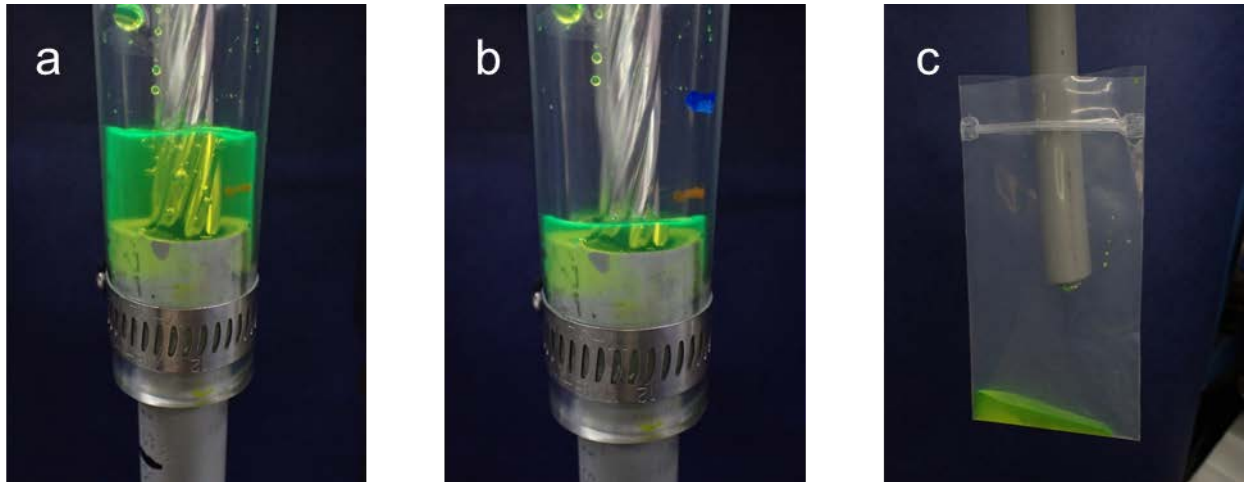


Figure 28. Representative photographs of liquid ingress testing performed on 17-kV ACSR CCs. (a) Liquid was introduced to the stripped end of a 17-kV ACSR CC at $t=0$. (b-c) After five minutes, the liquid level had dropped significantly at the stripped end (b), and liquid output was observed at the far end of the CC (c).

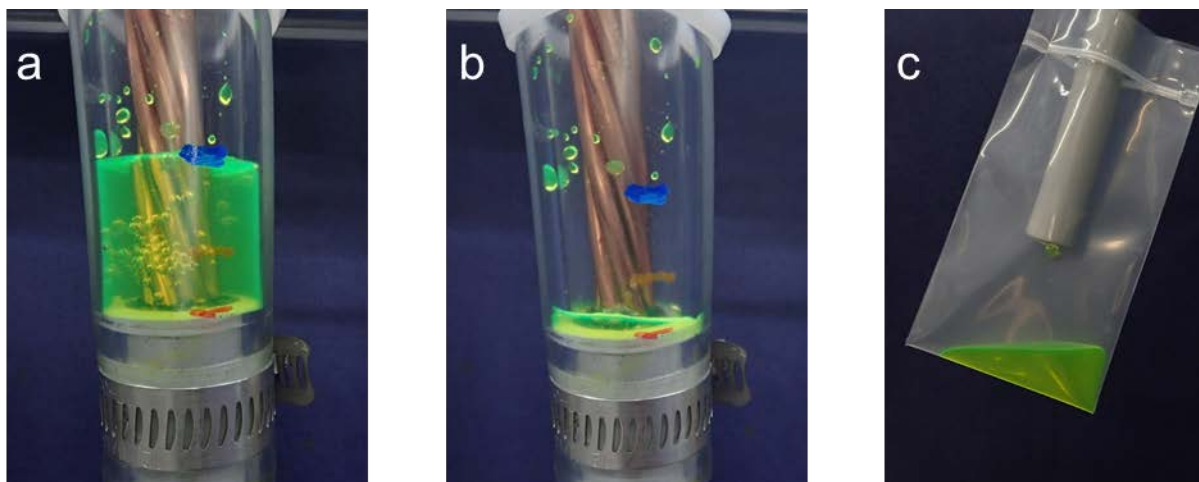


Figure 29. Representative photographs of liquid ingress testing performed on 17-kV copper CCs. (a) Liquid was introduced to the stripped end of a 17-kV copper CC at $t=0$. (b-c) After five minutes ($t=5$), the liquid level had dropped significantly at the stripped end (b), and liquid output was observed at the far end of the CC (c).

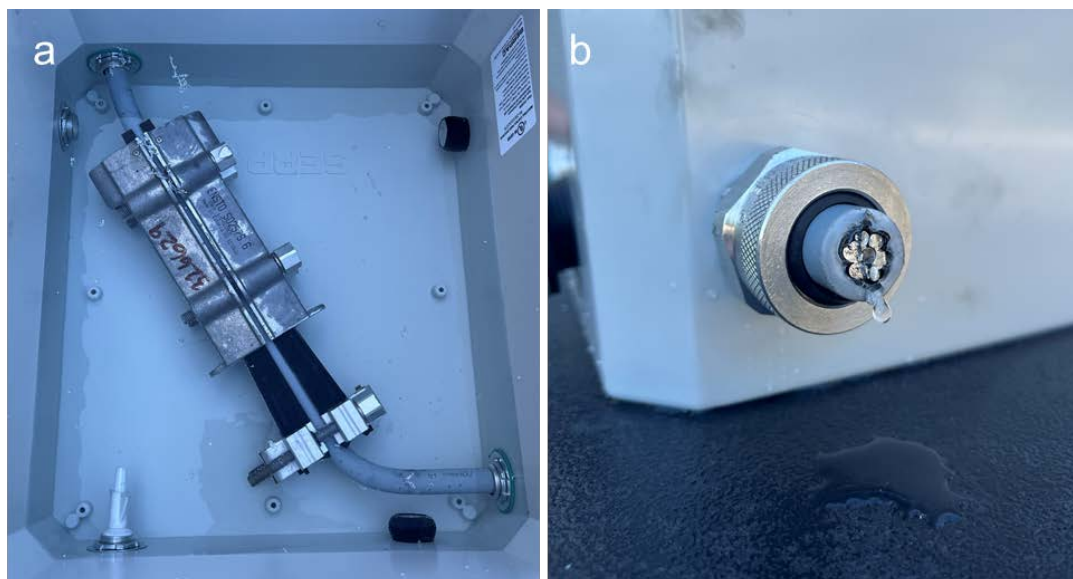


Figure 30. Representative photographs of liquid ingress testing performed on 15-kV ACSR CCs with IPC hardware. (a) The CC with IPC hardware was placed in a water reservoir with the cut ends outside of the reservoir. (b) Liquid output was observed at the cut ends outside of the reservoir.

Following testing of the 17-kV CCs, Exponent stripped and examined the conductors to determine the flow path. Figure 31 shows representative photographs of the flow paths in 17-kV ACSR and 17-kV copper CCs. In both cases, fluorescence was observed between individual strands and around the conductor core. All six 17-kV ACSR samples exhibited some evidence of flow on the stripped polymer sheath, while only one 17-kV copper conductor presented similar evidence. These results suggest that flow along the interface between the conductor

strands and polymer sheath may occur more readily in the ACSR CCs than in the copper CCs. However, further study would be required to better understand this observation. Figure 32 shows representative photographs of the flow paths on the polymer sheaths from 17-kV ACSR and copper CCs (Figure 32a, b, respectively). No clear differences in flow path or flow speed due to the stripping method (Ripley versus manual) were identified. The 22-kV AAC CCs and 15-kV ACSR CCs were not disassembled after testing, but in all samples tested liquid flow at the cable end was observed between the individual strands and around the conductor core.

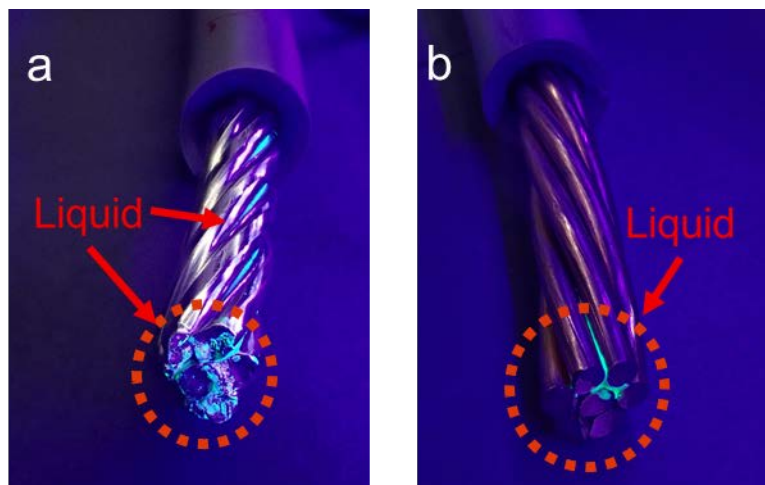


Figure 31. Representative photographs of (a) 17-kV ACSR and (b) 17-kV copper conductors after water ingress testing and sheath removal. Fluorescence was observed between the individual strands as well as around the core.

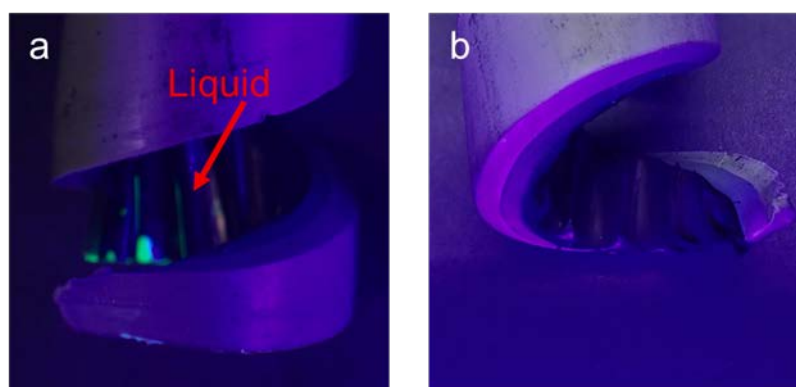


Figure 32. Representative photographs of polymer sheaths from (a) 17-kV ACSR and (b) 17-kV copper CCs after water ingress testing and sheath removal.

While these results indicate that liquid ingress may pose a risk for CCs, the conditions investigated present a far more extreme case than would likely be observed during actual operation. In addition to the extreme conditions (i.e., immersion of the stripped end and vertical mounting, full immersion of the IPC), this analysis neglects potential passive factors that may

reduce ingress (i.e., heating of the conductor improving evaporation and reducing crevice size due to thermal expansion) and active remediation methods (e.g., wildlife guards acting as rain shields). Nevertheless, this risk is worth considering, and appropriate mitigation measures may be warranted.

Salt Spray Testing

Salt spray testing was performed to evaluate the relative performance of bare conductors to CCs with stripped ends. This testing presents a highly aggressive environment containing both sodium chloride (NaCl) and sulfur dioxide (SO₂) fog to accelerate atmospheric corrosion over a short period of time. Although this environment is likely much more aggressive than what would be observed in the field, it does provide a means of comparing the relative corrosion performance of different types of conductor systems (bare versus CCs with exposed sites). This test is not designed to be representative of any specific duration of time in service. The test conditions were further exacerbated by introducing artificial crevices and/or localized damage (simulated midspan damage) to the polymer sheath to serve as positive controls.

Experimental Setup

Salt spray testing was performed using a salt spray chamber configured as shown in Figure 33. The tests were run in accordance with ASTM G85-19 Standard Practice for Modified Salt Spray (Fog) Testing using the conditions outlined in Annex 4.²¹ A standard 5 wt.% NaCl solution was used (5 parts NaCl and 95 parts H₂O by weight). The setup was arranged to prevent liquid pooling or dripping of one sample onto another. The salt fog was supplied continuously to the chamber, and SO₂ gas was introduced for one hour every six hours, as indicated in Figure 34. The salt fog and SO₂ were introduced via a large tube located centrally in the chamber. The samples were dispersed around the tube and were oriented approximately 60–75° off the vertical to mimic the orientation of overhead conductors under tension. The test chamber was held at 35° C ± 2° C, and the total exposure time was 168 hours (one week). These conditions simulate severe environmental conditions, which may be encountered only intermittently, if at all, in the field (i.e., very near the coastline or in the vicinity of heavy industry). At the end of the 168-hour exposure, the samples were rinsed with deionized water and allowed to dry for 24 hours. Approximately one week later, the samples were disassembled: the polymer sheath was stripped to expose regions that were covered during testing, and the conductors were disassembled into their constituent individual strands. The exposed conductor strands were further cleaned by rinsing under running tap water and cleaning with a soft brush. Samples were then visually inspected using an optical microscope, and tensile testing was performed on conductor strands to evaluate any reduction in strength due to corrosion.

²¹ ASTM G85-19 “Standard Practice for Modified Salt Spray (Fog) Testing,” American Society for Testing and Materials, 2019.

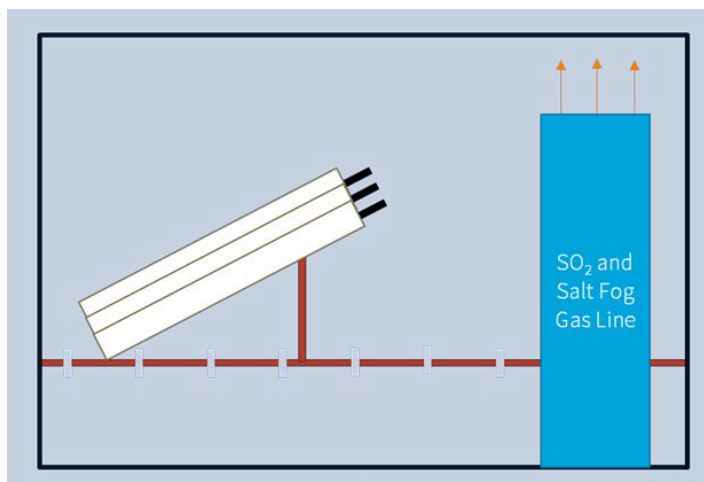


Figure 33. Schematic of salt spray testing apparatus. SO_2 and 5 wt.% salt fog were introduced through a central tube. Samples were arranged on a plastic platform with grid openings to prevent pooling of runoff. The samples were oriented approximately $60\text{--}75^\circ$ from vertical.

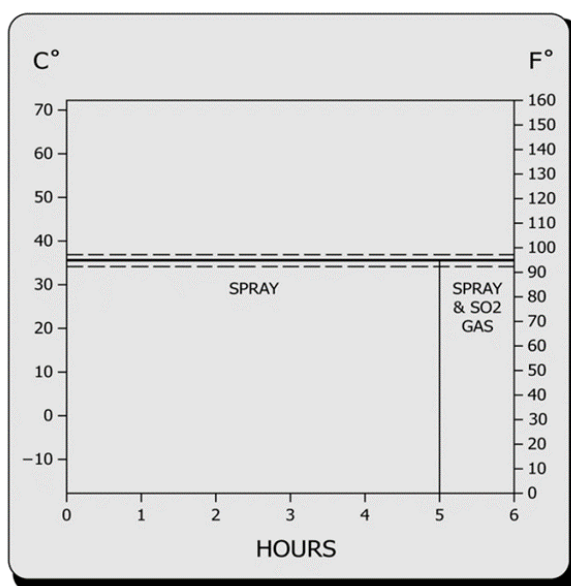


Figure 34. SO_2 /salt fog test conditions. The chamber was held at $35^\circ\text{C} \pm 2^\circ\text{C}$ and salt fog was introduced continually for 168 hours. SO_2 was introduced for one hour out of every six, as indicated. From ASTM G85-19: Standard Practice for Modified Salt Spray (Fog) Testing.²²

²² ASTM G85-19 “Standard Practice for Modified Salt Spray (Fog) Testing,” American Society for Testing and Materials, 2019.

Results

- Corrosion was observed on both bare conductors and on stripped CCs for 17-kV ACSR, 17-kV copper, and 22-kV AAC. Corrosion was observed on bare and CCs with midspan damage for 15-kV ACSR. Corrosion on CCs occurred both on regions that were exposed and on regions that were covered by the polymer sheath during testing.
- No corrosion was observed on 15-kV ACSR CCs with IPC hardware installed.
- Corrosion severity was variable, and in some tests the corrosion observed on regions beneath the polymer sheath was more severe than that observed on exposed, uncovered regions. Corrosion beneath the polymer sheath was observed to occur as far as 2–3 feet from the nearest exposed end. This distance also represents the maximum covered length used in these tests.
- For 17-kV ACSR conductors, corrosion occurred on both aluminum and galvanized steel strands. Similarly, corrosion was observed on both exterior and core strands for 17-kV copper conductors.
- For the 22-kV AAC conductors, corrosion primarily occurred on the outer aluminum strands.
- The stripping method and artificial crevicing at stripped ends did not appear to significantly affect the extent of corrosion on CCs. However, the presence of midspan damage did appear to result in corrosion that was more severe than that resulting from the stripped end.
- Salt spray testing was not observed to result in an appreciable change in the tensile strength of either copper conductor strands or ACSR steel core strands for the 17-kV and 15-kV conductors. A decrease in tensile strength was not observed for salt-spray-tested AAC CCs relative to either as-received or salt-spray-tested bare AAC conductors.
- Tensile testing on aluminum strands from salt spray tested ACSR CCs (without IPC hardware) showed a measurable difference in tensile strength relative to equivalent aluminum strands from both as-received bare conductors and bare conductors after salt spray testing. However, as this difference may be attributable to annealing of the conductor strands during the application of the polymer sheath, additional controls are needed to better elucidate the effect of corrosion on mechanical strength.
- Despite the measured decrease in strength of the aluminum strands from salt-sprayed ACSR CCs, the calculated overall conductor strength, which assumed six equivalent aluminum strands and a single steel strand, did not show a significant (> 10%) difference in ultimate tensile strength between salt-sprayed ACSR CCs (without IPC hardware) and either the as-received bare ACSR conductors or the bare ACSR conductors after salt spray testing.
- Tensile testing on aluminum strands from salt-sprayed ACSR CCs with IPC hardware showed a measurable decrease in tensile strength relative to equivalent aluminum strands from as-received bare conductors. This decrease is due to mechanical damage to the strands from IPC installation.
- Although Exponent expects that the testing conditions investigated here are much more extreme than what would typically be encountered in the field, the results indicate that it is possible for corrosion to occur beneath the polymer sheath of CCs near stripped ends.

Visual Characterization

17-kV ACSR Conductors (Stripped)—Aluminum Strands

Individual aluminum and steel strands from ACSR conductors were targeted for analysis. As the aluminum strands are in direct contact with the polymer sheath on the ACSR CCs and the galvanized steel core, they may be prone to crevice corrosion. Figure 35 presents representative optical microscopy images from salt-spray-tested aluminum conductor strands taken from bare 17-kV ACSR conductors (Figure 35a) and 17-kV ACSR CCs (Figure 35b-d). Both the bare and covered 17-kV ACSR conductors showed evidence of shallow localized corrosion (pitting) following salt spray testing. Given the aggressive nature of the test environment, the corrosion observed on both the bare conductors and the CCs was relatively minor. However, the CCs showed evidence of pitting both on areas that were exposed during testing and on areas that were underneath the polymer sheath. The pitting underneath the covered regions also appeared, in some cases, to be more severe (qualitatively) than the pitting observed on the bare conductor. There did not appear to be a clear correlation between extent of corrosion damage and stripping method. The most severe pitting was observed on the covered regions adjacent to midspan damage, as shown in Figure 35d. Exponent observed evidence of corrosion at the midpoint between the stripped end and the cut end, at least 10–15 cm from the nearest exposed metal (either the stripped end or the cut end). Salt spray testing thus demonstrated that corrosion can occur on the 17-kV ACSR CC at least 10–15 cm from the nearest exposed metal. Additional studies with longer sample lengths would be needed to conclusively determine the maximal longitudinal distance beneath the polymer sheath that corrosion may occur away from exposed metal.

As it is expected that damage to the polymer sheath may occur during stripping in the field, this testing additionally sought to determine if the presence of large, artificially induced crevices at the stripped ends would lead to more severe localized corrosion. However, unlike in the midspan damage case, the corrosion appears relatively similar between the artificially creviced and cleanly stripped samples (not shown). This observation suggests that large or intentionally introduced crevices are not a requirement for corrosion to occur beneath the polymer sheath.

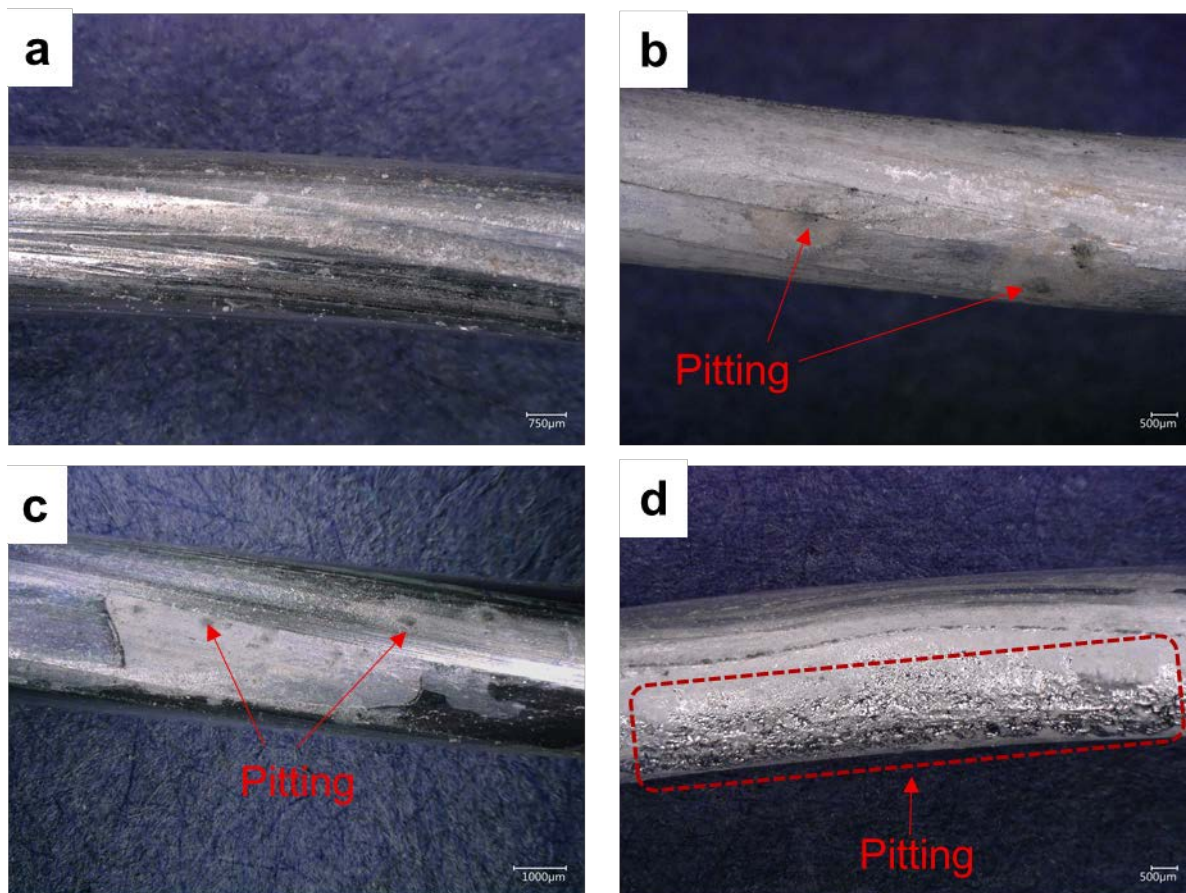


Figure 35. Representative optical microscopy images of aluminum conductor strands from (a) a bare 17-kV ACSR conductor and (b-d) covered regions of 17-kV ACSR CCs after salt spray testing. The polymer sheath was stripped from CCs samples prior to testing (b) using a Ripley tool or (c) manually; in addition to being stripped at one end, (d) was damaged along a midspan section. For CCs, pitting corrosion was observed underneath the polymer sheath regardless of the stripping method. The pitting associated with the midspan damage appeared to be the most severe of the four cases investigated (d).

17-kV ACSR Conductors (Stripped)—Steel Core

Galvanized steel core strands from both covered and bare 17-kV ACSR conductors were also inspected. Figure 36 presents a comparison of the galvanized steel core strand from a bare 17-kV ACSR conductor (Figure 36a) and the galvanized steel core strands from underneath the polymer sheaths of 17-kV ACSR CCs (Figure 36b-d). As shown in Figure 36b, a significant amount of an insoluble, white zinc-based corrosion product developed on the Ripley-stripped sample during testing. Although the differences from the bare conductor are more subtle, the manual stripping method also showed evidence of zinc corrosion (Figure 36c). The most severe corrosion was observed at the midspan damage site (Figure 36d). Localized areas of rust (steel

corrosion product) were occasionally observed, as shown in the inset to Figure 36d; these areas suggest potential penetration of the zinc layer.

In general, it was observed that the extent of corrosion appeared to be more severe for 17-kV ACSR CCs relative to the bare 17-kV ACSR conductors. This may be the result of longer duration of water entrapment underneath the polymer sheath in the CCs as opposed to bare conductors from which water may be able to drip off. Water may also be able to pool and concentrate in areas between the conductor strands and polymer sheath. Furthermore, when the exteriors of the samples were rinsed with deionized water post-testing, it is possible that only some of the liquid would have been removed from underneath the covered sections. If this were the case, the portions of the conductors underneath the polymer sheath would continue to undergo corrosion until the samples were fully disassembled and recleaned. This suggests that water entrapment and the concentration of corrosive species underneath the polymer sheath may present a potential issue in the field.

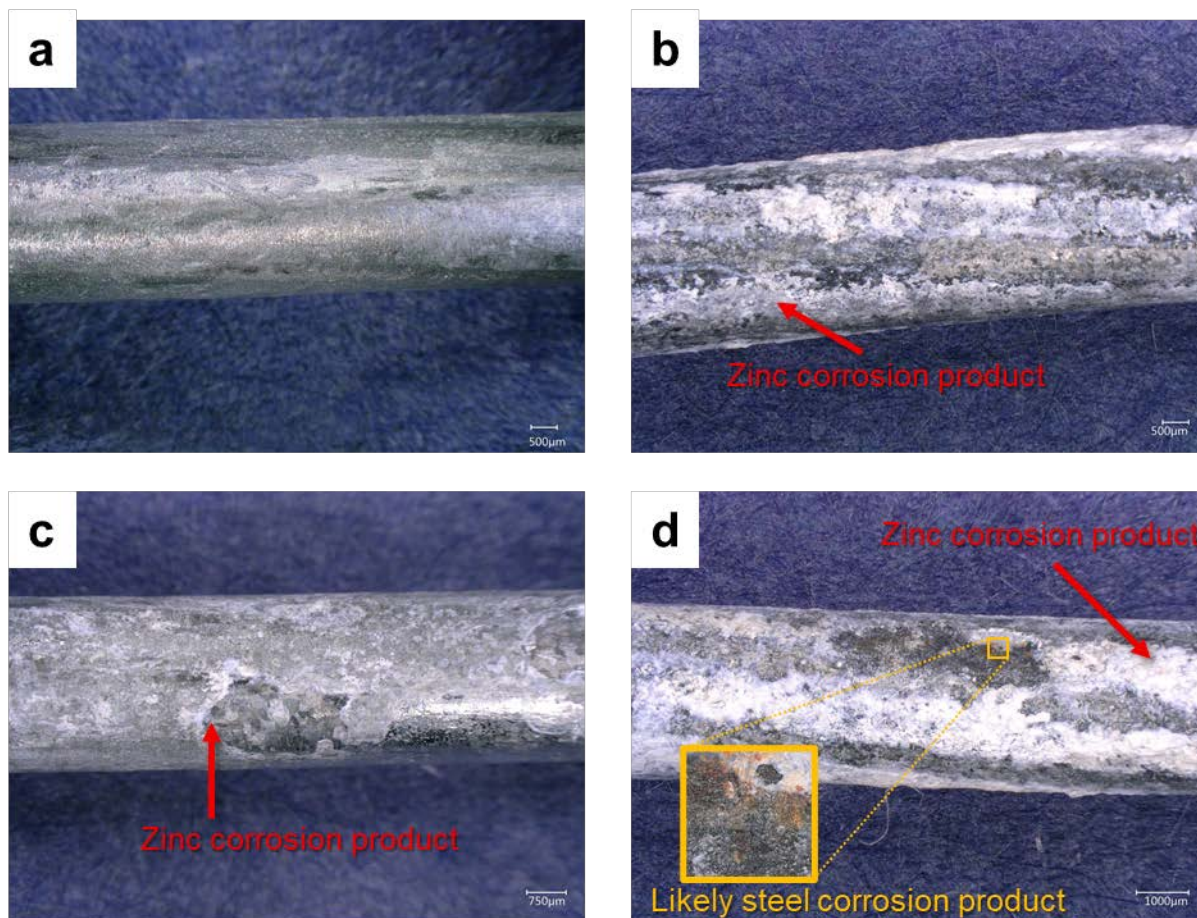


Figure 36. Representative optical microscopy images of galvanized steel conductor strands from (a) a bare 17-kV ACSR conductor and (b-d) covered regions of 17-kV ACSR CCs after salt spray testing. The polymer sheath was stripped from CCs samples prior to testing (b) using a Ripley tool or (c) manually; in addition to being stripped at one end, (d) was damaged along a midspan section.

15-kV ACSR Conductors with IPCs—Aluminum Strands

Bare and covered 15-kV ACSR conductors were analyzed after salt spray testing, as well as 15-kV ACSR CCs that had IPC hardware installed prior to salt spray testing. Figure 37 shows representative optical microscopy images from exterior aluminum strands of salt-spray-tested 15-kV ACSR conductors. The exterior strand from the bare 15-kV ACSR conductors (Figure 37a) showed some evidence of both uniform corrosion and pitting, as well as some general damage that was present prior to salt spray testing. No corrosion was observed on the exterior aluminum strands from the 15-kV ACSR CC with IPC hardware (Figure 37b). Some mechanical damage was observed where the IPC connector contacted the outer aluminum strands, which was a result of normal installation and was unrelated to the salt spray testing. Evidence of shallow localized corrosion was observed on aluminum strands of 15-kV ACSR CCs that had midspan damage, i.e., away from the IPC location (Figure 37c). This corrosion

occurred on regions under the polymer sheath during salt spray testing and appeared qualitatively similar to that observed on the bare conductor.

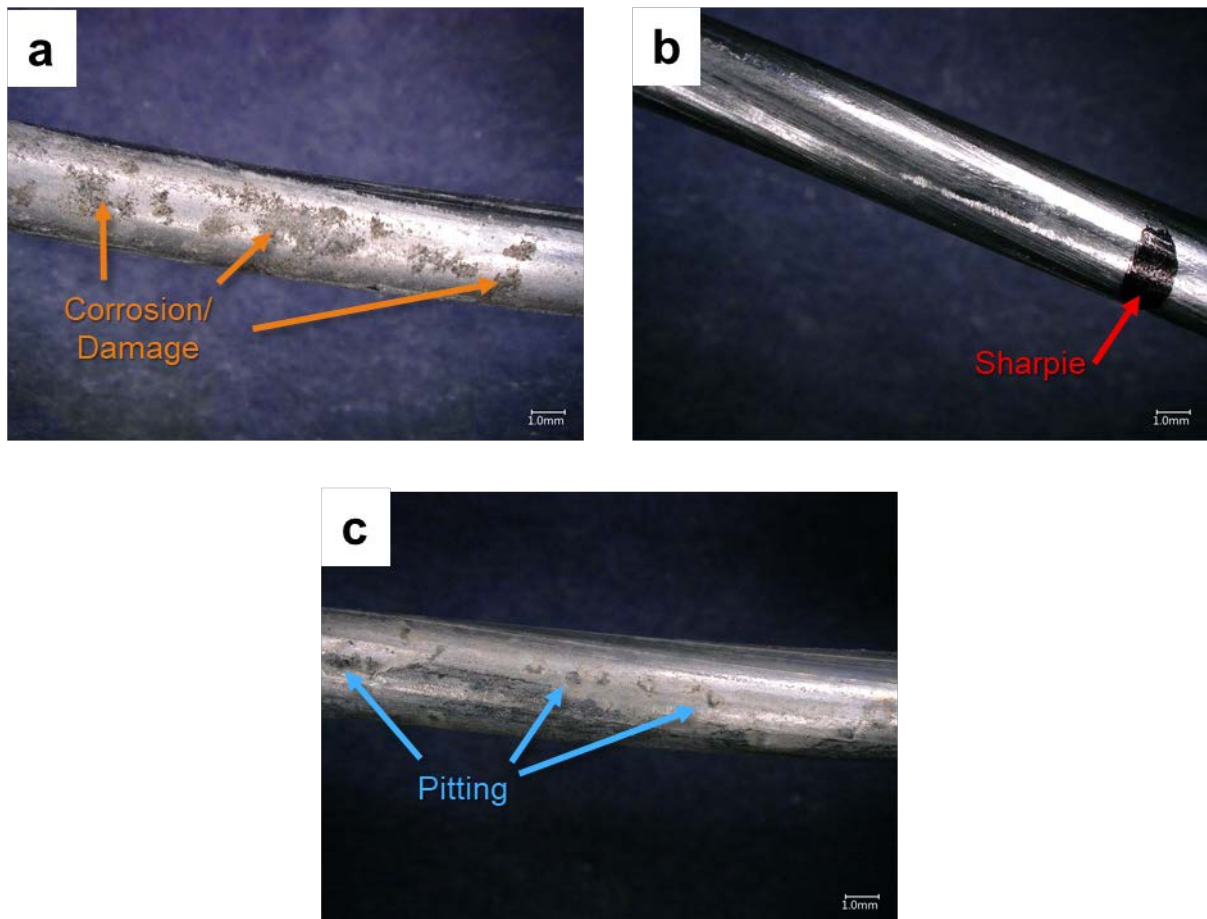


Figure 37. Representative optical microscopy images of aluminum conductor strands from a salt-spray-tested (a) bare 15-kV ACSR conductor, (b) 15-kV ACSR CC with IPC hardware, and (c) 15-kV ACSR CC with midspan damage. The areas in (b) and (c) were underneath the polymer sheath during salt spray testing.

15-kV ACSR Conductors with IPCs—Steel Core

The steel core strands from bare, covered, and IPC-covered 15-kV ACSR conductors were also inspected after salt spray testing. Figure 38 presents representative optical microscopy images from interior steel strands of salt-spray-tested 15-kV ACSR conductors. The core steel strands from the bare 15-kV ACSR conductors (Figure 38a) showed some evidence of minor corrosion and/or damage. No corrosion was observed on the core steel strands of the 15-kV ACSR CCs with IPC hardware (Figure 38b). Evidence of corrosion, including the presence of insoluble, white, zinc-based corrosion product, was observed on the core steel strands from the 15-kV ACSR CCs that had midspan damage (Figure 38c).

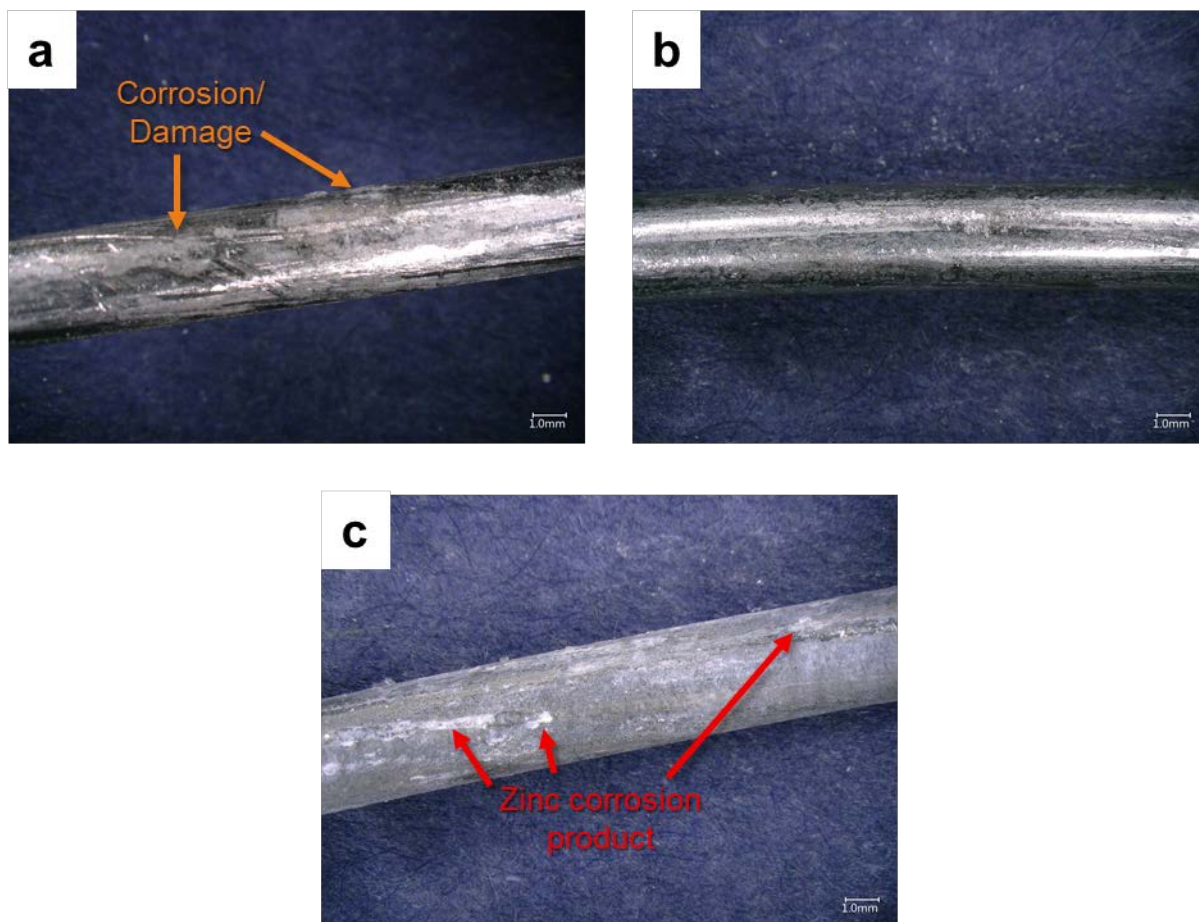


Figure 38. Representative optical microscopy images of steel conductor strands from a salt-spray-tested (a) bare 15-kV ACSR conductor, (b) 15-kV ACSR CC with IPC hardware, and (c) 15-kV ACSR CC with midspan damage. The areas in (b) and (c) were underneath the polymer sheath during salt spray testing.

17-kV Copper Conductors—Outer Strands

Individual strands from the 17-kV copper conductors, both bare and covered, were separated for targeted analysis. Figure 39 presents representative optical microscopy images from exterior strands of salt-spray-tested 17-kV copper conductors. The exterior strand from the bare copper conductor (Figure 39a) showed some evidence of both uniform corrosion and pitting. The corrosion observed on the exposed regions of CCs (Figure 39b-c) appeared similar to the corrosion observed on the bare conductor (Figure 39a). Note that the black spots observed in Figure 39b-d are marks added by Exponent to track the edge of the covered area. Additionally, it was observed that, in some cases, the black layer from the polymer sheath could not be cleanly removed from the copper conductors. This phenomenon was observed on as-received copper CCs and thus is likely not due to salt spray testing itself. Evidence of more severe corrosion and accumulation of corrosion product was observed on the sample with midspan damage (Figure 39d). However, because this likely occurs less frequently in the field than the others (i.e., accidental damage is likely less frequent than intentional sheath removal), this result should be considered an extreme case.

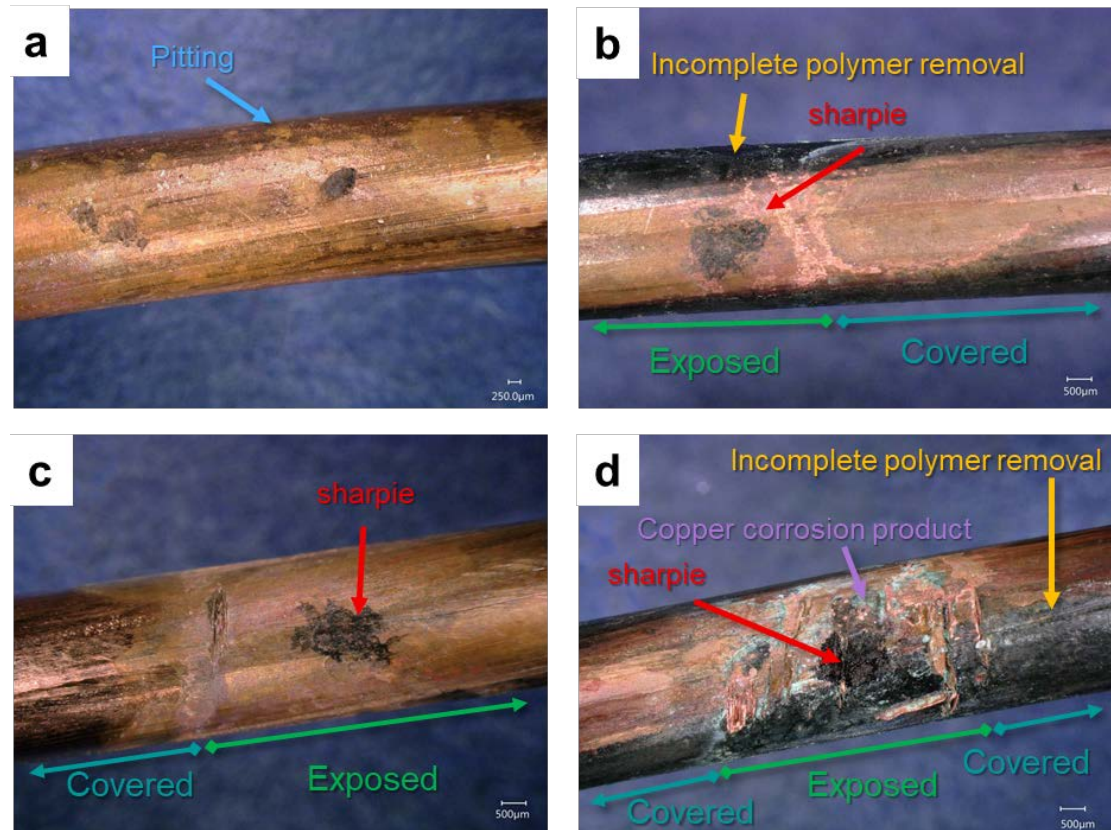


Figure 39. Representative optical microscopy images of exterior strands from a salt-spray-tested (a) bare 17-kV copper conductor, (b) Ripley-stripped 17-kV copper CC, (c) manually stripped 17-kV copper CC, and (d) 17-kV copper CC with midspan damage. The areas in (b-d) show the interfacial area between covered regions and exposed regions as indicated. The CCs showed evidence of corrosion underneath the polymer sheath (b-c) for both Ripley-stripped CC (b) and manually stripped CC (c). The midspan damage region appeared to have the most extensive corrosion of the four sample types (d).

17-kV Copper Conductors—Core Strands

The extent of corrosion on the core strands was also evaluated for salt-spray-tested 17-kV copper conductors, as shown in Figure 40. The core strand from the bare 17-kV copper conductor (Figure 40a) showed some evidence of both uniform corrosion and pitting. The localized corrosion observed on core strands from covered regions of 17-kV copper CCs appeared more severe than that observed on core strands from the bare conductor (Figure 40b-c). Additionally, evidence of localized corrosion was identified at the midpoint of the covered regions of these samples, at least 10–15 cm from the nearest exposed metal (either the stripped end or the cut end). Thus, these experiments indicate that corrosion can occur at least 10–15 cm from a stripped end, although additional studies with longer covered sample lengths would be needed to determine the maximal longitudinal distance beneath the polymer sheath that corrosion may occur away from exposed metal.

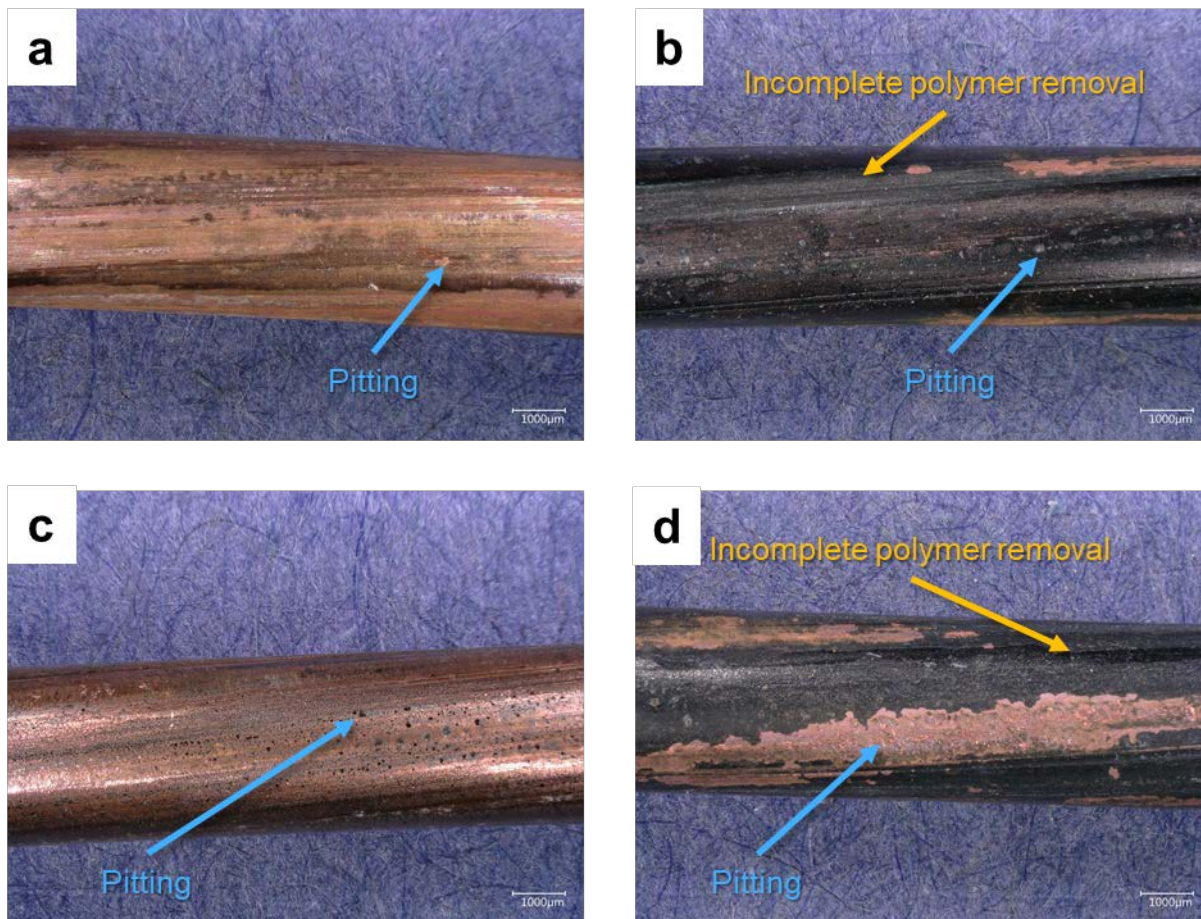


Figure 40. Representative optical microscopy images of core strands from a salt-spray-tested (a) bare 17-kV copper conductor, (b) Ripley-stripped 17-kV copper CC, (c) manually stripped 17-kV copper CC, and (d) 17-kV copper CC with midspan damage. The areas in (b-d) were underneath the polymer sheath during salt spray testing.

22-kV AAC Conductors

Bare and covered 22-kV AAC conductors were analyzed after salt spray testing. Figure 41 presents representative optical microscopy images of salt-spray-tested 22-kV AAC conductors. The images shown are taken prior to disassembly and show the outer strands of the conductor bundles; no corrosion was observed on the interior conductor strands following disassembly. The exterior strands from the bare AAC conductors (Figure 41a) showed minimal evidence of corrosion. Evidence of shallow localized corrosion (pitting) was observed on 22-kV AAC CCs (Figure 41b,c). This corrosion occurred on regions that were underneath the polymer sheath during salt spray testing and appeared qualitatively more severe than that observed on the bare conductor. There did not appear to be a significant difference in the severity of corrosion observed on CCs that had the ends of the polymer sheath removed versus those that had midspan damage. Evidence of corrosion was observed at the midpoint between the stripped end and the cut end, at least 1.5 feet from the nearest exposed metal.

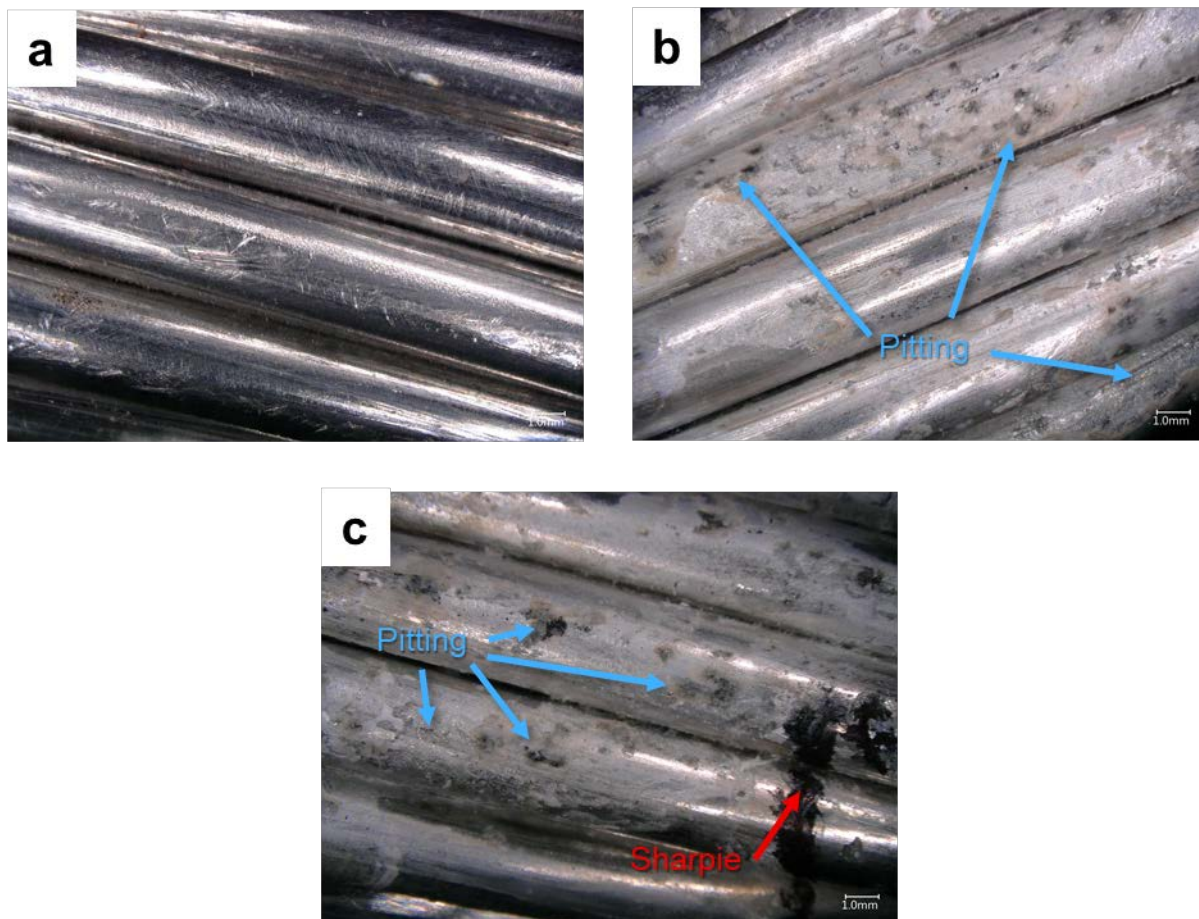


Figure 41. Representative optical microscopy images from a salt-spray-tested (a) bare 22-kV AAC conductor, (b) Ripley-stripped 22-kV AAC CC, and (c) 22-kV AAC CC with midspan damage. The areas in (b) and (c) were underneath the polymer sheath during salt spray testing. The optical microscopy images shown were taken of the entire conductor cable prior to disassembly and show multiple outer strands. No corrosion was observed on the inner strands.

Remaining Strength

Following salt spray exposure, Exponent performed tensile testing on a subset of samples to identify any changes in mechanical strength of the conductors using a 5982 Instron universal testing machine (UTM) equipped with a 100-kN load cell and an Instron AVE 2 non-contact video extensometer. To be consistent with prior conductor testing methodologies,^{23,24} individual conductor strands were tested rather than the full conductors. The conductor strands were pulled with a displacement rate of 5 mm/min. Tensile specimens generally have reduced cross-sectional areas to induce failure in between the grips (in the gauge section). However, as the

²³ Lequien, F., et al. "Characterization of an aluminum conductor steel reinforced (ACSR) after 60 years of operation." *Engineering Failure Analysis* 120 (2021): 105039.

²⁴ Refsnæs, S., Magnusson N., Ulleberg T. "Laboratory corrosion tests on overhead line conductors with bird protection systems." *Int. Trans. Electr. Energ. Syst.* 24(2014): 1185.

goal of this work was to assess differences in individual conductor strands arising from salt spray testing, machining the samples was not possible. Thus, the ends of the conductor strand were wrapped with aluminum foil to reduce the likelihood of failure at the grips. Figure 42 presents a representative sample with aluminum foil wrapped ends. Note that the aluminum foil wrapping was found to be less effective for copper samples.

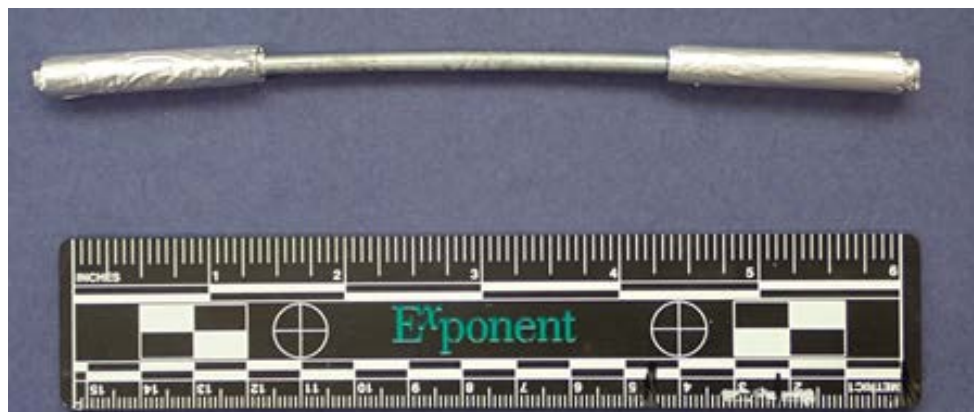


Figure 42. Representative photograph of a tensile specimen with aluminum foil wrapped ends. The aluminum foil reduces the likelihood of failure outside the gauge length.

17-kV ACSR Conductors (Stripped)

Figure 43 presents engineering stress-strain curves for aluminum strands (Figure 43a) and steel strands (Figure 43b) from 17-kV ACSR conductors. In these plots, sample IDs 316133, 316134, and 316139 are from salt-spray-tested CCs, and sample ID 316175 is a salt-spray-tested bare conductor. The as-received sample was a bare conductor that was not subjected to salt spray testing. The salt-spray-tested aluminum strands from CCs had lower tensile strengths than both the salt-spray-tested and as-received bare aluminum conductor strands by approximately 16–19%. However, the high-temperature processing of the polymer sheath likely leads to some annealing (and thus strength loss) of the aluminum conductor strands in CCs. Thus, understanding the degree of strength loss (if any) attributable to corrosion of these strands would require additional testing on aluminum strands from as-received 17-kV ACSR CCs. Both bare and covered salt-spray-tested steel strands showed higher ultimate tensile strengths than the as-received bare conductor. Thus, based on the limited tests conducted, changes to the steel strand were considered insignificant. It should be noted that a limited number of tests were performed to characterize strength loss after exposure to a corrosive environment. Should a greater level of statistical confidence be desired, more tests would be recommended.

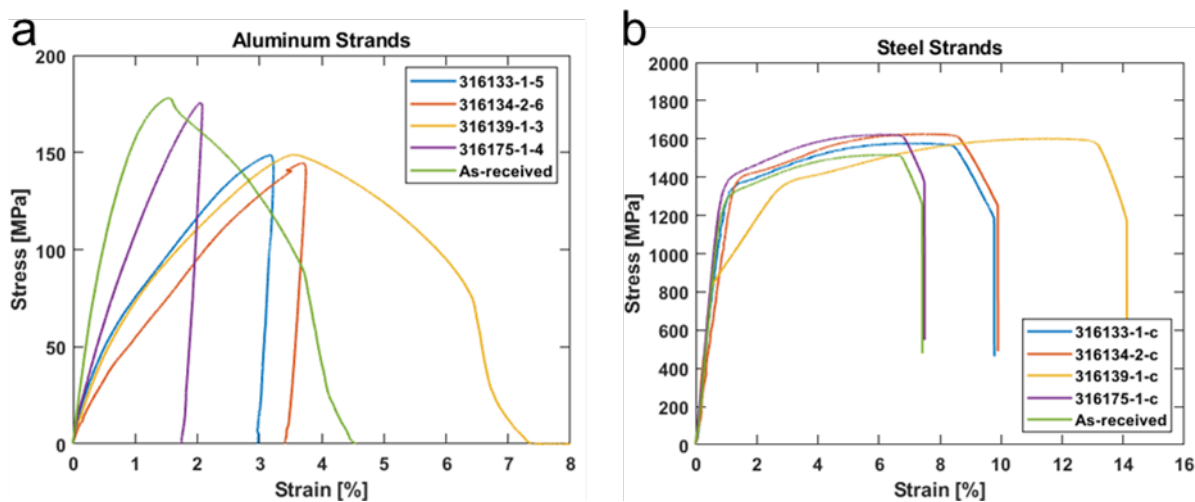


Figure 43. Engineering stress-strain curves for salt-spray-tested (a) aluminum and (b) steel strands from covered and bare 17-kV ACSR conductors. Sample IDs starting with 316133, 316134, and 316139 are from salt-spray-tested CCs. Sample IDs starting with 316175 are from a salt-spray-tested bare conductor. The as-received sample is also a bare conductor.

Table 14 summarizes the tensile strength results for salt-spray-tested and as-received 17-kV ACSR conductors. All samples with a sample ID number underwent salt spray testing. Three out of the four salt-spray-tested aluminum strands fractured outside the gauge length. This effect, coupled with the unquantified impacts of annealing expected during CC manufacturing, prevents firm conclusions from being drawn regarding the strength loss due to corrosion. Although grip failure in selected samples may hinder the ability to understand the maximum strength, the tested strands must be at least as strong as the load at grip failure. The salt spray testing does not appear to have had a significant impact on the steel strand strength. These results are consistent with the optical microscopy results that suggest widespread attack of the zinc galvanizing layer but very little attack of the underlying steel.

Table 14. Tensile strengths for single strands of 17-kV ACSR conductors. Samples listed with a sample ID had undergone salt spray testing prior to tensile testing. Samples denoted with * fractured outside the gauge length.

Sample ID	Strand Material	Sample Type	Tensile Strength [MPa]
316133-1-5	Aluminum	CC Ripley	148.62*
316134-2-6	Aluminum	CC Ripley Midspan	144.55*
316139-1-4	Aluminum	CC Manual Creviced	148.84
316175-1-4	Aluminum	Bare	175.61*
As-received	Aluminum	Bare	178.05
316133-1-c	Galvanized Steel	CC Ripley	1576.38
316134-2-c	Galvanized Steel	CC Ripley Midspan	1624.70
316139-1-c	Galvanized Steel	CC Manual Creviced	1600.70
316175-1-c	Galvanized Steel	Bare	1621.01
As-received	Galvanized Steel	Bare	1515.66

Lequien et al. report that the ultimate tensile strength (UTS) for ACSR conductors can be calculated using the following equation:²⁵

$$UTS_{ACSR} = \sum_{Al\ strands} [A_{Al} \times TS_{Al}] + \sum_{Steel\ Strands} [A_{steel} \times \sigma_{steel}(TE_{steel} = TUE_{Al})]$$

where UTS_{ACSR} is the ultimate tensile strength for the ACSR conductor (reported in the literature as a load in kN), A_{Al} and A_{steel} are the nominal cross-sectional areas for the aluminum and steel strands, respectively, and TS_{Al} is the measured tensile strength (in MPa) from Table 14 for the aluminum strands. Because the total elongation of the steel strands was much larger than the total uniform elongation of the aluminum strands (not shown), the aluminum strands should break first; thus, the final term $\sigma_{steel}(TE_{steel} = TUE_{Al})$ describes the steel stress σ_{steel} at the total elongation of the steel (TE_{steel}) corresponding to the total uniform elongation of the aluminum (TUE_{Al}).

Table 15 presents the calculated ultimate tensile strengths (in kN) for 17-kV ACSR conductors. By this method, the calculated ultimate tensile strength losses of salt-spray-tested 17-kV ACSR CCs are 2–7% relative to as-received and salt-spray-tested bare 17-kV ACSR conductors. Nevertheless, as noted previously, some of the calculated strength loss may be attributed to annealing during manufacturing, making it difficult to draw firm conclusions on the strength loss due to corrosion.

²⁵ Lequien, F., et al. "Characterization of an aluminum conductor steel reinforced (ACSR) after 60 years of operation." *Engineering Failure Analysis* 120 (2021): 105039.

Table 15. Calculated ultimate tensile strengths for 17-kV ACSR conductors. Samples listed with a sample ID had undergone salt spray testing prior to tensile testing.

Conductor	Conductor Type	Ultimate Tensile Strength [kN]
316133-1	CC Ripley	21.61
316134-2	CC Ripley Midspan	21.26
316139-1	CC Manual Creviced	20.55
316175-1	Bare	22.21
As-received	Bare	22.10

15-kV ACSR Conductors with IPCs

Tensile testing was performed on salt-spray-tested 15-kV ACSR conductors. Figure 44 presents engineering stress-strain curves for aluminum strands (Figure 44a) and steel strands (Figure 44b) from 15-kV ACSR conductors. Aluminum and steel strands from salt-spray-tested CCs with IPC hardware installed (Sample IDs: 326622 and 332625), CCs with midspan damage (Sample IDs: 332916 and 332917), and bare conductors (Sample IDs: 332932 and 332933) were tensile tested, as well as aluminum and steel strands from an as-received bare conductor that was not subjected to salt spray testing.

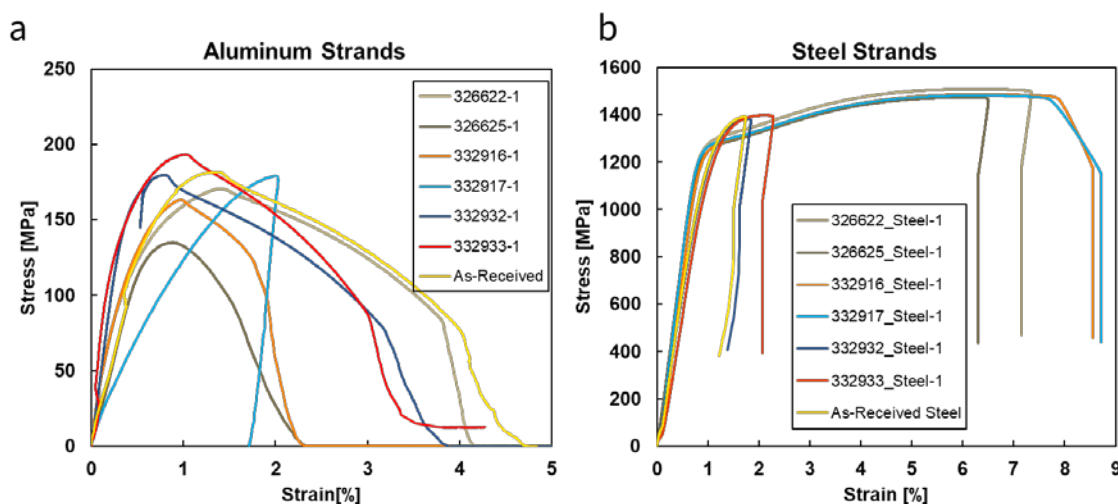


Figure 44. Engineering stress-strain curves for salt-spray-tested (a) aluminum and (b) steel strands from covered and bare 15-kV ACSR conductors. Sample IDs starting with 326622 and 332625 are from salt-spray-tested CCs with IPC hardware. Sample IDs starting with 332916 and 332917 are from salt-spray-tested CCs with midspan damage. Sample IDs starting with 332932 and 332933 are from a salt-spray-tested bare conductor. The as-received sample is also a bare conductor.

Table 16 summarizes the tensile strength results for individual aluminum and steel strands for salt-spray-tested and as-received 15-kV ACSR conductors as well as the calculated ultimate

tensile strengths (in kN) for these conductors. The ultimate tensile strength calculations were similar to those used for the 17-kV ACSR conductors discussed above. The lowest calculated ultimate tensile strength was for a salt-spray-tested ACSR CC with IPC hardware (326625-1), which showed a ~17% decrease in ultimate tensile strength compared to a bare, as-received conductor that did not undergo salt spray testing. The tensile strength of the aluminum strand for this sample was significantly lower than the other aluminum strands tested, likely due to the mechanical damage caused by IPC hardware installation, as shown in Figure 45. The lack of corrosion observed on the IPC hardware samples also supports the notion that the decrease in tensile strength is a result of mechanical damage to the conductor by the IPC installation rather than a result of corrosion of the conductor material. These results suggest that ACSR CCs with IPC hardware may have a measurable decrease in conductor strength relative to bare conductors, likely due to mechanical damage caused by the IPC installation.

Salt-spray-tested 15-kV ACSR CCs with midspan damage had ultimate tensile strength losses of ~1–9% compared to bare, as-received conductors that did not undergo salt spray testing. The ultimate tensile strength losses for salt-spray-tested bare conductors relative to bare, as-received conductors that did not undergo salt spray testing were ~4–14%. These results suggest that there may be some decrease in ultimate tensile strength for 15-kV ACSR CCs after salt spray testing, but the strength loss is not markedly different from bare conductors tested under the same conditions.

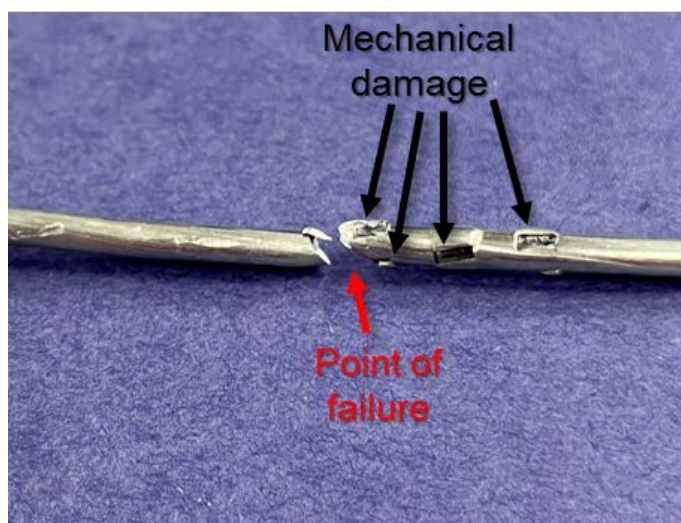


Figure 45. Photograph of a single aluminum strand from a 15-kV ACSR CC with IPC hardware after salt spray exposure and tensile testing. The mechanical damage was caused by the IPC hardware and was unrelated to either the salt spray testing or the tensile testing.

Table 16. Tensile strengths for single strands of 15-kV ACSR conductors and calculated ultimate tensile strengths. Samples listed with a sample ID had undergone salt spray testing prior to tensile testing. Samples denoted with * fractured outside the gauge length.

Sample ID	Sample Type	Aluminum Strand Tensile Strength [MPa]	Steel Strand Tensile Strength [MPa]	Ultimate Tensile Strength [kN]
326622-1	ACSR CC IPC	170.6	1507.9*	20.9
326625-1	ACSR CC IPC	134.9	1473.6*	18.1
332916-1	ACSR CC Midspan	163.3	1485.7	19.8
332917-1	ACSR CC Midspan	179.1*	1481.6	21.7
332932-1	ACSR Bare	179.7	1384.0*	18.7
332933-1	ACSR Bare	193.4	1397.7*	20.4
As-Received	ACSR Bare	181.6	1392.3*	21.9

17-kV Copper Conductors

Exponent also performed tensile testing on the salt-spray-tested 17-kV copper conductors; Exponent understands through discussions with SCE that CC installations in coastal areas will utilize copper conductors. Figure 46 presents the engineering stress-strain curves for salt-spray-tested CCs (Sample IDs 316068-2-5, 316068-1-2, and 316071-1-2) and bare conductors (Sample ID 316081-1-3). The curve for an as-received bare conductor that was not subjected to salt spray testing is also presented.

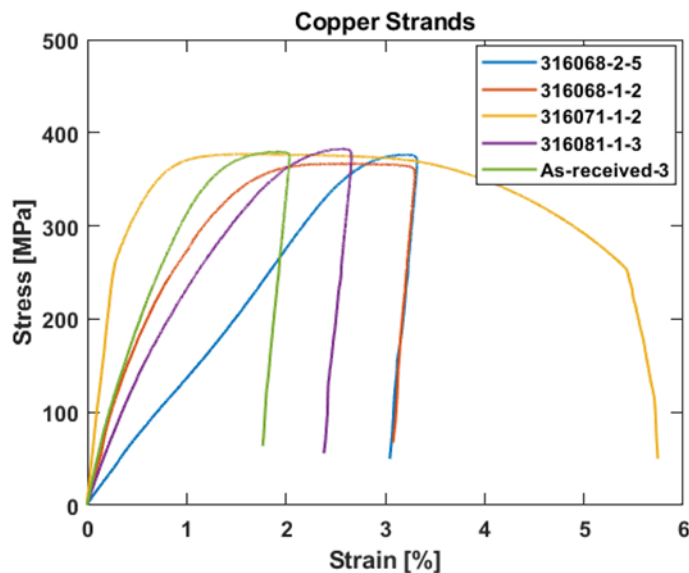


Figure 46. Engineering stress-strain curves for salt-spray-tested 17-kV copper strands from covered and bare conductors. Sample IDs 316068-2-5, 316068-1-2, and 316071-1-2 are from salt-spray-tested CCs. Sample ID 316081-1-3 is a salt-spray-tested bare conductor. The as-received sample is a bare conductor that did not undergo salt spray testing.

Table 17 summarizes the tensile strengths measured for the 17-kV copper conductors. Of the five samples tested, four fractured outside the gauge length. Although grip failure in selected samples may hinder the ability to understand the maximum strength, the tested strands must be at least as strong as the load at grip failure. Sample 316068-1-2 showed an approximately 3% decrease in tensile strength as compared to the bare as-received sample. However, as is the case with the 17-kV ACSR CCs, application of the polymer sheath may lead to some strength loss, making it difficult to attribute this decrease solely to corrosion. Furthermore, as this represents a relatively small change, additional studies on variations in tensile strength for individual copper conductor strength would be needed to rule out sample variation as an explanation for this difference.

Table 17. Tensile strength for single strands of 17-kV copper conductors. Samples listed with a sample ID had undergone salt spray testing prior to tensile testing. Samples denoted with * fractured outside the gauge length.

Sample ID	Sample Type	Tensile Strength [MPa]
316068-2-5	CC Ripley Midspan	376.52*
316068-1-2	CC Ripley	366.63*
316071-1-2	CC Manual	377.04
316081-1-3	Bare	382.54*
As-received-3	Bare	379.50*

22-kV AAC Conductors

Tensile testing was performed on salt-spray-tested 22-kV AAC conductors. Figure 47 presents engineering stress-strain curves for individual outer aluminum strands from salt-spray-tested CCs (Sample IDs 332921, 332923, and 332927) and bare conductors (Sample IDs 326619 and 326621), as well as for an individual aluminum strand from a bare, as-received conductor that did not undergo salt spray testing.

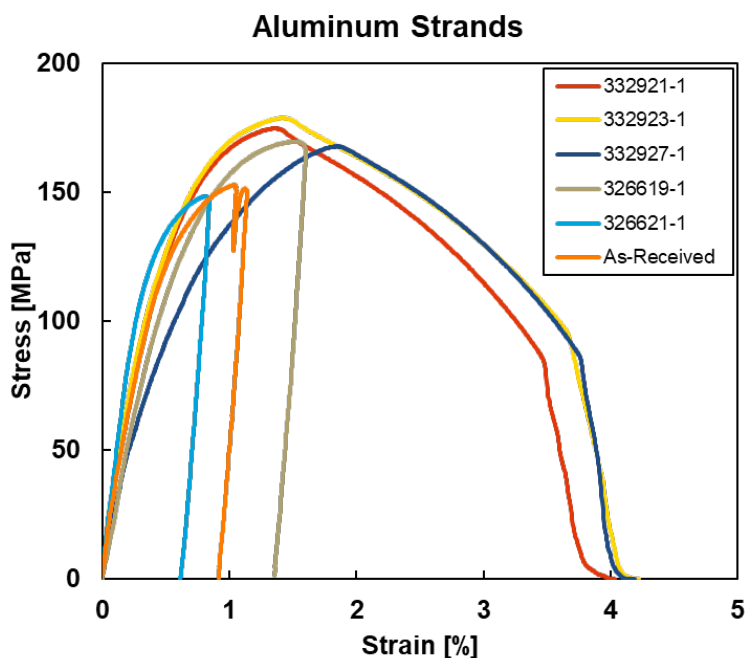


Figure 47. Engineering stress-strain curves for salt-spray-tested 22-kV AAC strands from covered and bare conductors. Sample IDs 332921, 332923, and 332927 are from salt-spray-tested CCs. Sample IDs 326619 and 326621 are from salt-spray-tested bare conductors. The as-received sample is a bare conductor that did not undergo salt spray testing.

Table 18 summarizes the tensile strengths measured for the 22-kV AAC conductors. The tensile strengths of all aluminum strands from CCs exposed to salt spray testing were larger than the average tensile strength for aluminum strands from bare conductors exposed to salt spray testing, as well as the tensile strength for a bare, as-received conductor. All aluminum strands from bare conductors fractured outside the gauge length. Although grip failure in these samples may hinder the ability to understand the maximum strength, the tested strands must be at least as strong as the load at grip failure. Further studies with larger sample sizes would be needed to draw firm conclusions about the mechanical properties of bare and covered conductors, but these results suggest that corrosion caused by salt spray testing does not lead to a significant decrease in tensile strength for AAC CCs relative to bare conductors.

Table 18. Tensile strength for single strands of 22-kV AAC conductors. Samples listed with a sample ID had undergone salt spray testing prior to tensile testing. Samples denoted with * fractured outside the gauge length.

Sample ID	Sample Type	Tensile Strength [MPa]
332921-1	AAC CC End Strip	174.6
332923-1	AAC CC Creviced End	178.6
332927-1	AAC CC Midspan	167.7
326619-1	AAC Bare	169.5*
326621-1	AAC Bare	148.4*
As-Received	AAC Bare	152.8*

Cyclic Polarization Testing

As mentioned previously, Phase 1 studies identified accelerated localized corrosion as a potential threat to CC systems. As the water ingress and salt spray testing demonstrated, stripping of the polymer sheath may facilitate liquid ingress and corrosion beneath the polymer sheath. Thus, to better understand this phenomenon, cyclic polarization testing was performed to electrochemically characterize the localized corrosion susceptibility of CCs with stripped ends in an aqueous environment. Specifically, the effects of material type, sheath removal method, presence of artificially induced crevices, and the age of the samples were investigated. Note that as pre-aged samples were not provided, some samples were put through an accelerated aging process to simulate extended use.

Experimental Setup

A detailed description of the conductor sample preparation and cyclic polarization testing is provided in Appendix A. Briefly, electrical connection was made to a small section of conductor and then the connection and each end of the conductor were sealed with silicone sealant. Testing was performed in 3.5% NaCl at 35 ° C. All electrochemical testing was conducted using Gamry potentiostats. All potentiostats used for testing successfully passed the criteria outlined in ASTM G5-14.²⁶ The sample was polarized from the rest potential (E_r), the potential measured when no net current is flowing through the system, to a vertex potential of 1.1 V versus a standard calomel reference electrode (or to a maximum vertex current of either 300 mA or 600 mA, depending on the potentiostat capabilities) and then the scan was reversed and scanned back to E_r . A schematic of the electrochemical test setup is provided in Figure 48.

Cyclic polarization testing was limited to only the 17-kV ACSR and 17-kV copper conductors. In addition to testing as-received ACSR and copper conductors, cyclic polarization was also performed on a set of samples that were subjected to cyclic immersion aging prior to testing. These samples were immersed in a 3.5% NaCl solution at 35° C for 16 hours and then taken out and allowed to dry at room temperature for 8 hours; the wet/dry cycling was repeated for a total

²⁶ ASTM G5-14 “Standard Reference Test Method for Making Potentiodynamic Anodic Polarization Measurements,” American Society for Testing and Materials, 2014.

of seven days. This immersion aging was intended to mimic exposure to harsh environmental conditions (i.e., near the ocean) and to evaluate the effect of such exposure on the corrosion resistance of the CCs and bare conductors. Figure 49 presents representative images of immersion-aged 17-kV ACSR and 17-kV copper CCs prior to cyclic polarization testing.

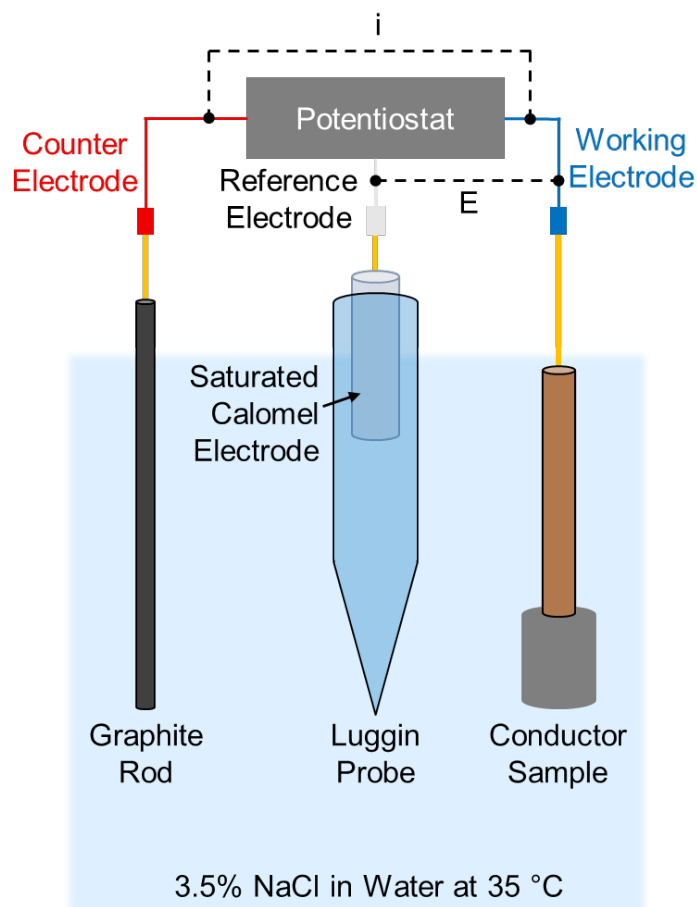


Figure 48. Schematic showing a typical setup for cyclic polarization testing. The potential of the sample was measured relative to a saturated calomel electrode. Graphite was used as the counter electrode. A 3.5% NaCl solution was used for the electrolyte and was held at 35° C.

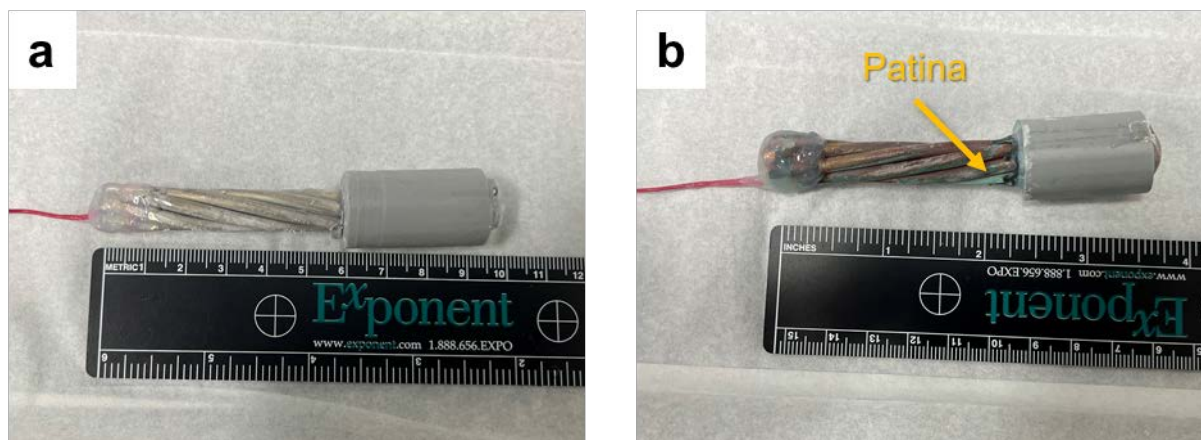


Figure 49. Representative pre-test photographs of aged (a) 17-kV ACSR and (b) 17-kV copper CCs. The immersion aging resulted in patina formation on copper conductors.

Following testing, the samples were visually inspected, and the cyclic polarization scans were evaluated for evidence of corrosion. Typically, large, sudden increases in current during the forward scan indicate localized corrosion and are referred to as breakdown. The potential at which breakdown occurs (E_b) and the relationship of E_b to E_r provide a metric for evaluating corrosion susceptibility, i.e., higher $E_b - E_r$ values indicate better corrosion resistance. In addition, the current density at E_r (j_{E_r}) was calculated by fitting the linear region of the current versus potential traces within the first few hundred millivolts of the forward scan and extrapolating back to E_r . Comparison of the current densities at E_r provides an analysis of the corrosion activity at the rest potential, wherein lower current densities indicate less corrosion.

Results

- No significant adverse effect in localized corrosion susceptibility for CCs compared to bare conductors was observed.
- The 17-kV ACSR conductors exhibited a mix of active and passive behavior, indicating that the breakdown potential in this test environment (3.5% NaCl) is close to the rest potential.
- All 17-kV copper conductors (bare and covered) exhibited active corrosion in this test environment and could not be differentiated.
- Both 17-kV copper and 17-kV ACSR conductors (bare and covered) are susceptible to localized corrosion if an aggressive environment is present. Care should be taken to prevent water ingress and the concentration of contaminants underneath the polymer sheath that can result in the formation of an aggressive environment.
- Neither the sheath removal method nor the presence of artificially created crevices had a significant effect on the corrosion resistance of the 17-kV copper and 17-kV ACSR conductors tested.

17-kV ACSR Conductors

Figure 50 presents representative plots of current density versus potential for 17-kV ACSR conductors and for individual, polished aluminum strands. An increase in current density is generally observed as the sample is polarized in the anodic direction. If a passive film forms, one would expect the current density to remain relatively constant until a breakdown potential is reached. At the breakdown potential, a rapid increase in current density is observed. The 17-kV ACSR conductors had a mix of active and passive behavior.

Table 19 presents average current density at the E_r (j_{Er}) measurements for 17-kV ACSR conductors and for individual, polished aluminum strands. The j_{Er} is a representation of the corrosion rate of the sample in a particular environment when no external bias is applied. It is of note that the average j_{Er} values measured for single, polished aluminum strands was much lower than the average j_{Er} values measured for either 17-kV ACSR bare conductors or CCs. This suggests that j_{Er} measurements on both bare conductors and CCs is driven primarily by creviced geometries resulting from the stranded nature of the conductor bundle rather than any potential crevices at the conductor/sheath interface (in the case of CCs). Note also that, in these results, the stripping method and presence of artificial end crevices did not appear to significantly affect the corrosion susceptibility, although variability in the data make it difficult to determine conclusively.

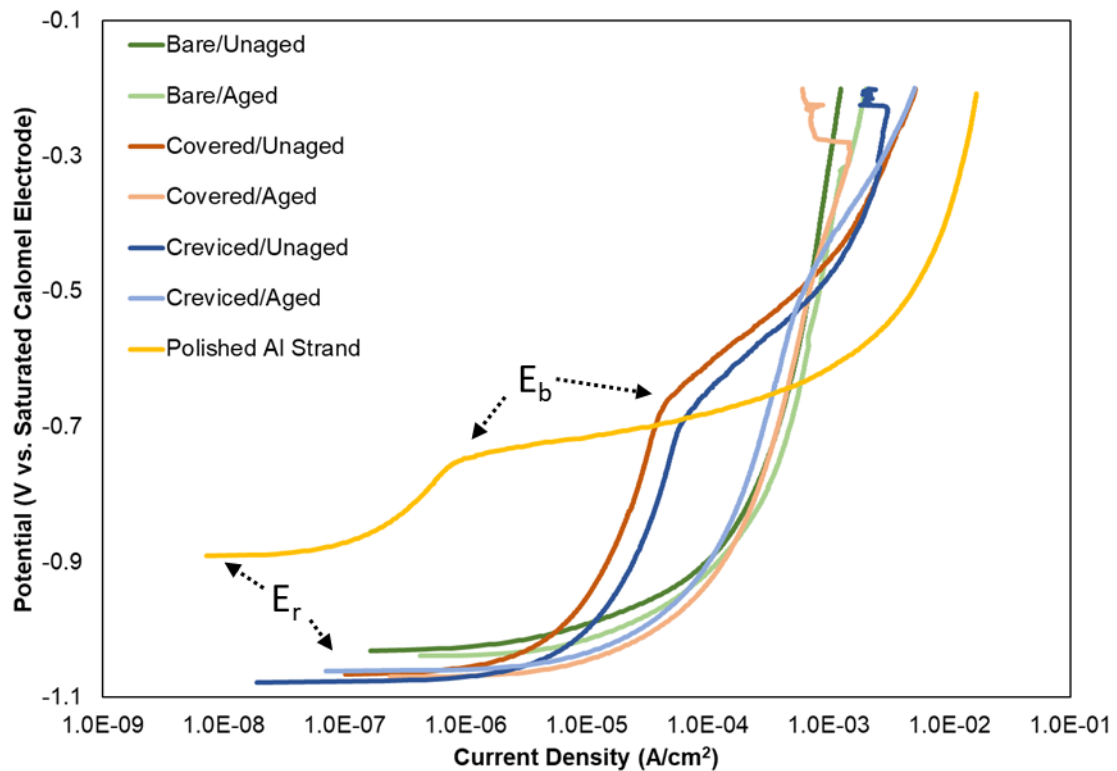


Figure 50. Representative plots of current density vs. potential for 17-kV ACSR conductor samples and for an individual polished aluminum strand. The plots shown here only present data from the forward scan up to -0.20 V vs. saturated calomel electrode for clarity and to highlight the particular regions of interest in evaluating the corrosion susceptibility. E_b and E_r denote the breakdown potential and the rest potential, respectively.

Table 19. Measured current densities at the rest potential (j_{Er}) for cyclic-polarization-tested 17-kV ACSR conductors and individual polished aluminum strands. Averaged values are reported with the standard deviation; some test conditions resulted in anomalies, and only a single test was considered reliable.

Conductor Type/Condition	j_{Er} ($\mu\text{A}/\text{cm}^2$)
Bare, Unaged	2.84 ± 0.47
Covered, Unaged	2.66 ± 1.44
Crevice End, Unaged	2.44
Bare, Aged	4.88
Covered, Aged	3.67 ± 1.81
Crevice End, Aged	3.49 ± 0.49
Individual Polished Al Strand	0.11 ± 0.00

Figure 51 presents representative optical microscopy images of exposed (Figure 51a) and covered (Figure 51b) regions of an unaged 17-kV ACSR CC after cyclic polarization testing. Extensive pitting was observed on exposed regions, consistent with the electrochemical data. In addition, pitting was observed on areas that were covered during testing; it is noted that these surfaces appeared similar to the surfaces that were covered during salt spray testing (Figure 35). These data indicate that water may ingress beneath the polymer sheath and cause corrosion of the underlying conductor in regions that are not directly exposed to the surrounding environment.

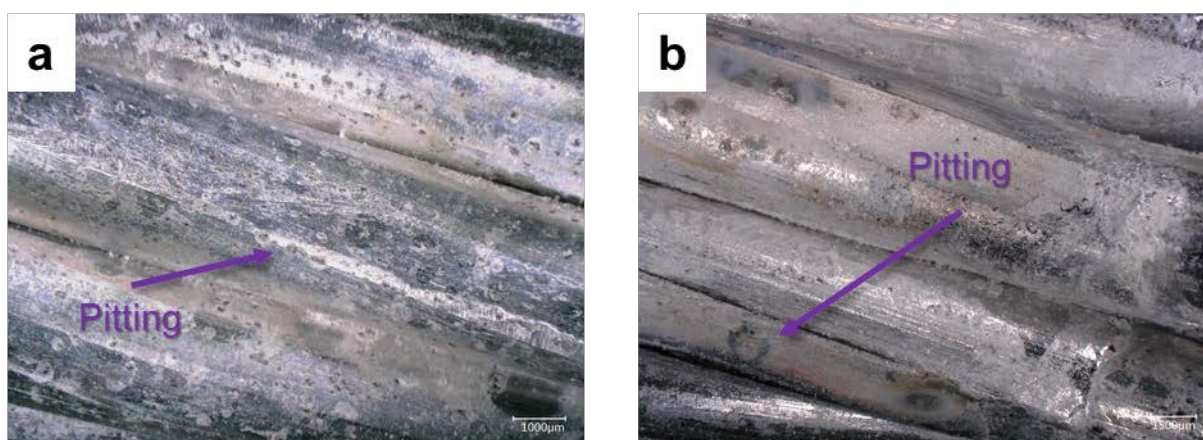


Figure 51. Representative optical microscopy images of (a) stripped and (b) covered portions of an unaged cyclic-polarization-tested 17-kV ACSR CC.

17-kV Copper Conductors

Figure 52 presents representative plots of current density versus potential for 17-kV copper conductors and for individual, polished copper strands. A breakdown potential was not observed in the electrochemical data for cyclic polarization of copper conductors. However, the rapid increase in current density to a very high value at the beginning of the polarization indicates that the samples do not exhibit passive behavior and undergo active corrosion at potentials very near E_r . Similar results were observed for single, polished copper strands.

Table 20 presents average j_{E_r} measurements for 17-kV copper conductors and for individual, polished copper strands. The average j_{E_r} values were similar for 17-kV copper bare conductors, CCs, and single, polished strands. This indicates that j_{E_r} is primarily a function of the active corrosion rate of copper and is not critically dependent on the sample geometry in this test environment investigated. No significant differences in behavior were observed between the stripping methods (not shown).

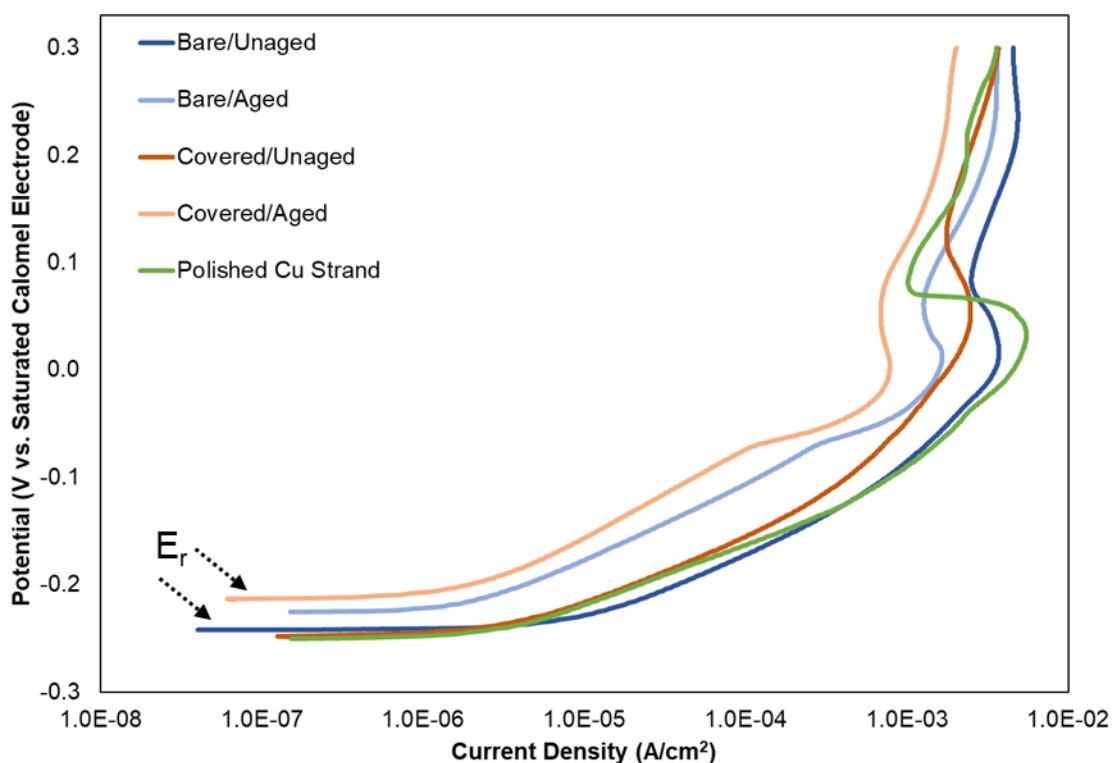


Figure 52. Representative plots of current density vs. potential for 17-kV copper conductor samples. The plots shown here only present data from the forward scan up to 0.30 V vs. saturated calomel electrode for clarity and to highlight regions of interest in evaluating the corrosion susceptibility. E_r denotes the rest potential.

Table 20. Measured current densities at the rest potential (j_{Er}) for cyclic-polarization-tested 17-kV copper conductors. Averaged values are reported with the standard deviation.

Conductor Type/Condition	j_{Er} ($\mu\text{A}/\text{cm}^2$)
Bare, Unaged	8.70 ± 0.92
Covered, Unaged	2.99 ± 0.62
Bare, Aged	1.81 ± 0.13
Covered, Aged	2.04 ± 0.37
Individual Polished Cu Strand	2.61 ± 0.47

Figure 53 presents representative optical microscopy images of exposed (Figure 53a) and covered (Figure 53b) regions of an unaged 17-kV copper CC after cyclic polarization testing. Both localized and general corrosion were observed on the exposed regions, consistent with the electrochemical data. A patina was observed on exposed and covered regions after cyclic polarization, as well as on exposed copper surfaces after immersion aging (Figure 49b). The observation of a patina on covered areas after cyclic polarization testing indicates that water may penetrate beneath the polymer sheath and cause corrosion of the copper conductor in regions that are not directly exposed to the surrounding environment.

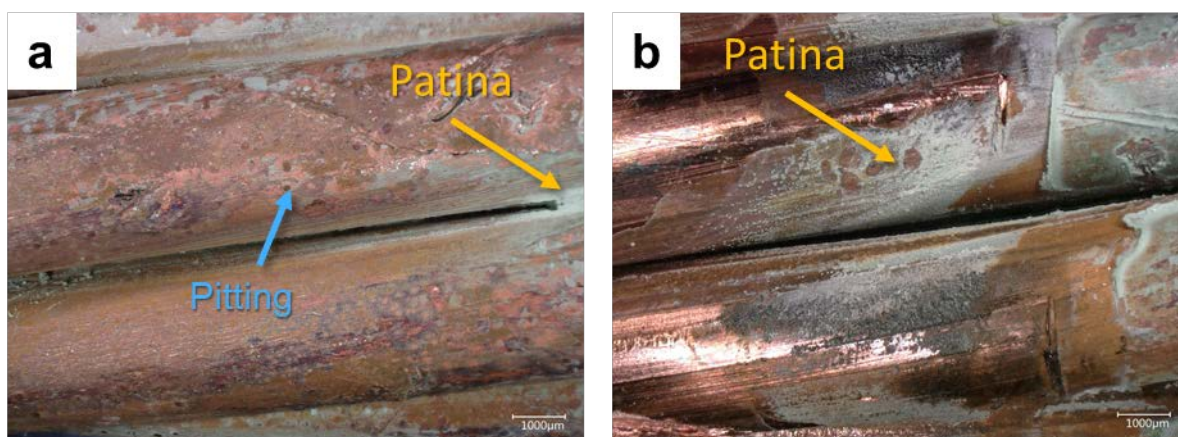


Figure 53. Representative optical microscopy images of (a) stripped and (b) covered portions of an unaged cyclic polarization tested 17-kV copper CC.

Discussion and Conclusions: Corrosion Testing

The testing described in this section investigated the corrosion susceptibility of CCs relative to bare conductors. To assess this, Exponent performed liquid ingress testing, salt spray testing, and cyclic polarization testing. The major conclusions from this combined set of tests are:

- Stripped ends of CCs, as well as CCs with IPC hardware, are susceptible to water ingress. The methods used here to test water ingress are more aggressive than what would typically be encountered in the field but indicate that water may penetrate and traverse through the conductor core to the nearest elevation minimum.
- Corrosion can occur beneath the polymer sheath in highly corrosive environments. Corrosion was observed at least 2–3 feet away from the nearest exposed metal under the tested conditions.
- Although the salt spray testing conditions used here are more severe than what would be encountered in the field, and no potential mitigation measures were considered, the results indicate that it is possible for corrosion to occur beneath the polymer sheath of CCs, and, in some cases, the corrosion that occurs beneath the sheath may be more severe than that which occurs on bare, exposed conductors.
- The condition of the stripped end, including the technique used to remove the polymer sheath and the presence of artificial crevices, did not appear to have a significant effect on the corrosion susceptibility of CCs. The presence of damage to the polymer sheath at midspan regions of CCs did appear to have potential for more severe corrosion than that observed at stripped ends. CCs with IPC hardware did not appear to be susceptible to corrosion at the IPC installation area under the tested conditions despite the previous evidence of water ingress. This apparent discrepancy is likely due to the aggressive nature of the ingress test (i.e., full immersion).
- The corrosion that was observed did not have a significant adverse effect on the tensile strength of the conductor strands. A small decrease in tensile strength was observed for salt-spray-tested aluminum and copper strands from CCs relative to salt-spray-tested aluminum and copper strands from bare conductors and to as-received aluminum and copper strands from bare conductors. This may be due to annealing of the conductor strands during application of the polymer sheath; additional testing would be needed to fully evaluate these differences.
- A decrease in tensile strength was observed for salt-spray-tested aluminum strands from ACSR CCs with IPC hardware relative to bare, as-received ACSR conductors; this decrease is likely due to mechanical damage to the conductor strands from IPC installation, as no visual evidence of corrosion was observed on the IPC samples.
- Electrochemical testing indicated that both ACSR and copper conductors are susceptible to localized corrosion at or very near their rest potentials. This may be due to crevices introduced by the stranding or mechanical damage from the stranding process. No significant difference in corrosion susceptibility between CCs and bare conductors was observed electrochemically.
- Pitting and general corrosion was evident on bare conductors and exposed areas of CCs after electrochemical testing. Corrosion was also observed beneath the polymer sheath after electrochemical testing, particularly for ACSR CCs.

Flammability Testing

Motivation and Scope

CCs may be subject to unique failure modes compared to traditional conductors. Specifically, the polymer sheath of a CC may be damaged from nearby wildfires or may have the potential to ignite under certain circumstances. To improve understanding of the latter, a cone calorimeter was utilized to determine the conditions under which heat from a nearby wildfire could ignite the polymer sheath. ASTM E1354 provides a methodology on determining the incident heat flux and time required to induce sustained flaming ignition of the sample.²⁷ However, as ASTM E1354 specifies a flat sample with dimensions of 10 cm x 10 cm, which was incompatible with testing CCs, the setup was modified to use a 10-centimeter-long CC in its place. The modified test setup was designed to subject the sample to a heat flux that is representative of its intended geometry and orientation without compromising the integrity of the data.

Table 21 describes the test cases used to assess the autoignition (ignition without a spark) properties of the polymer sheaths on CCs. Test cases are indicated in Table 21 with an “X.” Exponent performed heat flux testing on 15-kV, 17-kV, and 35-kV ACSR CCs; 22-kV AAC CCs; and 17-kV-rated copper CCs. The time to autoignition was assessed for all CCs at the following incident heat fluxes: 25, 30, 35, and 50 kW/m². Exponent evaluated the behavior of the copper CCs at one additional heat flux, 28 kW/m² to clarify its minimum autoignition temperature, and evaluated the ignition behavior of the 15-kV ACSR and 22-kV AAC at 65 and 80 kW/m² to confirm its propensity for ignition at higher heat flux values. Results were then compared with known heat flux values for wildland fires from the literature.

Table 21. Incident heat flux tests conducted to determine autoignition properties.

Heat Flux (kW m ⁻²)	2/0 Cu CC	1/0 ACSR CC			AAC CC
	17 kV	17 kV	35 kV	15 kV	22 kV
25	X	X	X	X	X
28	X	Not Tested	Not Tested	Not Tested	Not Tested
30	X	X	X	X	X
35	X	X	X	X	X
50	X	X	X	X	X
65	Not Tested	Not Tested	Not Tested	X	X
80	Not Tested	Not Tested	Not Tested	X	X

²⁷ ASTM E1354-17 “Standard Test Method for Heat and Visible Smoke Release Rates for Materials and Products Using an Oxygen Consumption Calorimeter,” American Society for Testing and Materials, 2017.

Experimental Setup

The heat flux testing setup is shown in the Figure 54 schematic. The use of a conical radiant electric heater ensured that the sample experienced a constant heat flux across its top surface. The 10-centimeter-long CC sample was positioned on top of a refractory fiber blanket to support the sample and to ensure that an adiabatic surface was maintained. Additional pieces of refractory fiber blanket were used to cover approximately 1.3 cm of the cut ends of the conductor to reduce their impact on the ignition behavior and to ensure that the ignition conditions are representative of an extended piece of cable used in the field. Thus, a 7.6 cm portion of the CC was exposed to the radiant heat flux with the top edge of the CC 2.5 cm below the bottom surface of the electric heater.

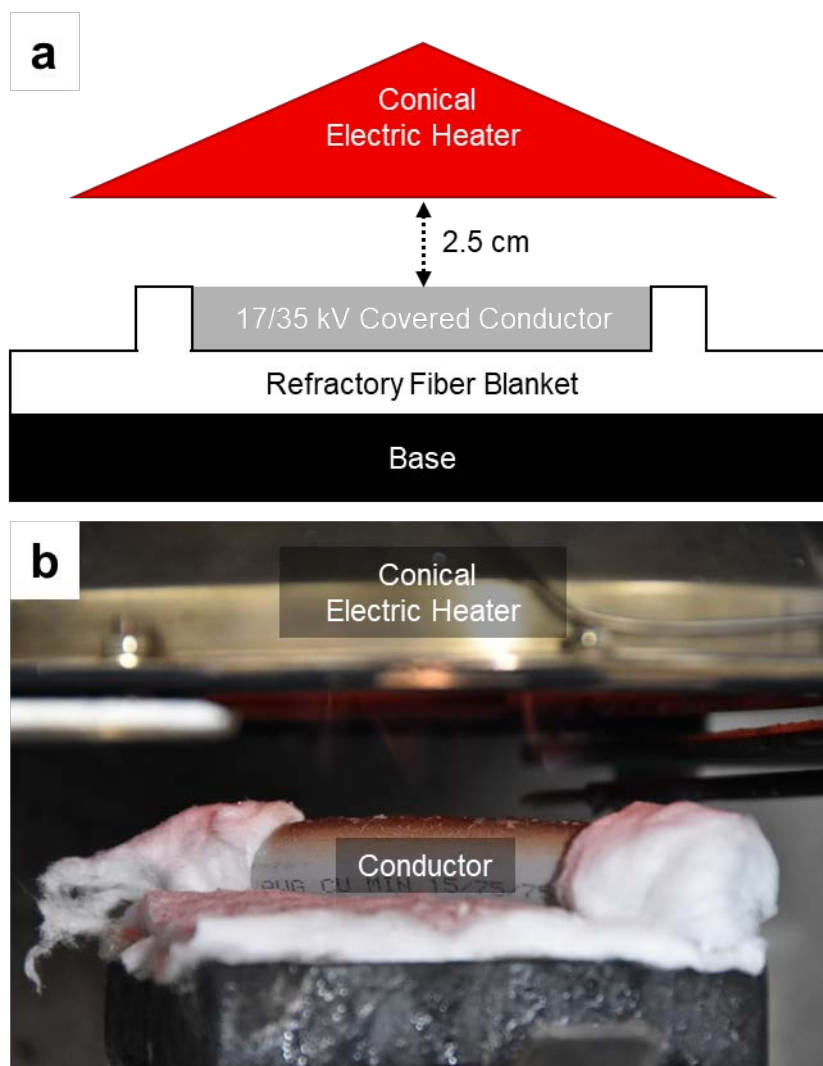


Figure 54. (a) Schematic and (b) representative photo of the heat flux testing apparatus. The top edge of the CC was spaced 2.5 cm from the bottom of the conical heat source. A refractory fiber blanket was used to provide an adiabatic back surface and protect the ends of the CC to reduce unwanted edge effects.

The test began when the CC was first exposed to the electric radiant heat source and was terminated when either no ignition occurred within a predetermined time or the combustible portion of the sample was fully consumed after ignition. The testing methodology evolved over the course of the experiment. Initially, Exponent imposed a 15-minute (900-second) time limit for testing. However, during testing it became clear that this time was insufficient to ignite the CCs for some of the heat fluxes of interest. Thus, in a few cases, the sample was heated until ignition occurred approximately 1,600 seconds after the test began.

Results

Table 22 presents the time to autoignition as a function of heat flux for all tested CCs. Note that due to the initial 900-second time limit on the test, the times to ignition for the 17-kV ACSR conductor, copper conductor, and AAC are unknown for 25 kW/m² because the tests were terminated before ignition occurred, indicating that more than 900 seconds of exposure would be required to ignite the materials at 25 kW/m², if ignition is possible at 25 kW/m². In practice, exposure times for CCs subjected to wildland fires are expected to be significantly less than 900 seconds. Therefore, higher heat fluxes would be required for autoignition.

Table 22. Autoignition times as a function of heat flux for all tested CCs.

Heat Flux (kW/m ²)	Cu t _{ig} (s)	ACSR t _{ig} (s)			AAC t _{ig} (s)
	17 kV	17kV	35kV	15kV	22kV
25	Unknown		1594 (26.6 min)	776 (12.9 min)	Unknown
28	1616 (26.9 min)	Not tested			
30	677 (11.3 min)	975 (16.3 min)	831 (13.9 min)	635 (10.6 min)	667 (11.1 min)
35	239 (4.0 min)	376 (6.3 min)	444 (7.4 min)	383 (6.4 min)	481 (8.0 min)
50	128 (2.1 min)	118 (2.0 min)	84 (1.4 min)	101 (1.7 min)	178 (3.0 min)
65	Not tested			63 (1.1 min)	44 (0.7 min)
80	Not tested			27 (0.5 min)	28 (0.5 min)

Discussion and Conclusions: Flammability Testing

Ignition of solid materials can be divided into two distinct regimes: thermally thin ignition and thermally thick ignition. In general, the time to autoignition (t_{ig}) for a thermally thin sample (i.e., one with a uniform temperature across the sample) is linearly related to the inverse incident heat flux (ϕ_q). For a thermally thick sample (i.e., one with a thermal gradient from the surface to the interior), the heat flux is expected to be inversely proportional to the square root of the time to ignition (i.e., $\phi_q \propto \frac{1}{\sqrt{t_{ig}}}$). In both instances, the time to ignition is expected to decrease as a function of increasing heat flux. Based on the thickness of the polymer sheath (see Table 2), Exponent expected that the CCs were best described using a thermally thick ignition regime. Thus, Figure 55 portrays the inverse square root of the ignition time, $\frac{1}{\sqrt{t_{ig}}}$ (using data from Table 22), as a function of incident heat flux. As expected, the ignition times and corresponding heat fluxes for ignition produce a linear trend of ignition times exponentially increasing as the heat flux decreases. Given that the CC polymer sheath is the same material for all conductor

types (copper, ACSR, and AAC) and a thermally thick regime is employed, the conductor material and sheath thickness do not impact the autoignition behavior. Thus, using the data from all conductor types, Exponent found a correlation between the ignition time (in seconds) and incident heat flux (in kW/m²) to be $t_{ig}^{-0.5} = 0.003\phi_q - 0.0543$.

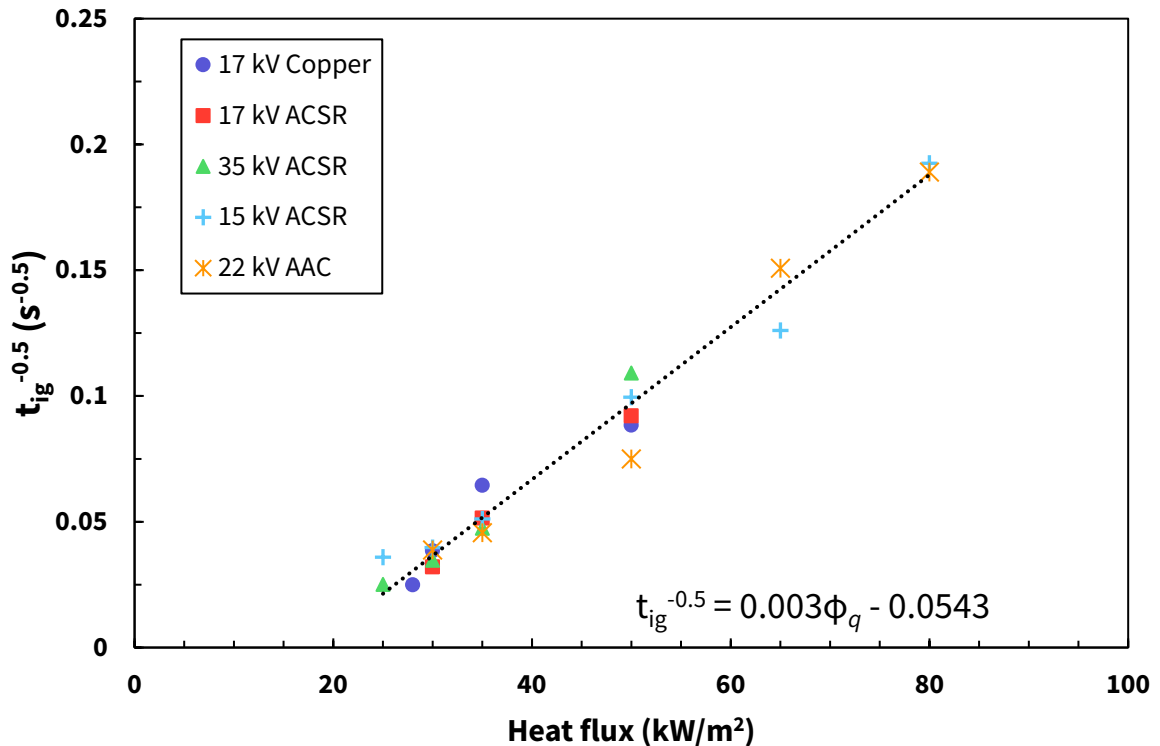


Figure 55. Symbols portray the autoignition time (plotted as the inverse square root) as a function of incident heat flux from cone calorimetry tests. The line is a linear best fit providing a correlation between heat flux and ignition times for the CCs.

Wildland fires are generally categorized into three different groups. The first group, surface fires, represent fires that primarily burn surface vegetation such as twigs and dried leaves. The second group, brush fires, include fires in which the fuel load significantly consists of grasses and brush vegetation that extends several meters above the ground. The third group, crown fires, include fires that burn primarily in the canopy of trees and spread from treetop to treetop. To evaluate the CCs' propensity for autoignition, experimental results from the cone calorimetry tests were compared to representative heat fluxes and corresponding residence times of wildland fires.

A detailed review of available literature was performed, and multiple sources that gathered real-world data from numerous actual wildland fires were identified.^{28,29,30,31} Representative time-averaged radiative heat fluxes and associated residence times from wildland fires were reviewed for each of the three wildland fire groups discussed previously. The residence time represents the duration in which the fire was in contact with the sensor (i.e., the duration used for the time-averaging). It was found that surface fires exhibited a range of time-averaged radiative heat fluxes of 18–77 kW/m² over a duration of approximately 4–42 seconds with an instantaneous peak recorded heat flux of 115 kW/m².

Next, the brush fires were found to have a time-averaged heat flux on the order of 97 to 110 kW/m² with a residence time of 10–40 seconds and a measured peak heat flux of 132 kW/m². Finally, the crown fires were shown to produce time-averaged radiative heat fluxes ranging from 179 to 263 kW/m² over a period of 50 seconds with a measured peak heat flux of 300 kW/m². It is important to note that for each of the heat flux ranges above, the measurements were collected from sensors positioned approximately one meter above the ground and were collected from sensors positioned inside the flame in direct contact with the flame of the passing fire front.

To provide a conservative comparison between the estimated autoignition heat flux and reported heat flux values from wildland fires, the peak radiative heat flux values discussed above were employed. Peak radiative heat fluxes and associated residence times from full-scale wildland fire measurements are shown as symbols in Figure 56 for surface, brush, and crown fires.³² The solid line in Figure 56 represents the minimum combination of heat flux and residence time for autoignition of the CCs computed using the correlation experimentally derived above. The region above the solid line represents a fire scenario (CC surface heat flux and exposure time) in which ignition is likely to occur, and the region below indicates fire regimes in which ignition of the CC sheath is unlikely.

²⁸ Butler, B., et al. “Measurements of radiant emissive power and temperatures in crown fires.” *Canadian Journal of Forest Research* (2004): 1577-1587.

²⁹ Morandini, F., et al. “Fire spread experiment across Mediterranean shrub: Influence of wind on flame front properties.” *Fire Safety Journal* 41 (2006) 229-235.

³⁰ Silvani, X., and Morandini, F. “Fire spread experiments in the field: Temperature and heat fluxes measurements.” *Fire Safety Journal* 44 (2009) 279-285.

³¹ Frankman, D., et al. “Measurements of convective and radiative heating in wildland fires.” *International Journal of Wildland Fire* 22.2 (2013): 157-167.

³² Ibid.

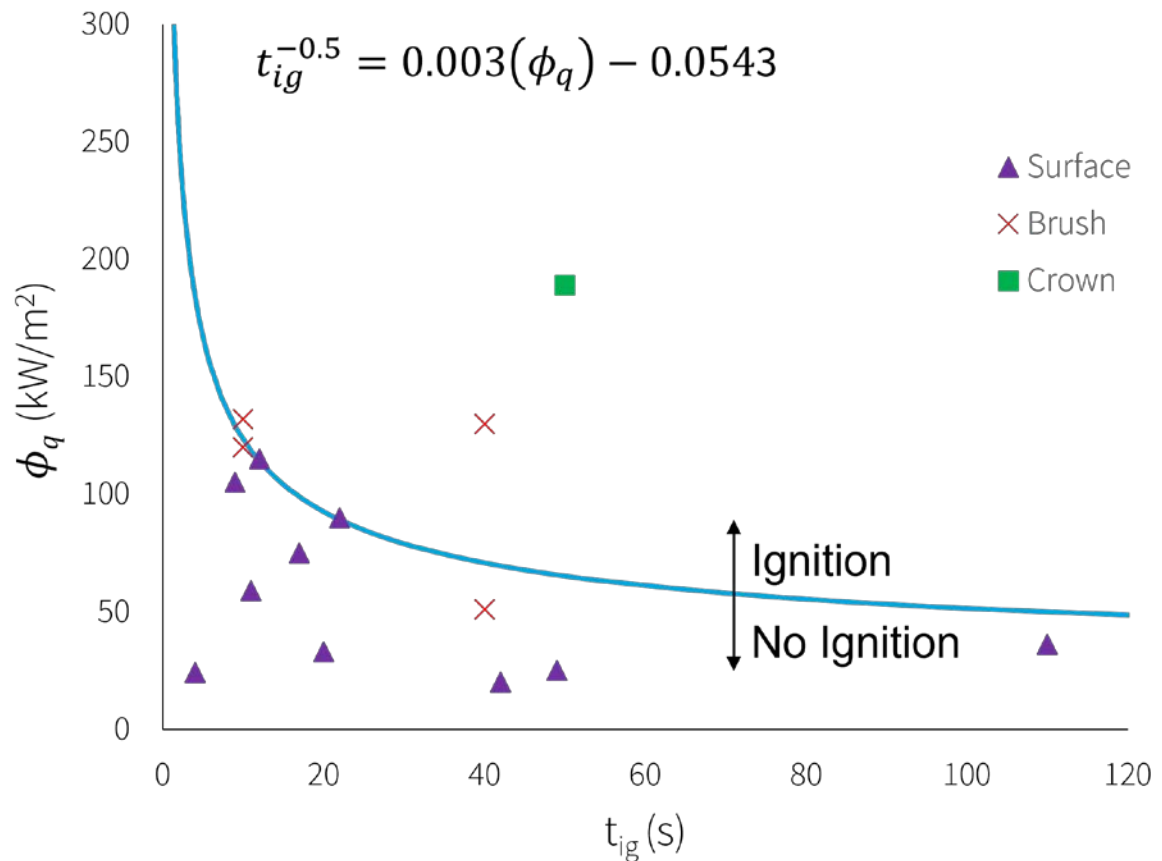


Figure 56. Critical heat flux and associated residence time for autoignition. Symbols represent full-scale wildland fire data. The blue line represents the theoretical minimum heat flux required for autoignition derived from cone calorimetry experiments and thermally thick ignition theory.

With respect to the ignition of CCs, which are often installed on poles high above the ground, Figure 56 demonstrates that certain scenarios have the potential to lead to an autoignition scenario while others are unlikely. Surface fires and low-lying brush fires exhibit a low probability that autoignition will occur, given the combination of average heat fluxes, associated residence times, and distance between the fire and the conductors. It is important to note that the individual data points presented in Figure 56 represent a peak value measured directly inside the flame. However, a typical crown/ canopy fire has the potential to ignite the CC due to its immense heat flux, extended residence times, and proximity to the distribution lines.

System Strength Testing

Scope

Mechanical strength testing was performed to measure the breaking strength of individual CC system components and to understand their failure modes/behaviors, as well as to understand their behavior within the context of the overall system. Testing was performed on 15-kV, 17-kV, and 35-kV 1/0 ACSR, as well as 22-kV-rated 397.5 kcmil AAC CCs. The specified dimensions, stranding, and rated tensile strengths of these CCs can be found in Table 3. Three unique tests were performed to achieve these goals:

1. **Splice Maximum Load Test:** This test was designed to measure the strength of the splice-conductor assembly under tension.
2. **Insulator Slip Test:** This test was designed to measure the tensile load at which conductor slippage relative to the tangent insulator occurs, and how the insulator may fail after the onset of slippage.
3. **Full-System Tree-Fall Test:** This test was intended to simulate the response of the full system (i.e., pole, cross-arm, insulators, and CC) if a tree were to fall into a span. Both load and failure behavior were recorded.

Further, SCE expressed specific interest in understanding the mechanical limits of selected combinations of dead-end hardware and equipment. Exponent worked with SCE to design and execute mechanical tests similar to the joint-IOU mechanical tests discussed here, but with use of dead-end hardware instead of tangent structures/insulators. The results of this dead-end testing are included in Appendix E.

Experimental Setup

Splice Maximum Load Test

Test Setup and Equipment

The maximum load tests were performed using unique splice designs/manufacturers for the 15-kV ACSR CCs, 17-kV and 35-kV ACSR CCs, and 22-kV AAC CC. Splices were provided pre-installed on the 15-kV conductor by SDG&E. All other splice installation was carried out using appropriate hydraulic crimping tools and dies.

Tests were performed in a hydraulic horizontal test machine, and epoxy resin dead-end fittings were used to terminate the free ends of the conductor and minimize stress concentration at the grips. ASO 398 bolted clamps were used to test the 15-kV ACSR CCs. The overall test sample length was approximately 12 feet for the 15-kV ACSR and 44 feet for all other conductors. In every case, the splice was positioned near the center of the span. Testing was performed in general accordance with the procedures outlined in ANSI C119.4-2016 (Clause 6.2.2.2,

Maximum Load)³³ and ANSI C119.0-2015.³⁴ A schematic diagram and representative photo of the test setup are shown in Figure 57 and Figure 58, respectively.

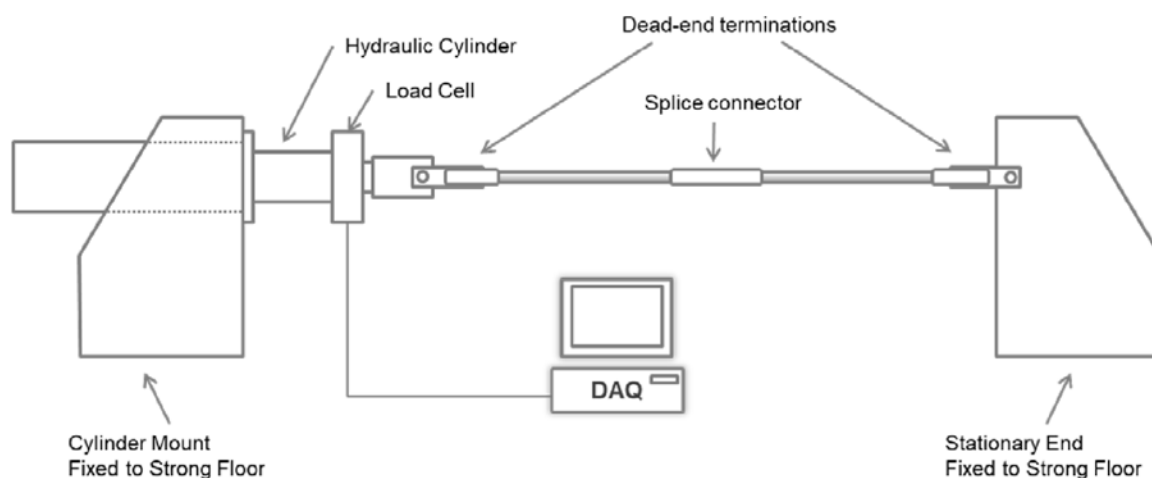


Figure 57. Schematic diagram of splice maximum load test.

³³ ANSI C119.4-2016, “American National Standard for Electric Connectors – Connectors for Use Between Aluminum-to-Aluminum and Aluminum-to-Copper Conductors Designed for Normal Operation at or Below 93C,” Clause 6.2.2.2 (Maximum Load).

³⁴ ANSI C119.0-2015, “American National Standard for Electric Connectors – Testing Methods and Equipment Common to the ANSI C119 Family of Standards.”

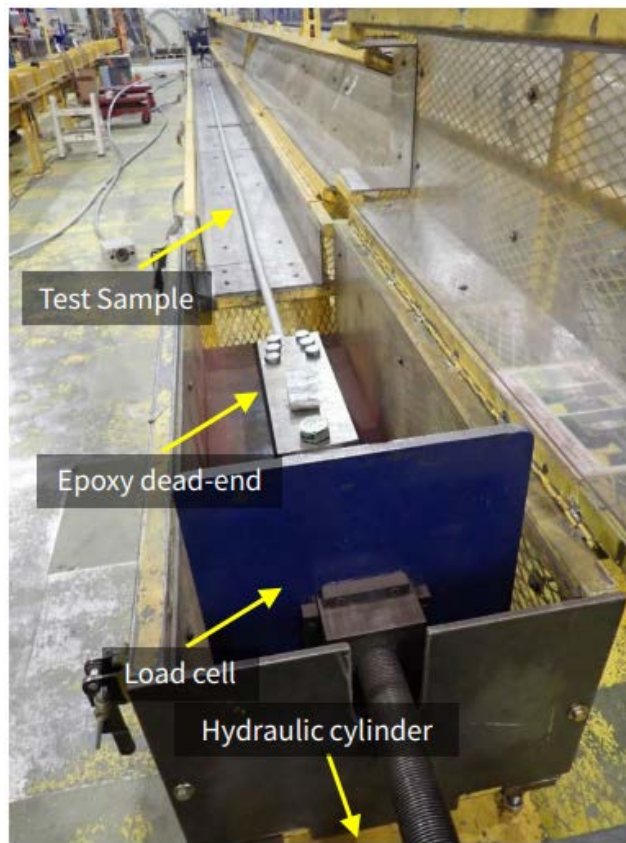


Figure 58. Representative photo of splice maximum load test.

Testing Procedure

The test sample (conductor-splice assembly) was installed in the horizontal test machine and was pre-tensioned to approximately 10% of the rated tensile strength (RTS) of the tested conductor. The conductor was marked with paint at the entrance points on each end of the splice to monitor movement of the conductor relative to the splice during the test. The south end was painted red and the north end was painted blue, where north and south relate to the orientation of the horizontal load frame.

The load was then increased to approximately 60% RTS and held for five minutes. The conductor was visually monitored for slippage at both ends of the splice. Upon completing the five-minute hold, the load was increased until failure was observed. A representative load versus time plot for this loading profile is shown in Figure 59. Tests on each conductor type were performed in triplicate.

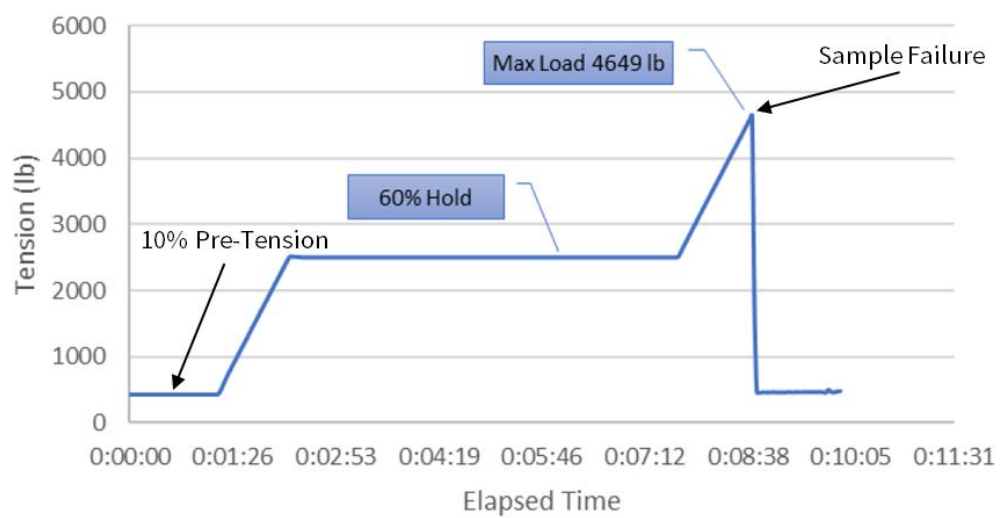


Figure 59. Representative load vs. time plot for the splice maximum load test (Test 1.1).

Insulator Slip Test

Test Setup and Equipment

The insulator slip tests were performed on vise-top pin insulators on all four CC types, as well as clamp-top post insulators on the 17-kV and 35-kV ACSR CCs. Insulators were installed on wooden blocks to simulate a typical cross-arm center phase connection.

Tests were performed in a hydraulic horizontal test machine, and epoxy resin dead-end fittings were used to terminate the free ends of the conductor and minimize stress concentration at the grips. Multiple insulator “stations” were positioned along the conductor in 10-foot intervals such that subsequent tests could be performed on the same conductor span in an area unaffected by the previous test. A schematic diagram and representative photo of the test setup are shown in Figure 60 and Figure 61, respectively.

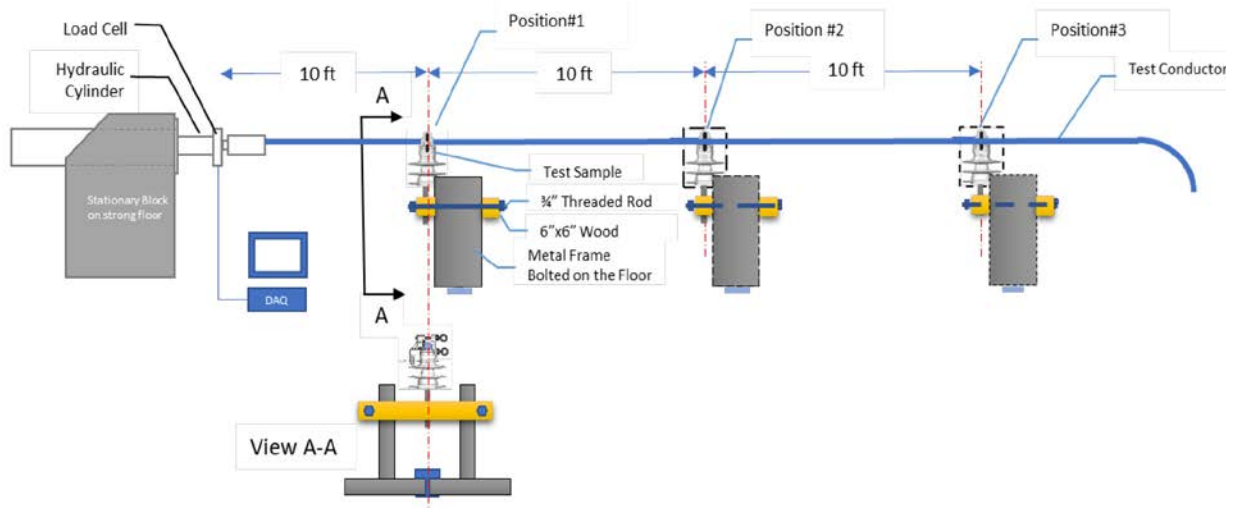


Figure 60. Schematic diagram of insulator slip test.

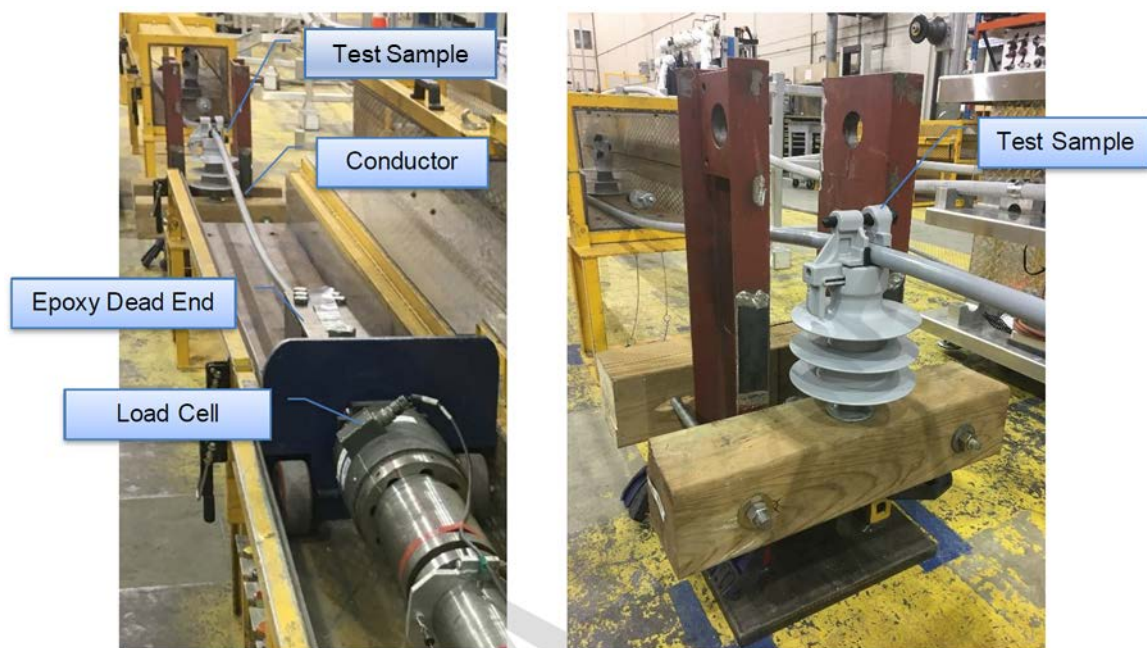


Figure 61. Representative photos of insulator slip test.

Testing Procedure

The insulators were installed on the simulated cross-arm, and the conductor was clamped into position atop the insulator. The conductor tension was increased to 10% RTS, and the conductor ends were marked at the entry points to the insulator clamp. The tension was then increased to

20% RTS, and the conductor was visually inspected for signs of slippage. Once complete, the tensile load was continuously increased at a rate of 1000 lb/min until slippage of the conductor inside the clamp occurred. A representative load versus time plot for this loading profile is shown in Figure 62. Tests on each conductor type were performed in triplicate.

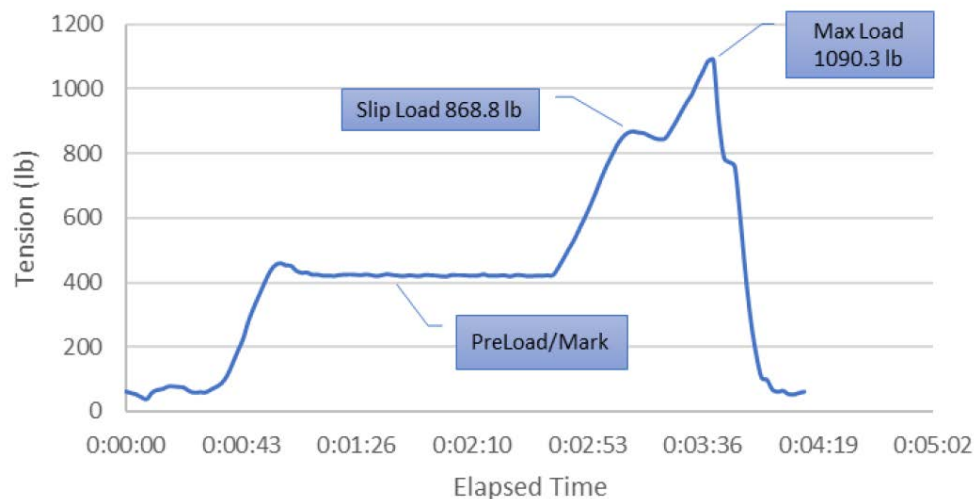


Figure 62. Representative load vs. time plot for the insulator slip test.

Full System Tree-Fall Test

Test Setup and Equipment

Full system mock-up tests were performed using all four conductor types and corresponding hardware, including representative insulators and composite cross-arms. Both vise-top pin and clamp-top insulators were tested for the 17-kV and 35-kV ACSR CCs. The cross-arm assemblies were mounted to a pole stub with standard hardware to simulate a realistic distribution pole configuration.

The tests were performed in a hydraulic horizontal test machine, and dead-ends were used to terminate the free ends of the conductor. A pulley system was implemented to induce a vertical loading component at the cross-arm, and a load cell was attached to the pulley adjacent to the cross-arm to measure vertical loads. The deflection of the conductor toward the pulley was approximately 40 degrees on the insulator side (north). The conductor span on the unloaded (north) side of the insulator was fixed at the end but was kept slack to simulate an adjacent conductor span. A schematic diagram and representative photo of the test setup are shown in Figure 63 and Figure 64, respectively.

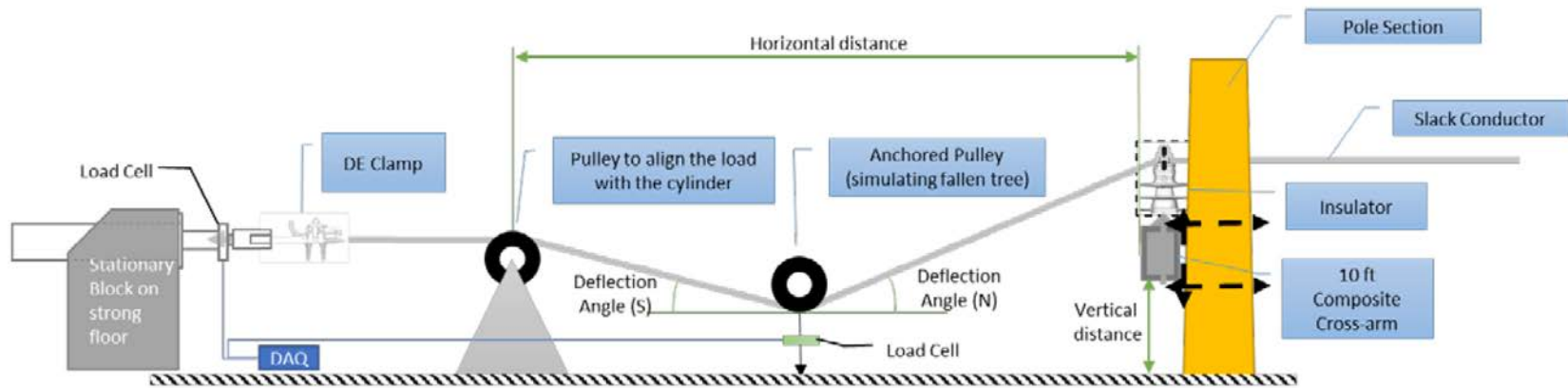


Figure 63. Schematic diagram of the full-system tree-fall test.

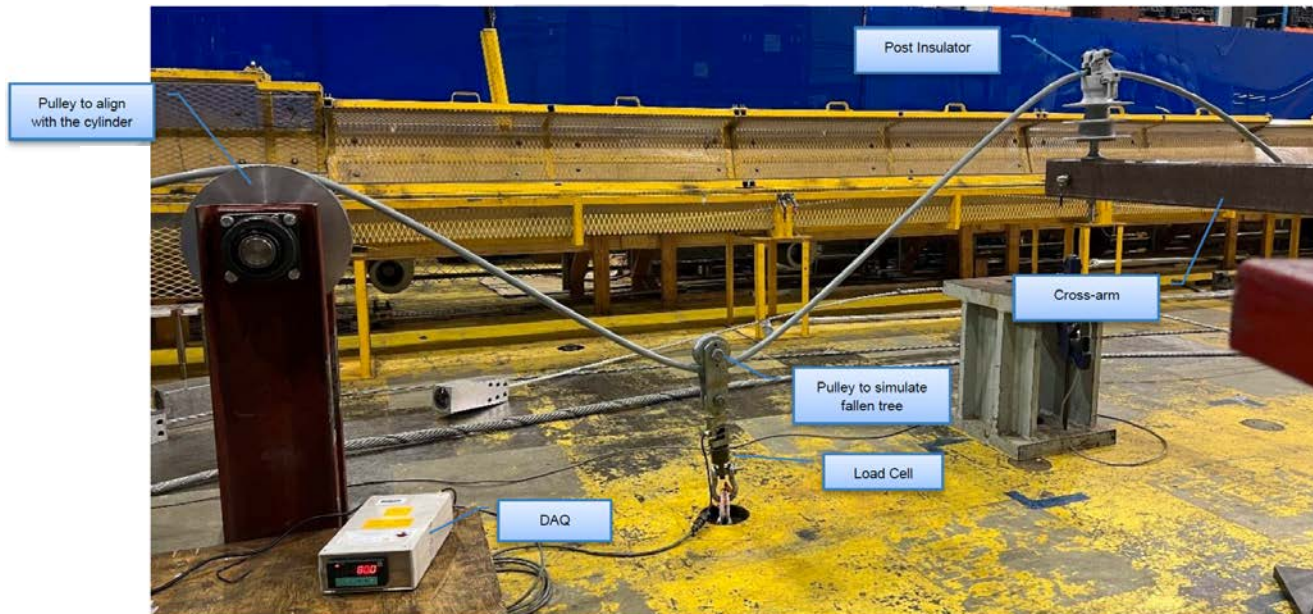


Figure 64. A representative photo of the full-system tree-fall test.

Testing Procedure

The test system including conductor, insulator, and cross-arm is shown in Figure 64. A small pre-tension was applied to remove the slack from the conductor, and the conductor was marked at the insulator clamp entry points to monitor for slippage. The horizontal load was continuously increased at a rate of 1,000 lb/min until damage to the cross-arm or slippage of the conductor occurred. The target vertical load on the pulley was approximately 1000 lb. Loads at the hydraulic cylinder and at the pulley attached to the floor were monitored throughout the test. The permanent deflection of the cross-arm was measured by referencing the vertical distance of the insulator attachment point on the cross-arm to the floor.

Results

Splice Maximum Load Test

Tabulated results of the splice maximum load tests are presented in Table 23. All tested splices exceeded 100% of the rated conductor strength. Further, no slippage was observed either at the five-minute hold at 60% RTS or just prior to failure. Complete test details, including load versus time plots and photos, can be found in Appendix F.

Separation of conductor strands, or “birdcaging,” was observed following installation of splices on both 17-kV and 35-kV ACSR CCs. An example of the birdcaging is shown in Figure 65. Subsequent failure of the conductor occurred in the birdcaged area in four out of six tests (66%). Despite this, all 17-kV and 35-kV spliced conductors exceeded 100% of the conductor RTS when tested.

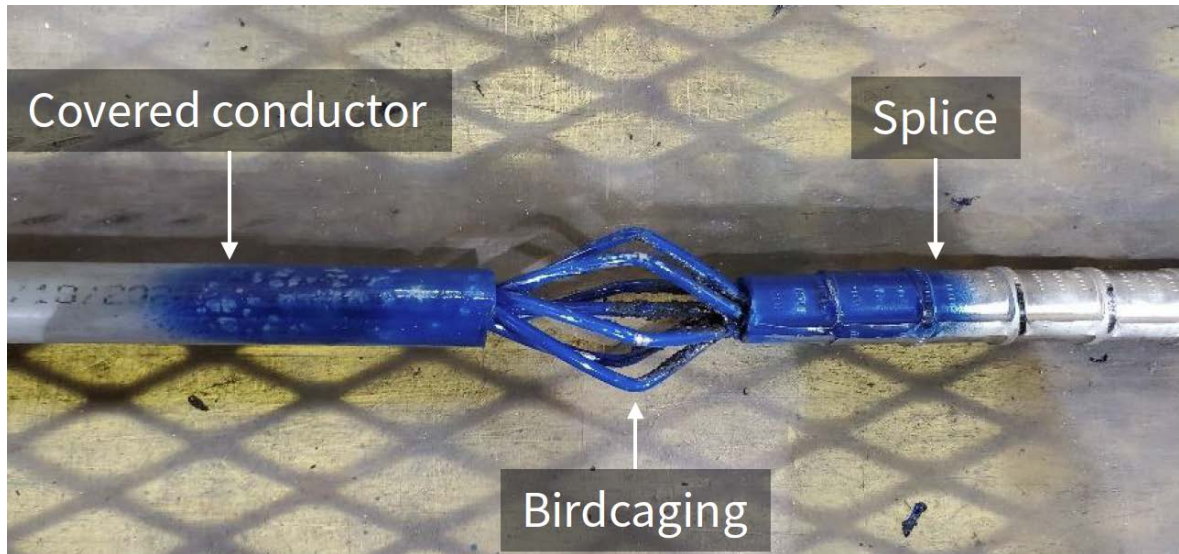


Figure 65. A representative photograph showing the birdcaging behavior of splices on 17-kV and 35-kV ACSR CCs.

Table 23. Results of splice maximum load tests.

Sample #	Conductor Type	Max. Load		Observations
		(lb)	(% RTS)	
1.1.1	17-kV, 1/0 AWG ACSR	4,659	112%	No slippage at 60% RTS. Aluminum strands broke near south end of splice. Steel core intact.
1.1.2	17-kV, 1/0 AWG ACSR	4,724	114%	No slippage at 60% RTS. Aluminum strands broke near south end of splice. Steel core intact.
1.1.3	17-kV, 1/0 AWG ACSR	4,517	109%	No slippage at 60% RTS. Conductor broke at north epoxy block. Steel core pulled out completely.
1.2.1	35-kV, 1/0 AWG ACSR	4,454	107%	No slippage at 60% RTS. Conductor broke near south end of splice. Steel core pulled out completely.
1.2.2	35-kV, 1/0 AWG ACSR	4,623	111%	No slippage at 60% RTS. Aluminum strands broke at south end of splice. Steel core intact.
1.2.3	35-kV, 1/0 AWG ACSR	4,213	101%	No slippage at 60% RTS. Conductor broke at north epoxy block.
1.3.1	22-kV, 397.5 kcmil AAC	6,979	103%	No slippage at 60% RTS. Conductor broke at south end of splice.
1.3.2	22-kV, 397.5 kcmil AAC	7,152	106%	No slippage at 60% RTS. Conductor broke at south end of splice.
1.3.3	22-kV, 397.5 kcmil AAC	7,245	107%	No slippage at 60% RTS. Conductor broke at south end of splice.
1.4.1	15-kV, 1/0 AWG ACSR	4,263	102%	No slippage at 60% RTS. Conductor pulled out of south dead-end.
1.4.2	15-kV, 1/0 AWG ACSR	4,625	111%	No slippage at 60% RTS. Conductor broke at north end of splice.
1.4.3	15-kV, 1/0 AWG ACSR	4,626	111%	No slippage at 60% RTS. Conductor broke at south dead-end.

Insulator Slip Test

Tabulated results of the insulator slip tests are presented in Table 24. Insulator slip behavior showed a minor dependence on conductor size (i.e., larger diameter conductor generally had a higher maximum load) likely due to increased contact area with the clamping hardware. Additionally, the slip behavior of vise-top and clamp-top insulators was different. Vise-top insulators held the conductor firmly in the plastic inserts, which resulted in deformation of the insulator at the mounting pin, as shown in Figure 66. This created a misalignment between the conductor and the insulator vise top, allowing the conductor to lift out of the plastic insert and start to slip. No damage to the insulator apart from the deformation of the pin was observed after testing. The conductor also remained largely undamaged except for some superficial damage to the polymer sheath, an example of which is shown in Figure 67.

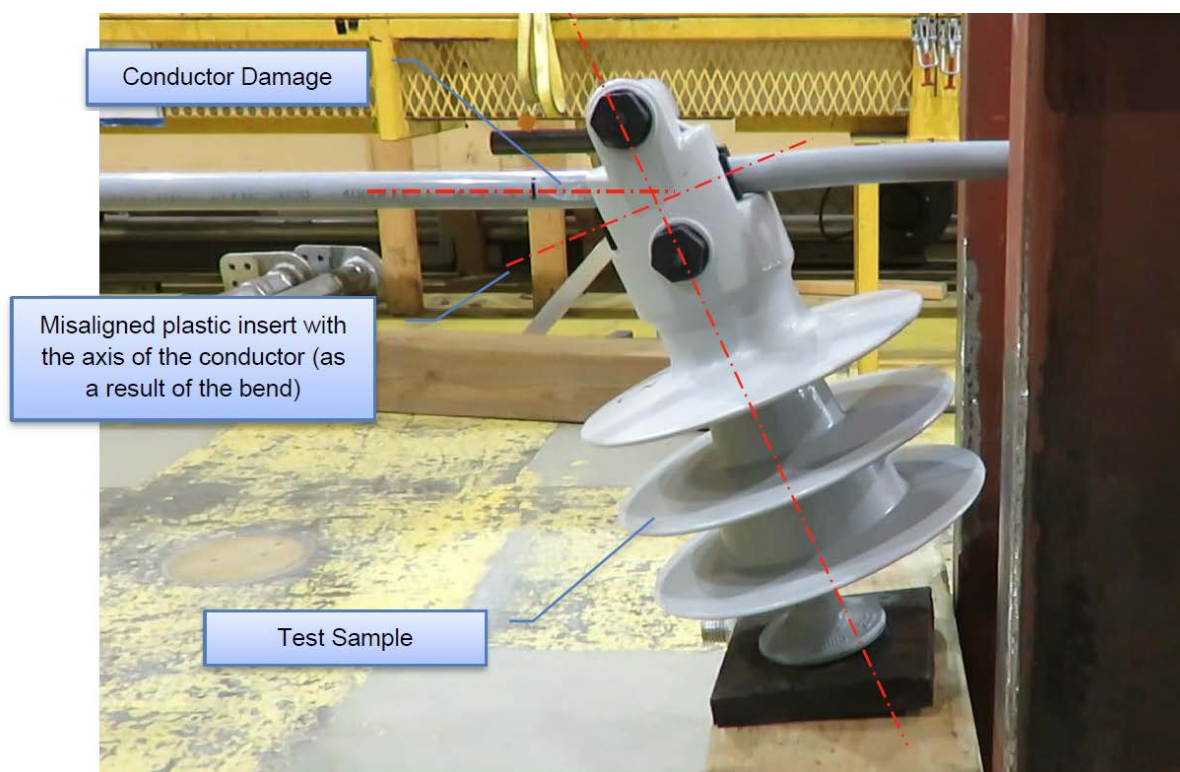


Figure 66. A representative post-test image of a vise-top insulator illustrating the bending behavior of the insulator that leads to conductor slippage (1/0 ACSR).



Figure 67. A representative post-test image of a 17-kV ACSR CC showing superficial damage to the polymer sheath caused by slippage.

Slippage of clamp-top post insulators (tested for the 17-kV and 35-kV ACSR CC only) occurred at significantly lower tensile loads relative to the vise-top pin insulators, with an average maximum load of 355 lb for 17-kV and 442 lb for 35-kV compared with 1,058 lb for 17-kV and 1,014 lb for 35-kV with the vise-top insulators. The mechanism of slippage was also different; despite a moderate forward “bend” during testing, no gross deformation was observed on the insulator or mounting hardware post-test. Rather, the conductors began to slip when tensile loads exceeded the clamping force of the insulator. A representative image illustrating the extent of conductor slippage is shown in Figure 68. No damage to the polymer sheath of the conductor was observed following slippage in the clamp-top insulators. Complete test details, including load versus time plots and photos, can be found in Appendix F.



Figure 68. A representative post-test image of a clamp-top insulator illustrating the extent of conductor slippage (1/0 ACSR).

Table 24. Results of insulator slip tests.

Sample #	Insulator	Conductor Type	Max. Load		Observations
			(lb)	(% RTS)	
2.1.1	Vise-top pin	17-kV, 1/0 AWG ACSR	1090.3	26.2%	Slippage started at 868.8 lb.
2.1.2	Vise-top pin	17-kV, 1/0 AWG ACSR	1040.6	25.0%	Slippage started at 865.5 lb.
2.1.3	Vise-top pin	17-kV, 1/0 AWG ACSR	1043.9	25.1%	Slippage started at 870.2 lb.
2.2.1	Vise-top pin	35-kV, 1/0 AWG ACSR	970.9	23.3%	Slippage started at 879.8 lb.
2.2.2	Vise-top pin	35-kV, 1/0 AWG ACSR	1048.3	25.2%	Slippage started at 862.7 lb.
2.2.3	Vise-top pin	35-kV, 1/0 AWG ACSR	1024.1	24.6%	Slippage started at 872.0 lb.
2.3.1	Vise-top pin	22-kV, 397.5 kcmil AAC	1107.3	16.4%	Minimal slippage before max. load.
2.3.2	Vise-top pin	22-kV, 397.5 kcmil AAC	1195.1	17.7%	Minimal slippage before max. load.
2.3.3	Vise-top pin	22-kV, 397.5 kcmil AAC	1142.9	16.9%	Minimal slippage before max. load.
2.4.1	Vise-top pin	15-kV, 1/0 AWG ACSR	863.3	20.8%	Minimal slippage before max. load.
2.4.2	Vise-top pin	15-kV, 1/0 AWG ACSR	847.4	20.4%	Minimal slippage before max. load.
2.4.3	Vise-top pin	15-kV, 1/0 AWG ACSR	872.6	21.0%	Minimal slippage before max. load.
2K.1.1	Clamp-top post	17-kV, 1/0 AWG ACSR	380.4	9.1%	Slippage started before hold.
2K.1.2	Clamp-top post	17-kV, 1/0 AWG ACSR	391.8	9.4%	Slippage started before hold.
2K.1.3	Clamp-top post	17-kV, 1/0 AWG ACSR	291.9	7.0%	Slippage started before hold.
2K.2.1	Clamp-top post	35-kV, 1/0 AWG ACSR	486.7	11.7%	Slippage started before hold.
2K.2.2	Clamp-top post	35-kV, 1/0 AWG ACSR	393.1	9.4%	Slippage started before hold.
2K.2.3	Clamp-top post	35-kV, 1/0 AWG ACSR	446.7	10.7%	Slippage started before hold.

Full-System Tree-Fall Test

Tabulated results of the full-system tree-fall tests are presented in Table 25. The tree-fall tests all exhibited significant bending/damage to the insulator and cross-arm hardware, or insulator slippage well below the rated tensile strength of the tested CC. Like the insulator slip tests described above, the deformation and slip behavior showed a strong dependence on the insulator type (vise top versus clamp top). Tests with vise-top insulators exhibited no slippage of the conductor in the insulator grip up to the maximum vertical test load, and only superficial marks were observed on the conductor at the grip location after the test (see Figure 69). The steel insulator pin and fiberglass cross-arm deformed significantly under load and retained a permanent deflection after test completion. Additionally, tilting of the steel insulator flange during loading resulted in cracking and damage to the cross-arm at the mounting location, as shown in Figure 70. This cracking eventually led to full splitting of the cross-arm and pull-out of the insulator pin at final failure (Figure 71).



Figure 69. A representative post-test image showing superficial marks on the conductor at the vise-top insulator grip location (17-kV 1/0 ACSR).

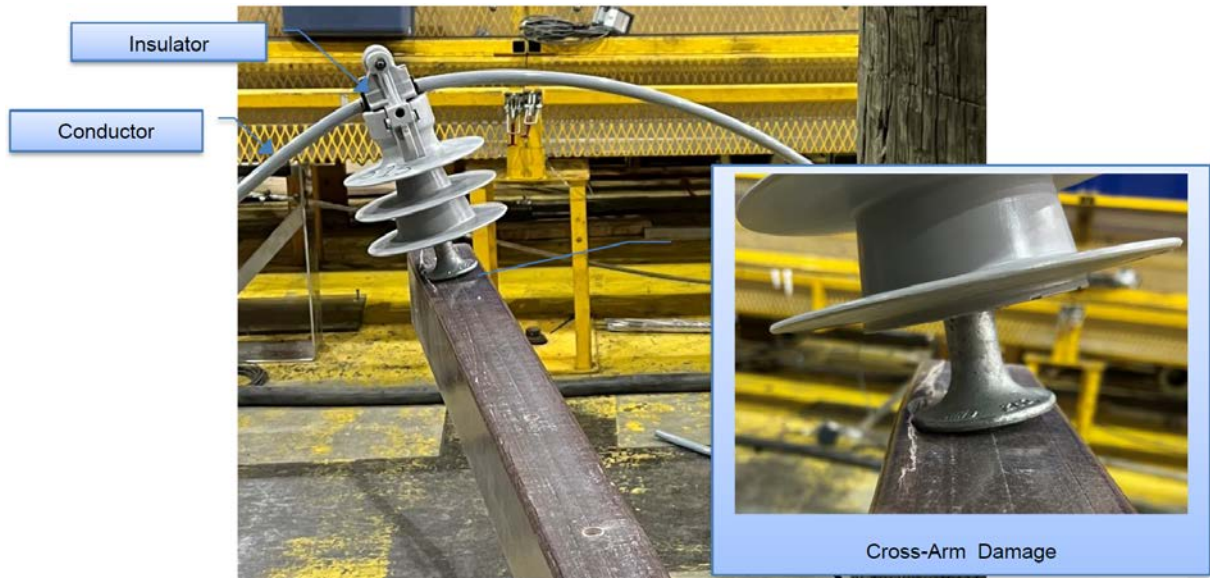


Figure 70. A representative post-test image showing insulator deformation and damage to the cross-arm at its connection point (35-kV 1/0 ACSR).



Figure 71. A representative post-test image showing pull-out of the insulator pin at final failure (17-kV 1/0 ACSR).

Tree-fall tests performed with clamp-top insulators exhibited insulator slippage at relatively low loads between approximately 400 and 700 lb, and none of the tests reached the target load of 1,000 lb. In contrast to the vise-top insulator tests, no bending or other damage was observed on the clamp-top insulators or fiberglass cross-arms, as shown in Figure 72. The moderate forward “bend” observed during insulator slip testing was not observed during the tree-fall tests, likely due to the relative compliance of the cross-arm in this configuration. Additionally, no damage was observed on the conductor polymer sheath post-test. Complete test details, including load vs. time plots and photos, can be found in Appendix F.

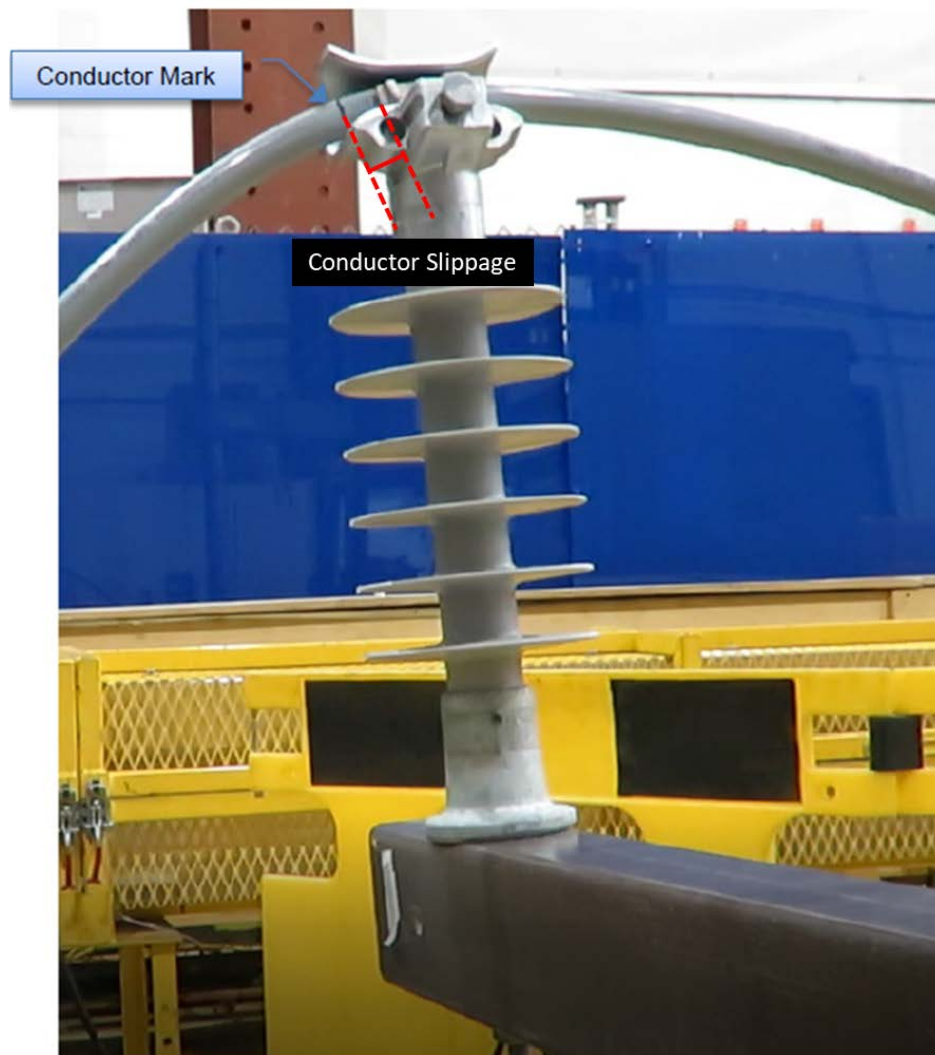


Figure 72. A representative post-test image of a clamp-top insulator tree-fall test (35-kV 1/0 ACSR).

Table 25. Results of full-system tree-fall tests.

Sample #	Conductor Type	Max. Vertical Load	Vertical Deflection of Cross-arm		Observations
		(lb)	West* (in.)	East* (in.)	
3.1.1	17-kV, 1/0 AWG ACSR	939	-2.40	2.30	Cross-arm damaged at insulator flange. No slippage or conductor damage.
3.1.2	17-kV, 1/0 AWG ACSR	1,095	-3.00	2.64	No cross-arm damage, no slippage, no conductor damage.
3.1.3	17-kV, 1/0 AWG ACSR	1,042	-2.36	2.28	Cross-arm damaged at insulator flange. No slippage or conductor damage.
3.2.1	35-kV, 1/0 AWG ACSR	1,063	-1.97	1.65	Cross-arm damaged at insulator flange. No slippage or conductor damage.
3.2.2	35-kV, 1/0 AWG ACSR	985	-2.04	1.97	Cross-arm damaged at insulator flange. No slippage or conductor damage.
3.2.3	35-kV, 1/0 AWG ACSR	1,019	-1.26	1.02	Cross-arm damaged at insulator flange. No slippage or conductor damage.
3.3.1	22-kV, 397.5 kcmil AAC	1,326	-1.93	1.57	Cross-arm damaged at insulator flange. No slippage or conductor damage.
3.3.2	22-kV, 397.5 kcmil AAC	1,060	-1.77	1.61	Cross-arm damaged at insulator flange. No slippage or conductor damage.
3.3.3	22-kV, 397.5 kcmil AAC	988	-2.60	2.40	Cross-arm damaged at insulator flange. No slippage or conductor damage.
3.4.1	15-kV, 1/0 AWG ACSR	880	-0.35	0.35	Cross-arm damaged at insulator flange. No slippage or conductor damage.
3.4.2	15-kV, 1/0 AWG ACSR	1,090	-2.00	1.46	Cross-arm damaged at insulator flange. No slippage or conductor damage.
3.4.3	15-kV, 1/0 AWG ACSR	789	-1.54	1.42	Cross-arm damaged at insulator flange. No slippage or conductor damage.
3K.1.1	17-kV, 1/0 AWG ACSR	573	-1.57	1.57	Conductor slippage at clamp. No damage to cross-arm or conductor.
3K.1.2	17-kV, 1/0 AWG ACSR	396	-0.24	0.24	Conductor slippage at clamp. No damage to cross-arm or conductor.
3K.1.3	17-kV, 1/0 AWG ACSR	508	-0.20	0.12	Conductor slippage at clamp. No damage to cross-arm or conductor.
3K.2.1	35-kV, 1/0 AWG ACSR	555	-0.20	0.16	Conductor slippage at clamp. No damage to cross-arm or conductor.
3K.2.2	35-kV, 1/0 AWG ACSR	548	-0.08	0.04	Conductor slippage at clamp. No damage to cross-arm or conductor.
3K.2.3	35-kV, 1/0 AWG ACSR	693	-0.08	0.04	Conductor slippage at clamp. No damage to cross-arm or conductor.

* "East" and "west" refer to downward deflection on the insulator side of the cross-arm and upward deflection at the free end of the cross-arm, respectively. Negative values are toward the floor.

Discussion and Conclusions: System Strength

The major conclusions from the system strength tests are:

- All tested splices on CCs exceeded 100% of the rated conductor strength, and no conductor slippage was observed prior to failure.
- Insulator slip tests showed distinct slip behavior depending on insulator type. Vise-top pin insulators exhibited bending of the insulator pin and lift-out of the conductor from the plastic insert prior to slippage. Clamp-top post insulators showed slippage at significantly lower tensile loads with no damage to the insulator hardware.
- The full-system tree-fall tests all resulted in significant bending/damage to the insulator and cross-arm hardware or insulator slippage well below the rated tensile strength of the tested CC (i.e., no conductor breakage was observed).
- The failure mode of the tree-fall tests also exhibited a dependence on insulator type. Vise-top insulators showed bending of the insulator pin, permanent deflection of the cross-arm, and cracking/splitting of the cross-arm due to impingement of the insulator mounting flange. Clamp-top insulators showed insulator slippage at lower loads with no accompanying damage to the conductor, insulator, or cross-arm. These results are consistent with observations from the insulator slip tests and suggest that while clamp-top insulators have a lower threshold for conductor slippage, they may be less likely to result in damage to the conductor or supporting structure in the event of a tree fall.
- The tree-fall tests were performed under quasi-static loading conditions (approximately 1,000 lb/min). The dynamic loads experienced during a real-world tree-fall event will depend on many factors, including tree height and weight, as well as crown size and density. Although the strain rate sensitivity of the covered conductor system components is not well understood, the system-level behavior and component interactions observed in these tests give valuable insight into the most likely failure modes for individual pole configurations. Further, these results can be used to inform future modeling efforts to analyze specific scenarios and to study the sensitivity to various structural and environmental factors.

Limitations

At the request of SCE, SDG&E, and PG&E, Exponent has investigated the effectiveness of CCs for overhead distribution systems. Exponent investigated specific issues relevant to this technology, as requested by the three utilities. Not all risks have been investigated as part of this work. The scope of services performed during this investigation may not adequately address the needs of other users of this report, and any reuse of this report or its findings, conclusions, or recommendations presented herein is at the sole risk of the user. The opinions and comments formulated during this assessment are based on observations and information available at the time of the investigation. No guarantee or warranty as to future life or performance of any reviewed condition is expressed or implied.

The findings presented herein are made to a reasonable degree of engineering certainty. We have made every effort to accurately and completely investigate all areas of concern identified during our investigation. If new data become available or there are perceived omissions or misstatements in this report regarding any aspect of those conditions, we ask that they be brought to our attention as soon as possible so we have the opportunity to fully address them.

Appendix A

Methods

Appendix A: Methods

One-Line Diagrams

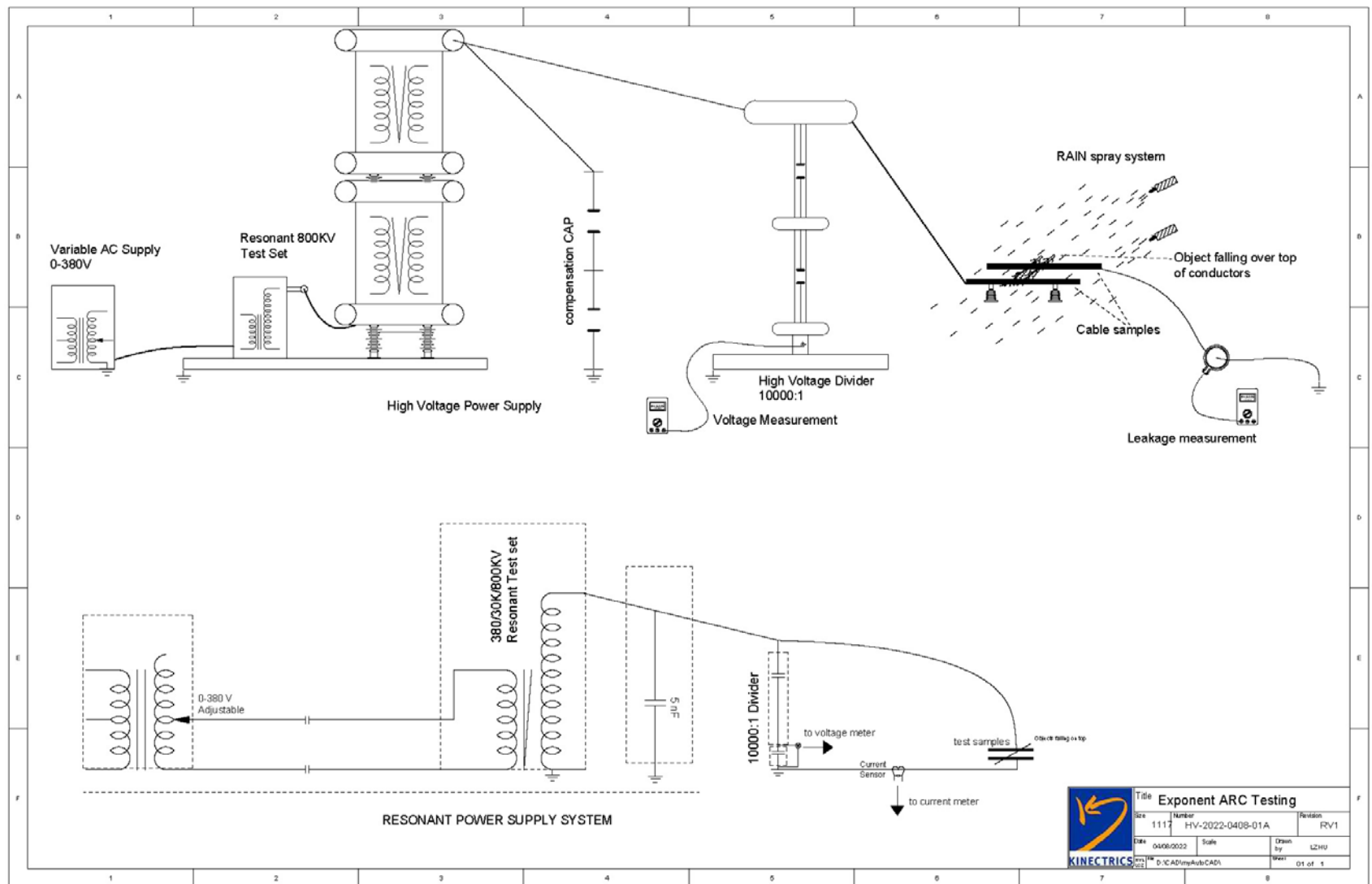


Figure A1. Phase-to-phase contact tests.

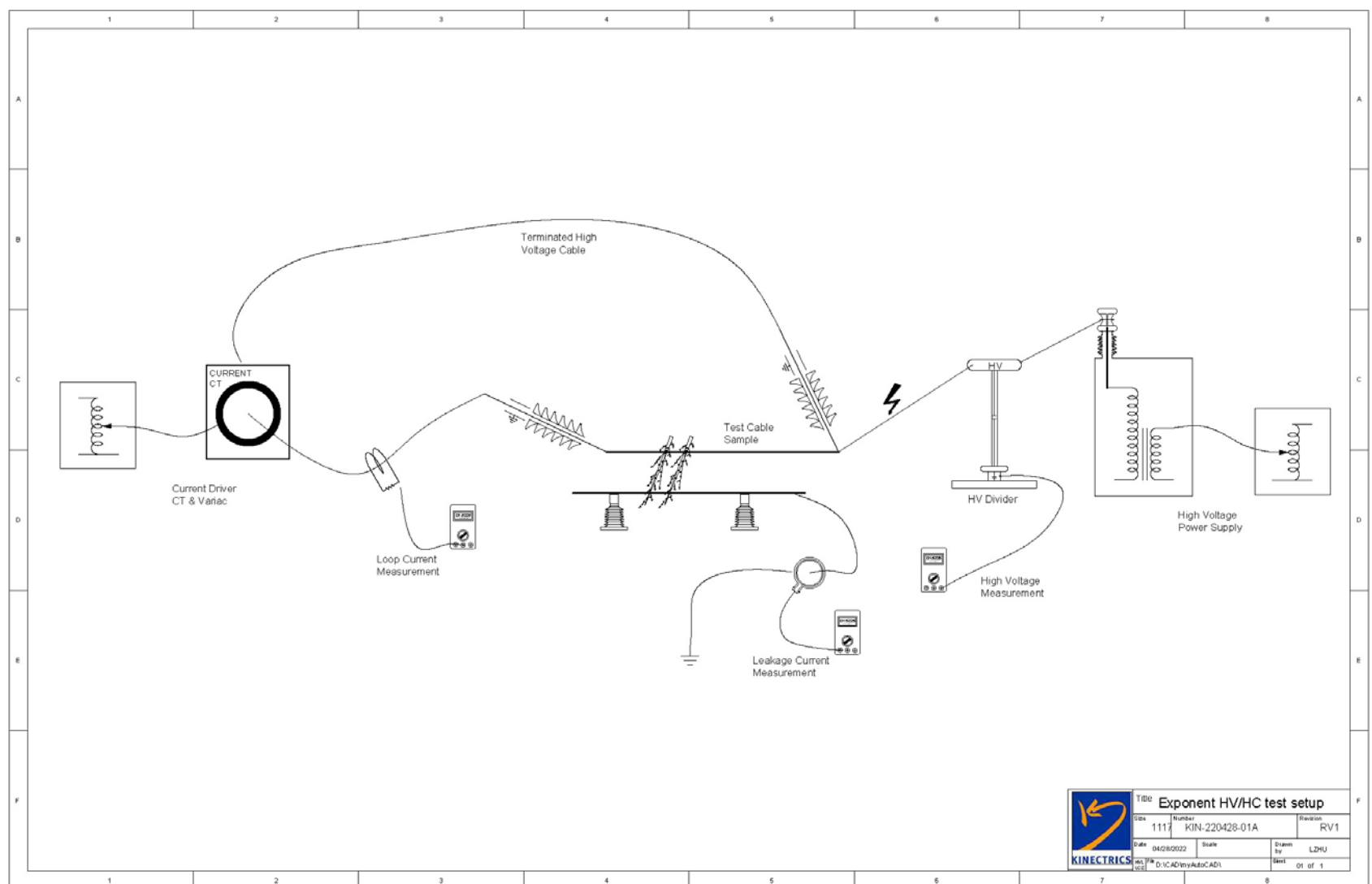


Figure A2. Extended phase-to-phase contact tests.

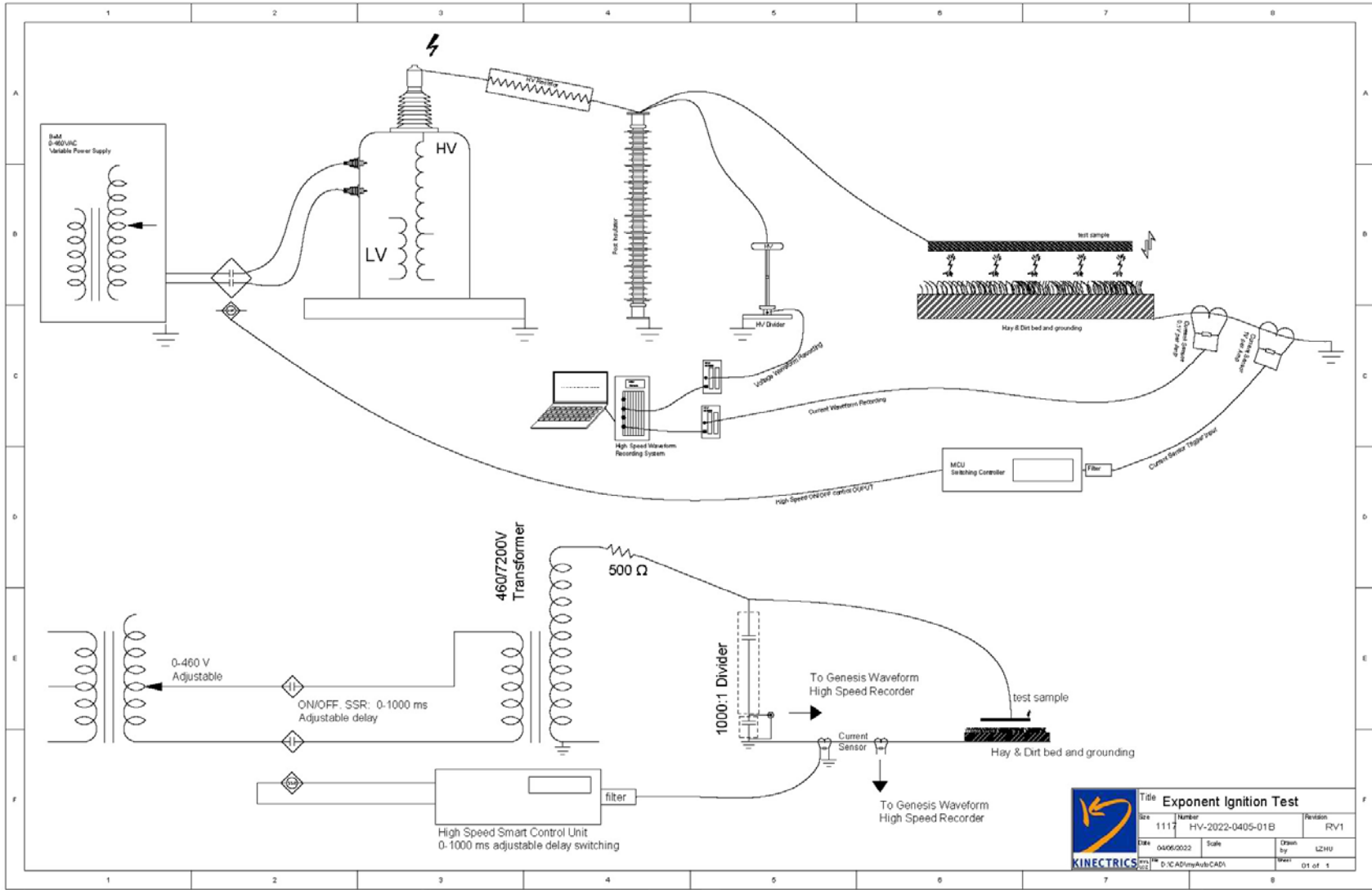


Figure A3. Simulated wire-down tests.

Phase-to-Phase Contact Testing in Wet Conditions



Figure A4. Wet test setup for phase-to-phase contact tests.

Table A1. Precipitation conditions for wet tests met IEEE Standard 4-2013 requirements.

Rain Parameter	Average and Std Dev	IEEE4 Standard
Vertical Rate	1.31 ± 0.20 mm/min	1.0 to 2.0 mm/min
Horizontal Rate	1.47 ± 0.22 mm/min	1.0 to 2.0 mm/min
Water Temperature	19.4 ± 1.2 °C	Ambient ± 15 °C
Water Conductivity	102.0 ± 4.5 μ S/cm	100 ± 15 μ S/cm

Vegetation, Branch Preparation, and Quality Control

Three mature eucalyptus cinerea trees were sourced from Gilroy, California, and were consistently watered with 12 gallons of water per day to maintain their freshness and moisture. Branches were cut into 4.5-foot sections and labeled according to their original position on the tree. Diameter and moisture measurements were made at the cut end and center of each branch. Branch diameters varied from 0.4 inches to 2.28 inches and averaged 1.15 inches.

Immediately after sectioning, the cut ends were painted with Anchor Seal, a water-based emulsion wax sealer used to prevent moisture loss from freshly cut wood. The painted end was then wrapped with industrial plastic wrap and secured with a rubber band. The prepped branches were placed in 100 gallon / 6 mil thick plastic bags. Two 84% relative humidity (RH) humidifier seasoning packets were placed in each bag for humidity control. The air inside was fully evacuated with a vacuum, and the plastic bags were sealed shut with a heat gun. The prepped and sealed branches were placed in a wooden crate and shipped to the high-voltage testing facility. Moisture measurements were repeated upon receipt at the testing lab to ensure that the moisture content of each branch was consistent with live vegetation.



Figure A5. Cutting and preparation of leafy eucalyptus branches for phase-to-phase arc testing.

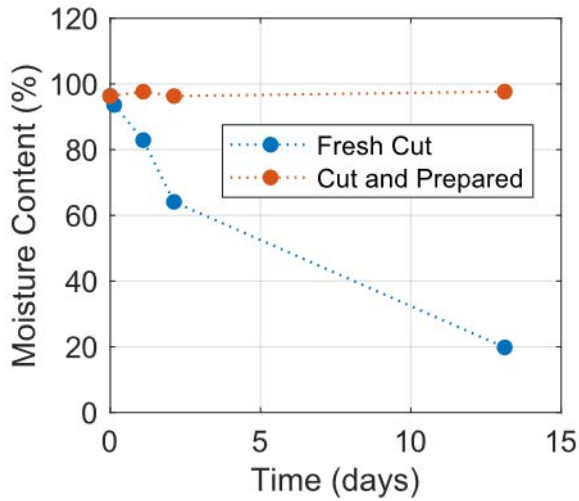


Figure A6. Moisture content as a function of time for a fresh-cut branch and a cut and prepared branch. The fresh-cut branch was exposed to atmosphere and lost 80% of its moisture over 14 days. The prepared branch retained its moisture over 14 days. Moisture meter readings were quantified by comparing to the oven-dry mass.

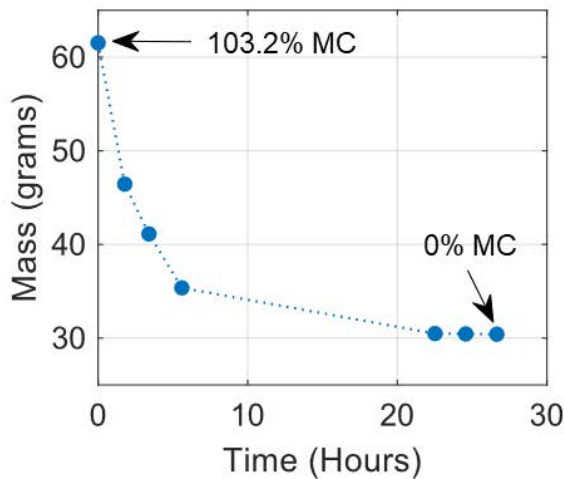


Figure A7. Mass of a fresh-cut branch as a function of time during heating in convection oven at 104° C to oven-dry condition, consistent with ASTM D4442-20.

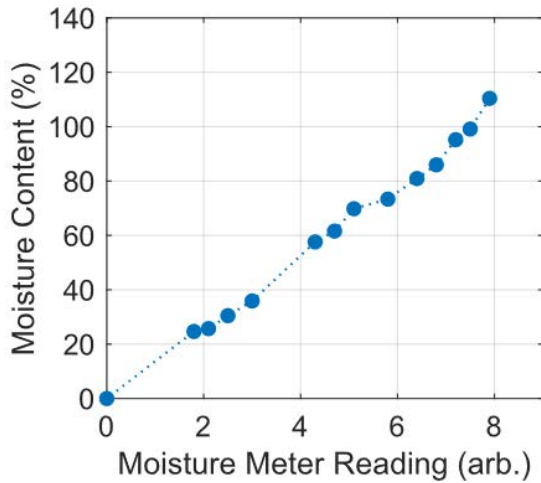


Figure A8. Method for quantifying moisture meter readings and converting to moisture content. The ASTM D4442-20 method of oven-dry mass was used. A fresh branch was cut and weighed, and its moisture content was measured with the moisture meter. The branch was allowed to dry in atmosphere over time. The mass and moisture meter readings were measured over time, until the mass of the branch was constant, indicating that the oven-dry mass was reached. Moisture meter readings above 5 (MC \approx 60%) were considered to be valid for phase-to-phase contact tests.

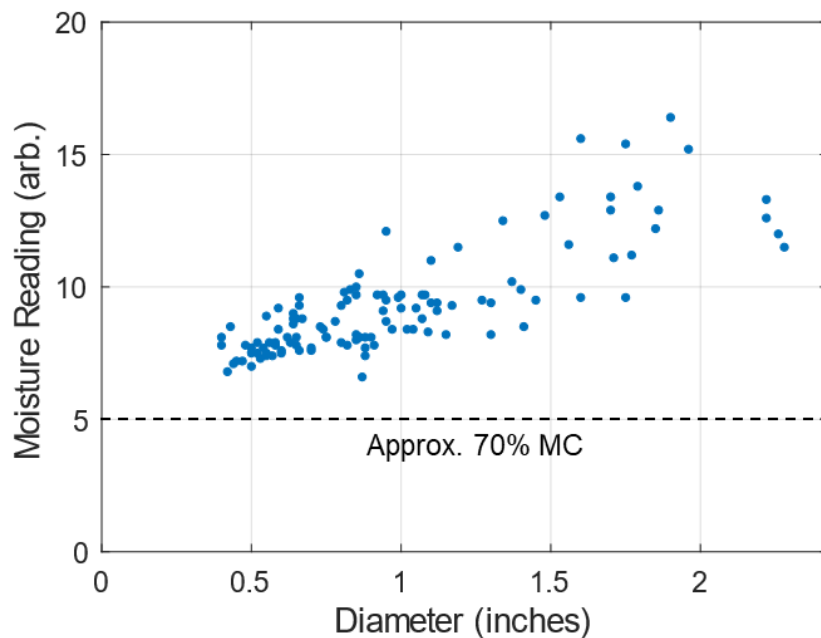


Figure A9. Leafy eucalyptus branch moisture content as a function of branch diameter. As branch diameter increases, moisture content trends upward.

Cyclic Polarization Sample Preparation

To prepare the samples for cyclic polarization testing, CCs and bare conductors were cut into ~4 inch pieces and the polymer sheath was removed from ~2.5 inches of one end of each of the CC samples. Electrical connection was made to each sample using a conductive silver epoxy. Silicone sealant was used to mask the silver epoxy connection and seal over both ends of the conductor. For bare conductors, silicone was applied along an additional length of conductor near the ends to achieve a similar exposed surface area to the exposed surface area of the CCs. Additional control samples were prepared in a similar manner using individual strands of disassembled bare conductors. The strands were polished prior to making electrical connection to minimize any surface scratches or defects to elucidate the electrochemical response of the conductor material without any geometry effects (i.e., without crevices). Figure A10 presents representative images of CCs and bare conductors prepared for cyclic polarization testing. For bare conductors, the length of exposed conductor (i.e., not covered with silicone sealant) for each sample was measured three times and averaged. The exposed conductor surface area of each sample was calculated using the average measured length and assuming the exposed area to be a cylinder. For CCs, because corrosion was observed beneath the polymer sheath, the entire length of the conductor was assumed to be active, but the calculation was otherwise the same. Due to the stranded nature of the conductors, the actual exposed surface areas are somewhat higher than the calculated values. Thus, the reported current densities (current per unit area) should be considered upper bounds. However, as the strand geometries of the CCs should be identical to their bare counterparts, relative comparisons of corrosion susceptibility between bare and CCs can be made.

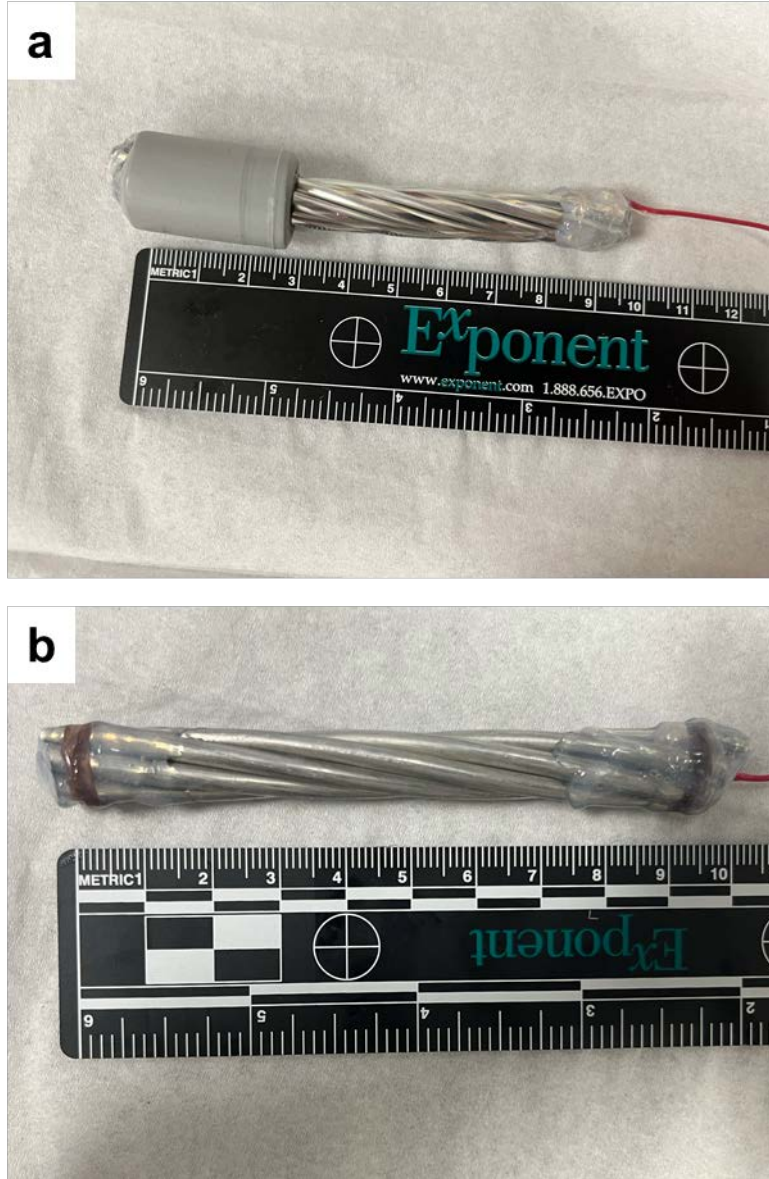


Figure A10. Representative photographs showing (a) CC and (b) bare conductor samples prepared for cyclic polarization testing. Electrical contact was made to one end of the conductor with conductive silver epoxy. The electrical connection and the other exposed end of the conductor were masked with silicone sealant.

Appendix B

Simulated Wire-Down Tests: Additional Figures

Appendix B: Simulated Wire-Down Tests: Additional Figures

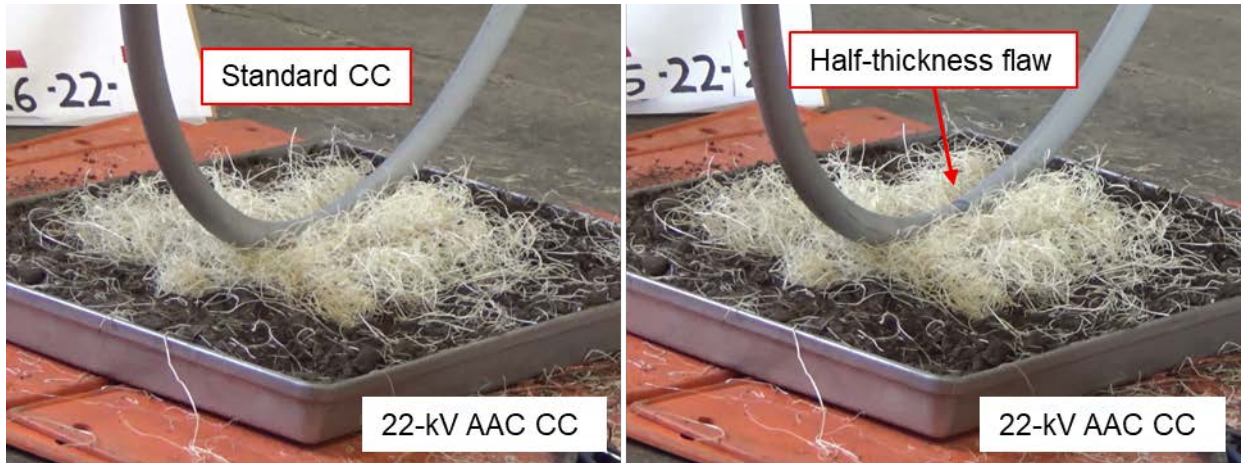


Figure B1. (Left) Simulated wire-down test of a 22-kV AAC CC. No ignition was observed after three tests. (Right) Simulated wire-down test of a 22-kV AAC CC with a half-thickness flaw. No ignition was observed after three tests.



Figure B2. Simulated wire-down test of a bare AAC demonstrating the potential for ignition of the dry brush.

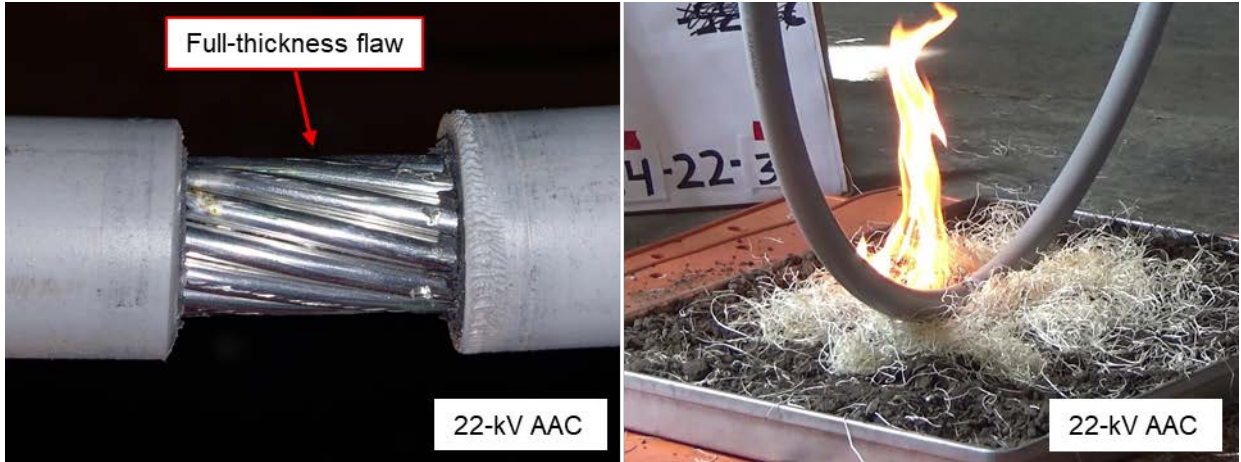


Figure B3. Simulated wire-down test of a 22-kV AAC CC with a full-thickness flaw demonstrating the potential for ignition of the dry brush.



Figure B4. Simulated wire-down test of a 22-kV AAC CC with a broken end demonstrating the potential for ignition of the dry brush.



Figure B5. (Left) Simulated wire-down test of a 15-kV ACSR CC. No ignition was observed after three tests. (Right) Simulated wire-down test of a 15-kV ACSR CC with a half-thickness flaw. No ignition was observed after three tests.

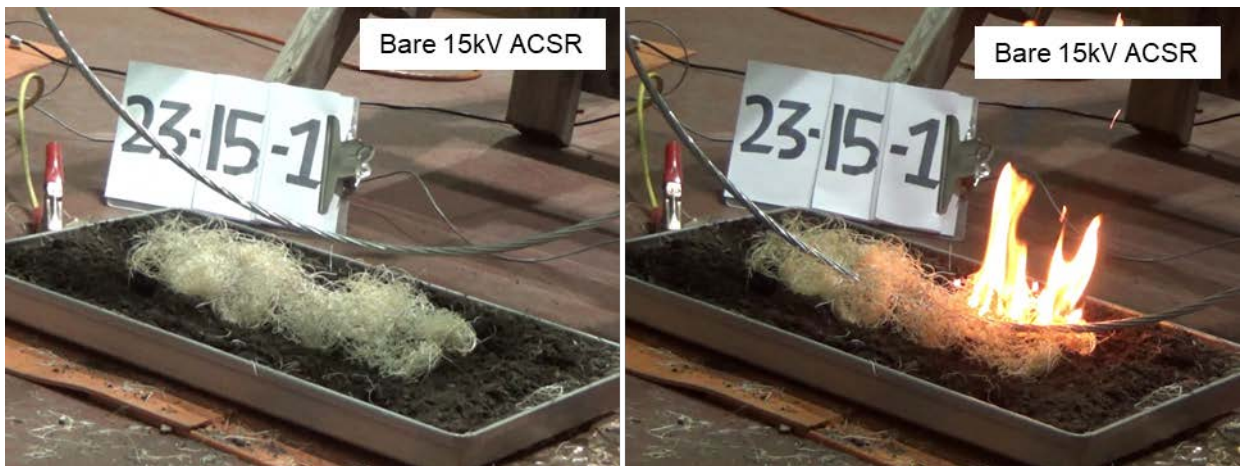


Figure B6. Simulated wire-down test of a bare 15-kV ACSR conductor demonstrating the potential for ignition of the dry brush.

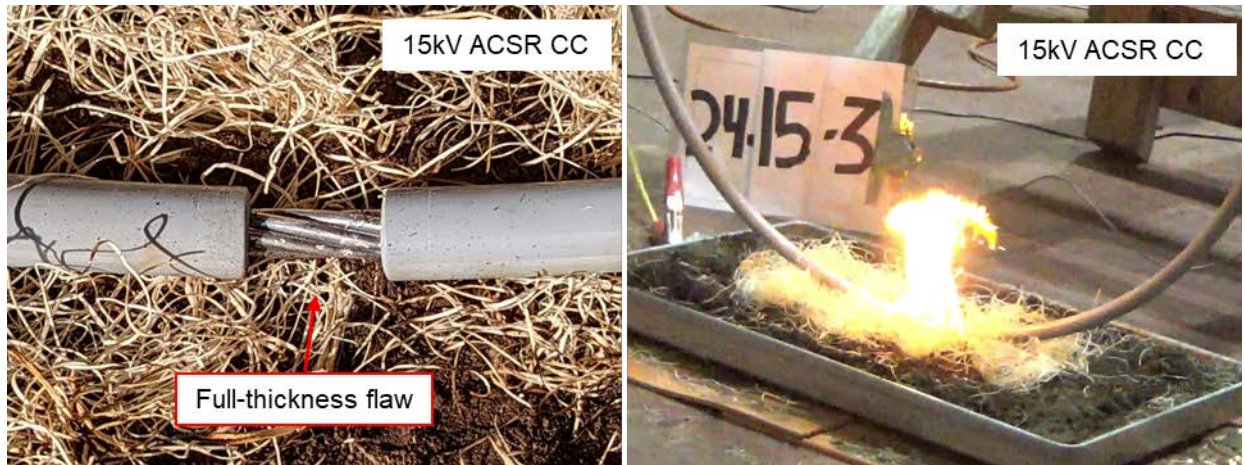


Figure B7. Simulated wire-down test of a 15-kV ACSR CC with a full-thickness flaw demonstrating the potential for ignition of the dry brush.

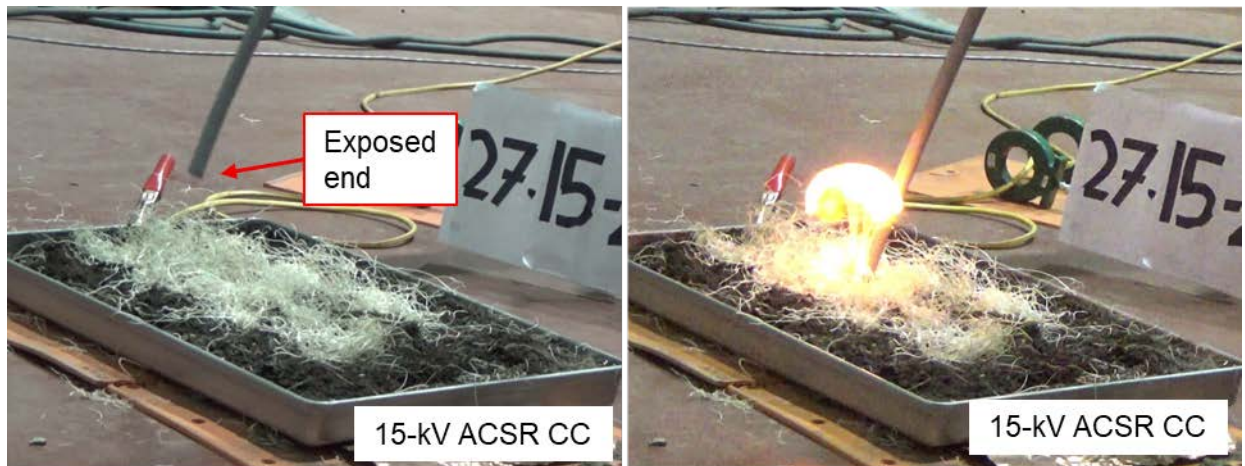


Figure B8. Simulated wire-down test of a 15-kV ACSR CC with a broken end demonstrating the potential for ignition of the dry brush.

Appendix C

Standards and Guidelines

Appendix C: Standards and Guidelines

Standards and Guidelines are listed with the footnote number of their first appearance.

3. California Public Utilities Commission (CPUC) General Order (GO) 95. Section III. Requirements for All Lines.
5. Southern California Edison Covered Conductor Data Sheet for 17-kV and 35 kV. 2020.
10. IEEE Std. 4TM-2013 “IEEE Standard for High Voltage Testing Techniques,” Institute of Electrical and Electronics Engineers, 2013.
20. ICEA T-31-610-2018 “Test Method for Conducting Longitudinal Water Penetration Resistance Tests on Blocked Conductors,” Insulated Cable Engineers Association, 2018.
21. ASTM G85-19 “Standard Practice for Modified Salt Spray (Fog) Testing,” American Society for Testing and Materials, 2019.
26. STM G5-14 “Standard Reference Test Method for Making Potentiodynamic Anodic Polarization Measurements,” American Society for Testing and Materials, 2014.
27. ASTM E1354-17 “Standard Test Method for Heat and Visible Smoke Release Rates for Materials and Products Using an Oxygen Consumption Calorimeter,” American Society for Testing and Materials, 2017
33. ANSI C119.4-2016, “American National Standard for Electric Connectors – Connectors for Use Between Aluminum-to-Aluminum and Aluminum-to-Copper Conductors Designed for Normal Operation at or Below 93C,” Clause 6.2.2.2 (Maximum Load).
34. ANSI C119.0-2015, “American National Standard for Electric Connectors – Testing Methods and Equipment Common to the ANSI C119 Family of Standards.”

Appendix D

Literature References

Appendix D: Literature References

Literature references are listed with the footnote number of their first appearance.

6. McBride, J.R. (2014) The History, Ecology and Future of Eucalyptus Plantations in the Bay Area: A lecture at the Commonwealth Club of San Francisco Understanding Eucalyptus in the Bay Area. San Francisco Forest Alliance.
7. Nance, A. (2014). The Plight of the Eucalyptus Trees in San Francisco: A Case Study on the Values and Considerations Involved in a Decision that Requires Comparative Valuation of Species. *Hastings W.-Nw. J. Env't'l L. & Pol'y*, 20, 429.
8. Dickinson, K. J. M., and J. B. Kirkpatrick. 1985. The flammability and energy content of some important plant species and fuel components in the forests of southeastern Tasmania. *Journal of Biogeography* 12:121-134.
9. Yousefpour, K. "Effect of Ambient Conditions on Insulation Strength of High Voltage Protection Devices." HAL Open Science. 2020.
12. Goodfellow and Appelt. "How Trees Cause Outages." Environmental Consultants, Inc.
15. Marxsen, T. "Powerline Bushfire Safety Program, Vegetation Conduction Ignition Test Report-Final." 2015.
16. R. Storie and W. Weir. "Generalized Soil Map of California." California Agricultural Experiment Station Extension Service.
18. Tony Marxsen. "Ignition Tests – lo-sag conductor." Powerline Bushfire Safety Program. 2015.
24. Refsnæs, S., Magnusson N., Ulleberg T. "Laboratory corrosion tests on overhead line conductors with bird protection systems," *Int. Trans. Electr. Energ. Syst.* 24(2014): 1185.
25. Lequien, F., et al. "Characterization of an aluminum conductor steel reinforced (ACSR) after 60 years of operation." *Engineering Failure Analysis* 120 (2021): 105039.28. Butler, B., et al. "Measurements of radiant emissive power and temperatures in crown fires." *Canadian Journal of Forest Research* (2004): 1577-1587.
29. Morandini, F., et al. "Fire spread experiment across Mediterranean shrub: Influence of wind on flame front properties." *Fire Safety Journal* 41 (2006) 229-235.
30. Silvani, X., and Morandini, F. "Fire spread experiments in the field: Temperature and heat fluxes measurements." *Fire Safety Journal* 44 (2009) 279-285.
31. Frankman, D., et al. "Measurements of convective and radiative heating in wildland fires." *International Journal of Wildland Fire* 22.2 (2013): 157-167.

Appendix E

SCE Covered Conductor Dead-End Strength Testing

Appendix E: SCE Covered Conductor Dead-End Strength Testing

Scope

Mechanical strength testing of covered conductor dead-end assemblies provided by SCE was performed to understand the failure behavior of a typical dead-end configuration. This testing was intended to simulate the response of a full dead-end “system” (i.e., cross-arm, insulator, dead-end clamp, and CC) if a tree were to fall into a span. Both load and failure behavior were recorded.

Experimental Setup

Test Setup and Equipment

Tests were performed using a total of seven conductor/dead-end clamp combinations provided by SCE, as shown in Table E1. Dead-end suspension insulators and composite cross-arms, also provided by SCE, were held constant for all tests. The cross-arm assemblies were mounted with standard hardware to simulate a realistic distribution pole configuration. Initial testing using a wood pole stub resulted in failure of the pole itself as the mounting plate tilted and impinged on the pole (see results section for more details). This failure mode is thought to be unique to the test setup, as the available pole was old, dry, and had been drilled many times, compromising its integrity. A steel plate fixture was substituted for the pole to eliminate this issue in subsequent tests.

Table E1. Conductor and hardware combinations used for dead-end testing.

Sample ID	Conductor	Conductor RTS (lb)*	Dead-End	Insulator	Cross-Arm
1	#2 CU (7 HDCU)	2,898	Type A	15 kV DE suspension	10 ft
2	2/0 CU (19 HDCU)	5,634	Type A	15 kV DE suspension	10 ft
3	4/0 CU (19 HDCU)	8,702	Type A	15 kV DE suspension	10 ft
4	1/0 ACSR (6/1)	4,160	Type A	15 kV DE suspension	10 ft
5	336.4 kcmil ACSR (18/1)	8,246	Type B	15 kV DE suspension	10 ft
6	336.4 kcmil ACSR (30/7)	16,435	Type C	15 kV DE suspension	10 ft
7	653.9 kcmil ACSR (18/3)	14,060	Type D	15 kV DE suspension	10 ft

* Conductor rated tensile strength (RTS) values were obtained from SCE Specification MS-0511-2020 Rev. 1.

The tests were performed in a hydraulic horizontal test machine, and matching dead-ends were used to terminate the free ends of the conductor. A pulley system was implemented to induce a vertical loading component at the cross-arm, and a load cell was attached to the pulley adjacent to the cross-arm to measure vertical loads. The deflection angles of the conductor on either side of the pulley were dependent on the test configuration and are reported in the results table below (Table E2). A schematic diagram and representative photo of the test setup are shown in Figure E1 and Figure E2, respectively.

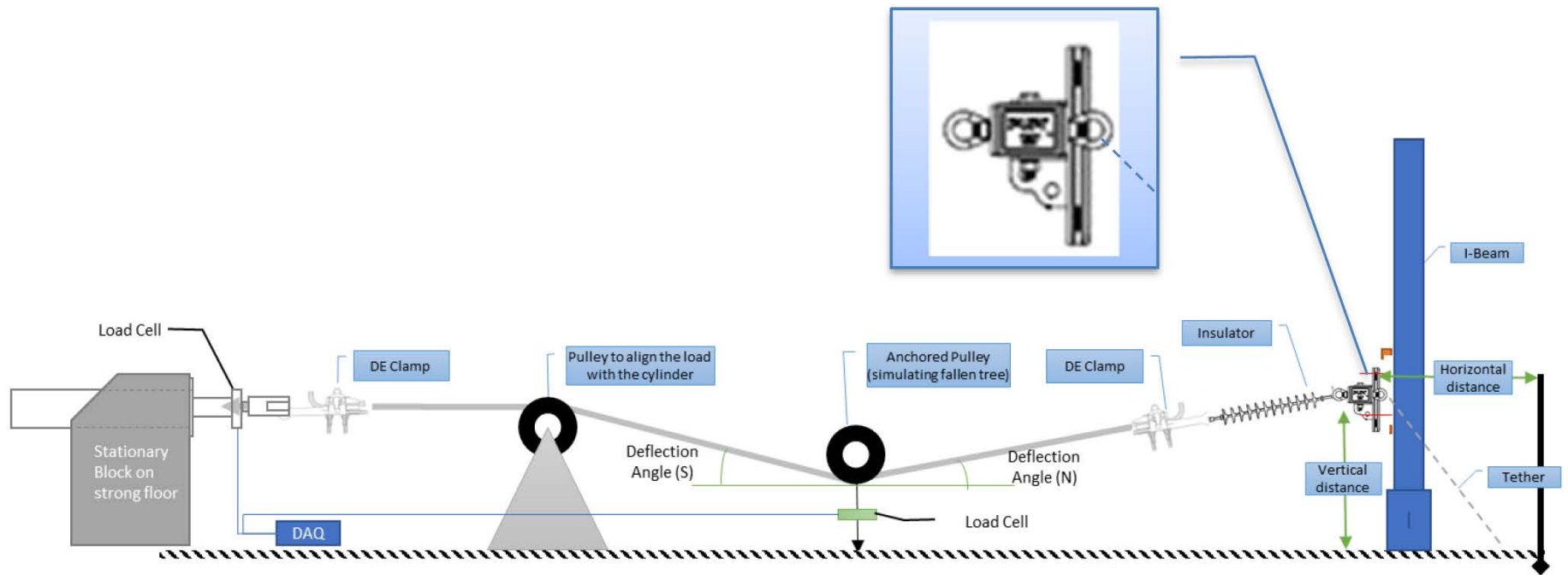


Figure E1. Schematic diagram of the dead-end tree fall test. The hydraulic actuator is located on the south end (left), and the cross-arm is located on the north end (right).

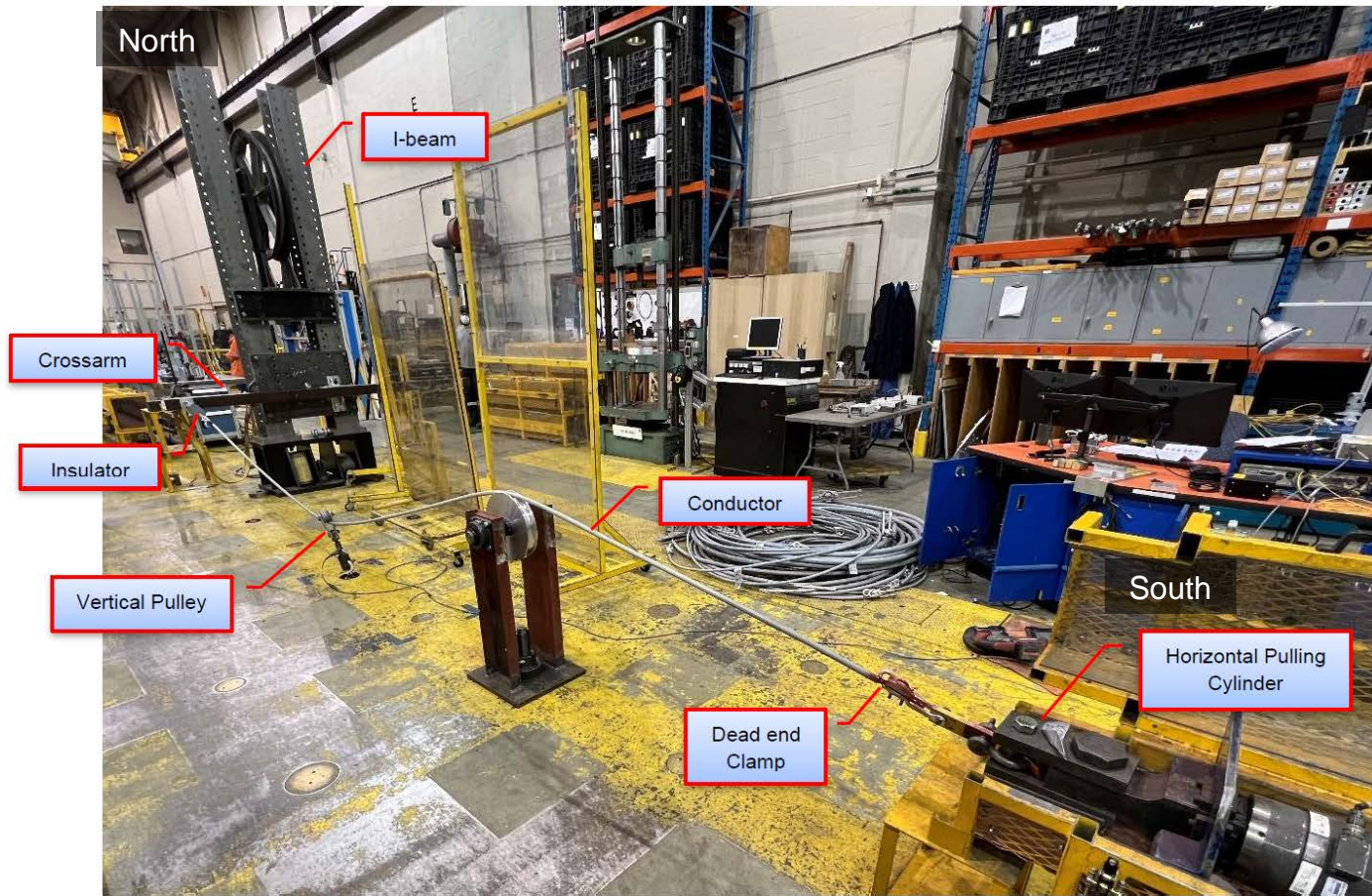


Figure E2. A representative photo of the dead-end tree fall test.

Testing Procedure

The test system including conductor, dead-end clamp, insulator, and cross-arm is shown in Figure E2. A small pre-tension was applied to remove the slack from the conductor, and the conductor was marked at the dead-end clamp entry points to monitor for slippage. The horizontal load was continuously increased at a rate of 1,000 lb/min until failure occurred. Vertical loads at the hydraulic cylinder and at the pulley attached to the floor were monitored throughout the test.

Results

Tabulated results of the dead-end tree-fall tests are presented in Table E2. For smaller size conductors (#2 Cu, 2/0 CU, 4/0 Cu, and 1/0 ACSR), failure occurred as a result of the conductor slipping out of the dead-end clamp (see Figure E3). For conductors with higher RTS (336.4 kcmil and 653.9 kcmil ACSRs), the typical failure point was the cross-arm. The failure of the cross-arm started at the bolts connecting the cross-arm to the mounting plate (see Figure E4). Deformation of the cross-arm mounting plate occurred in all instances, regardless of final failure mode. A representative image of the mounting plate deformation is shown in Figure E5. The deformation behavior of the mounting plate was likely influenced by the rigid fixturing method employed here; a standard wood pole may reduce the magnitude of the plate deformation. Complete test details, including load versus time plots and photos, can be found in Appendix F.

Table E2. Results of dead-end tree-fall tests.

Sample #	Conductor	Dead-End Hardware	Max. Vertical Load	Deflection Angle*		Observations
			(lb)	South (°)	North (°)	
1.1	#2 CU	Type A	1443	15.1	12.4	Conductor broke at south* dead-end; deformed cross-arm mounting plate.
1.2	#2 CU		1365	15.3	11.9	Conductor pulled out of south* dead-end; deformed cross-arm mounting plate.
1.3	#2 CU		1352	15.7	12.2	Conductor pulled out of south* dead-end; deformed cross-arm mounting plate.
2.1	2/0 CU		567	16.3	15.0	Conductor pulled out of north* dead-end; deformed cross-arm mounting plate.
2.2	2/0 CU		767	16.0	14.6	Conductor pulled out of south* dead-end; deformed cross-arm mounting plate.
2.3	2/0 CU		1375	16.9	16.8	Conductor pulled out of south* dead-end; deformed cross-arm mounting plate.
3.1	4/0 CU		693	17.0	12.3	Conductor pulled out of north* dead-end; deformed cross-arm mounting plate.
3.2	4/0 CU		1503	15.9	11.4	Conductor pulled out of south* dead-end; deformed cross-arm mounting plate.
3.3	4/0 CU		1509	17.0	16.0	Conductor pulled out of south* dead-end; deformed cross-arm mounting plate.
4.1	1/0 ACSR (6/1)		1776	15.8	13.5	Cross-arm fractured at center bolt. No conductor slippage at clamp.
4.2	1/0 ACSR (6/1)		1410	15.5	13.4	Conductor pulled out of north* dead-end; deformed cross-arm mounting plate.
4.3	1/0 ACSR (6/1)		1418	16.8	15.6	Conductor pulled out of south* dead-end; deformed cross-arm mounting plate.
5.1	336.4 kcmil ACSR (18/1)		Type B	1739	14.5	16.4
5.2	336.4 kcmil ACSR (18/1)	1771		16.5	12.3	Complete cross-arm failure. No conductor slippage at clamp.
5.3	336.4 kcmil ACSR (18/1)	1720		16.6	12.6	Complete cross-arm failure. No conductor slippage at clamp.
6.1	336.4 kcmil ACSR (30/7)	Type C	1628	16.1	13.2	Complete cross-arm failure. No conductor slippage at clamp.
6.2	336.4 kcmil ACSR (30/7)		1831	15.9	12.4	Complete cross-arm failure. No conductor slippage at clamp.
6.3	336.4 kcmil ACSR (30/7)		1786	16.2	12.0	Complete cross-arm failure. No conductor slippage at clamp.
7.1	653.9 kcmil ACSR (18/3)	Type D	2130	17.1	17.3	Complete cross-arm failure. No conductor slippage at clamp.
7.2	653.9 kcmil ACSR (18/3)		1973	17.2	14.6	Complete cross-arm failure. No conductor slippage at clamp.
7.3	653.9 kcmil ACSR (18/3)		1858	17.3	13.2	Complete cross-arm failure. No conductor slippage at clamp.

* North dead-end was attached to the insulator and cross-arm. South dead-end was attached to the hydraulic actuator.



Figure E3. A representative post-test image showing pull-out of the conductor at the dead-end clamp attached to the insulator (north end). 2/0 CU with Type A dead-end shown.



Figure E4. A representative post-test image showing splitting and failure of the composite cross-arm. 336.4 kcmil ACSR (30/7) with Type C dead-end shown.



Figure E5. A representative post-test image showing typical deformation of the cross-arm mounting plate.

Discussion and Conclusions: System Strength

The major conclusions from the system strength tests are:

- For smaller size conductors (#2 Cu, 2/0 CU, 4/0 Cu, and 1/0 ACSR), failure occurred as a result of the conductor slipping out of the dead-end clamp.
- For conductors with higher RTS (336.4 kcmil and 653.9 kcmil ACSRs), the typical failure point was the cross-arm. The failure of the cross-arm started at the bolts attaching the cross-arm to the mounting plate.
- Deformation of the cross-arm mounting plate occurred in all instances, regardless of final failure mode. The deformation behavior of the mounting plate was likely influenced by the rigid fixturing method employed in this testing; a standard wood pole may reduce the magnitude of the plate deformation.
- The tree-fall tests were performed under quasi-static loading conditions (approximately 1,000 lb/min). The dynamic loads experienced during a real-world tree-fall event will depend on many factors, including tree height and weight, as well as crown size and density. Although the strain rate sensitivity of the covered conductor system components is not well understood, the system-level behavior and component interactions observed in these tests give valuable insight into the most likely failure modes for individual pole configurations. Further, these results can be used to inform future modeling efforts to analyze specific scenarios and to study the sensitivity to various structural and environmental factors.

Appendix F

Kinectrics Mechanical Testing Reports



NOTE: Component manufacturer information has been redacted from this report.


MECHANICAL TESTING OF SPLICE CONNECTORS AND PIN INSULATOR CLAMPS FOR 1/0 AWG ACSR AND 397.5 KCMIL AAC COVERED CONDUCTORS

K-580740-RP-001 R00

Prepared for

Exponent

Purchase Order No. 00062928

<p>Prepared by</p> <p> Digitally signed by GORJA Genti Date: 2022.10.03 14:22:57 -04'00'</p> <p><i>Signature & Date</i></p> <p>Genti Gorja P.Eng. Principal Engineer Line Asset Management</p>	<p>Reviewed by</p> <p> Digitally signed by André Maurice Date: 2022.10.03 14:29:28 -04'00'</p> <p><i>Signature & Date</i></p> <p>André Maurice Service Line Manager Line Asset Management</p>	<p>Approved by</p> <p>PETER Zsolt  Digitally signed by PETER Zsolt Date: 2022.10.03 14:53:20 -04'00'</p> <p><i>Signature & Date</i></p> <p>Zsolt Peter Ph.D. Business Area Director Line Asset Management</p>
---	--	---

Revision History

Rev 00	Description: Original issue			
	Issue Date: 2022-09-28	Prepared by: Genti Gorja	Reviewed by: André Maurice	Approved by: Zsolt Peter

DISCLAIMER

Kinectrics prepared this report as a work of authorship sponsored by their client. This report has been prepared solely for the benefit of the Client and may not be used or relied upon in whole or in part by any other person or entity without Client permission or without Kinectrics' permission if required by the Contract between Client and Kinectrics Inc. . Neither Kinectrics, their client nor any person acting on behalf of them: (a) makes any warranty or representation whatsoever, express or implied, or assumes any legal liability of responsibility for any third party's use, or the results of such use, with respect to (i) the use of any information, apparatus, method, process, or similar item disclosed in this report including the merchantability or fitness for any particular purpose of any information contained in this report or the respective works or services supplied or performed or (ii) that such use does not infringe on or interfere with privately owned rights, including any party's intellectual property; or (b) assumes responsibility for any damages or other liability whatsoever (including any consequential damages resulting from a third party's selection or use of this report or any information, apparatus, method, process, or similar item disclosed).

Copyright © Kinectrics Inc. 2022. All rights reserved.



Table of Contents

1	Executive Summary	4
2	Test Objective and Test Standard	5
3	Test Sample.....	5
3.1	Test Conductor	6
3.2	Test Connectors and Installation Procedure.....	7
4	Test Setup	8
5	Test Procedure	10
6	Test Results.....	10
7	Acceptance Criteria.....	20
8	Conclusion	20
Appendix A	Acronyms and Abbreviations	21
Appendix B	Product Specification of Splices	22
Appendix C	Conductor Data Sheet (<i>as provided by Exponent</i>).....	28
Appendix D	Instrument Sheet.....	30
Appendix E	Kinectrics ISO 9001 Certificate of Registration	31
Appendix F	Distribution	32

1 Executive Summary

This report describes the mechanical test program conducted for Exponent™ to evaluate the performance of splice connectors designed to be used with 15 kV 1/0 AWG ACSR covered conductor, 17 kV 1/0 AWG ACSR covered conductor, 35 kV 1/0 AWG ACSR covered conductor and 22 kV 397.5 kcmil AAC covered conductor.

The test were conducted in accordance with client’s requirements as outlined in the relevant sections of this document. The test program and completion dates are summarized in Table 1-1.

Table 1-1: Test Program

Test ID	Sample ID	Conductor	Splice	Date Completed	
Maximum Load Test on the Splice	1.1	1.1.1	17 kV 1/0 AWG ACSR	██████████	June 2, 2022
		1.1.2	17 kV 1/0 AWG ACSR	██████████	June 3, 2022
		1.1.3	17 kV 1/0 AWG ACSR	██████████	June 2, 2022
	1.2	1.2.1	35 kV 1/0 AWG ACSR	██████████	May 19, 2022
		1.2.2	35 kV 1/0 AWG ACSR	██████████	May 26, 2022
		1.2.3	35 kV 1/0 AWG ACSR	██████████	June 3, 2022
	1.3	1.3.1	22 kV 397.5 kcmil AAC	██████████	May 16, 2022
		1.3.2	22 kV 397.5 kcmil AAC	██████████	May 18, 2022
		1.3.3	22 kV 397.5 kcmil AAC	██████████	May 18, 2022
	1.4	1.4.1	15 kV 1/0 AWG ACSR	██████████	August 26, 2022
		1.4.2	15 kV 1/0 AWG ACSR	██████████	August 26, 2022
		1.4.3	15 kV 1/0 AWG ACSR	██████████	August 26, 2022

Exponent supplied samples and accessories required for testing. Kinectrics received all connectors and conductor assemblies, in good condition, on May 2, 2022.

Except for installation of ██████████, which was supplied pre-installed on conductor, the installation of the splice connectors on conductor and the test setup were performed by Kinectrics personnel.

The tests were performed by Kinectrics personnel at 800 Kipling Avenue, Toronto, Ontario, M8Z 5G5, Canada. The work was conducted under Exponent Purchase Order No. 00062928 dated January 14, 2022.

The tests were performed under Kinectrics’ ISO 9001 Quality Management System. A copy of ISO 9001 Certificate of Registration is included in Appendix E.

2 Test Objective and Test Standard

A Maximum Load Test was performed to verify the tensile strength of the connector/conductor assembly. The test was performed in general accordance with the procedures outlined in the following standards:

ANSI C119.4-2016, “*American National Standard for Electric Connectors – Connectors for Use Between Aluminum-to-Aluminum and Aluminum-to-Copper Conductors Designed for Normal Operation at or Below 93°C and Copper-to-Copper Conductors Designed for Normal Operation at or Below 100°C*”, Clause 6.2.2.2 (Maximum Load)

ANSI C119.0-2015, “*American National Standard for Electric Connectors – Testing Methods and Equipment Common to the ANSI C119 Family of Standards*”.

A five (5) minute hold at 60% of conductor’s Rated Tensile Strength (RTS) was introduced during the loading sequence to evaluate the performance of connectors under sustained (design) load.

3 Test Sample

A total of twelve (12) samples were tested. All test samples consisted of two (2) lengths of covered conductor, joined by a splice and terminated with epoxy dead-end or bolted dead-end clamp at the free ends of the conductor.

A schematic of a typical test sample is shown in Figure 3-1 and a summary of the test samples configuration is shown Table 3-1.

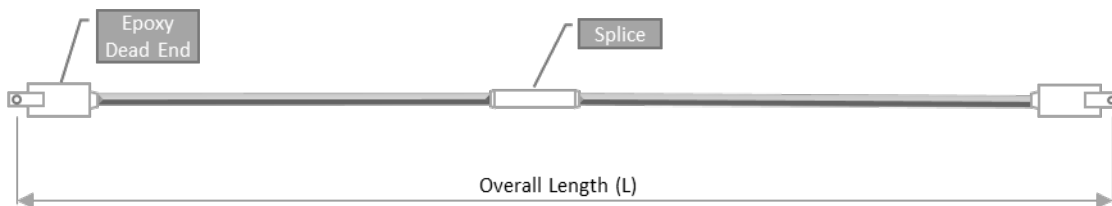


Figure 3-1: Schematic of Typical Test Sample for Maximum Load Test

Table 3-1: Test Sample Configuration

Sample No.	Connector Identification		Conductor Size (AWG or kcmil)	Overall Length [ft]
	Dead-end	Splice		
1.1.1	Epoxy Resin	██████████	17 kV, 1/0 AWG ACSR	44
1.1.2	Epoxy Resin	██████████	17 kV 1/0 AWG ACSR	44
1.1.3	Epoxy Resin	██████████	17 kV 1/0 AWG ACSR	44
1.2.1	Epoxy Resin	██████████	35 kV 1/0 AWG ACSR	44
1.2.2	Epoxy Resin	██████████	35 kV 1/0 AWG ACSR	44
1.2.3	Epoxy Resin	██████████	35 kV 1/0 AWG ACSR	44
1.3.1	Epoxy Resin	██████████	22 kV 397.5 kcmil AAC	44
1.3.2	Epoxy Resin	██████████	22 kV 397.5 kcmil AAC	44
1.3.3	Epoxy Resin	██████████	22 kV 397.5 kcmil AAC	44
1.4.1	Bolted Clamp ASO 398	██████████	15 kV, 1/0 AWG ACSR	12
1.4.2	Bolted Clamp ASO 398	██████████	15 kV 1/0 AWG ACSR	12
1.4.3	Bolted Clamp ASO 398	██████████	15 kV 1/0 AWG ACSR	12

3.1 Test Conductor

All test conductors used to prepare the test samples, comprised of a concentrically stranded conductor (1/0 AWG ACSR or 397.5 kcmil AAC) covered with a thin semi-conducting layer, a crosslinked low-density polyethylene (XL-LDPE) inner layer and a high-density XL-HDPE outer layer (see Figure 3-2).

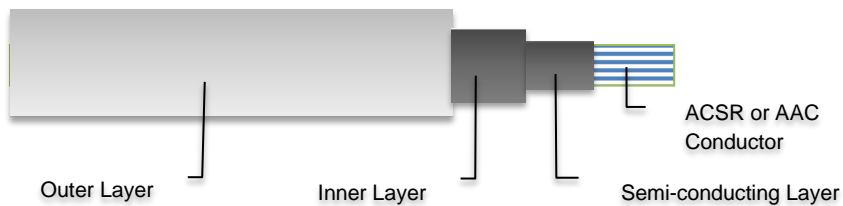


Figure 3-2: Schematic of Covered Conductor

The main conductor properties, as provided by Exponent, are shown in Table 3-2. See Appendix C for complete conductor data sheets.

Table 3-2: Test Conductor Main Characteristics

Conductor Description	Conductor Diameter [in]	Covering Thickness [mils]			Maximum Overall Diameter [in]	RTS [lb]
		Semi-conducting Layer	Inner Layer	Outer Layer		
██████ - 15 kV 1/0 AWG, 6/1 st. ACSR covered conductor	0.398	15	75	75	0.748	4,160
██████ - 17 kV 1/0 AWG, 6/1 st. ACSR covered conductor	0.398	15 - 25	75	75	0.748	4,160
██████ - 35 kV 1/0 AWG, 6/1 st. ACSR covered conductor	0.398	15 - 25	175	125	1.048	4,160
██████ - 22 kV 397.5 kcmil, 19 st. AAC covered conductor	0.723	25	75	75	1.074	6,754

3.2 Test Connectors and Installation Procedure

Test connectors are rated Class 1 in accordance with ANSI C119.4 and are identified as follows:

- ██████ for 17 kV 1/0 AWG ACSR covered conductor
- ██████ for 35 kV 1/0 AWG ACSR covered conductor
- ██████ for 22 kV 397.5 kcmil AAC covered conductor
- ██████ for 15 kV 1/0 AWG ACSR covered conductor

The installation of the ██████ splices was carried out by Kinectrics personnel using ██████ hydraulic crimping tool and ██████ dies U247 (for ██████) and U468 (for ██████). Note that the installation of the ██████ on 1/0 AWG ACSR resulted in significant bird-caging of the conductor on both ends of the splice (see Figure 3-3).

The ██████ was provided pre-installed on conductor by San Diego Gas & Electric (SDG&E).



Figure 3-3: ██████ installed on 35 kV 1/0 AWG, 6/1 ACSR



Figure 3-4: [REDACTED] Installed on 22 kV 397.5 kcmil, 19 strands AAC



Figure 3-5: [REDACTED] Installed on 15 kV 1/0 AWG, 6/1 ACSR

The insulating cover on the connectors was not installed as it was deemed not to affect the mechanical strength of the splice and would prevent observing slippage on the conductor at the ends of the splice.

Kinectrics personnel prepared and installed the epoxy resin dead-end fittings used to terminate the free ends of the conductor. The length of the exposed conductor between the splice and the epoxy dead-end was greater than 24 inches as recommended in Table 12 of ANSI C119.0-2015 (see Table 3-1 for actual lengths).

Product Specifications for all splices, as supplied by Exponent, are shown in Appendix B.

4 Test Setup

The Maximum Load Test was performed in a hydraulically-activated horizontal test machine. A schematic for the Maximum Load Test is shown in Figure 4-1 and representative picture of the typical setup is shown in Figure 4-2.

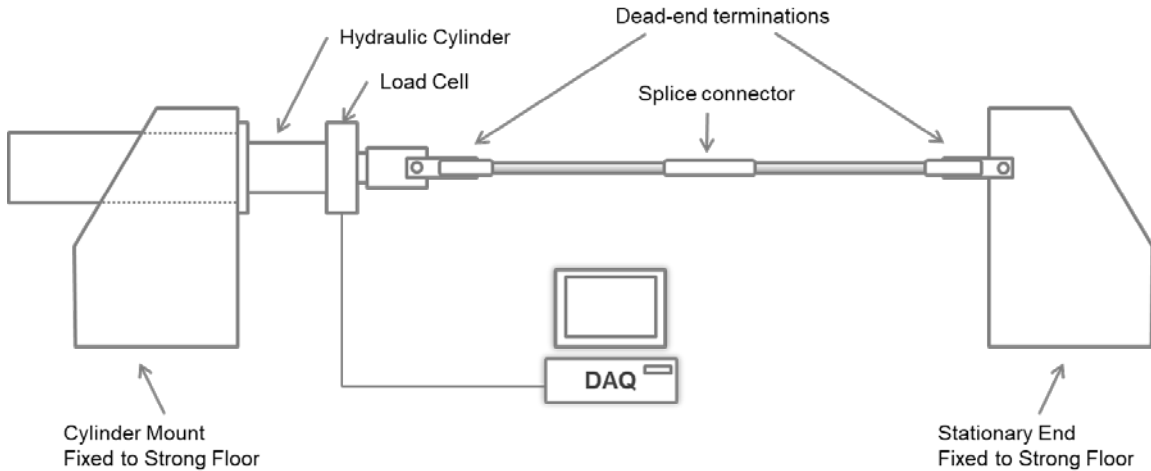


Figure 4-1: Maximum Load Test – Schematic of the Setup



Figure 4-2: Maximum Load Test - Typical Setup

The tension applied to the test assembly was measured by a load cell located at one end of the sample and was monitored continuously using a digital data logging system. The data logging rate was every one (1) second during loading and every ten (10) seconds during hold. The test was performed in a temperature-controlled laboratory at $22\text{ }^{\circ}\text{C} \pm 2\text{ }^{\circ}\text{C}$. The measuring instruments and equipment used in this test are listed in Appendix D.

5 Test Procedure

One at a time, the test samples were installed in the horizontal tensile machine and pre-tensioned to 10% of the conductor's RTS, corresponding to 400 lb for the 1/0 AWG ACSR, or 670 lb for the 397.5 kcmil AAC.

The conductor entrance points at the epoxy dead-end splice connector were marked with paint to monitor movement of conductor relative to the connector during the test. Red color paint was used to mark the conductor on the South end of the setup and blue color paint was used to mark the conductor on the North side of the setup. Note that North and South labels relate to the orientation of the horizontal test machine.

The load was then increased to 60% RTS and held for five (5) minutes. The conductor was visually monitored for slippage at both ends of the connector. Upon completing the five (5) minute hold, the load was increased until sample failure occurred.

6 Test Results

The maximum load recorded during the test and the failure location are summarized in Table 6-1. The graphical representation of the tensile load vs. elapsed time are shown in Figure 6-1 to Figure 6-4.

The sample appearing after testing and the failure locations are shown in Figure 6-3 to Figure 6-13.

[The remainder of this page is intentionally left blank.]

Table 6-1: Maximum Load Test Results

Sample No.	Splice	Conductor Size (AWG or kcmil)	Max. Load Recorded		Comments (Failure Location)
			[lb]	[%RTS]	
1.1.1	████████	17 kV, 1/0 AWG ACSR	4,659	112%	No slippage at 60% RTS. Conductor aluminum strands broke approx. 1" from the South end of the splice. Steel core was intact.
1.1.2	████████	17 kV 1/0 AWG ACSR	4,724	114%	No slippage at 60% RTS. Conductor aluminum strands broke near South end of the splice. Steel core was intact.
1.1.3	████████	17 kV 1/0 AWG ACSR	4,517	109%	No slippage at 60% RTS. Conductor broke at the North epoxy dead-end block. Steel core pulled out completely.
1.2.1	████████	35 kV 1/0 AWG ACSR	4,454	107%	No slippage at 60% RTS. Conductor broke near South end of the splice. Steel core pulled out completely.
1.2.2	████████	35 kV 1/0 AWG ACSR	4,623	111%	No slippage at 60% RTS. Conductor aluminum strands broke at the South end of the splice. Steel core was intact.
1.2.3	████████	35 kV 1/0 AWG ACSR	4,213	101%	No slippage at 60% RTS. Conductor broke at the North epoxy dead-end block.
1.3.1	████████	22 kV 397.5 kcmil AAC	6,979	103%	No slippage at 60% RTS. Conductor broke at the south entrance of the splice
1.3.2	████████	22 kV 397.5 kcmil AAC	7,152	106%	No slippage at 60% RTS. Conductor broke at the south entrance of the splice.
1.3.3	████████	22 kV 397.5 kcmil AAC	7,245	107%	No slippage at 60% RTS. Conductor broke at the south entrance of the splice
1.4.1	████████	15 kV, 1/0 AWG ACSR	4,263	102%	No slippage at 60% RTS. Conductor pulled out of South DE.
1.4.2	████████	15 kV 1/0 AWG ACSR	4,625	111%	No slippage at 60% RTS. Conductor broke at the North mouth of splice.
1.4.3	████████	15 kV 1/0 AWG ACSR	4,626	111%	No slippage at 60% RTS. Conductor broke at the South DE.

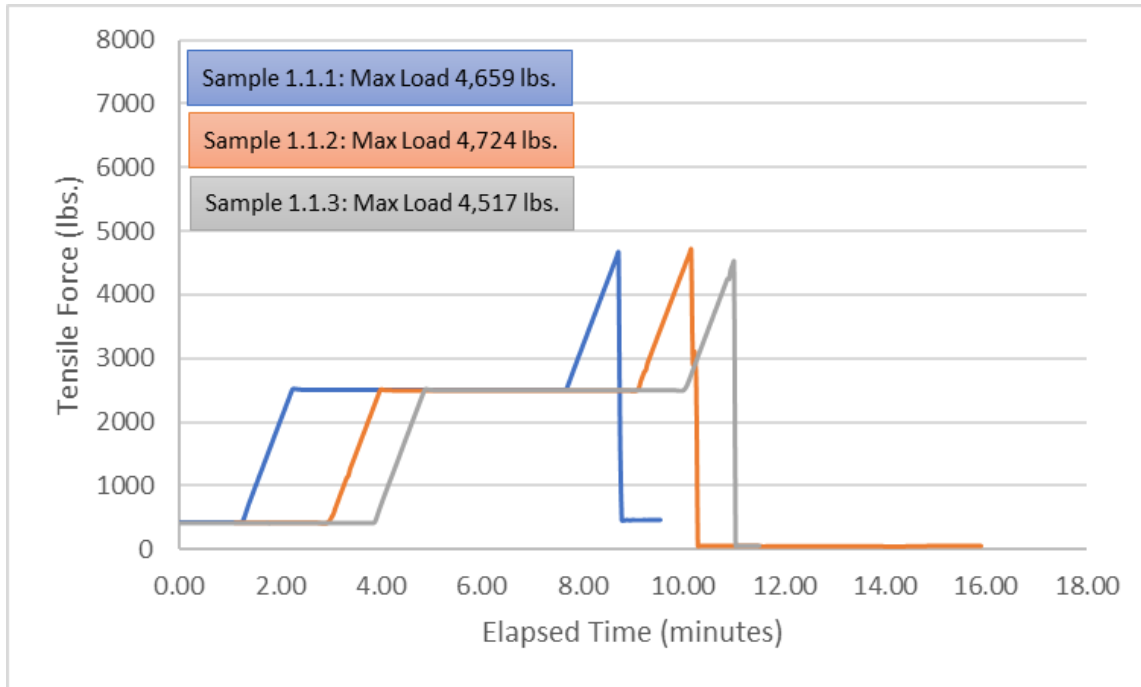


Figure 6-1: Maximum Load Test – 17 kV, 1/0 AWG ACSR

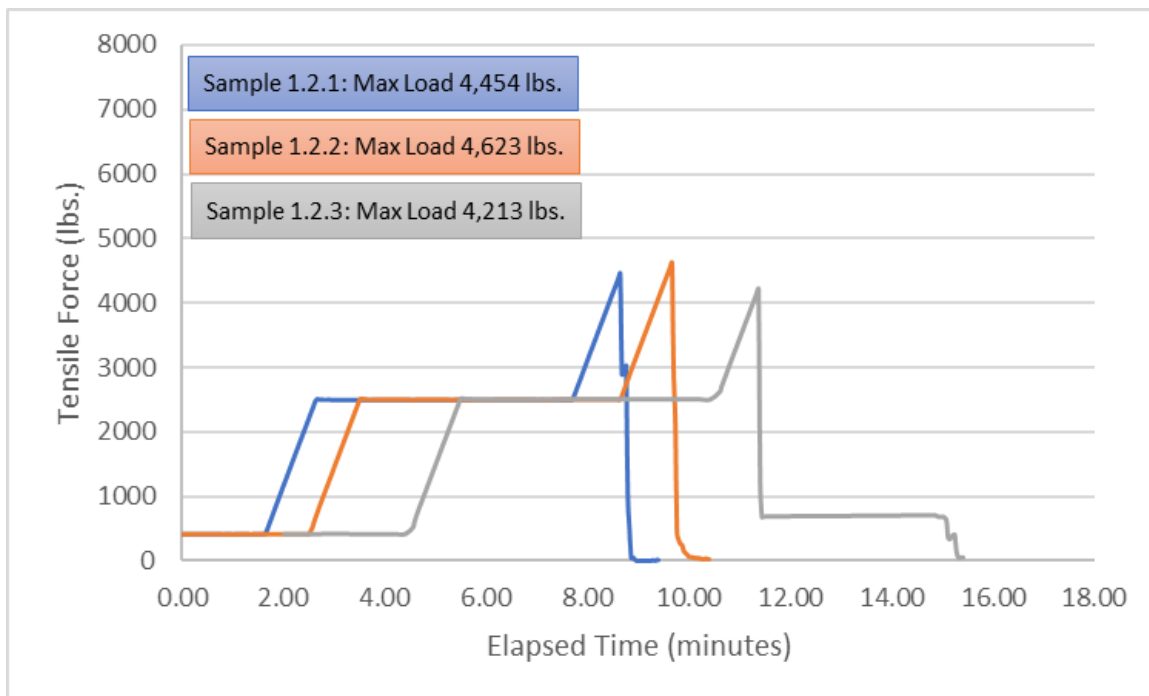


Figure 6-2: Maximum Load Test – 35 kV, 1/0 AWG ACSR

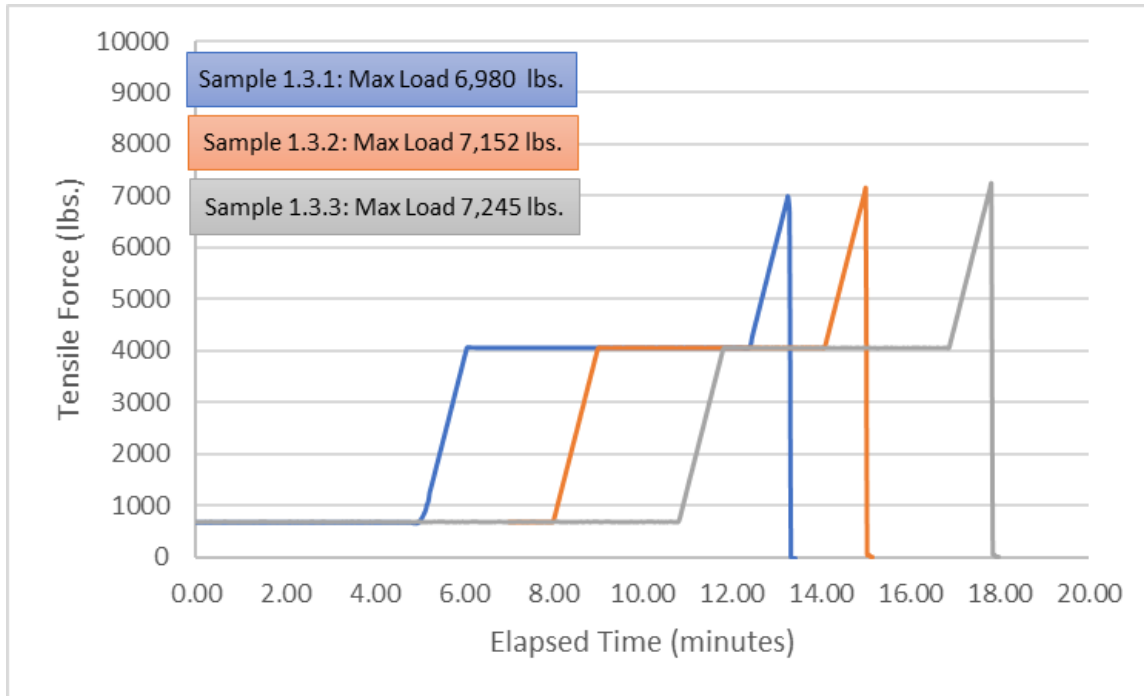


Figure 6-3: Maximum Load Test – 22 kV, 397.5 kcmil AAC

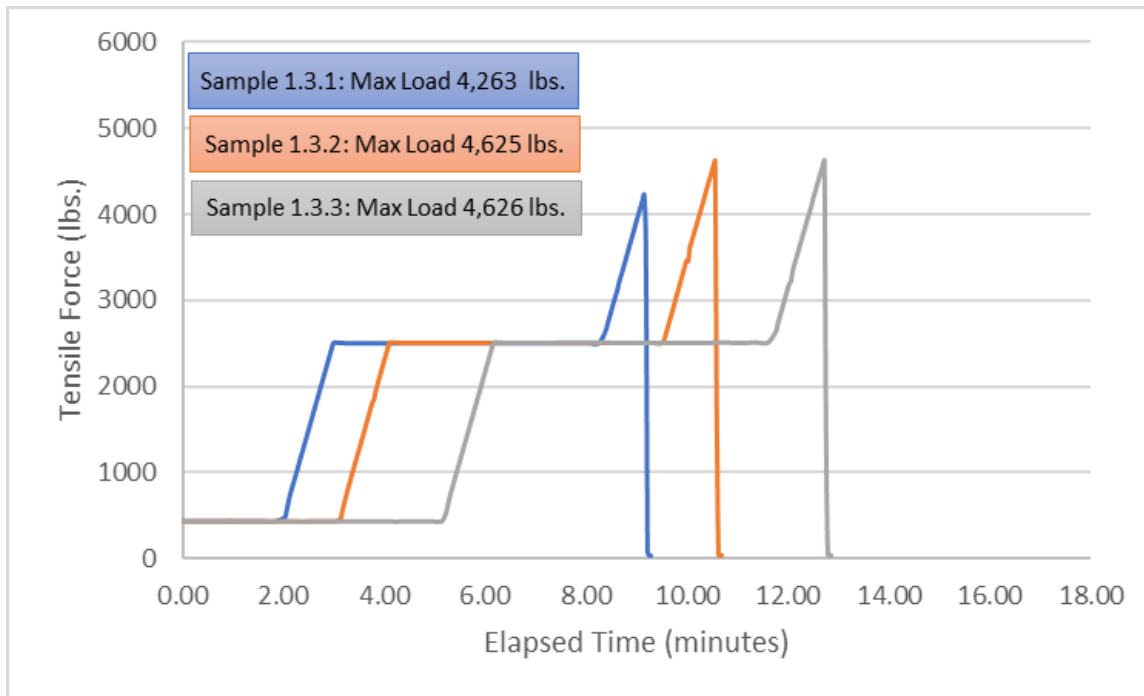


Figure 6-4: Maximum Load Test – 15 kV, 1/0 AWG ACSR

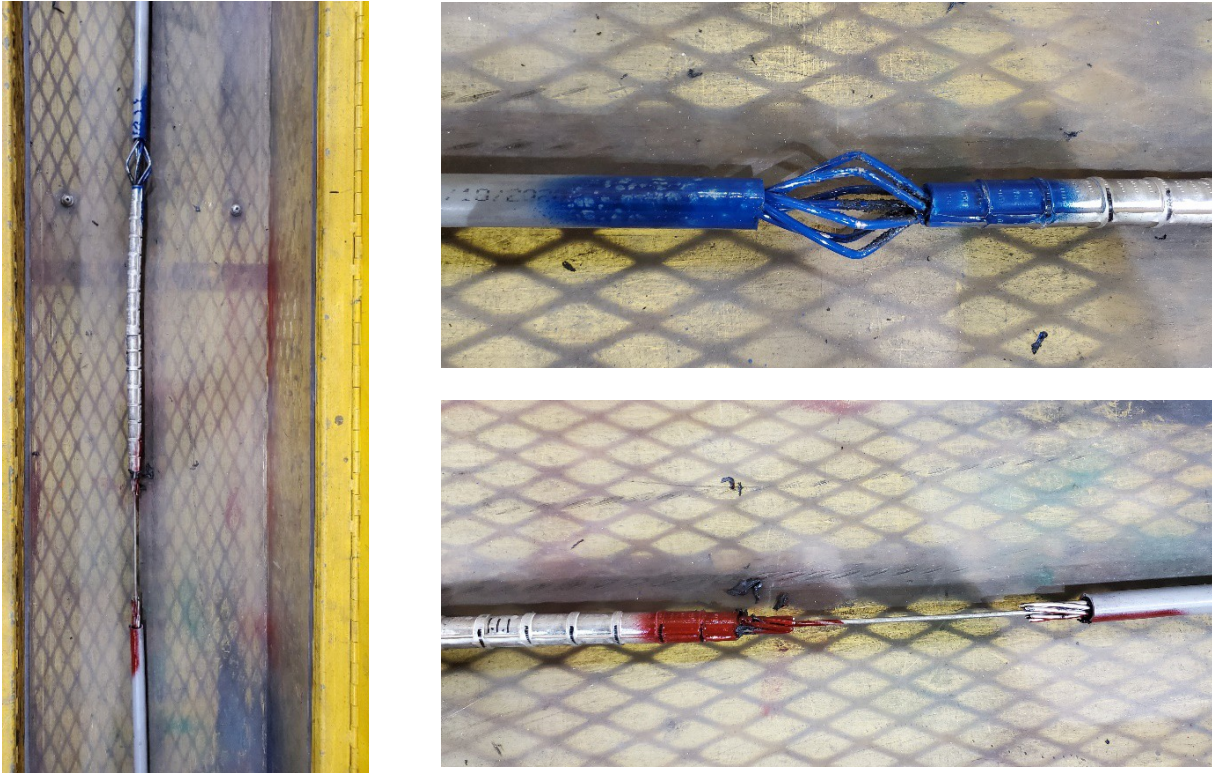


Figure 6-5: Sample 1.1.1 after test (conductor failed at South end of splice)

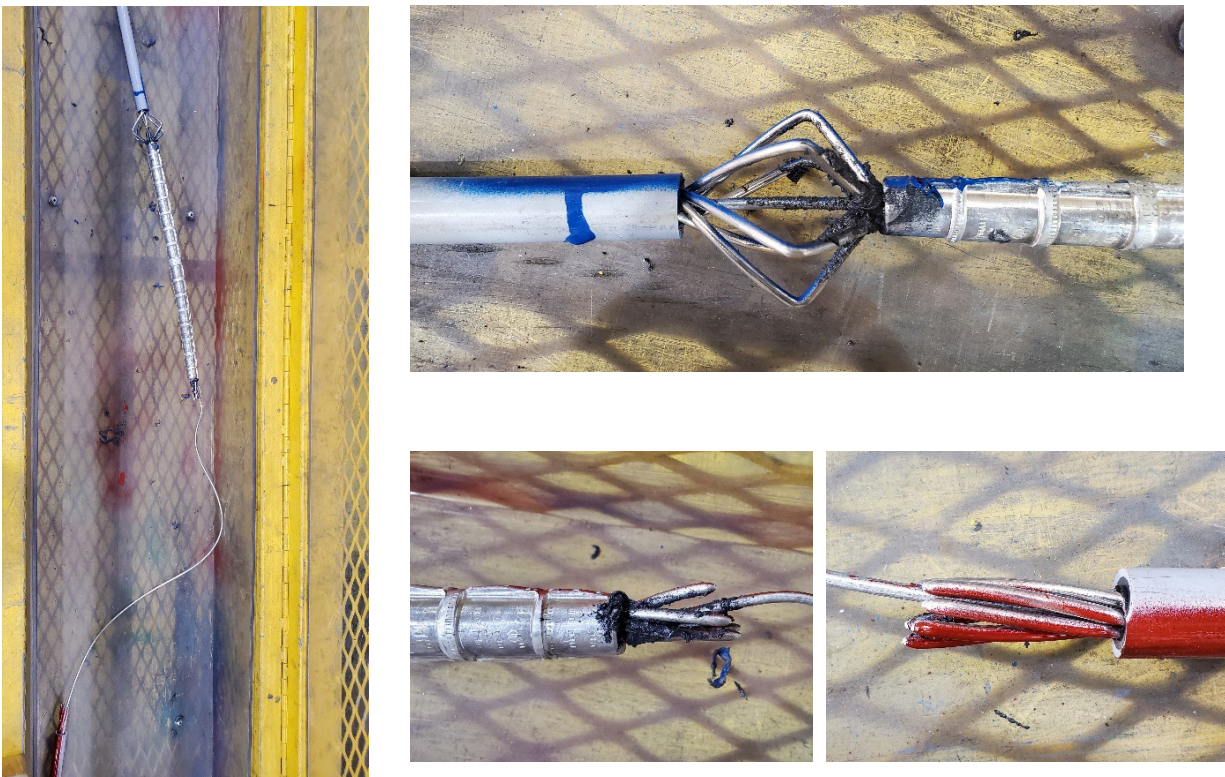


Figure 6-6: Sample 1.1.2 after test (conductor failed at South end of splice)

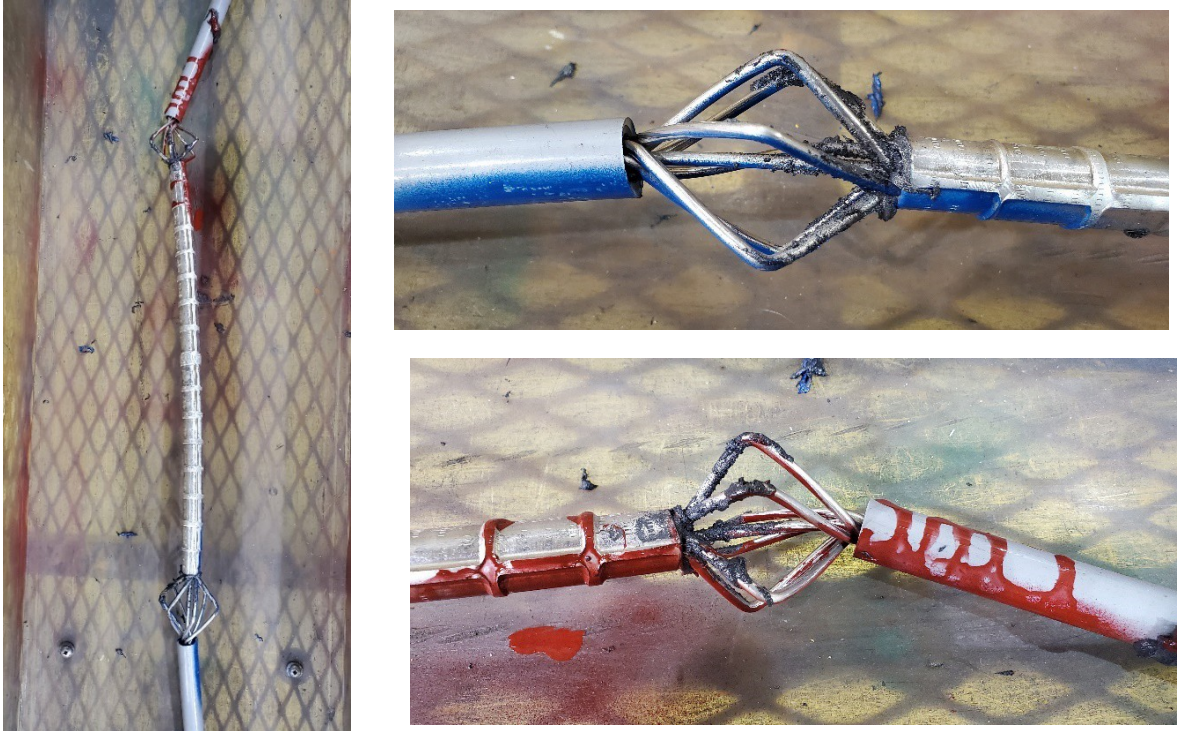


Figure 6-7: Sample 1.1.3 after test (conductor failed at North epoxy dead-end)



Figure 6-8: Sample 1.2.1 after test (conductor failed at North end of splice)

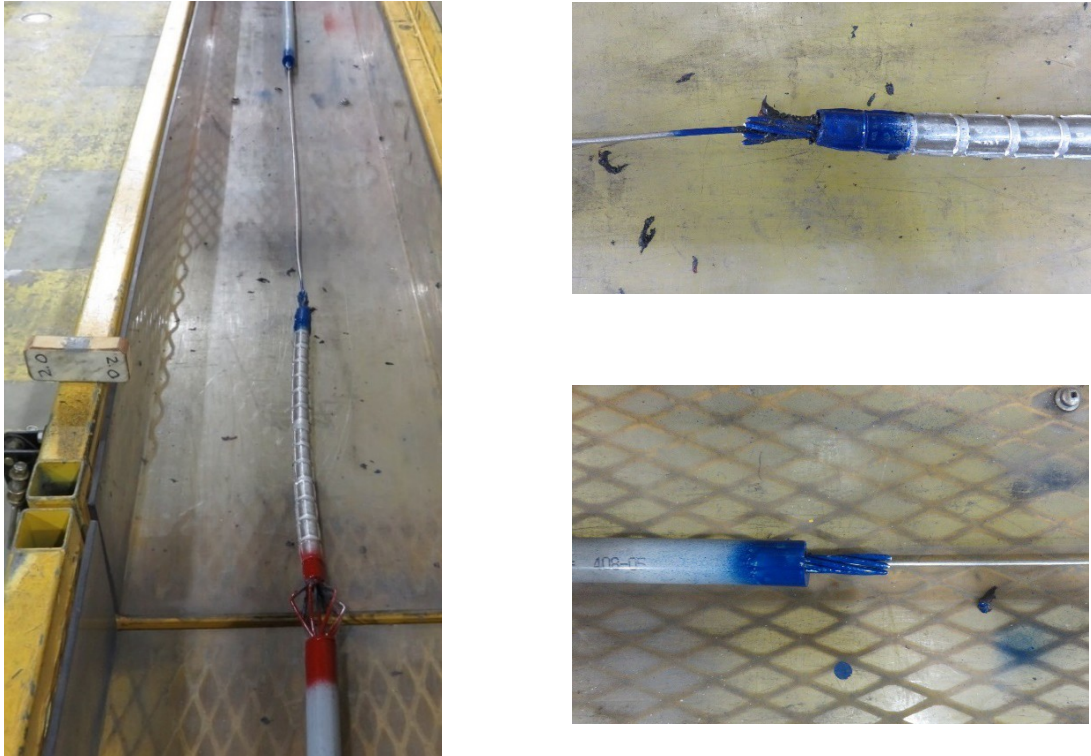


Figure 6-9: Sample 1.2.2 after test (conductor failed at North end of splice)

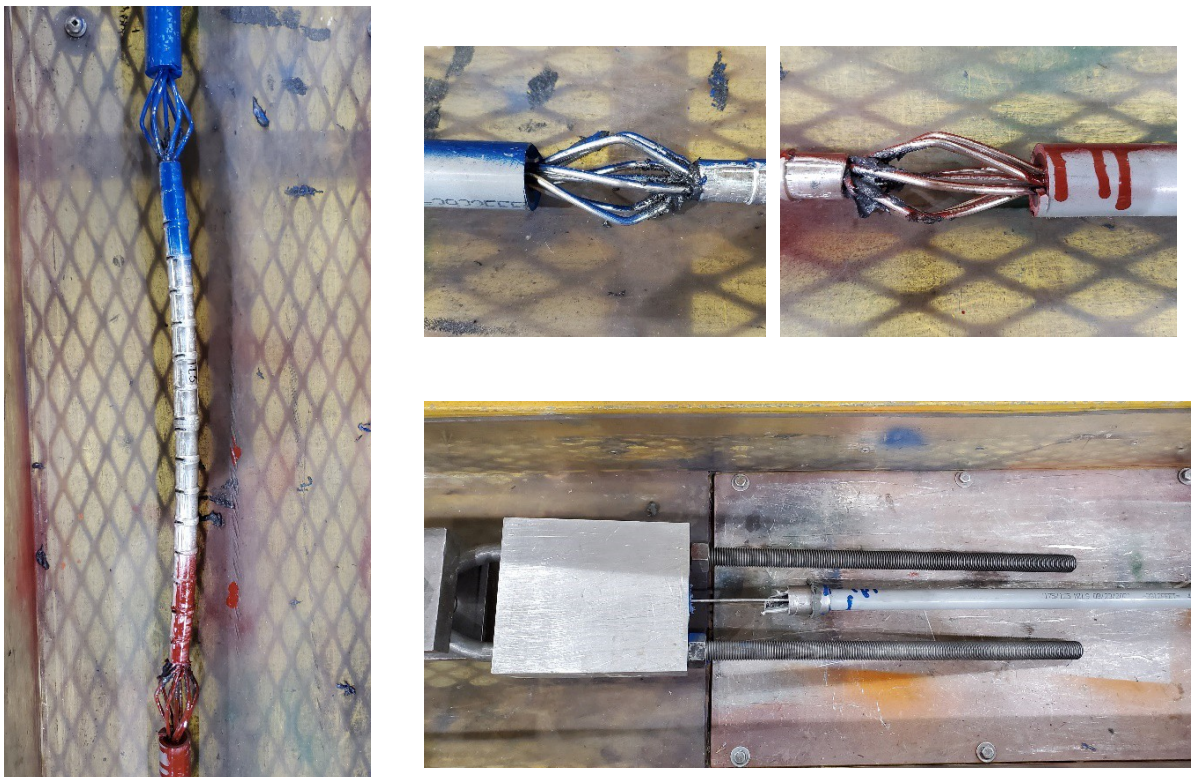


Figure 6-10: Sample 1.2.3 after test (failed at epoxy dead-end)

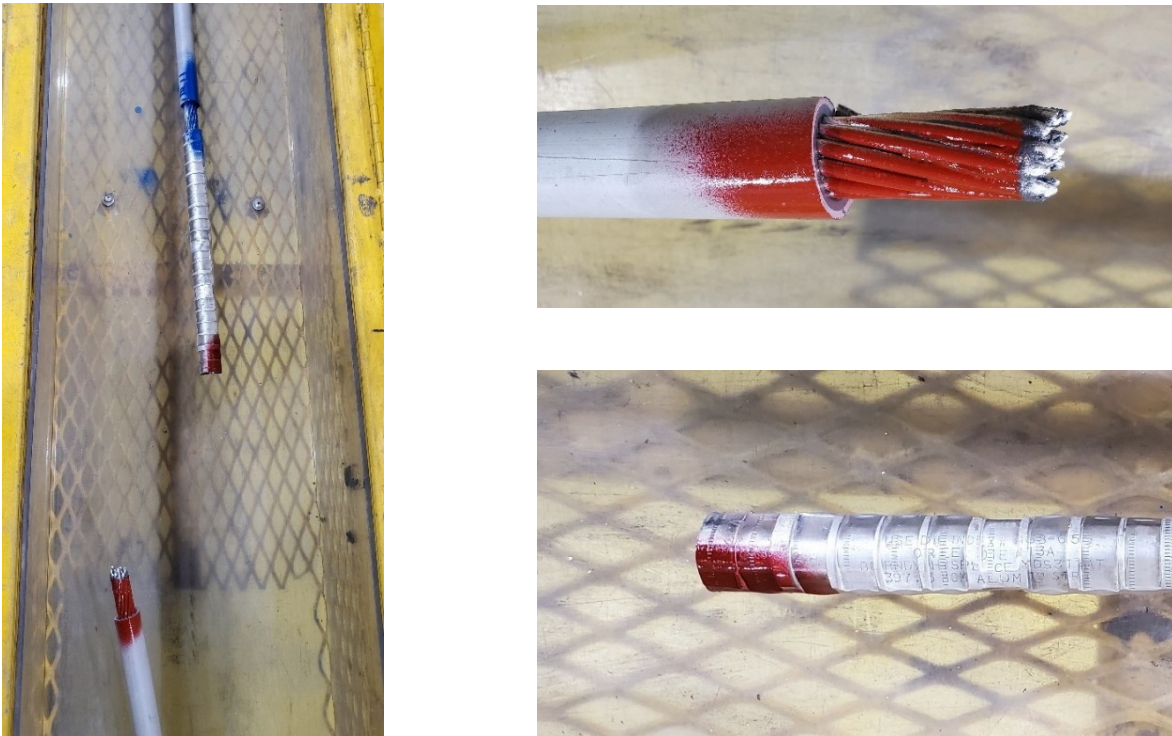


Figure 6-11: Sample 1.3.1 after test

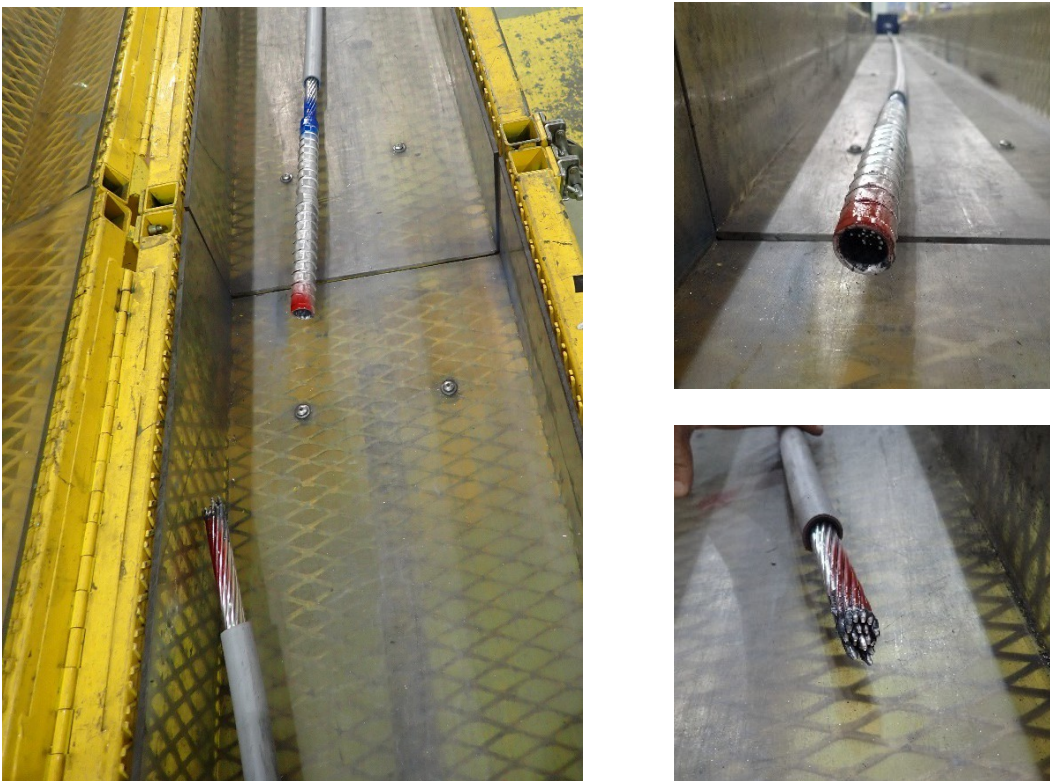


Figure 6-12: Sample 1.3.2 after test



Figure 6-13: Sample 1.3.3 after test

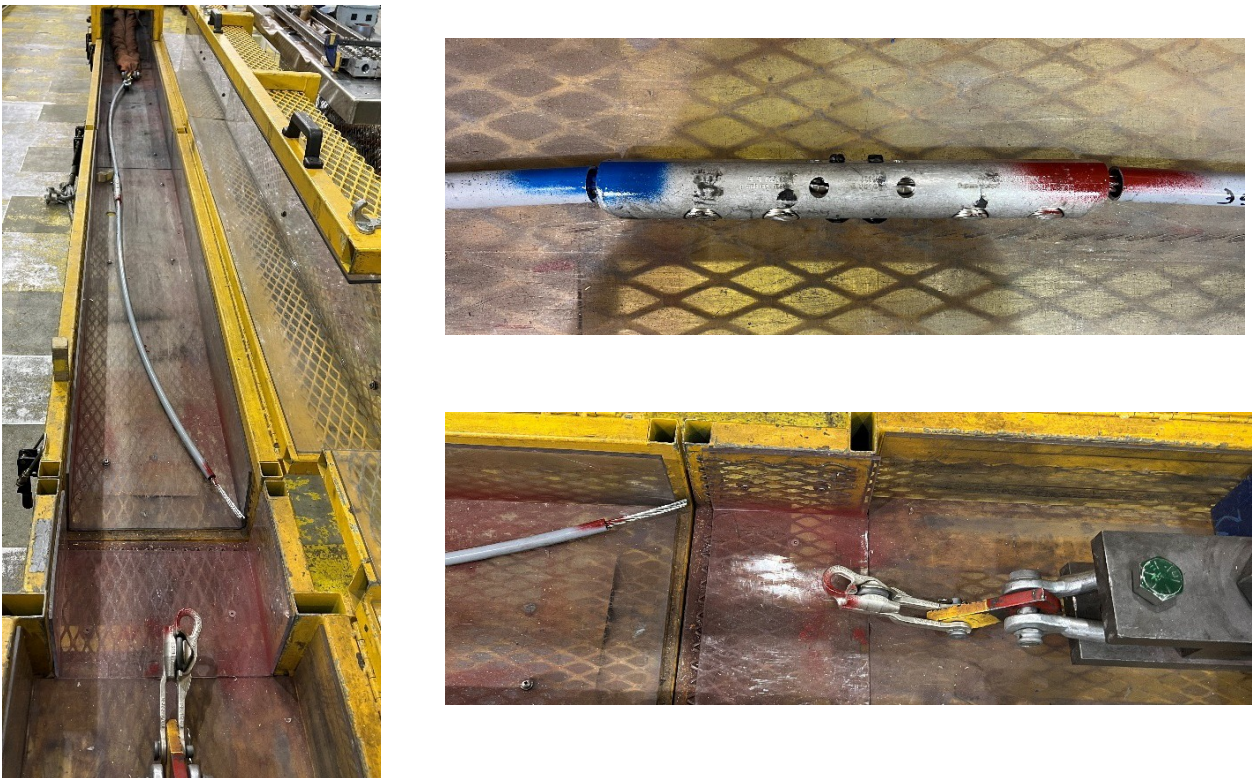


Figure 6-14: Sample 1.4.1 after test

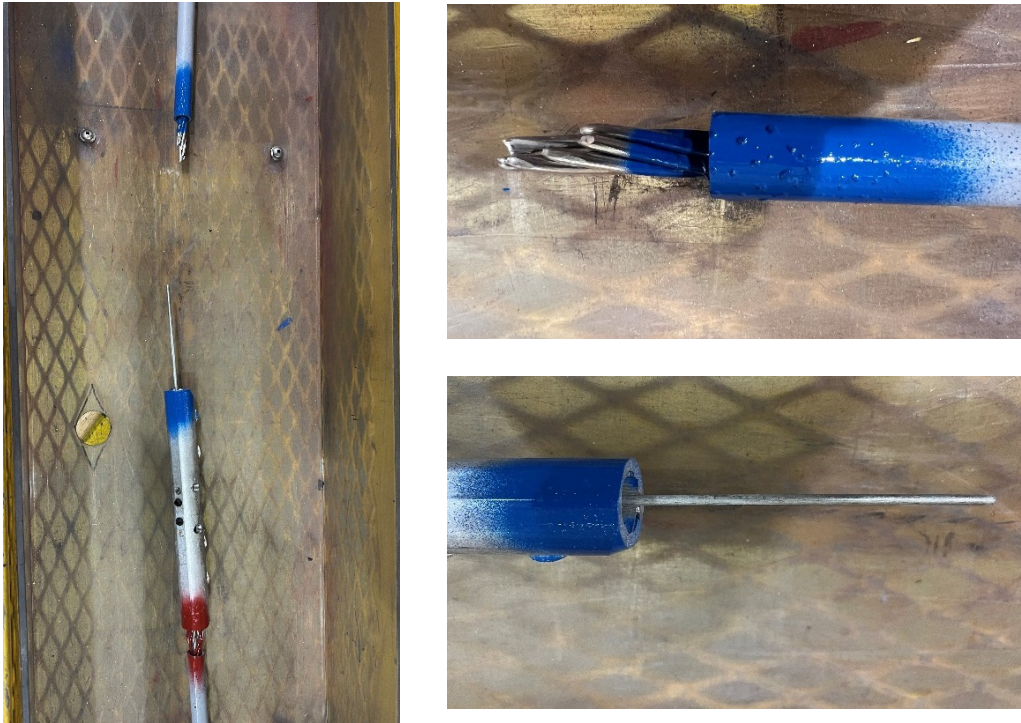


Figure 6-15: Sample 1.4.2 after test



Figure 6-16: Sample 1.4.3 after test

7 Acceptance Criteria

There were no acceptance criteria provided by the client. The objective of the test program was to:

1. Evaluate the performance of the connectors (i.e. conductor slippage) at the end of five (5) minutes hold at 60% RTS; and,
2. Evaluate the maximum tensile strength of the connector/conductor assembly.

8 Conclusion

Test results show that the connectors tested performed without slippage during the five (5) minute hold at 60% RTS and that there was no slippage or breakage of the conductor strands below 100% RTS.

[The remainder of this page is intentionally left blank.]



Appendix A Acronyms and Abbreviations

AAC	- All Aluminum Conductor
ACSR	- Aluminum Conductor Steel Reinforced
ANSI	- The American National Standards Institute
AWG	- American Wire Gauge
DE	- Dead-end
ISO	- International Organization for Standardization
RTS	- Rated Tensile Strength
SDG&E	- San Diego Gas & Electric
XLPE	- Crosslinked Polyethylene

[The remainder of this page is intentionally left blank.]

Appendix B Product Specification of Splices

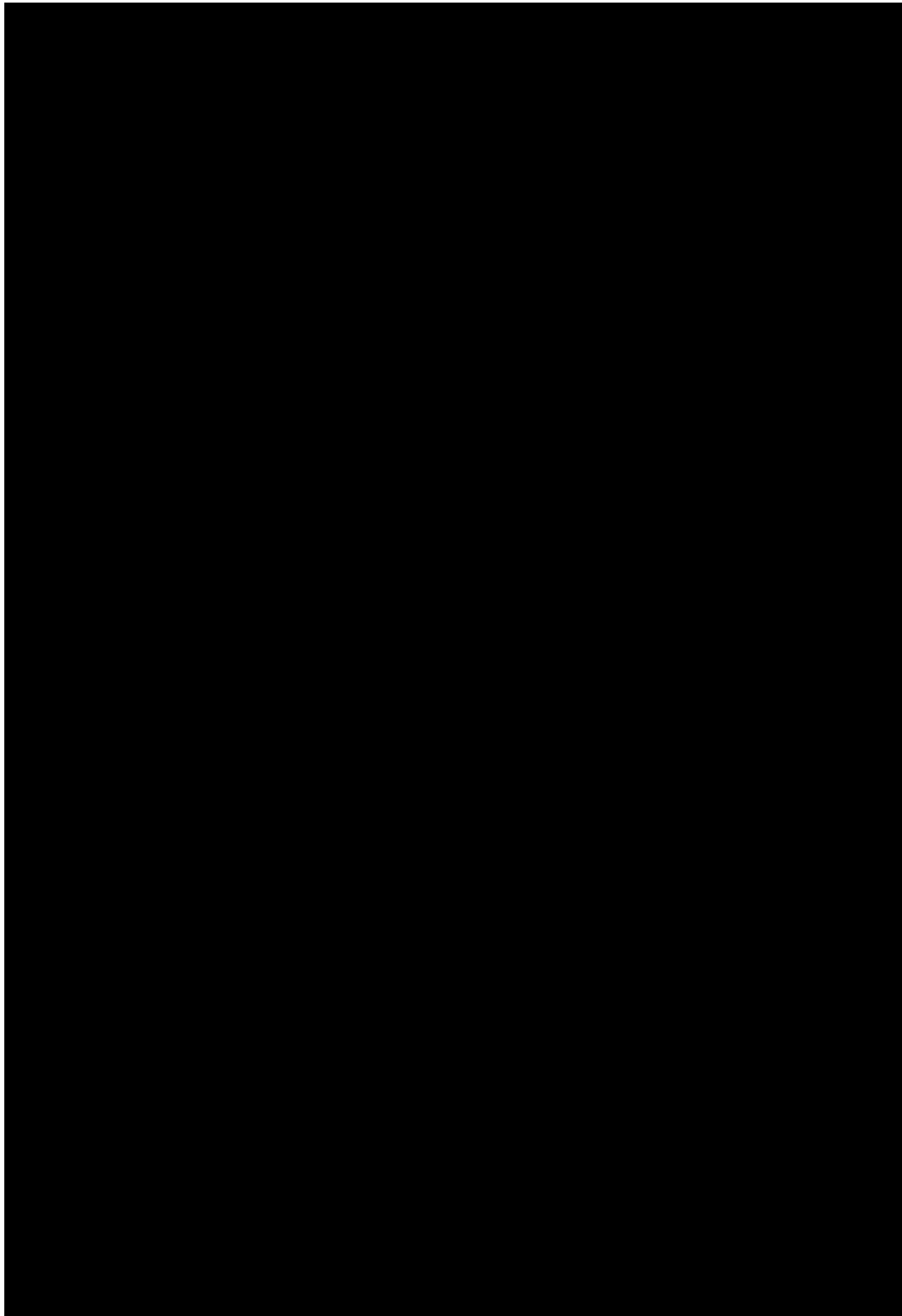


Figure B - 1: [REDACTED] (Page 1 of 2)

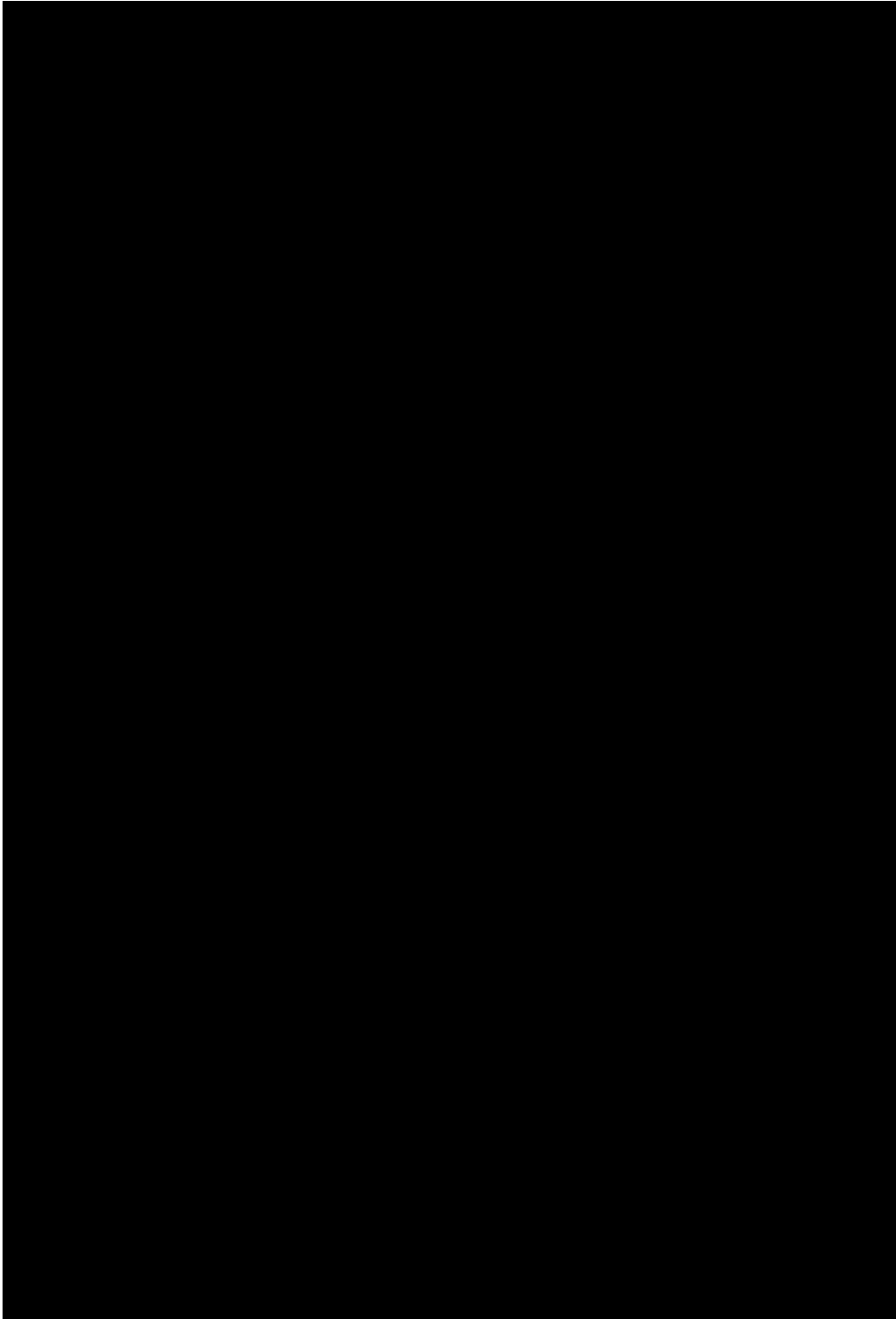


Figure B - 2:  (Page 2 of 2)

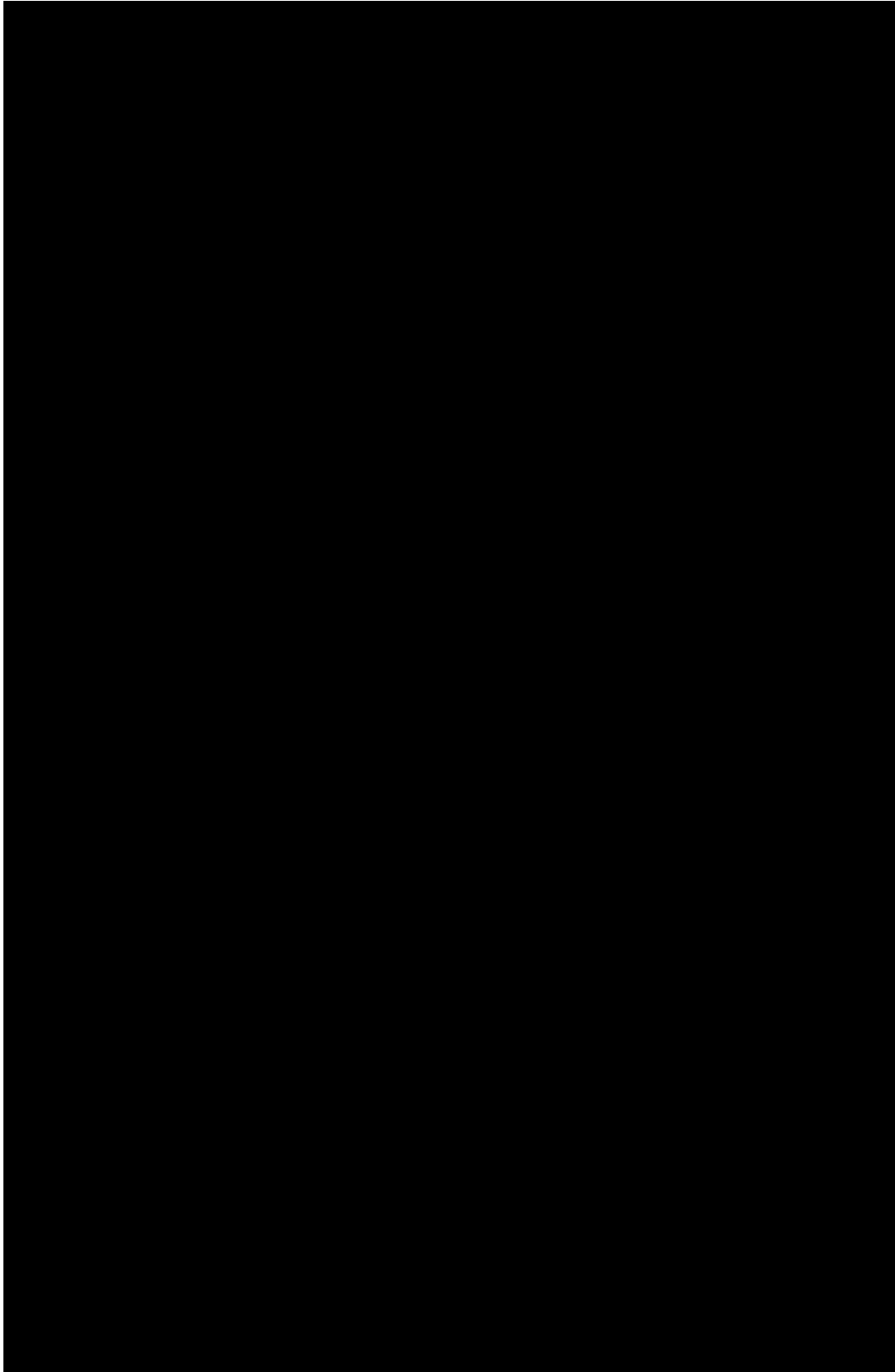


Figure B - 3: [REDACTED] (installation drawing)

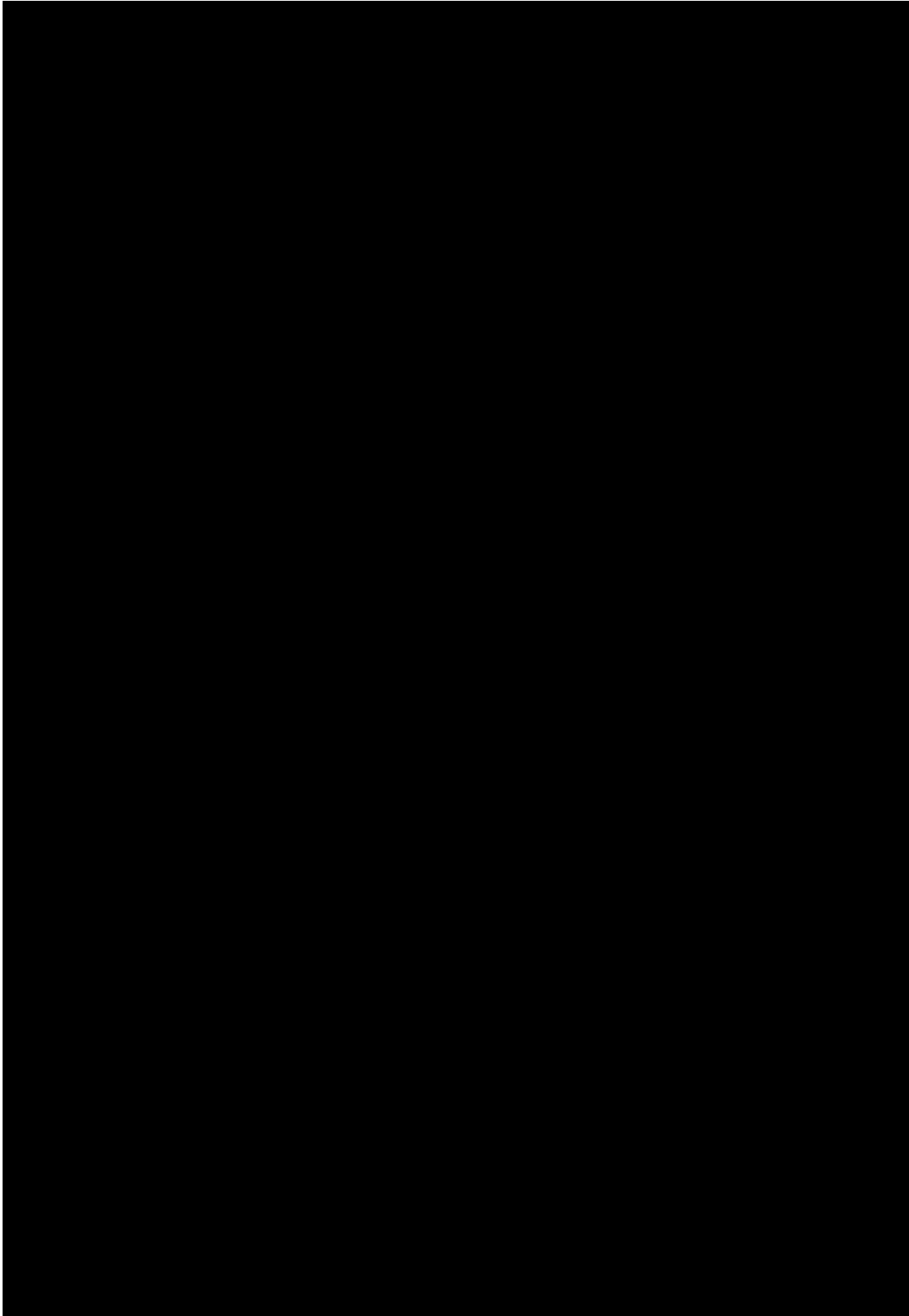


Figure B - 4: 

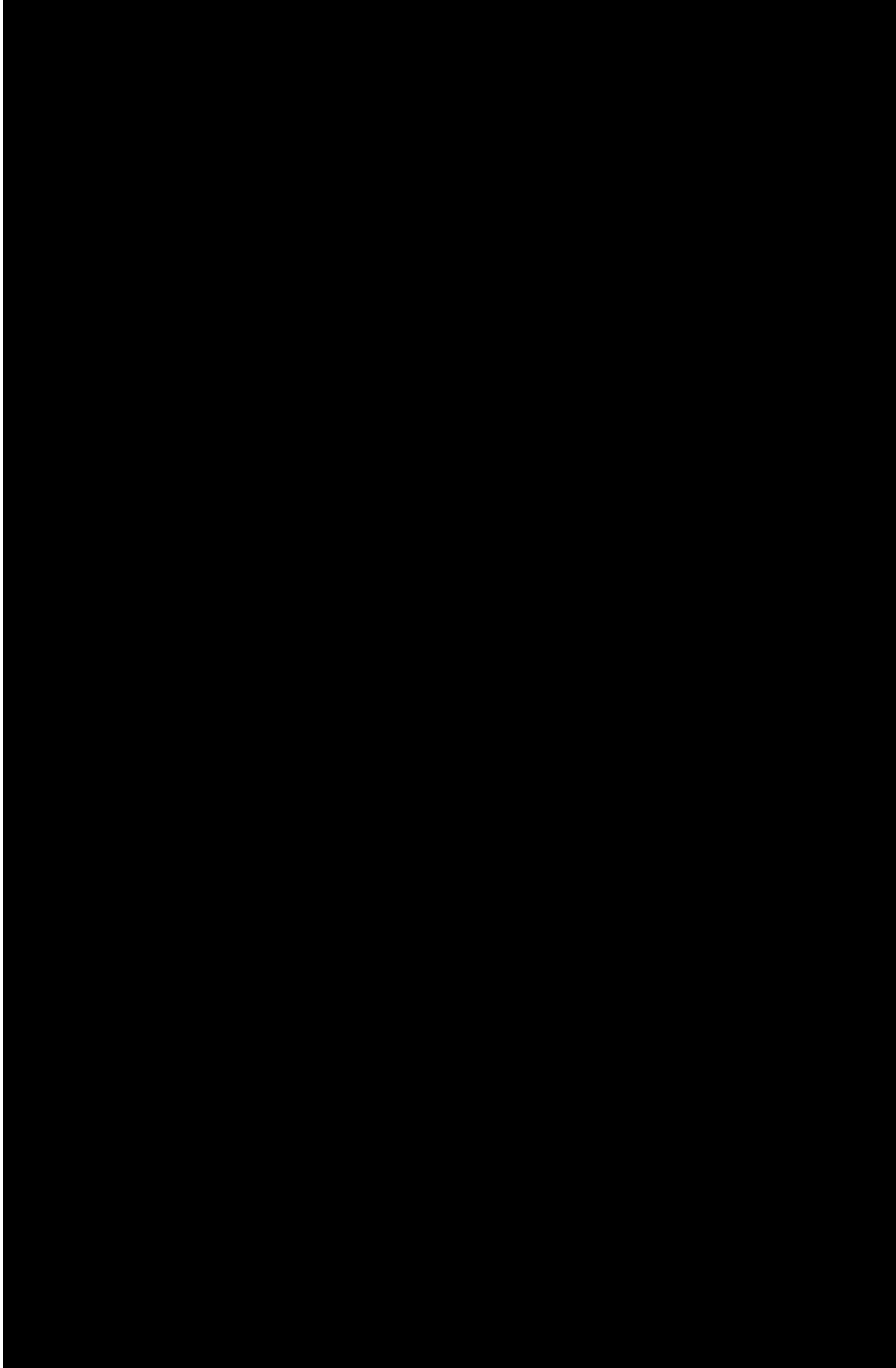


Figure B - 5: 

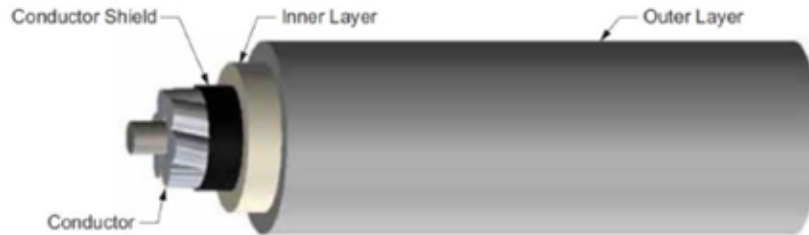


Figure B - 6:  datasheet

Appendix C Conductor Data Sheet (as provided by Exponent)

Covered Conductor Data Sheet

Covered Conductor for 17kV and 35kV



- Conductor:
 - Aluminum Conductor Steel-Reinforced (ACSR) or
 - Hard Drawn Copper (HDCU)
- Conductor Shield: Semiconducting Thermoset Polymer
- Inner Layer: Crosslinked Low Density Polyethylene (XL-LDPE)
- Outer Layer: Crosslinked High Density Polyethylene (XL-HDPE)
 - Track Resistant
 - Abrasion Resistant

Temperature Rating:

Normal Operating Temperature: 90°C

Emergency Operating Temperature: 130°C

Short Circuit Temperature: 250°C

17kV Covered Conductor

ACSR

Conductor Size (AWG)	Conductor Type (Stranding)	Weight (lb/ft)	Conductor Diameter (in)	Conductor Shield Thickness (in)	Inner Layer Thickness (in)	Outer Layer Thickness (in)	Max Nominal Overall Diameter (in)	Maximum Rated Strength (lb.)	Ampacity per Conductor ¹ (Amps)
1/0	ACSR (6x1)	0.289	0.398	0.015 - 0.025	0.075	0.075	0.748	4,160	271
336.4	ACSR (18x1)	0.584	0.684	0.015 - 0.025	0.075	0.075	1.034	8,246	550
336.4	ACSR (30/7)	0.750	0.741	0.015 - 0.025	0.075	0.075	1.091	16,435	561
653.9	ACSR (18x3)	0.998	0.953	0.020 - 0.025	0.080	0.080	1.323	14,060	835

¹ Covered Conductor Cable Normal Operating Rating Criteria:

Ambient Temperature = 40°C

Conductor Temperature = 90°C

Load Factor = 100%

Wind Speed = 4 ft/sec

Coefficient of Emissivity = 0.5

Coefficient of Absorption = 0.5

Latitude = 34°

Elevation of Conductor above Sea Level = 0 ft

Atmosphere = Clear

Local Sun Time = 1:00 pm

Figure C - 1: [REDACTED], 17 kV 1/0 AWG ACSR Conductor Data

35kV Covered Conductor

ACSR

Conductor Size (AWG)	Conductor Type (Stranding)	Weight (lb/ft)	Conductor Diameter (in)	Conductor Shield Thickness (in)	Inner Layer Thickness (in)	Outer Layer Thickness (in)	Max Nominal Overall Diameter (in)	Maximum Rated Strength (lb.)	Ampacity per Conductor ¹ (Amps)
1/0	ACSR (6x1)	0.460	0.398	0.015 - 0.025	0.175	0.125	1.048	4,160	255
336.4	ACSR (18x1)	0.850	0.684	0.015 - 0.025	0.175	0.125	1.334	8,246	518
336.4	ACSR (30x7)	0.981	0.741	0.015 - 0.025	0.175	0.125	1.391	16,435	529
653.9	ACSR (18x3)	1.242	0.953	0.020 - 0.025	0.175	0.125	1.602	14,060	784

¹ Covered Conductor Cable Normal Operating Rating Criteria:

- Ambient Temperature = 40°C
- Conductor Temperature = 90°C
- Load Factor = 100%
- Wind Speed = 4 ft/sec
- Coefficient of Emissivity = 0.5
- Coefficient of Absorption = 0.5
- Latitude = 34°
- Elevation of Conductor above Sea Level = 0 ft
- Atmosphere = Clear
- Local Sun Time = 1:00 pm

Specifications

Must be manufactured to the latest editions of the following standards:

- ASTM B8
- ASTM B232
- ICEA S-121-733

Figure C - 2: [REDACTED], 35 kV 1/0 AWG ACSR Conductor Data



Appendix D Instrument Sheet

EQUIPMENT DESCRIPTION	ASSET No.	ACCURACY CLAIMED	CALIBRATION DATE	CALIBRATION DUE DATE	TEST USE
Data Logger	KIN-01836	±0.1% of Reading	May 20, 2021 May 27, 2022	May 20, 2022 May 27, 2023	Data acquisition
Load Cell/ Conditioner	KIN-01725/ KIN-01724	±1% of Reading	October 26, 2021	October 26, 2022	Load
Tape Measure	KIN-06890	< 0.05% of Reading	June 8, 2021 Jun 29, 2022	June 8, 2022 Jun 29, 2022	Length
Thermocouple/ Transmitter	KIN-00918/ KIN-00919	± 1 °C	October 28, 2021 October 21, 2021	October 28, 2022/ October 21, 2022	Ambient Temperature

[The remainder of this page is intentionally left blank.]

Appendix E Kinectrics ISO 9001 Certificate of Registration



Registered by:
QMI-SAI Canada Limited (SAI Global), 20 Carlton Court, Suite 200, Toronto, Ontario M5W 7Y5 Canada. This registration is subject to the SAI Global Terms and Conditions for Certification. While all due care and skill was exercised in carrying out the assessment, SAI Global accepts responsibility only for proven negligence. This certificate remains the property of SAI Global and must be returned to them upon request.
To verify that this certificate is current, please refer to the SAI Global On-Line Certification Register:
https://www.sai-global.com/en-us/assurance/auditing_and_certification/certification_registry/





Appendix F Distribution

Mr. Matt Bowers, Ph.D., P.E. Exponent
17000 Science Drive, Suite 200
Bowie, Maryland 20715
Email: mbowers@exponent.com

Mr. Genti Gorja Kinectrics AES Inc.
800 Kipling Ave, Unit No.2
Toronto, ON
Canada M8Z 5G5
Email: genti.gorja@kinectrics.com

[The remainder of this page is intentionally left blank.]



NOTE: Component manufacturer information has been redacted from this report.

SLIP LOAD TEST ON INSULATOR CLAMPS WITH COVERED CONDUCTORS

K-580740-RP-002 R01

Prepared for

Exponent

Purchase Order No. 00062928

<p>Prepared by</p> <p> Digitally signed by GORJA Genti Date: 2022.11.04 16:30:41 -04'00'</p> <p><i>Signature & Date</i></p> <p>Genti Gorja P.Eng. Principal Engineer Line Asset Management</p>	<p>Reviewed by</p> <p> Digitally signed by André Maurice Date: 2022.11.07 13:38:25 -05'00'</p> <p><i>Signature & Date</i></p> <p>André Maurice Service Line Manager Line Asset Management</p>	<p>Approved by</p> <p>PETER Zsolt  Digitally signed by PETER Zsolt Date: 2022.11.08 07:48:48 -05'00'</p> <p><i>Signature & Date</i></p> <p>Zsolt Peter Ph.D. Business Area Director Line Asset Management</p>
---	--	--

Revision History

Rev 00	Description: Original issue			
	Issue Date: 2022-09-28	Prepared by: Genti Gorja	Reviewed by: André Maurice	Approved by: Zsolt Peter
Rev 01	Description: The %RTS values reported for the [REDACTED] insulator in Table 6-1 are incorrect.			
	Issue Date: 2022-11-04	Prepared by: Genti Gorja	Reviewed by: André Maurice	Approved by: Zsolt Peter

DISCLAIMER

Kinectrics prepared this report as a work of authorship sponsored by their client. This report has been prepared solely for the benefit of the Client and may not be used or relied upon in whole or in part by any other person or entity without Client permission or without Kinectrics' permission if required by the Contract between Client and Kinectrics Inc. . Neither Kinectrics, their client nor any person acting on behalf of them: (a) makes any warranty or representation whatsoever, express or implied, or assumes any legal liability of responsibility for any third party's use, or the results of such use, with respect to (i) the use of any information, apparatus, method, process, or similar item disclosed in this report including the merchantability or fitness for any particular purpose of any information contained in this report or the respective works or services supplied or performed or (ii) that such use does not infringe on or interfere with privately owned rights, including any party's intellectual property; or (b) assumes responsibility for any damages or other liability whatsoever (including any consequential damages resulting from a third party's selection or use of this report or any information, apparatus, method, process, or similar item disclosed).

Copyright © Kinectrics Inc. 2022. All rights reserved.



Table of Contents

1	Executive Summary	4
2	Test Objective and Test Standard	5
3	Test Sample	5
4	Test Setup	6
5	Test Procedure	8
6	Test Results	8
7	Acceptance Criteria	18
8	Conclusion	18
Appendix A	Acronyms and Abbreviations	19
Appendix B	Conductor Data Sheet (<i>as provided by Exponent</i>)	20
Appendix C	Insulator Data Sheet	22
Appendix D	Instrument Sheet	24
Appendix E	Kinectrics ISO 9001 Certificate of Registration	25
Appendix F	Distribution	26

1 Executive Summary

This report describes the Slip Load Test performed on [redacted] Vise Top pin insulator (model [redacted] - [redacted] and [redacted] Clamp Top post insulator (model [redacted] and [redacted]

The Slip Load Test was conducted for Exponent™ to evaluate the performance of [redacted] and [redacted] post insulator clamps designed for use with 15 kV 1/0 AWG ACSR covered conductor, 17 kV 1/0 AWG ACSR covered conductor, 35 kV 1/0 AWG ACSR covered conductor and 22 kV 397.5 kcmil AAC covered conductor.

The test were conducted in accordance with client’s requirements as outlined in the relevant sections of this document. The test program and completion dates are summarized in Table 1-1.

Table 1-1: Test Program

Test ID	Sample ID	Conductor	Insulator Cat.ID.	Date Completed
2.1	2.1.1	17 kV 1/0 AWG ACSR	[redacted]	May 11, 2022
	2.1.2	17 kV 1/0 AWG ACSR	[redacted]	May 11, 2022
	2.1.3	17 kV 1/0 AWG ACSR	[redacted]	May 11, 2022
2.2	2.2.1	35 kV 1/0 AWG ACSR	[redacted]	May 12, 2022
	2.2.2	35 kV 1/0 AWG ACSR	[redacted]	May 12, 2022
	2.2.3	35 kV 1/0 AWG ACSR	[redacted]	May 12, 2022
2.3	2.3.1	22 kV 397.5 kcmil AAC	[redacted]	May 13, 2022
	2.3.2	22 kV 397.5 kcmil AAC	[redacted]	May 13, 2022
	2.3.3	22 kV 397.5 kcmil AAC	[redacted]	May 13, 2022
2.4	2.4.1	15 kV 1/0 AWG ACSR	[redacted]	July 26, 2022
	2.4.2	15 kV 1/0 AWG ACSR	[redacted]	July 26, 2022
	2.4.3	15 kV 1/0 AWG ACSR	[redacted]	July 26, 2022
2k.1	2k.1.1	17 kV 1/0 AWG ACSR	[redacted]	July 27, 2022
	2k.1.2	17 kV 1/0 AWG ACSR	[redacted]	July 27, 2022
	2k.1.3	17 kV 1/0 AWG ACSR	[redacted]	July 27, 2022
2k.2	2k.2.1	35 kV 1/0 AWG ACSR	[redacted]	July 27, 2022
	2k.2.2	35 kV 1/0 AWG ACSR	[redacted]	July 27, 2022
	2k.2.3	35 kV 1/0 AWG ACSR	[redacted]	July 27, 2022

Exponent™ supplied samples and accessories required for testing. Kinectrics received all samples, in good condition, on May 2, 2022.

The tests were performed by Kinectrics personnel at 800 Kipling Avenue, Toronto, Ontario, M8Z 5G5, Canada. The work was conducted under Exponent™ Purchase Order No. 00062928 dated January 14, 2022.

The tests were performed under Kinectrics’ ISO 9001 Quality Management System. A copy of ISO 9001 Certificate of Registration is included in Appendix E.

2 Test Objective and Test Standard

The intent of the Slip Test was to determine the tensile load which resulted in conductor slippage relative to the clamp of a [REDACTED] Vise Top pin insulator or [REDACTED] Clamp Top post insulator. The test was designed to simulate clamp/conductor system mechanical loading during field installation and operation. The test was performed in accordance with the procedures requested by Exponent™.

3 Test Sample

A total of eighteen (18) samples were tested. The test samples consisted of the following insulators (see Appendix C for the insulator data sheet):

- Twelve (12) [REDACTED] Vise Top pin insulator, model [REDACTED]
- Three (3) [REDACTED] Clamp Top post insulator, model [REDACTED]
- Three (3) [REDACTED] Clamp Top post insulator, model [REDACTED]

A 45 ft length of each conductor type was terminated with one dead-end for testing in conjunction with the corresponding insulator. Detailed data of the conductors used in this test program are shown in Appendix B. A summary of the test sample configurations is shown in Table 3-1.

Table 3-1: Test Sample Configuration

Sample No.	Connector Identification		Conductor Size (AWG or kcmil)	Overall Length [ft]
	Dead-end	Insulator		
2.1.1	Epoxy Resin	[REDACTED]	17 kV, 1/0 AWG ACSR	45
2.1.2		[REDACTED]		
2.1.3		[REDACTED]		
2.2.1	Epoxy Resin	[REDACTED]	35 kV 1/0 AWG ACSR	45
2.2.2		[REDACTED]		
2.2.3		[REDACTED]		
2.3.1	Epoxy Resin	[REDACTED]	22 kV 397.5 kcmil AAC	45
2.3.2		[REDACTED]		
2.3.3		[REDACTED]		
2.4.1	[REDACTED]	[REDACTED]	15 kV 1/0 AWG ACSR	45
2.4.2		[REDACTED]		
2.4.3		[REDACTED]		
2k.1.1	[REDACTED]	[REDACTED]	17 kV, 1/0 AWG ACSR	45
2k.1.2		[REDACTED]		
2k.1.3		[REDACTED]		
2k.2.1	[REDACTED]	[REDACTED]	35 kV, 1/0 AWG ACSR	45
2k.2.2		[REDACTED]		
2k.2.3		[REDACTED]		

4 Test Setup

The Slip Load Test was performed in a hydraulically-activated horizontal test machine. The conductor sample, terminated with the dead-end fitting installed at one end, was used for all three (3) insulator clamps. A different section of conductor was used for testing each new insulator.

The dead-end fitting, installed at one end of the conductor length was attached directly to the hydraulic piston. The test insulator (Vise Top or Clamp Top) was setup vertically, on a support pedestal, to ensure that the center of the clamps was in line with the pulling axis of the cylinder.

Schematic of the slip test set-up is shown in Figure 4-1. The actual setup and clamp slip test is shown in Figure 4-2.

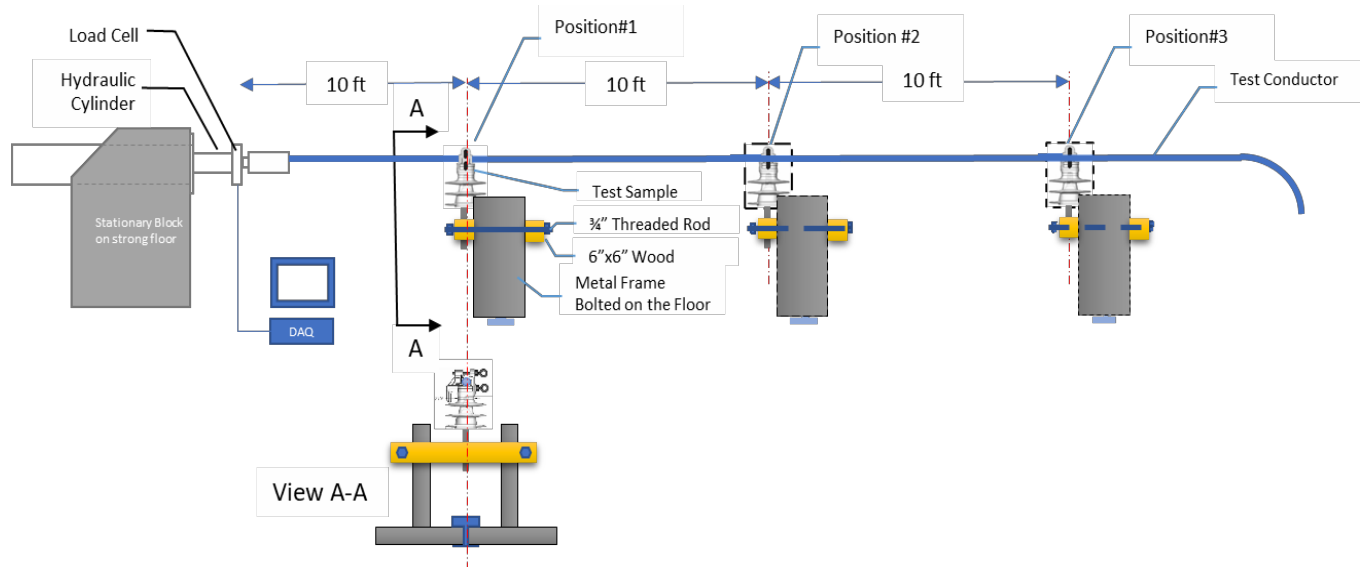


Figure 4-1: Clamp Slip Test Schematic

The Slip Load Test was performed by gradually increasing the load until slippage of the conductor inside the clamp occurred. The conductor tension and clamp slip load were measured by a load cell located at the end of the hydraulic cylinder. The test was performed in a temperature-controlled laboratory at $22\text{ }^{\circ}\text{C} \pm 2\text{ }^{\circ}\text{C}$. The measuring instruments and equipment used in this test are listed in Appendix D.



Test Sample

Conductor

Epoxy Dead End

Load Cell



Test Sample
Insulator



Test Sample
Insulator

Figure 4-2: Clamp Slip Test Setup

5 Test Procedure

The Slip Load Test was conducted as follows:

- The insulator was setup in the first position location approximately 10 ft from the cylinder (Position #1),
- The dead-end installed on the conductor was attached to the cylinder of the horizontal test machine and the conductor was secured in the vise top clamp of the insulator following manufacturer's instructions. When testing [REDACTED] Clamp Top insulators, a 40 ft-lb torque was used to secure the conductor in the clamp.
- The conductor tension is increased to 10% of RTS (pre-tension value) and the conductor was marked at the entry points in the clamp.
- The conductor tension is increased to 20% of RTS. The conductor was visually monitored for slippage.
- Tensile load was continuously increased at a rate of 1000 lb/min until continuous slippage of the conductor inside the clamp occurred, and the load could not be increased further.

Upon completing the test on the first sample, the same setup was repeated at a distance of 10 ft North of the first setup.

Upon completing the test on the second sample, the same setup was repeated at a distance of 10 ft North of the second setup.

6 Test Results

Test results are summarized in Table 6-1 and the loading profiles for each sample during test are shown in Figure 6-12 to Figure 6-17. Typical pictures of insulator and conductor condition after the test is shown in Figure 6-1 through Figure 6-6 for [REDACTED] insulators and Figure 6-7 through Figure 6-11 for [REDACTED] insulators.

Observations from the results of the test are listed below:

- When testing with [REDACTED] Vise Top insulators
 - o The slippage in all samples occurred as a result of the insulator bending under the tension applied to the conductor. This caused the conductor to come off a portion of the plastic inserts in the insulator clamp and slip. When testing the clamp with 397.5 AAC covered conductor, the larger diameter of the conductor made it easier to come off the clamp, as the insulator was bending under the effect of the tensile load on the conductor.
 - o There was no damage of the insulator (cracks or failure of the component). The insulator pin was bent in all test samples.
 - o There was some superficial damage on the outer jacket of the conductor.
- When testing with [REDACTED] Clamp Top insulators
 - o The slippage in all samples occurred at a lower tensile load as compared to the [REDACTED] Vise Top when tested with the same conductor

- The maximum tensile force achieved during the test with 35 kV 1/0 AWG ACSR conductor was higher than when testing with 17 kV 1/0 AWG ACSR conductor.
- There was no damage on the outer jacket of the conductor after the test.

Table 6-1: Suspension Clamps: Slip Test Results

Sample No.	Test Sample (Insulator)	Conductor Size (AWG or kcmil)	Max Slip Load Recorded		Comments (Observations)
			[lb]	[%RTS]	
2.1.1	██████████	17 kV, 1/0 AWG ACSR	1090.3	26.2 %	Slippage started at 868.8 lb
2.1.2	██████████	17 kV 1/0 AWG ACSR	1040.6	25.0 %	Slippage started at 865.5 lb
2.1.3	██████████	17 kV 1/0 AWG ACSR	1043.9	25.1 %	Slippage started at 870.2 lb
2.2.1	██████████	35 kV 1/0 AWG ACSR	970.9	23.3 %	Slippage started at 879.8 lb
2.2.2	██████████	35 kV 1/0 AWG ACSR	1048.3	25.2 %	Slippage started at 862.7 lb
2.2.3	██████████	35 kV 1/0 AWG ACSR	1024.1	24.6 %	Slippage started at 872.0 lb
2.3.1	██████████	22 kV 397.5 kcmil AAC	1107.3	16.4 %	Minimal slippage before reaching maximum load
2.3.2	██████████	22 kV 397.5 kcmil AAC	1195.1	17.7 %	Minimal slippage before reaching maximum load
2.3.3	██████████	22 kV 397.5 kcmil AAC	1142.9	16.9 %	Minimal slippage before reaching maximum load
2.4.1	██████████	15 kV, 1/0 AWG ACSR	863.3	20.8 %	Minimal slippage before reaching maximum load
2.4.2	██████████	15 kV 1/0 AWG ACSR	847.4	20.4 %	Minimal slippage before reaching maximum load
2.4.3	██████████	15 kV 1/0 AWG ACSR	872.6	21.0 %	Minimal slippage before reaching maximum load
2K.1.1	██████	17 kV, 1/0 AWG ACSR	380.4	9.1%	Slippage started before the hold.
2K.1.2	██████	17 kV 1/0 AWG ACSR	391.8	9.4%	Slippage started before the hold.
2K.1.3	██████	17 kV 1/0 AWG ACSR	291.9	7.0%	Slippage started before the hold.
2K.2.1	██████	35 kV 1/0 AWG ACSR	486.7	11.7%	Slippage started before the hold.
2K.2.2	██████	35 kV 1/0 AWG ACSR	393.1	9.4%	Slippage started before the hold.
2K.2.3	██████	35 kV 1/0 AWG ACSR	446.7	10.7%	Slippage started before the hold.

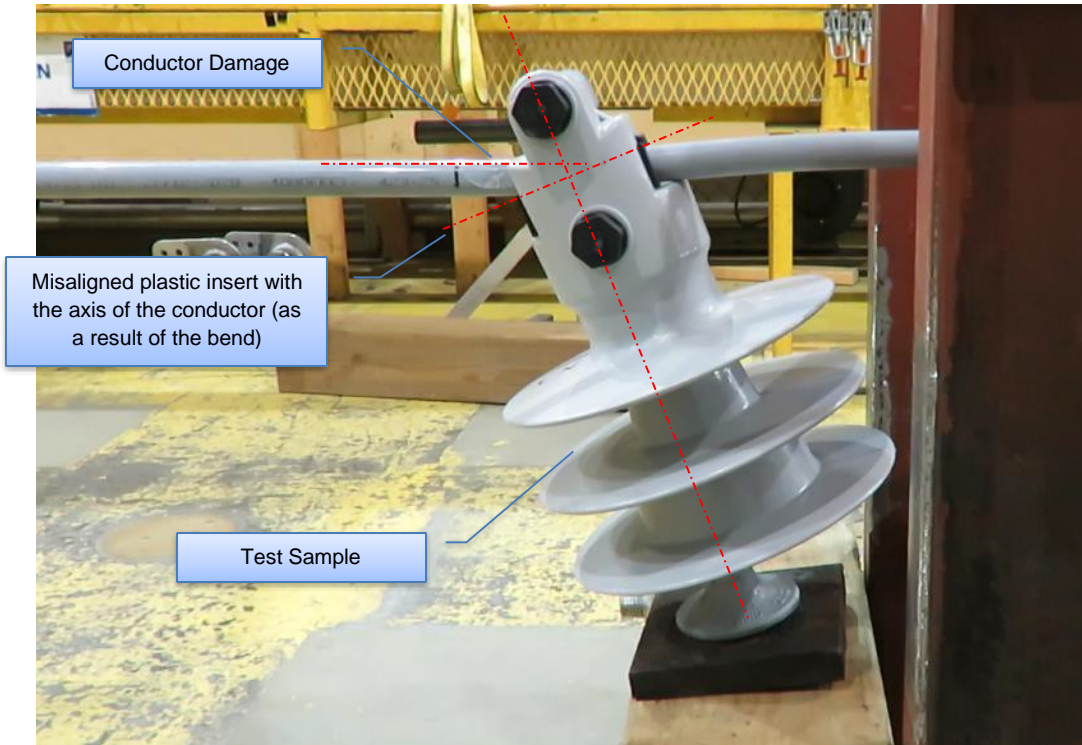


Figure 6-1: [REDACTED] - Typical Clamp and 1/0 AWG (17 kV) ACSR Conductor Position after Slip Test

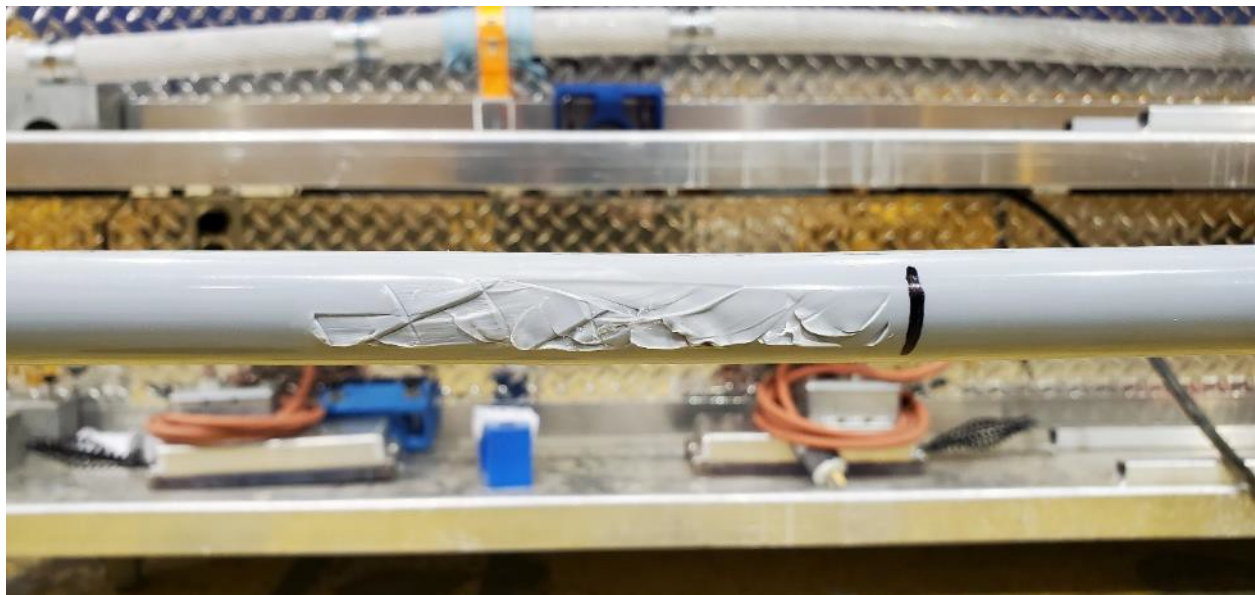


Figure 6-2: [REDACTED] - Typical 1/0 AWG (17 kV) ACSR Conductor Condition after Slip Test

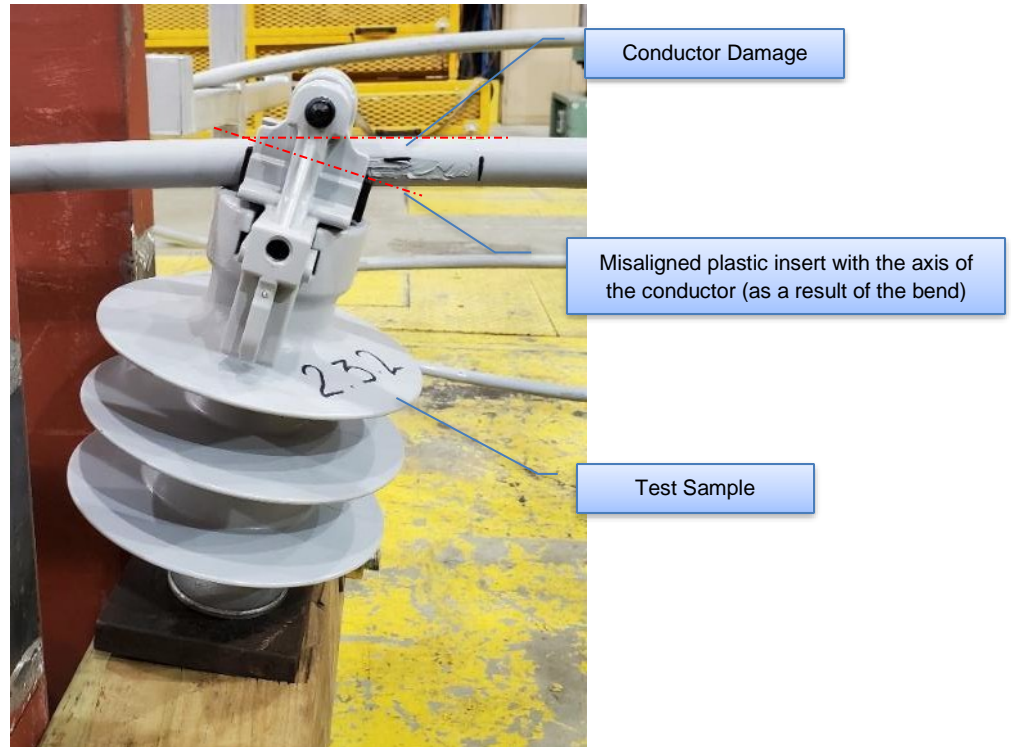


Figure 6-3: [REDACTED] - Typical Clamp and 397.5 kcmil (22 kV) AAC Conductor Position after Slip Test



Figure 6-4: [REDACTED] - Typical 397.5 kcmil (22 kV) AAC Conductor Condition after Slip Test



Figure 6-5: [REDACTED] - Typical Bend in Insulator Pin after Slip Test

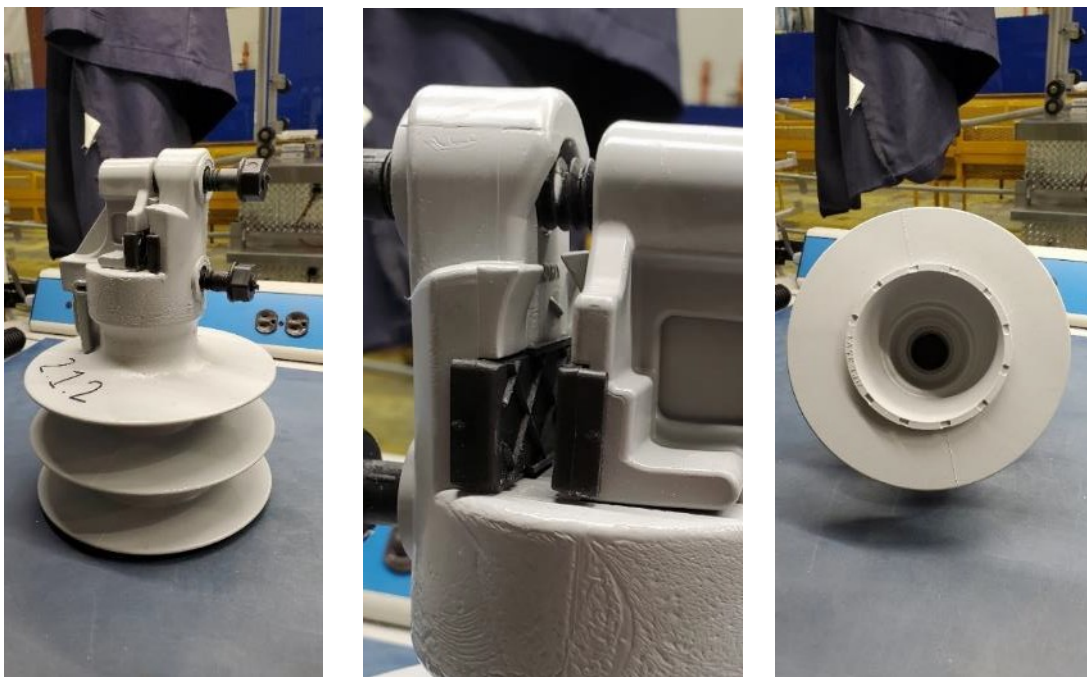


Figure 6-6: [REDACTED] - Typical Insulator Condition after Slip Test (no damage)

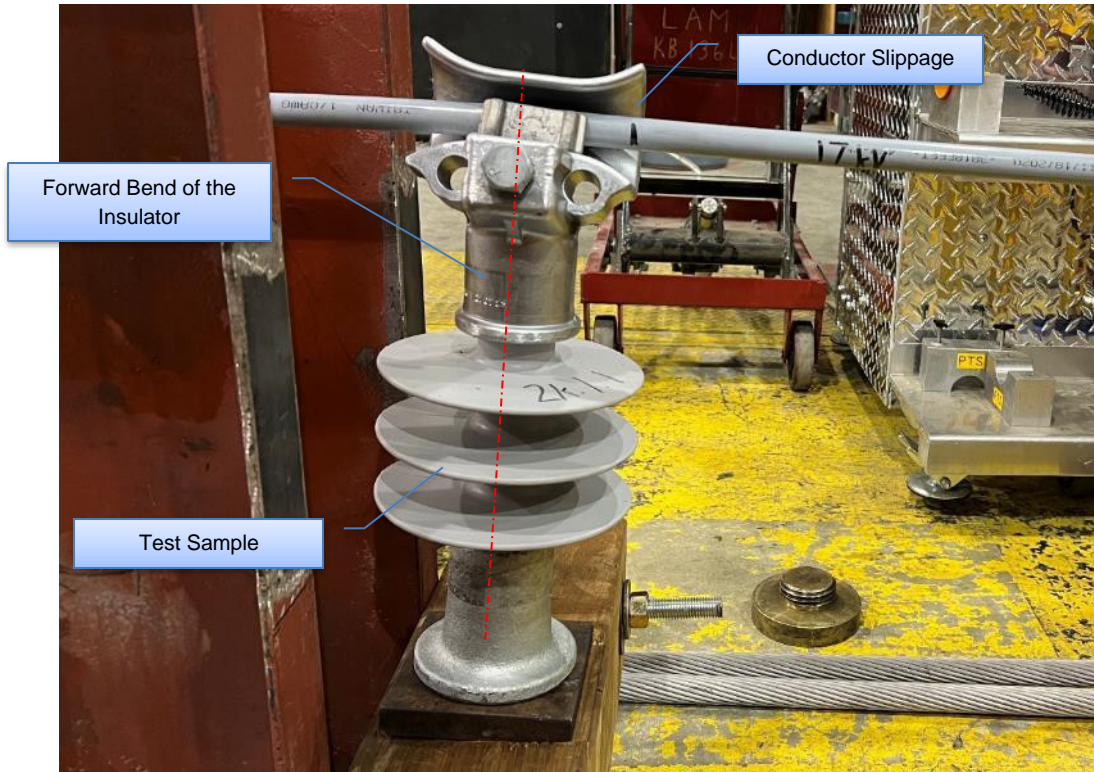


Figure 6-7: [REDACTED] - Typical Clamp and 1/0 AWG ACSR (17 kV) Conductor Position after Slip Test



Figure 6-8: [REDACTED] - Typical 1/0 AWG ACSR (17 kV) Conductor Condition after Slip Test

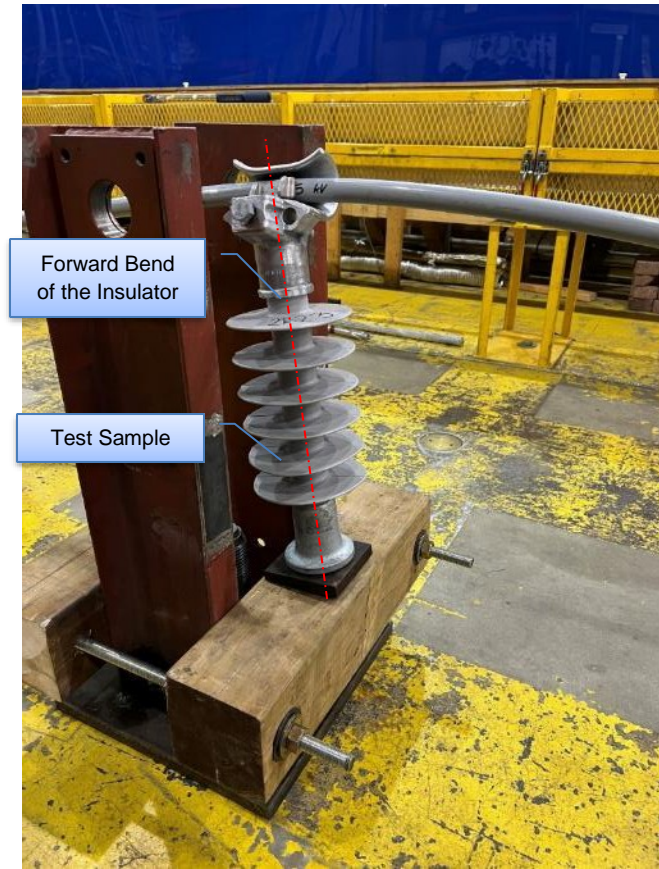


Figure 6-9: [REDACTED] - Typical Clamp and 1/0 AWG ACSR (35 kV) Conductor Position after Slip Test



Figure 6-10: [REDACTED] - Typical 1/0 AWG ACSR (35 kV) Conductor Condition after Slip Test



Figure 6-11: [REDACTED] - Typical Insulator and Pin Condition after Slip Test (no damage)

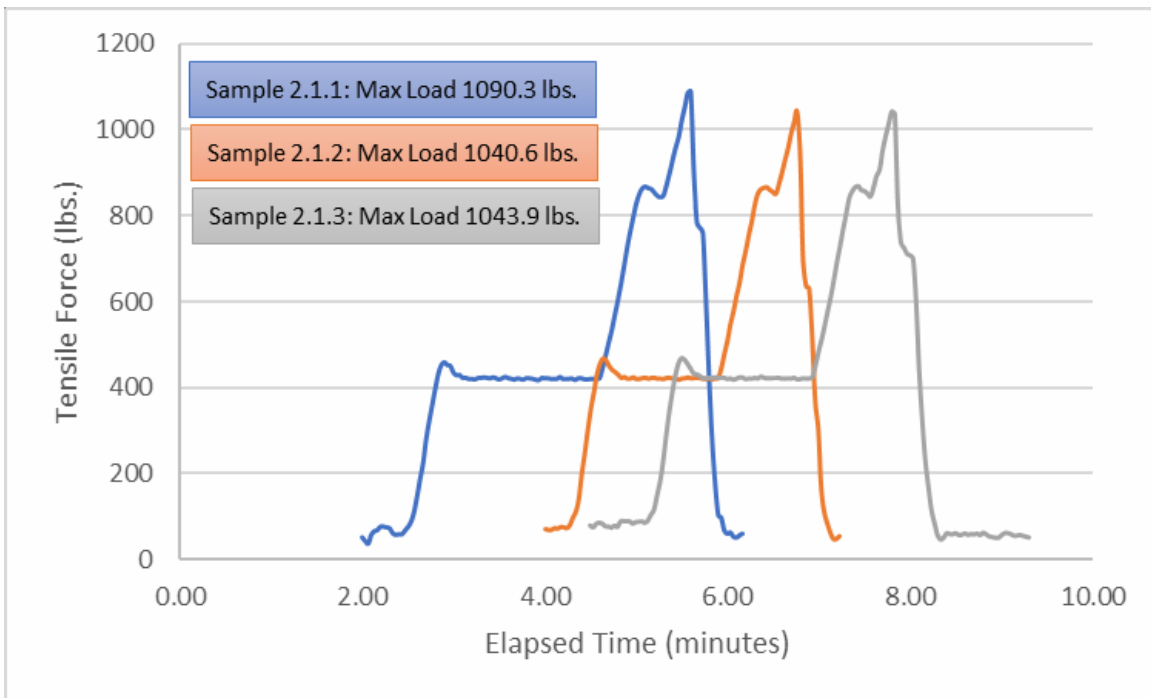


Figure 6-12: Slip Load Test – 17kV, 1/0 AWG ACSR with [REDACTED]

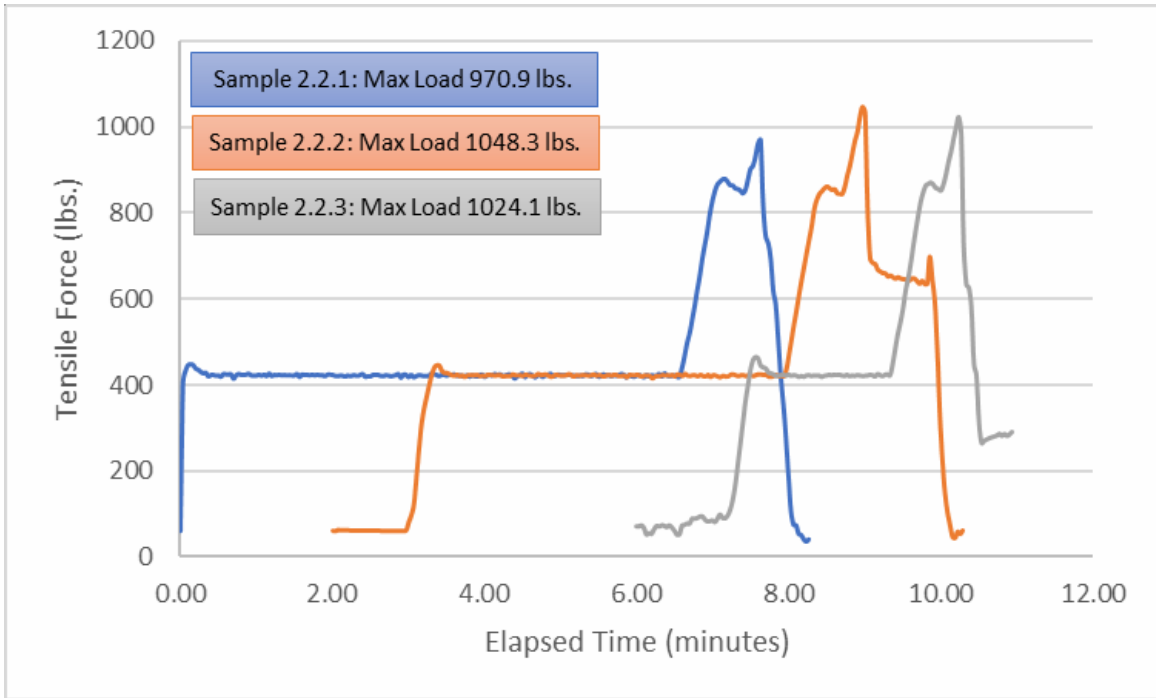


Figure 6-13: Slip Load Test – 35kV, 1/0 AWG ACSR with [REDACTED]

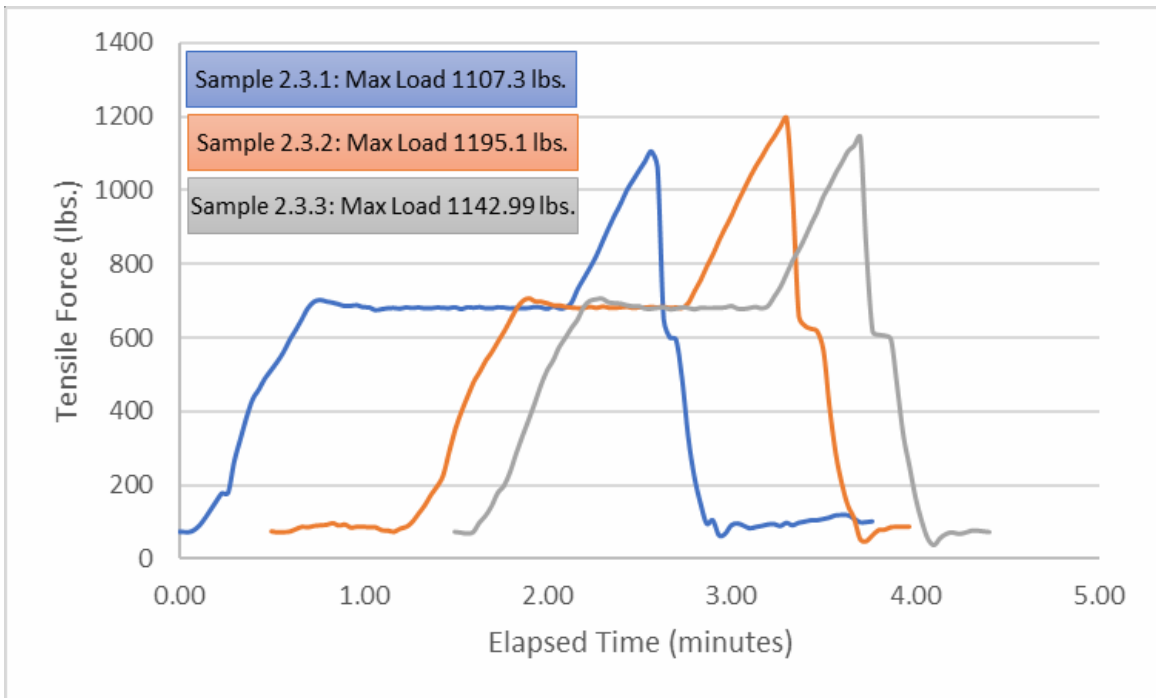


Figure 6-14: Slip Load Test – 22kV, 397.5 kcmil AAC with [REDACTED]

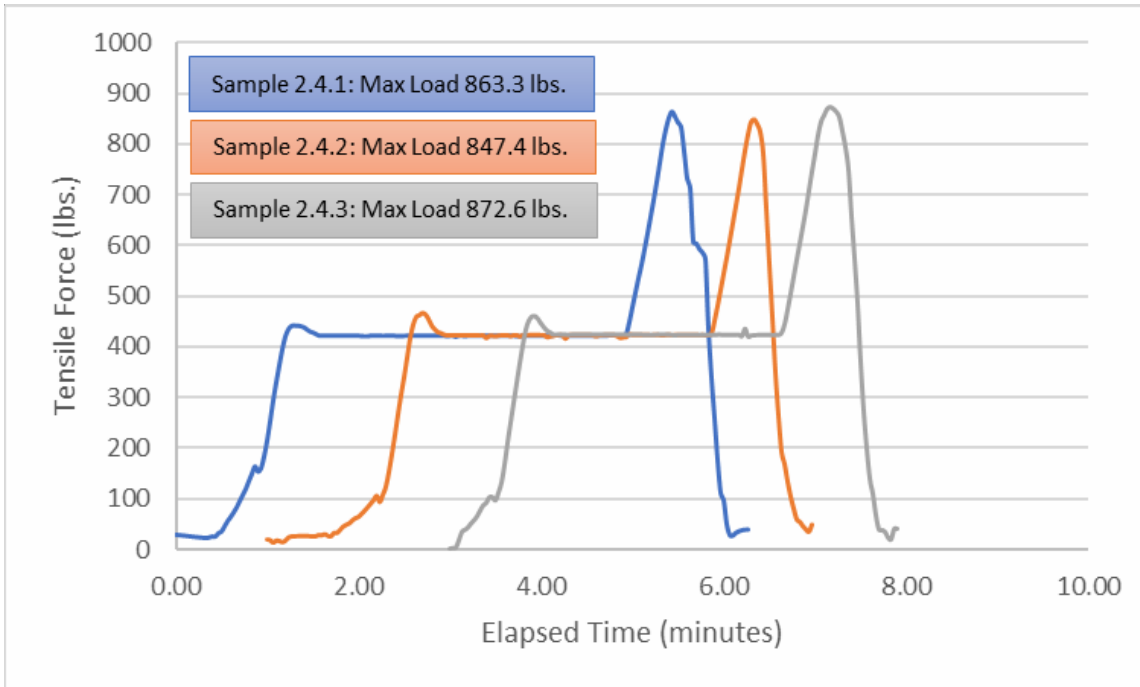


Figure 6-15: Slip Load Test – 15kV, 1/0 AWG ACSR with [REDACTED]

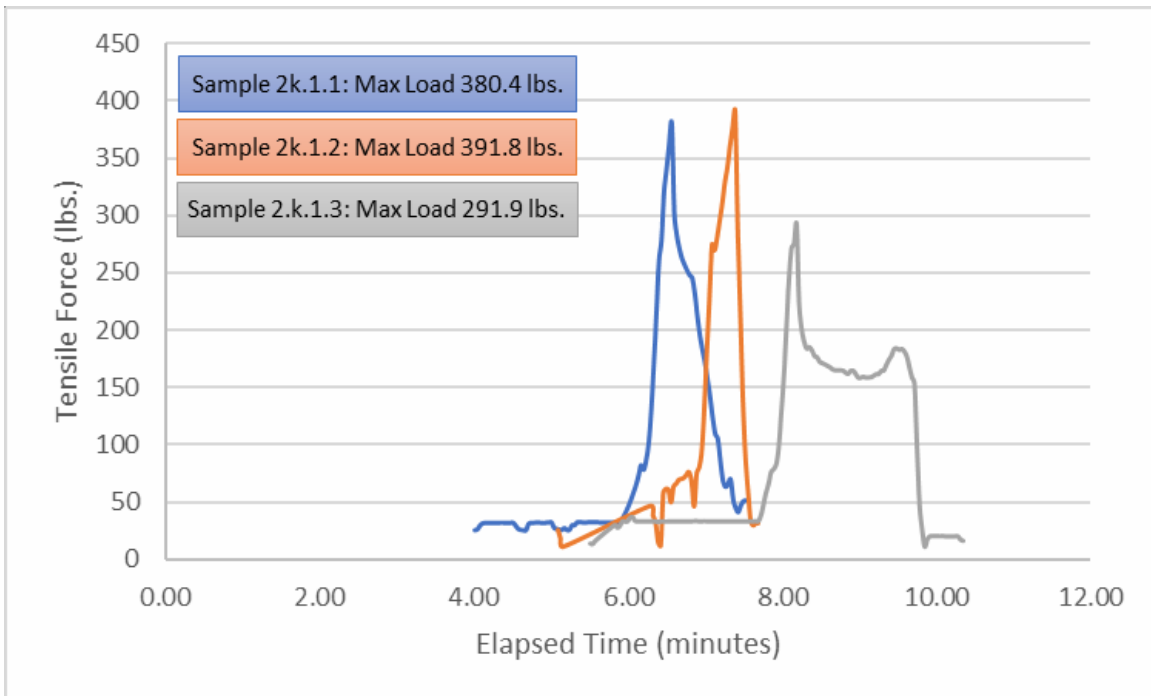


Figure 6-16: Slip Load Test – 17kV, 1/0 AWG ACSR with [REDACTED]

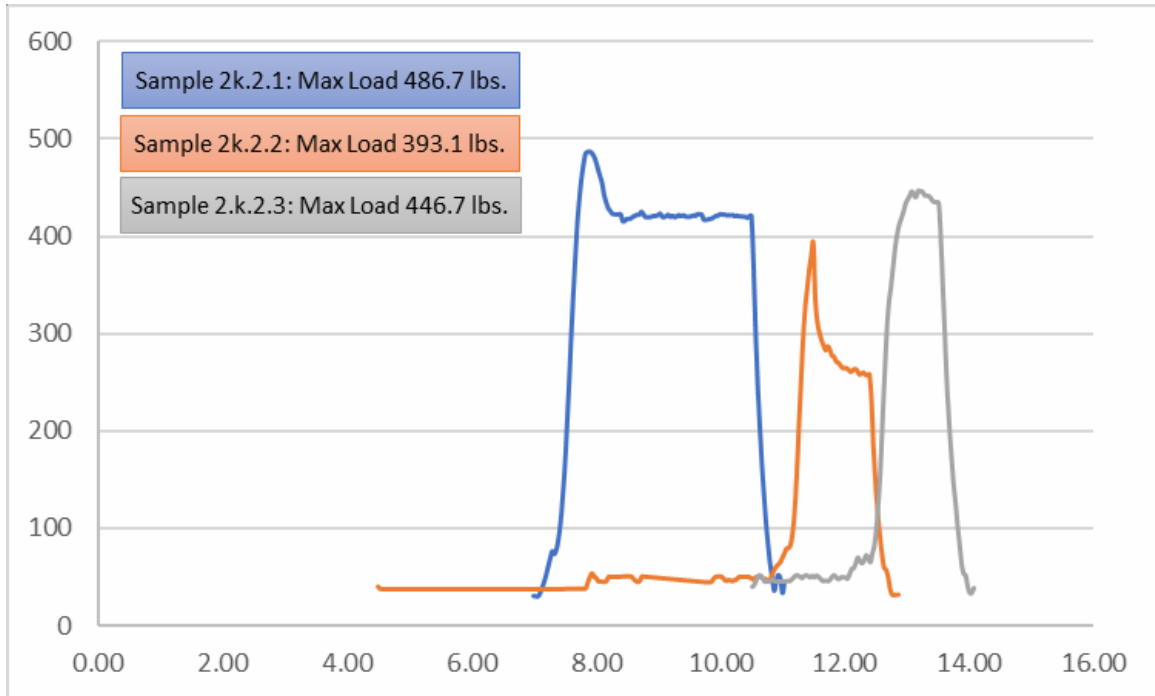


Figure 6-17: Slip Load Test – 35kV, 1/0 AWG ACSR with [REDACTED]

7 Acceptance Criteria

There were no acceptance criteria provided by the client. The objective of the test program was to determine the tensile load which resulted in conductor slippage relative to the clamp of a [REDACTED] Vise Top pin insulator or [REDACTED] Clamp Top post insulator.

8 Conclusion

When testing with [REDACTED] Vise Top insulators, the slip mechanism was the same for all samples: the slip occurred as a result of the insulator bending, causing the conductor to come off the plastic inserts in the insulator clamp. It is notable that all samples performed consistently around 1000 lb, regardless of the thickness of the insulation or conductor size.

When testing with [REDACTED] Clamp top insulators, the holding strength of the clamp was significantly lower than that of the [REDACTED] Vise Top insulator when installed on the same conductor. It is notable that when testing with the 35 kV 1/0 AWG conductor, the test samples performed better than when testing with 17 kV 1/0 AWG, suggesting that the thickness of the insulation could affect the results of the test.



Appendix A Acronyms and Abbreviations

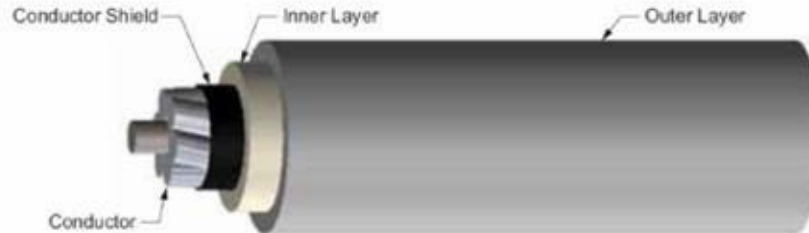
AAC	- All Aluminum Conductor
ACSR	- Aluminum Conductor Steel Reinforced
ANSI	- The American National Standards Institute
AWG	- American Wire Gauge
Cat. ID.	- Catalogue Identification
ISO	- International Organization for Standardization
RTS	- Rated Tensile Strength
XLPE	- Crosslinked Polyethylene

[The remainder of this page is intentionally left blank.]

Appendix B Conductor Data Sheet (as provided by Exponent)

Covered Conductor Data Sheet

Covered Conductor for 17kV and 35kV



- Conductor:
 - Aluminum Conductor Steel-Reinforced (ACSR) or
 - Hard Drawn Copper (HDCU)
- Conductor Shield: Semiconducting Thermoset Polymer
- Inner Layer: Crosslinked Low Density Polyethylene (XL-LDPE)
- Outer Layer: Crosslinked High Density Polyethylene (XL-HDPE)
 - Track Resistant
 - Abrasion Resistant

Temperature Rating:

Normal Operating Temperature: 90°C

Emergency Operating Temperature: 130°C

Short Circuit Temperature: 250°C

17kV Covered Conductor

ACSR

Conductor Size (AWG)	Conductor Type (Stranding)	Weight (lb/ft)	Conductor Diameter (in)	Conductor Shield Thickness (in)	Inner Layer Thickness (in)	Outer Layer Thickness (in)	Max Nominal Overall Diameter (in)	Maximum Rated Strength (lb.)	Ampacity per Conductor ¹ (Amps)
1/0	ACSR (6x1)	0.289	0.398	0.015 - 0.025	0.075	0.075	0.748	4,160	271
336.4	ACSR (18x1)	0.584	0.684	0.015 - 0.025	0.075	0.075	1.034	8,246	550
336.4	ACSR (30/7)	0.750	0.741	0.015 - 0.025	0.075	0.075	1.091	16,435	561
653.9	ACSR (18x3)	0.998	0.953	0.020 - 0.025	0.080	0.080	1.323	14,060	835

¹ Covered Conductor Cable Normal Operating Rating Criteria:

Ambient Temperature = 40°C

Conductor Temperature = 90°C

Load Factor = 100%

Wind Speed = 4 ft/sec

Coefficient of Emissivity = 0.5

Coefficient of Absorption = 0.5

Latitude = 34°

Elevation of Conductor above Sea Level = 0 ft

Atmosphere = Clear

Local Sun Time = 1:00 pm

Figure C - 1: [REDACTED] 17 kV 1/0 AWG ACSR Conductor Data

35kV Covered Conductor

ACSR

Conductor Size (AWG)	Conductor Type (Stranding)	Weight (lb/ft)	Conductor Diameter (in)	Conductor Shield Thickness (in)	Inner Layer Thickness (in)	Outer Layer Thickness (in)	Max Nominal Overall Diameter (in)	Maximum Rated Strength (lb.)	Ampacity per Conductor ¹ (Amps)
1/0	ACSR (6x1)	0.460	0.398	0.015 - 0.025	0.175	0.125	1.048	4,160	255
336.4	ACSR (18x1)	0.850	0.684	0.015 - 0.025	0.175	0.125	1.334	8,246	518
336.4	ACSR (30x7)	0.981	0.741	0.015 - 0.025	0.175	0.125	1.391	16,435	529
653.9	ACSR (18x3)	1.242	0.953	0.020 - 0.025	0.175	0.125	1.602	14,060	784

¹ Covered Conductor Cable Normal Operating Rating Criteria:

- Ambient Temperature = 40°C
- Conductor Temperature = 90°C
- Load Factor = 100%
- Wind Speed = 4 ft/sec
- Coefficient of Emissivity = 0.5
- Coefficient of Absorption = 0.5
- Latitude = 34°
- Elevation of Conductor above Sea Level = 0 ft
- Atmosphere = Clear
- Local Sun Time = 1:00 pm

Specifications

Must be manufactured to the latest editions of the following standards:

- ASTM B8
- ASTM B232
- ICEA S-121-733

Figure C - 2: XXXXXXXXXX 35 kV 1/0 AWG ACSR Conductor Data

Appendix C Insulator Data Sheet

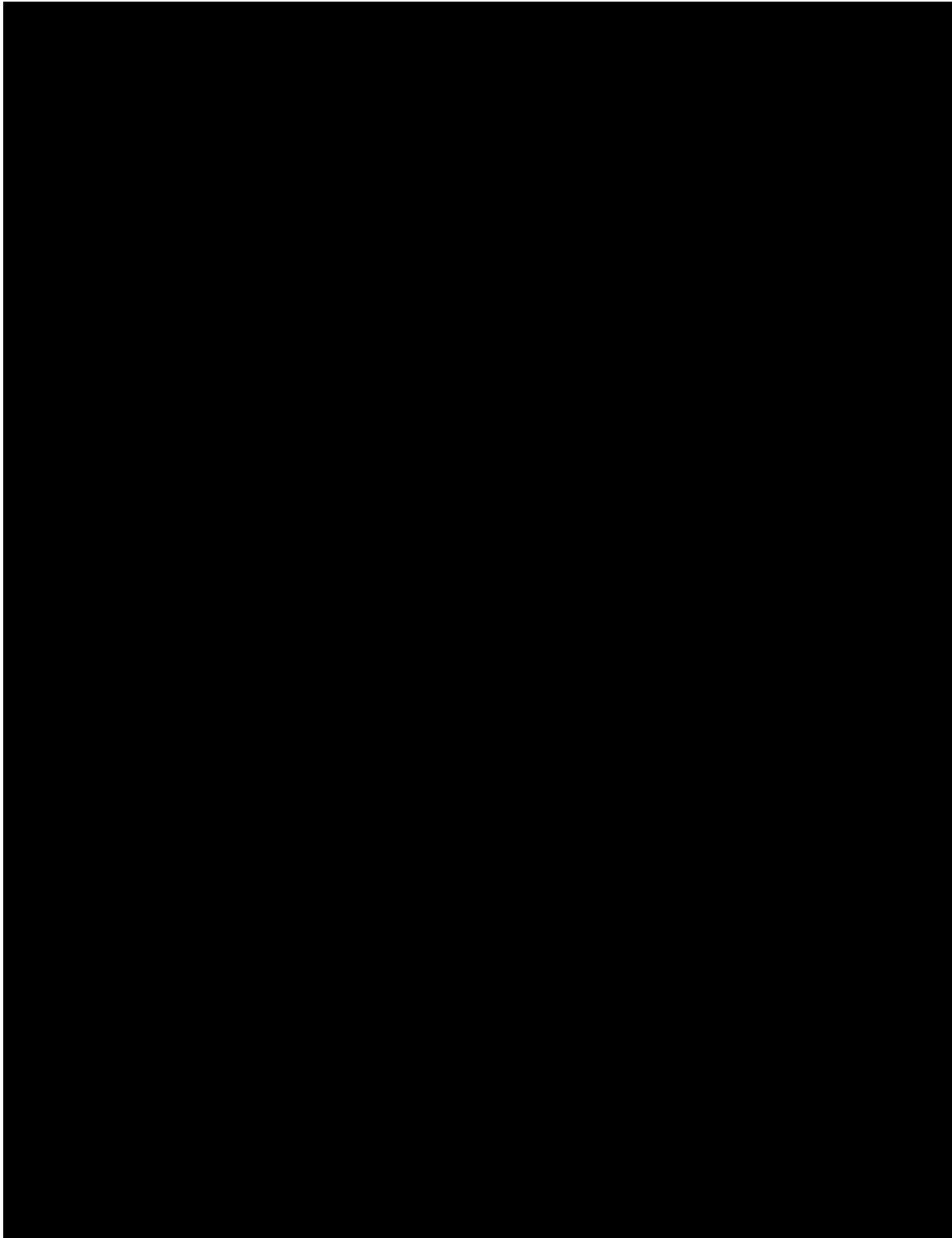


Figure D 1: [REDACTED] 35 kV Insulator [REDACTED]

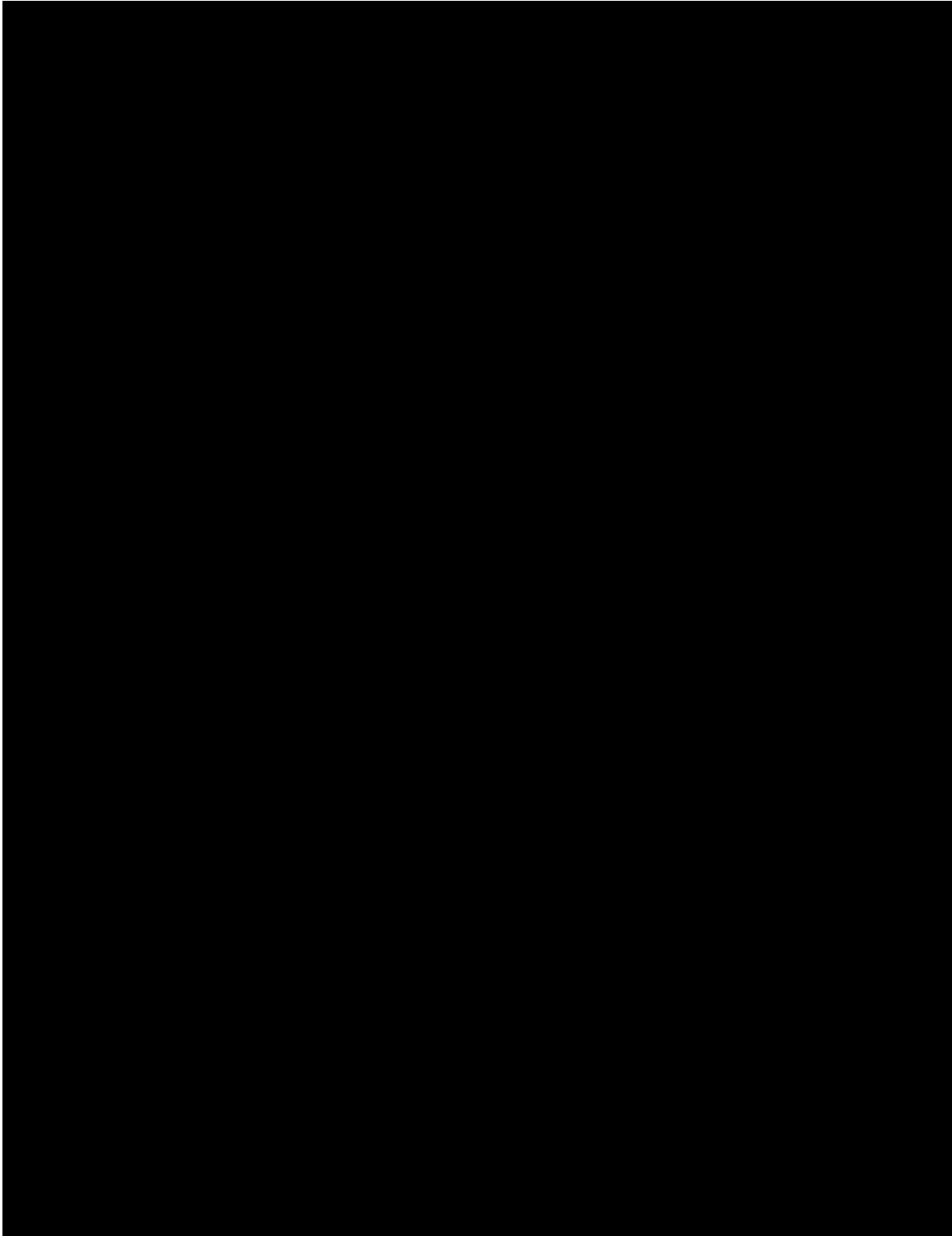


Figure D 2: [REDACTED] Post Insulators [REDACTED] and [REDACTED]

Appendix D Instrument Sheet

EQUIPMENT DESCRIPTION	ASSET No.	ACCURACY CLAIMED	CALIBRATION DATE	CALIBRATION DUE DATE	TEST USE
Data Logger	KIN-01836	±0.1% of Reading	May 20, 2021 May 27, 2022	May 20, 2022 May 27, 2023	Data acquisition
Load Cell/ Conditioner	KIN-01725/ KIN-01724	±1% of Reading	October 26, 2021	October 26, 2022	Load
Tape Measure	KIN-06890	< 0.05% of Reading	June 8, 2021 Jun 29, 2022	June 8, 2022 Jun 29, 2023	Length
Thermocouple/ Transmitter	KIN-00918/ KIN-00919	± 1 °C	October 28, 2021/ October 21, 2021	October 28, 2022/ October 21, 2022	Ambient Temperature

[The remainder of this page is intentionally left blank.]

Appendix E Kinectrics ISO 9001 Certificate of Registration



 **CERTIFICATE OF REGISTRATION**

This is to certify that
Kinectrics Inc.
Kinectrics North America Inc., Kinectrics International Europe ApS or Kinectrics International Inc.
800 Kipling Avenue, Unit 2, Toronto, Ontario M8Z 5G5 Canada

Refer to Attachment to Certificate of Registration dated November 5, 2021 for additional certified sites
operates a
Quality Management System
which complies with the requirements of
ISO 9001:2015
for the following scope of certification
This registration covers the Quality Management System for engineering, consulting, design, testing, project management, research, software development, assessments, operations support, and analysis within our facilities, and at field sites, for customers in the electricity industry and related energy sectors; both nuclear and conventional; as well as processing of radiological and conventional laundry and manufacture, inspection, and repair of personal protection equipment.

Certificate No.:	CERT-0119296	Original Certification Date:	July 7, 1998
File No.:	006555	Certification Effective Date:	May 23, 2021
Issue Date:	November 5, 2021	Certification Expiry Date:	May 22, 2024


Frank Camasta
Global Head of Technical Services
SAI Global Assurance

Registered by:
QMI-SAI Canada Limited (SAI Global), 20 Carlton Court, Suite 200, Toronto, Ontario M5W 7Y5 Canada. This registration is subject to the SAI Global Terms and Conditions for Certification. While all due care and skill was exercised in carrying out this assessment, SAI Global accepts responsibility only for gross negligence. This certificate remains the property of SAI Global and must be returned to them upon request.
To verify that this certificate is current, please refer to the SAI Global On-Line Certification Register:
https://www.sai-global.com/en-us/assurance/auditing_and_certification/certification_register/





Appendix F Distribution

Mr. Matt Bowers, Ph.D., P.E.

Exponent
17000 Science Drive, Suite 200
Bowie, Maryland 20715
Email: mbowers@exponent.com

Mr. Genti Gorja

Kinectrics AES Inc.
800 Kipling Ave, Unit No.2
Toronto, ON
Canada M8Z 5G5

Email: genti.gorja@kinectrics.com

[The remainder of this page is intentionally left blank.]



NOTE: Component manufacturer information has been redacted from this report

FULL MOCK-UP TEST ON COVERED CONDUCTORS & INSULATORS INSTALLED ON FIBERGLASS CROSS-ARM

K-580740-RP-003 R00

Prepared for

Exponent

Purchase Order No. 00062928

<p>Prepared by</p> <p> Digitally signed by GORJA Genti Date: 2022.10.03 14:24:16 -04'00'</p> <p><i>Signature & Date</i></p> <p>Genti Gorja P.Eng. Principal Engineer Line Asset Management</p>	<p>Reviewed by</p> <p> Digitally signed by André Maurice Date: 2022.10.03 14:31:13 -04'00'</p> <p><i>Signature & Date</i></p> <p>André Maurice Service Line Manager Line Asset Management</p>	<p>Approved by</p> <p>PETER Zsolt  Digitally signed by PETER Zsolt Date: 2022.10.03 14:59:09 -04'00'</p> <p><i>Signature & Date</i></p> <p>Zsolt Peter Ph.D. Business Area Director Line Asset Management</p>
---	--	---

Revision History

Rev 00	Description: Original issue			
	Issue Date: 2022-09-28	Prepared by: Genti Gorja	Reviewed by: André Maurice	Approved by: Zsolt Peter

DISCLAIMER

Kinectrics prepared this report as a work of authorship sponsored by their client. This report has been prepared solely for the benefit of the Client and may not be used or relied upon in whole or in part by any other person or entity without Client permission or without Kinectrics' permission if required by the Contract between Client and Kinectrics Inc . Neither Kinectrics, their client nor any person acting on behalf of them: (a) makes any warranty or representation whatsoever, express or implied, or assumes any legal liability of responsibility for any third party's use, or the results of such use, with respect to (i) the use of any information, apparatus, method, process, or similar item disclosed in this report including the merchantability or fitness for any particular purpose of any information contained in this report or the respective works or services supplied or performed or (ii) that such use does not infringe on or interfere with privately owned rights, including any party's intellectual property; or (b) assumes responsibility for any damages or other liability whatsoever (including any consequential damages resulting from a third party's selection or use of this report or any information, apparatus, method, process, or similar item disclosed.

Copyright © Kinectrics Inc. 2022. All rights reserved.



Table of Contents

1	Executive Summary	4
2	Test Objective and Test Standard	5
3	Test Sample.....	5
4	Test Setup	6
5	Test Procedure	7
6	Test Results.....	7
7	Acceptance Criteria.....	32
8	Conclusion	32
Appendix A	Acronyms and Abbreviations	33
Appendix B	Conductor Data Sheet (<i>as provided by the client</i>).....	34
Appendix C	Insulator Datasheet	36
Appendix D	Dead-End Bolted Clamps used in the test	38
Appendix E	Instrument Sheet.....	40
Appendix F	Kinectrics ISO 9001 Certificate of Registration	41
Appendix G	Distribution	42

1 Executive Summary

This report describes the “Full Mock-Up” Test performed on [redacted] Vise Top pin insulator (model [redacted]) and [redacted] Clamp Top post insulator (model [redacted] and [redacted]). The “Full Mock-Up” Test program was conducted for Exponent™ to evaluate the performance of [redacted] and [redacted] post insulators, installed on fiberglass crossarm, when used with:

- 15 kV 1/0 AWG, ACSR covered conductor
- 17 kV 1/0 AWG, ACSR covered conductor
- 35 kV 1/0 AWG, ACSR covered conductor and
- 22 kV 397.5 kcmil, AAC covered conductor.

Exponent™ supplied samples and accessories required for testing. Kinectrics received all samples, in good condition, on May 2, 2022. The test program and completion dates are summarized in Table 1-1.

Table 1-1: Test Program

Test ID	Sample ID	Conductor	Insulator Cat.ID.	Date Completed
3.1	3.1.1	17 kV 1/0 AWG ACSR	[redacted]	August 16, 2022
	3.1.2	17 kV 1/0 AWG ACSR	[redacted]	August 17, 2022
	3.1.3	17 kV 1/0 AWG ACSR	[redacted]	August 17, 2022
3.2	3.2.1	35 kV 1/0 AWG ACSR	[redacted]	August 17, 2022
	3.2.2	35 kV 1/0 AWG ACSR	[redacted]	August 17, 2022
	3.2.3	35 kV 1/0 AWG ACSR	[redacted]	August 18, 2022
3.3	3.3.1	22 kV 397.5 kcmil AAC	[redacted]	August 19, 2022
	3.3.2	22 kV 397.5 kcmil AAC	[redacted]	August 19, 2022
	3.3.3	22 kV 397.5 kcmil AAC	[redacted]	August 19, 2022
3.4	3.4.1	15 kV 1/0 AWG ACSR	[redacted]	August 18, 2022
	3.4.2	15 kV 1/0 AWG ACSR	[redacted]	August 18, 2022
	3.4.3	15 kV 1/0 AWG ACSR	[redacted]	August 18, 2022
3k.1	3k.1.1	17 kV 1/0 AWG ACSR	[redacted]	August 18, 2022
	3k.1.2	17 kV 1/0 AWG ACSR	[redacted]	August 18, 2022
	3k.1.3	17 kV 1/0 AWG ACSR	[redacted]	August 18, 2022
3k.2	3k.2.1	35 kV 1/0 AWG ACSR	[redacted]	August 18, 2022
	3k.2.2	35 kV 1/0 AWG ACSR	[redacted]	August 18, 2022
	3k.2.3	35 kV 1/0 AWG ACSR	[redacted]	August 18, 2022

The tests were conducted in accordance with Exponent™ requirements as outlined in the relevant sections of this document. The tests were performed by Kinectrics personnel at 800 Kipling Avenue, Toronto, Ontario, M8Z 5G5, Canada. The work was conducted under Exponent™ Purchase Order No. 00062928 dated January 14, 2022.

The tests were performed under Kinectrics’ ISO 9001 Quality Management System. A copy of ISO 9001 Certificate of Registration is included in Appendix F.

2 Test Objective and Test Standard

The Full Mock-up Test was intended to simulate mechanical loading in the event of a tree falling on the line and evaluate its effect on components (conductor, insulator, cross arm). The test was performed in general accordance with the procedures requested by Exponent™.

3 Test Sample

Three (3) insulator samples were tested for each conductor. The test samples consisted of [REDACTED] Vise Top pin insulator, model [REDACTED] or [REDACTED] Clamp Top pin insulator mounted on a fiberglass tangent crossarm, as indicated in Table 3-1.

A 45 ft length of each conductor type was terminated with one dead-end for testing in conjunction with the corresponding insulator design. Data sheets for the conductors, insulators and bolted dead-ends used in this test are shown in Appendix B through Appendix D.

Table 3-1: Full Mock-up Test: Sample ID and Configuration

Sample No.	Test Sample (Insulator Cat. ID.)	Conductor Size (AWG or kcmil)	Dead-end
3.1.1	[REDACTED]	17 kV, 1/0 AWG ACSR	[REDACTED]
3.1.2	[REDACTED]		
3.1.3	[REDACTED]		
3.2.1	[REDACTED]	35 kV 1/0 AWG ACSR	[REDACTED]
3.2.2	[REDACTED]		
3.2.3	[REDACTED]		
3.3.1	[REDACTED]	22 kV 397.5 kcmil AAC	[REDACTED]
3.3.2	[REDACTED]		
3.3.3	[REDACTED]		
3.4.1	[REDACTED]	15 kV 1/0 AWG ACSR	[REDACTED]
3.4.2	[REDACTED]		
3.4.3	[REDACTED]		
3K.1.1	[REDACTED]	17 kV, 1/0 AWG ACSR	[REDACTED]
3K.1.2	[REDACTED]		
3K.1.3	[REDACTED]		
3K.2.1	[REDACTED]	35 kV, 1/0 AWG ACSR	[REDACTED]
3K.2.2	[REDACTED]		
3K.2.3	[REDACTED]		

4 Test Setup

The test was performed in a hydraulically-activated horizontal test machine. The conductor length, terminated with the dead-end fitting installed at one end, was used for all three (3) insulator clamps. A different section of conductor was used for testing each new insulator.

The insulator was setup vertically, mounted on the fiberglass cross-arm supplied by Exponent™. The insulator was aligned in the vertical plane with the pulling cylinder. The cross-arm was mounted on a pole section, which was firmly fixed on the floor.

A system of pulleys ensured that the conductor was at an angle coming off the insulator clamp. The deflection angle of the conductor at the pulley was approximately 35° toward the cylinder (South) and 40° toward the insulator clamp (North). A schematic of the test set-up is shown in Figure 4-1 and a picture of the actual setup is shown in Figure 4-2.

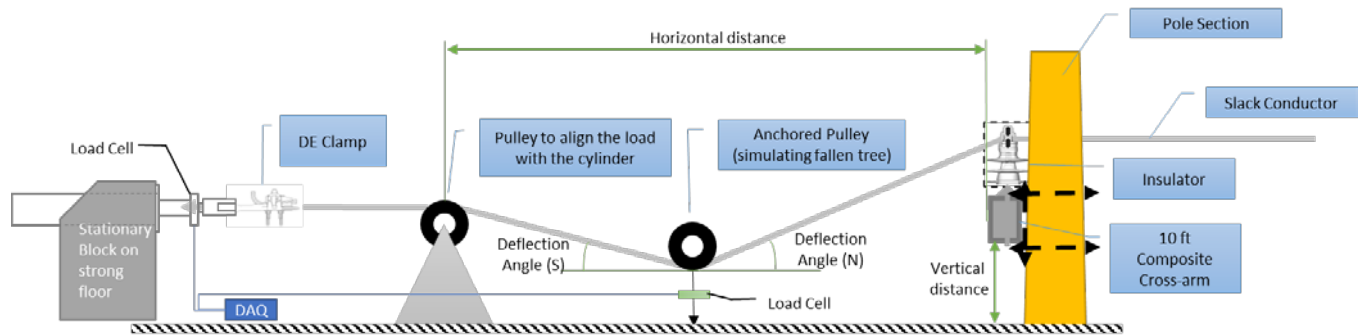


Figure 4-1: Full Mock-up Test - Schematic of the Setup

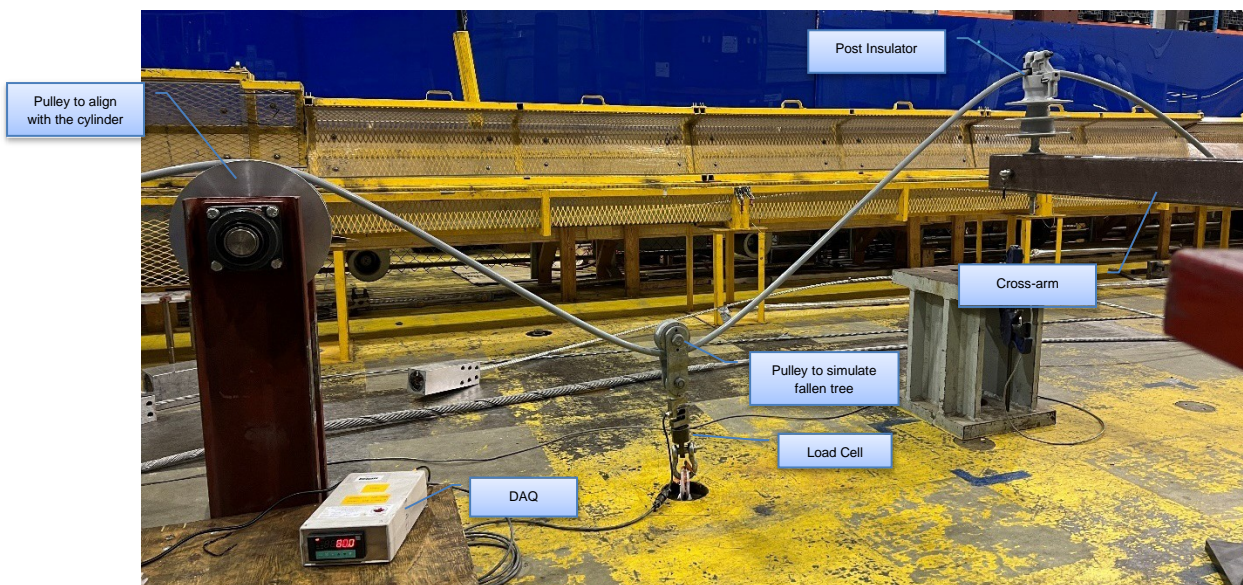


Figure 4-2: Full Mock-up Test - Picture of the Setup

The Full Mock-up Test was performed by increasing the horizontal tension until the vertical load on the pulley (simulating the fallen tree) reached 1,000 lb. The vertical load on the pulley was measured directly by attaching a load cell between the pulley and the floor. The vertical permanent deflection of both ends of the cross-arm was measured by referencing the vertical distance of the insulator attachment point on the cross-arm to the floor. The measurement of the vertical deflection on the side of the crossarm where the insulator was mounted (the force was applied) was labeled as “West” and the measurement on the opposite end of the crossarm was labeled as “East”. The data logging rate during the test was every one (1) second. The test was carried out in a temperature-controlled laboratory at $20\text{ }^{\circ}\text{C} \pm 2\text{ }^{\circ}\text{C}$.

5 Test Procedure

The Full Mock-up Test procedure was conducted as follows:

- The insulator/cross-arm and conductor assembly were setup as shown in Figure 4-2
- A small pretension value was applied (to remove the slack from the conductor) and the conductor was marked at the entry points in the clamp.
- The conductor tension was increased until the vertical load reached 1,000 lb on the pulley simulating the fallen tree. The conductor at the insulator clamp was visually monitored for slippage.
- The horizontal tensile load was continuously increased at a rate of 1,000 lb/min until damage to the cross-arm or slippage of the conductor inside the clamp occurred.

Upon completion of the test on the first sample, the same steps were repeated on a new insulator (second and third sample) on an unused section on the conductor (approx. 10 ft North of the first setup). A new cross-arm was installed in cases where the previous test resulted in damage. Video recordings of the tests were also provided for Exponent’s future reference.

6 Test Results

The load and conductor slippage during the test were monitored and recorded. Test results are summarized in Table 6-1 to Table 6-6. Loading profiles for each sample are shown in Figure 6-1 to Figure 6-6. Photos of the slippage and the sample after the test were taken for documentation purposes. Typical pictures of sample condition after the test are shown in Figure 6-7 through Figure 6-34. General observations from the test, common for all samples are provided below:

- When testing with [REDACTED] Vise Top insulators, the majority of test samples, achieved the target vertical load of 1,000 lb without slippage of the conductor at the clamp. There was no damage to the conductor (superficial marks only on the outer jacket), however there was damage on the fiberglass cross arm caused by the flange of the insulator pin.

- When testing with [redacted] Clamp Top insulators, the slippage in all samples occurred below the target vertical load of 1000 lb (and at a lower tensile load as compared to the [redacted] Vise Top when tested with the same conductor). There was no damage on the outer jacket of the conductor after the test and there was no damage observed on the fiberglass cross-arm after the test.

Table 6-1: Test Results: [redacted] and 17 kV 1/0 AWG ACSR

Sample No.	Max. Vertical Load	Vertical Deformation of Cross Arm		Comments (Observations)
	[lb]	West* [inch]	East** [inch]	
3.1.1	939.0	- 2.40	2.30	Cross-arm damaged under the flange of the insulator pin. No slippage at the clamp. No damage to conductor.
3.1.2	1095.0	- 3.00	2.64	No damage on the Cross-arm. No slippage at the clamp. No damage to conductor.
3.1.3	1042.0	- 2.36	2.28	Cross-arm damaged under the flange of the insulator pin. No slippage at the clamp. No damage to conductor.

(*) "West" references the downward deformation at the crossarm where the insulator was mounted

(**) "East" references the upward deformation at the free end of the crossarm, opposite to the side where the insulator was mounted

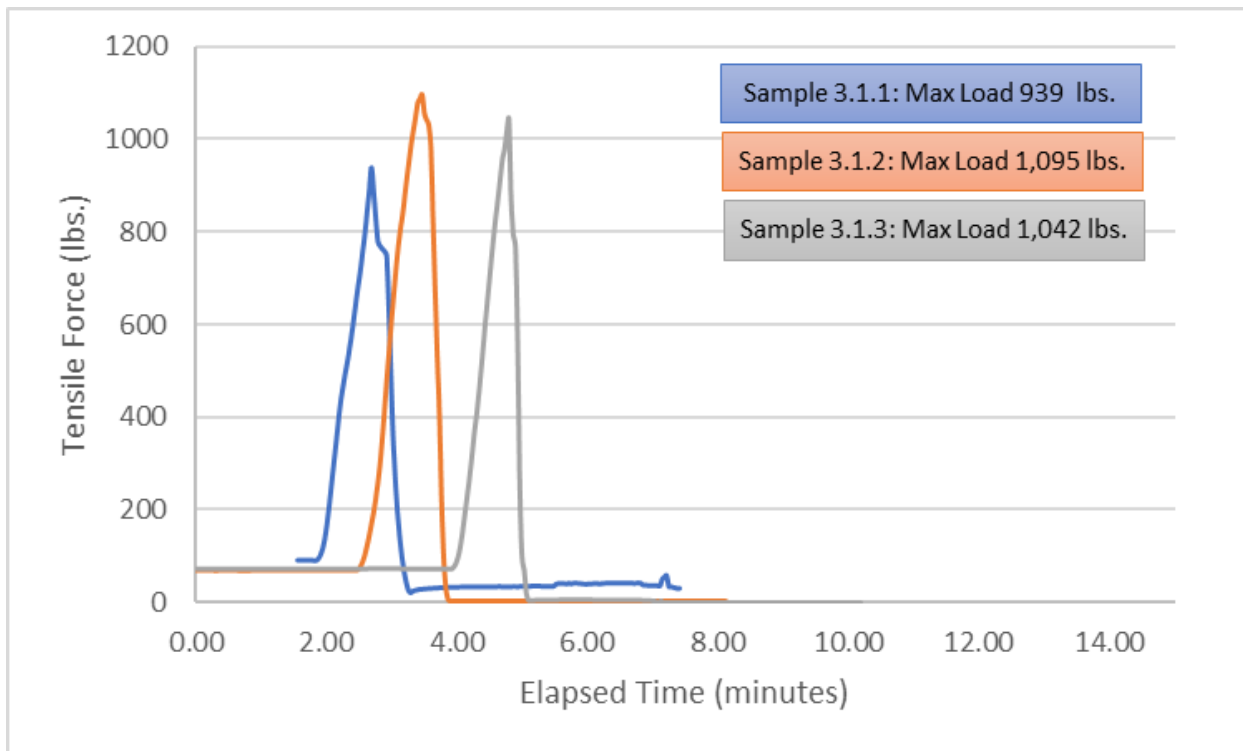


Figure 6-1: Test Load Profile: [redacted] and 17 kV 1/0 AWG ACSR

Table 6-2: Test Results: [REDACTED] and 35 kV 1/0 AWG ACSR

Sample No.	Max. Vertical Load	Vertical Deformation of Cross Arm		Comments (Observations)
	[lb]	West* [inch]	East** [inch]	
3.2.1	1063.0	- 1.97	1.65	Cross-arm damaged under the flange of the insulator pin. No slippage at the clamp. No damage to conductor.
3.2.2	985.0	- 2.04	1.97	Cross-arm damaged under the flange of the insulator pin. No slippage at the clamp. No damage to conductor.
3.2.3	1019.0	- 1.26	1.02	Cross-arm damaged under the flange of the insulator pin. No slippage at the clamp. No damage to conductor.

(*) "West" references the downward deformation at the crossarm where the insulator was mounted

(**) "East" references the upward deformation at the free end of the crossarm, opposite to the side where the insulator was mounted

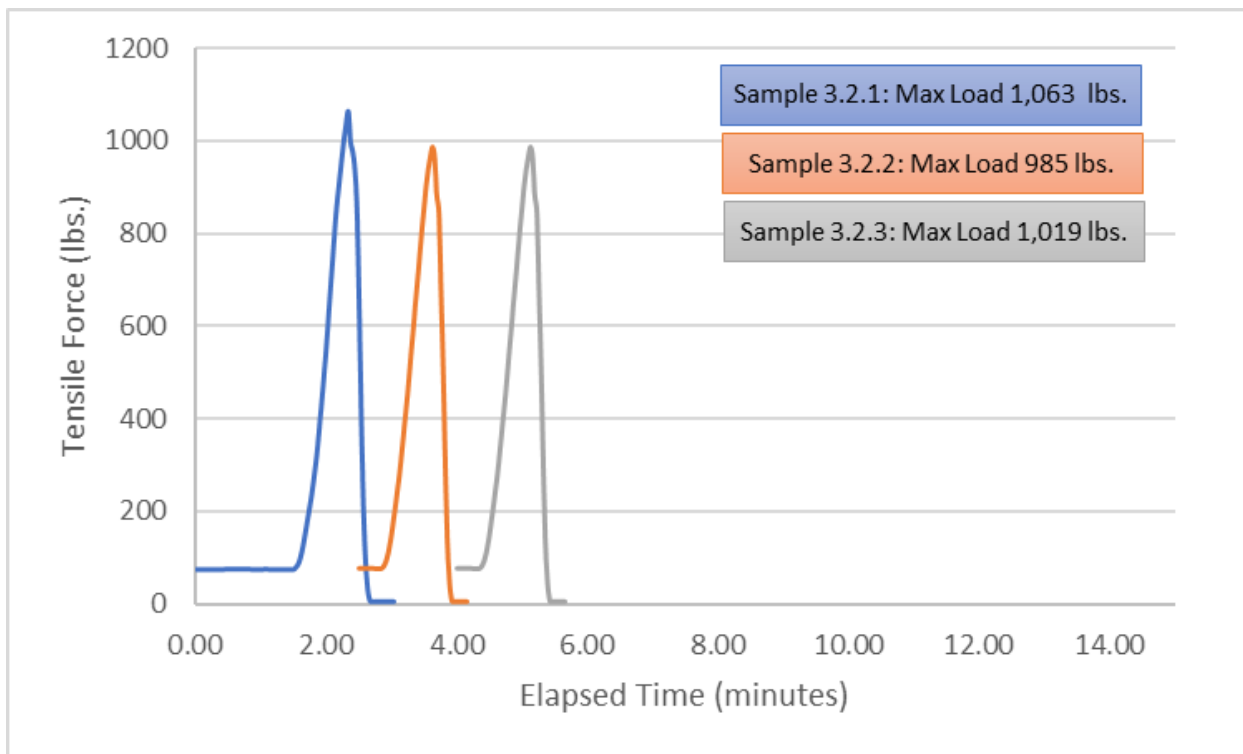


Figure 6-2: Test Load Profile: [REDACTED] and 35 kV 1/0 AWG ACSR

Table 6-3: Test Results: [REDACTED] and 22 kV 397.5 kcmil AAC

Sample No.	Max. Vertical Load	Vertical Deformation of Cross Arm		Comments (Observations)
	[lb]	West* [inch]	East** [inch]	
3.3.1	1326.0	- 1.93	1.57	Cross-arm damaged under the flange of the insulator pin. No slippage at the clamp. No damage to conductor.
3.3.2	1060.0	- 1.77	1.61	Cross-arm damaged under the flange of the insulator pin. No slippage at the clamp. No damage to conductor.
3.3.3	988.0	- 2.60	2.40	Cross-arm damaged under the flange of the insulator pin. No slippage at the clamp. No damage to conductor.

(*) "West" references the downward deformation at the crossarm where the insulator was mounted

(**) "East" references the upward deformation at the free end of the crossarm, opposite to the side where the insulator was mounted

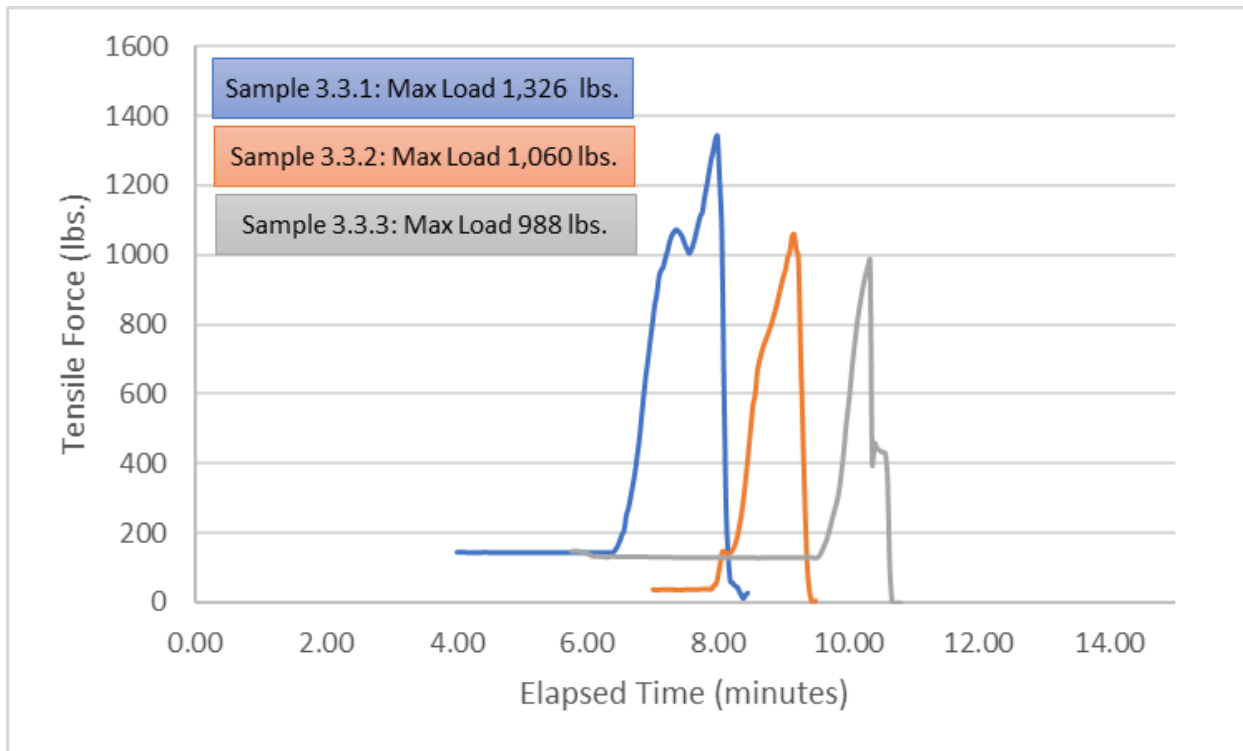


Figure 6-3: Test Load Profile: [REDACTED] and 22 kV 397.5 kcmil AAC

Table 6-4: Test Results: [REDACTED] and 15 kV 1/0 AWG ACSR

Sample No.	Max. Vertical Load	Vertical Deformation of Cross Arm		Comments (Observations)
	[lb]	West* [inch]	East** [inch]	
3.4.1	880.0	- 0.35	0.35	Cross-arm damaged under the flange of the insulator pin. No slippage at the clamp. No damage to conductor.
3.4.2	1090.0	- 2.00	1.46	Cross-arm damaged under the flange of the insulator pin. No slippage at the clamp. No damage to conductor.
3.4.3	789.0	- 1.54	1.42	Cross-arm damaged under the flange of the insulator pin. No slippage at the clamp. No damage to conductor.

(*) "West" references the downward deformation at the crossarm where the insulator was mounted

(**) "East" references the upward deformation at the free end of the crossarm, opposite to the side where the insulator was mounted

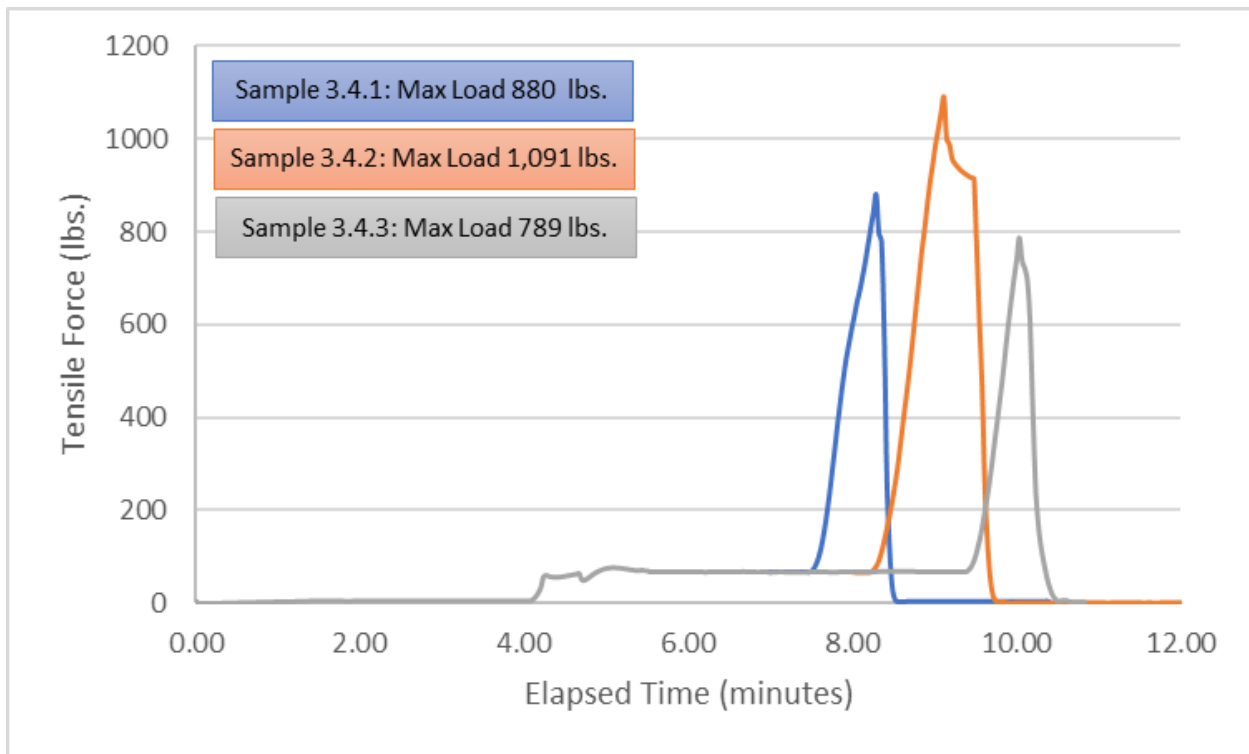


Figure 6-4: Test Load Profile: [REDACTED] and 15 kV 1/0 AWG ACSR

Table 6-5: Test Results: [REDACTED] and 17 kV 1/0 AWG ACSR

Sample No.	Max. Vertical Load	Vertical Deformation of Cross Arm		Comments (Observations)
	[lb]	West* [inch]	East** [inch]	
3K.1.1	573.0	- 1.57	1.57	Conductor slip at the clamp. No damage to the Cross-arm under the flange of the insulator pin. No damage to conductor
3K.1.2	396.0	- 0.24	0.24	Conductor slip at the clamp. No damage to the Cross-arm under the flange of the insulator pin. No damage to conductor
3K.1.3	508.0	- 0.20	0.12	Conductor slip at the clamp. No damage to the Cross-arm under the flange of the insulator pin. No damage to conductor.

(*) "West" references the downward deformation at the crossarm where the insulator was mounted

(**) "East" references the upward deformation at the free end of the crossarm, opposite to the side where the insulator was mounted

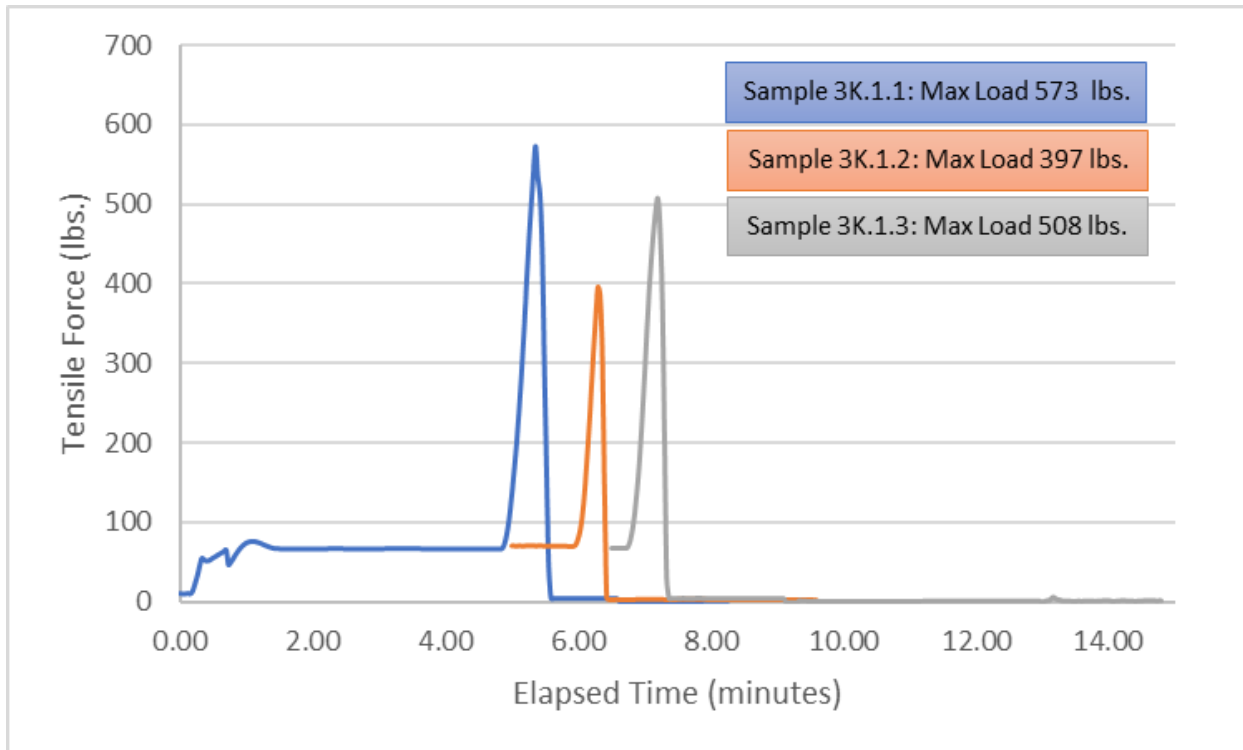


Figure 6-5: Test Load Profile: [REDACTED] and 17 kV 1/0 AWG ACSR

Table 6-6: Test Results: [REDACTED] and 35 kV 1/0 AWG ACSR

Sample No.	Max. Vertical Load	Vertical Deformation of Cross Arm		Comments (Observations)
	[lb]	West* [inch]	East** [inch]	
3K.2.1	555.0	- 0.20	0.16	Conductor slip at the clamp. No damage to the Cross-arm under the flange of the insulator pin. No damage to conductor
3K.2.2	548.0	- 0.08	0.04	Conductor slip at the clamp. No damage to the Cross-arm under the flange of the insulator pin. No damage to conductor
3K.2.3	693.0	- 0.08	0.04	Conductor slip at the clamp. No damage to the Cross-arm under the flange of the insulator pin. No damage to conductor

(*) "West" references the downward deformation at the crossarm where the insulator was mounted

(**) "East" references the upward deformation at the free end of the crossarm, opposite to the side where the insulator was mounted

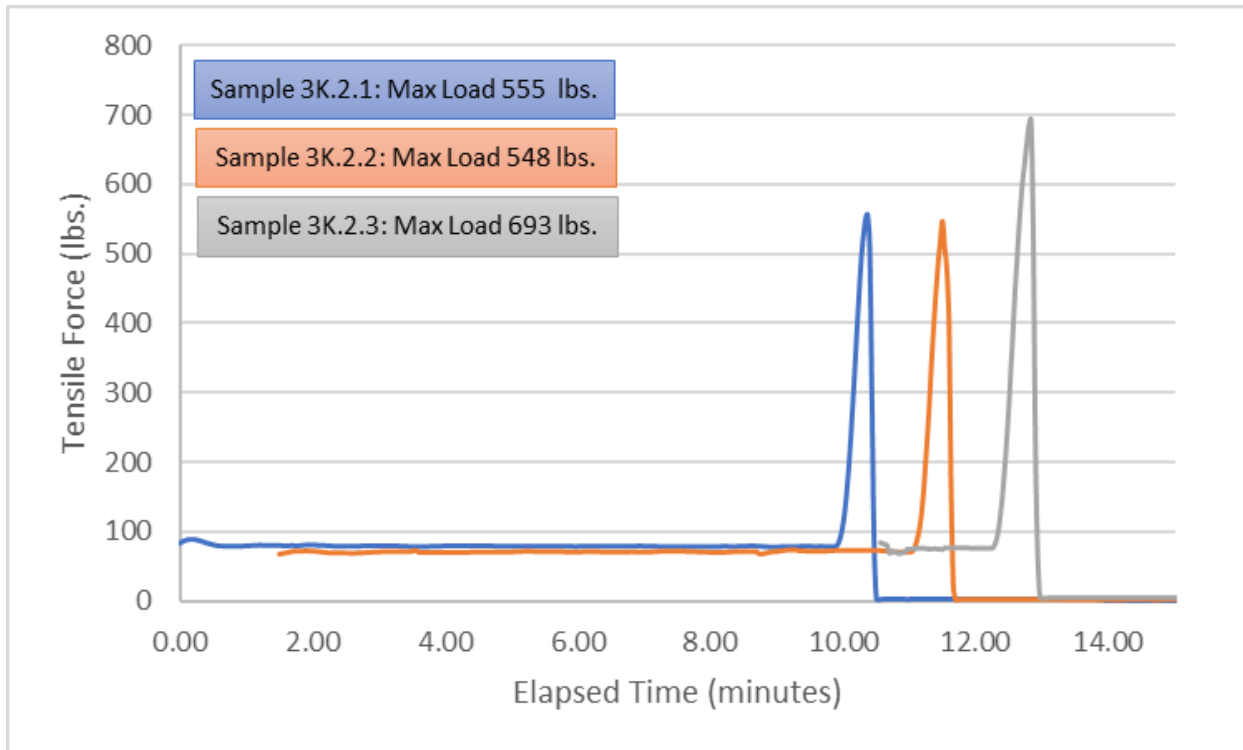


Figure 6-6: Test Load Profile: [REDACTED] and 35 kV 1/0 AWG ACSR

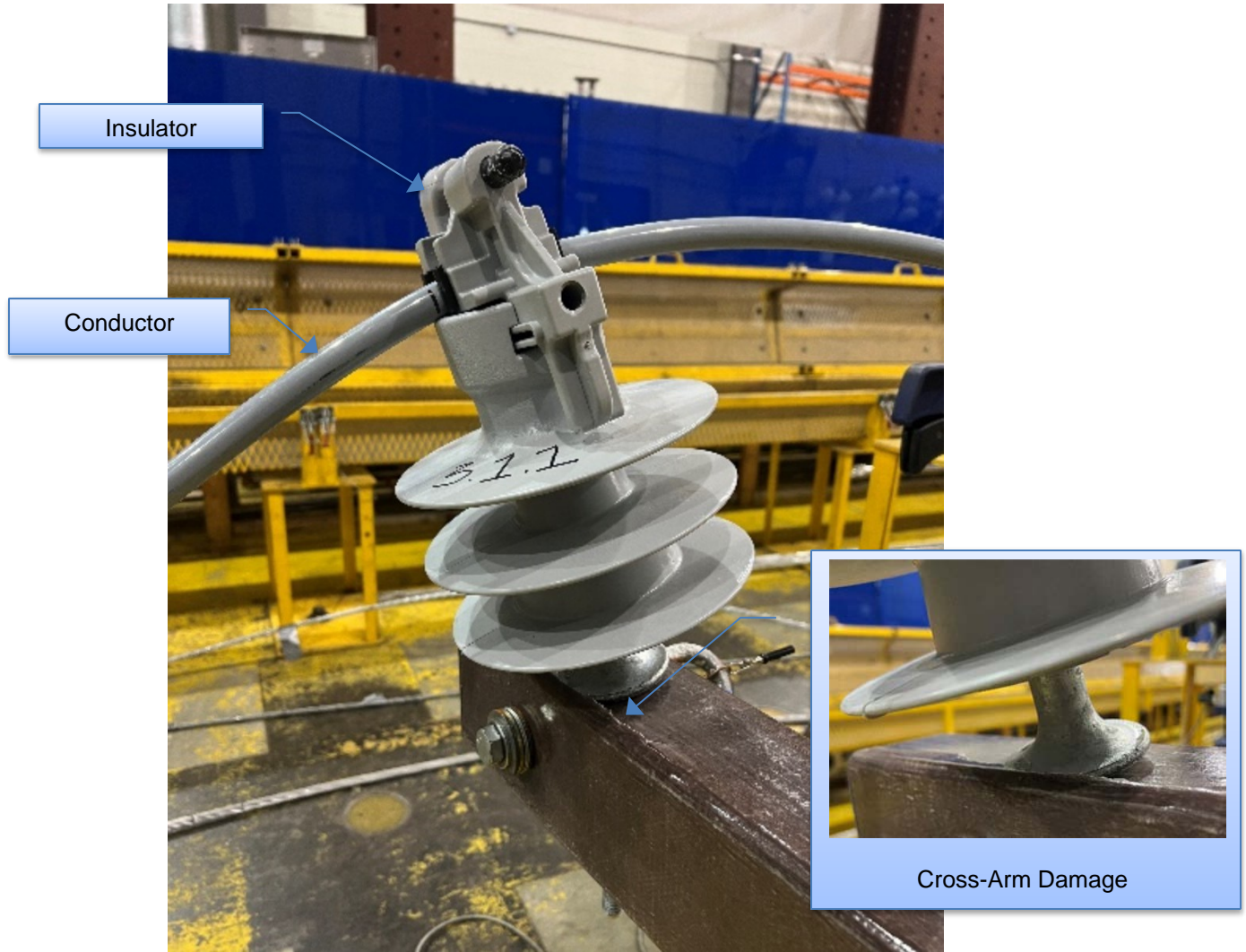


Figure 6-7: Sample 3.1.1 – Insulator and Cross-arm Condition after Test



Figure 6-8: Sample 3.1.1 - 17 kV, 1/0 AWG ACSR Condition after Test

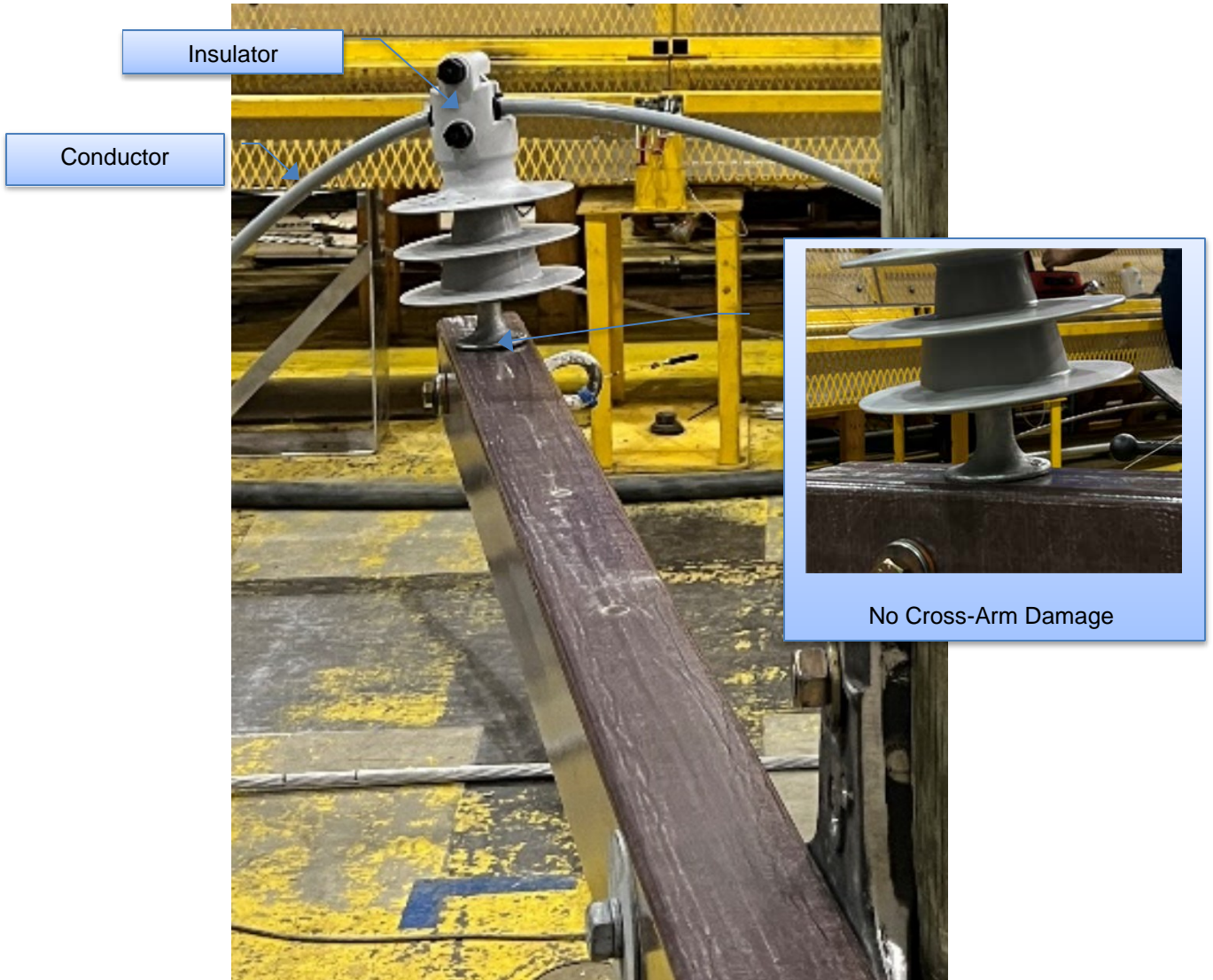


Figure 6-9: Sample 3.1.2 - – Insulator and Cross-arm Condition after Test



Figure 6-10: Sample 3.1.2 - 17 kV, 1/0 AWG ACSR Condition after Test

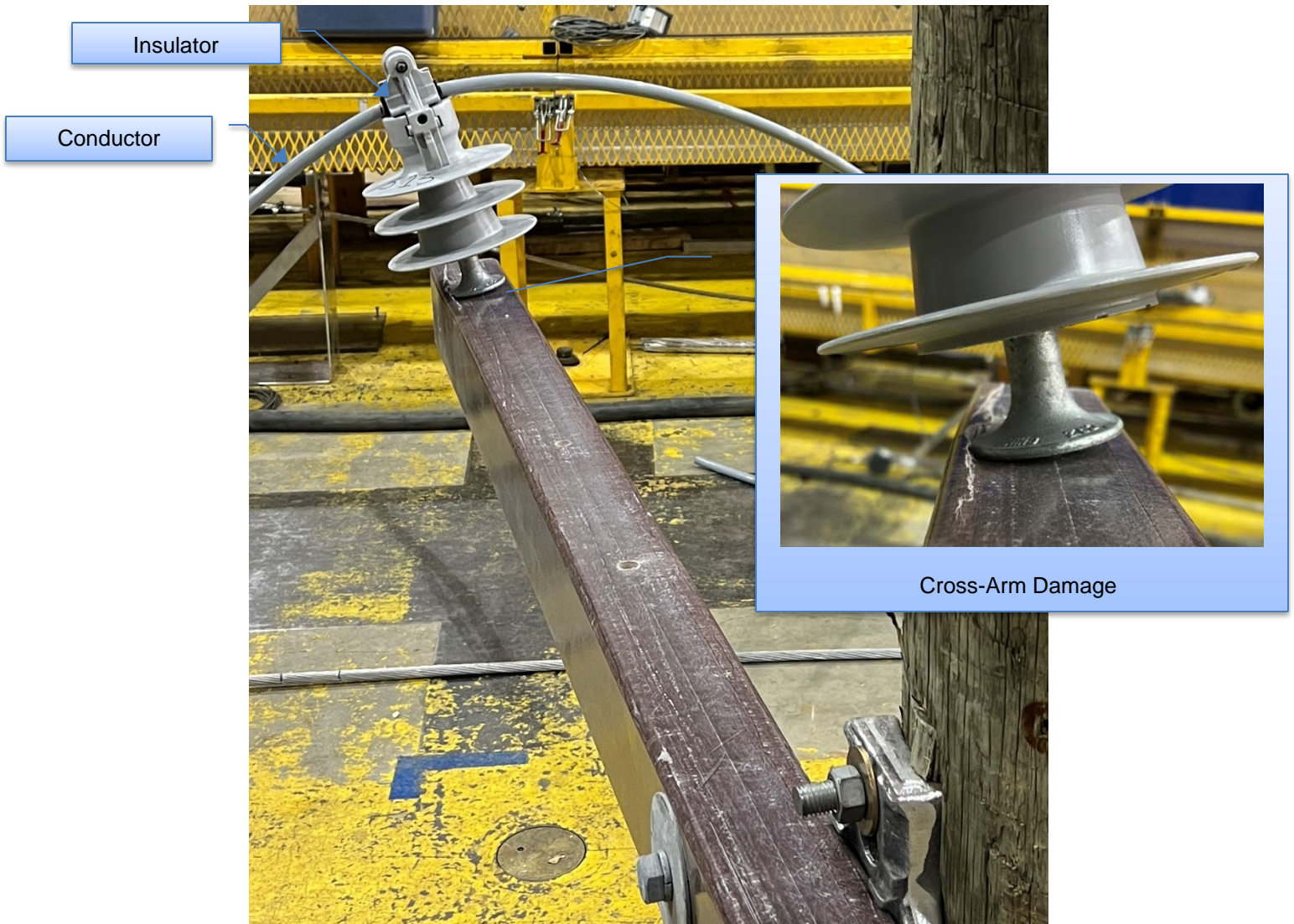


Figure 6-11: Sample 3.1.3 – Insulator and Cross-arm Condition after Test



Figure 6-12: Sample 3.1.3 - 17 kV, 1/0 AWG ACSR Condition after Test

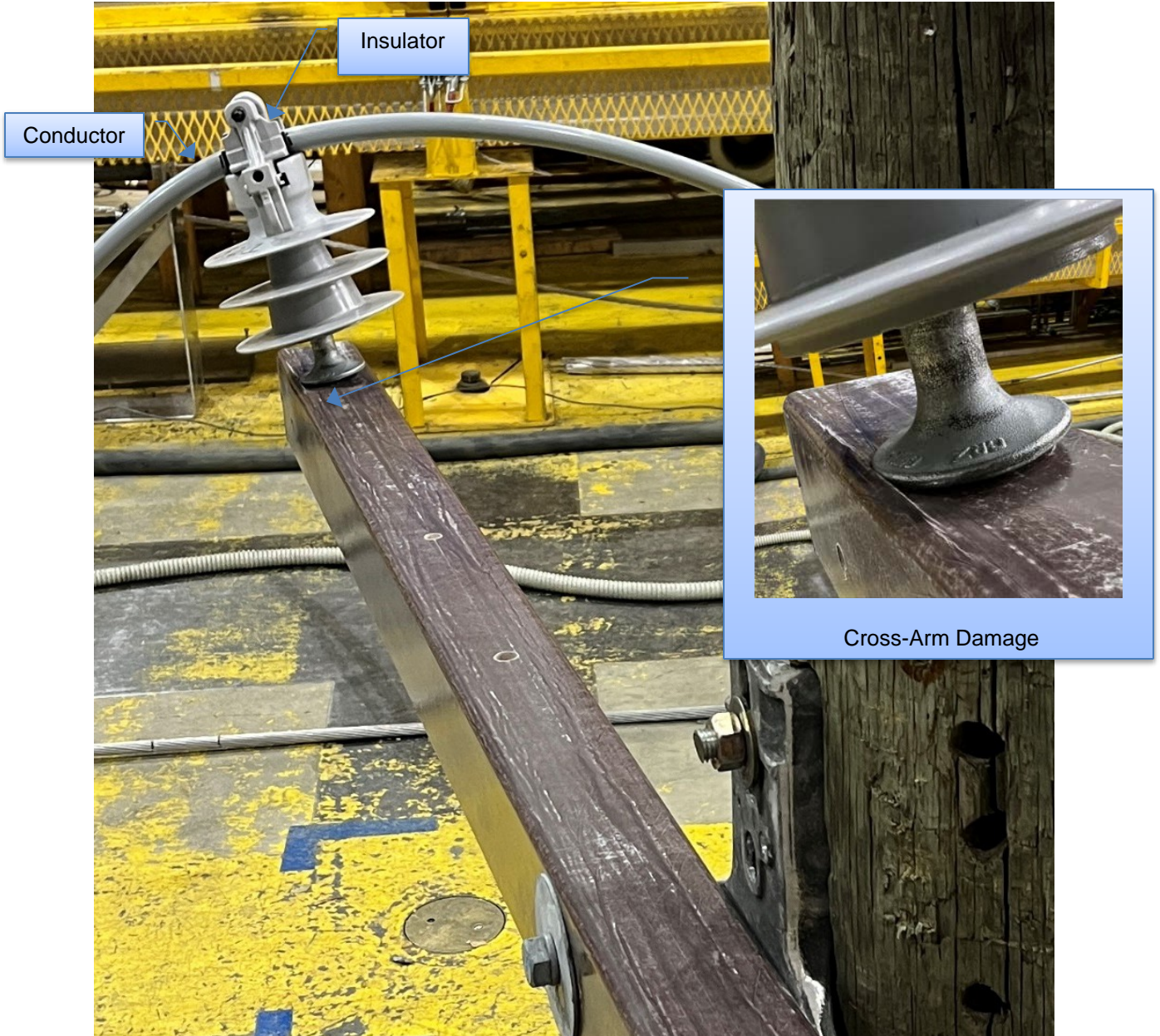


Figure 6-13: Sample 3.2.1 – Insulator and Cross-arm Condition after Test

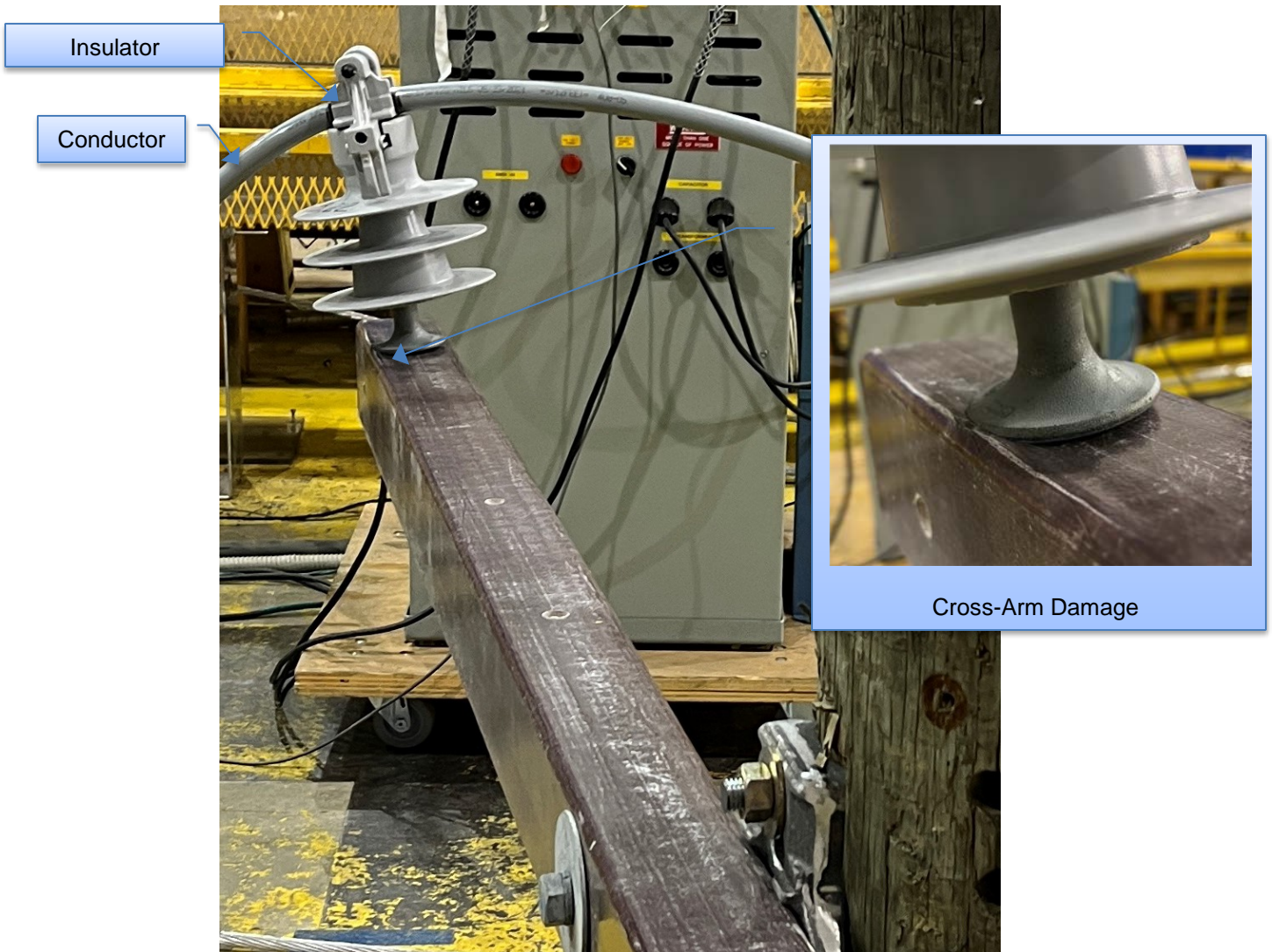


Figure 6-14: Sample 3.2.2 – Insulator and Cross-arm Condition after Test



Figure 6-15: Sample 3.2.2 - 35 kV, 1/0 AWG ACSR Condition after Test

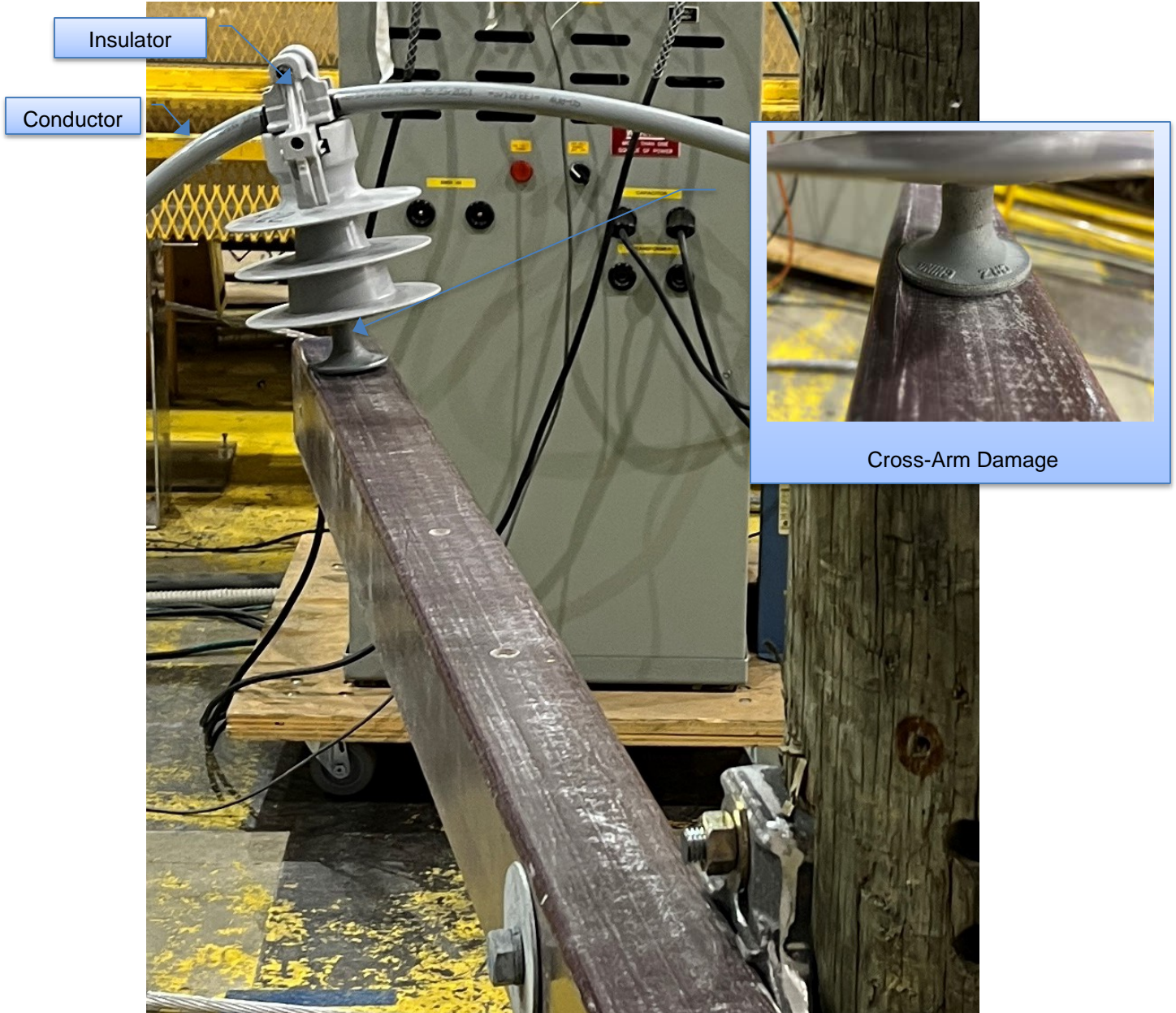


Figure 6-16: Sample 3.2.3 – Insulator and Cross-arm Condition after Test

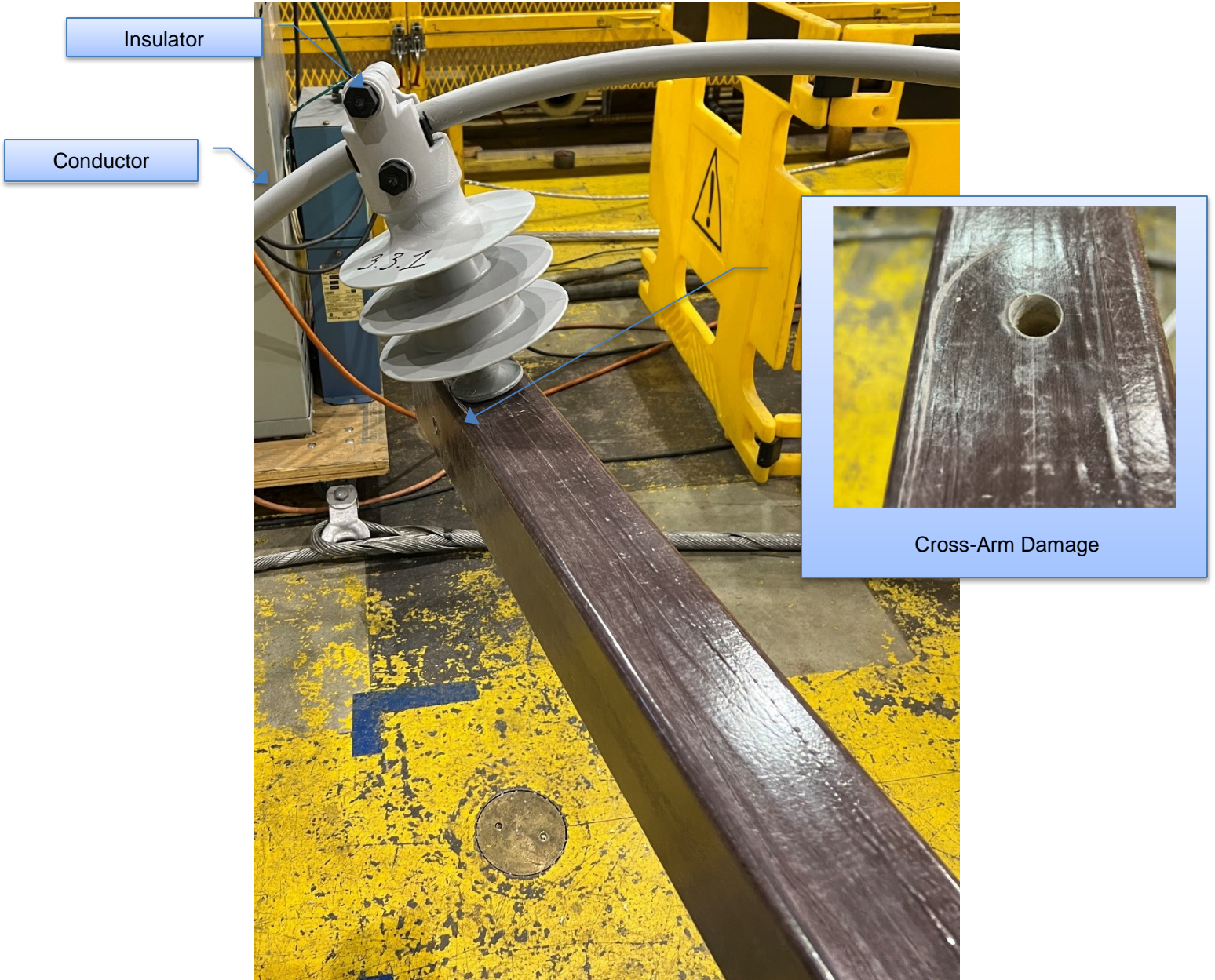


Figure 6-17: Sample 3.3.1 – Insulator and Cross-arm Condition after Test

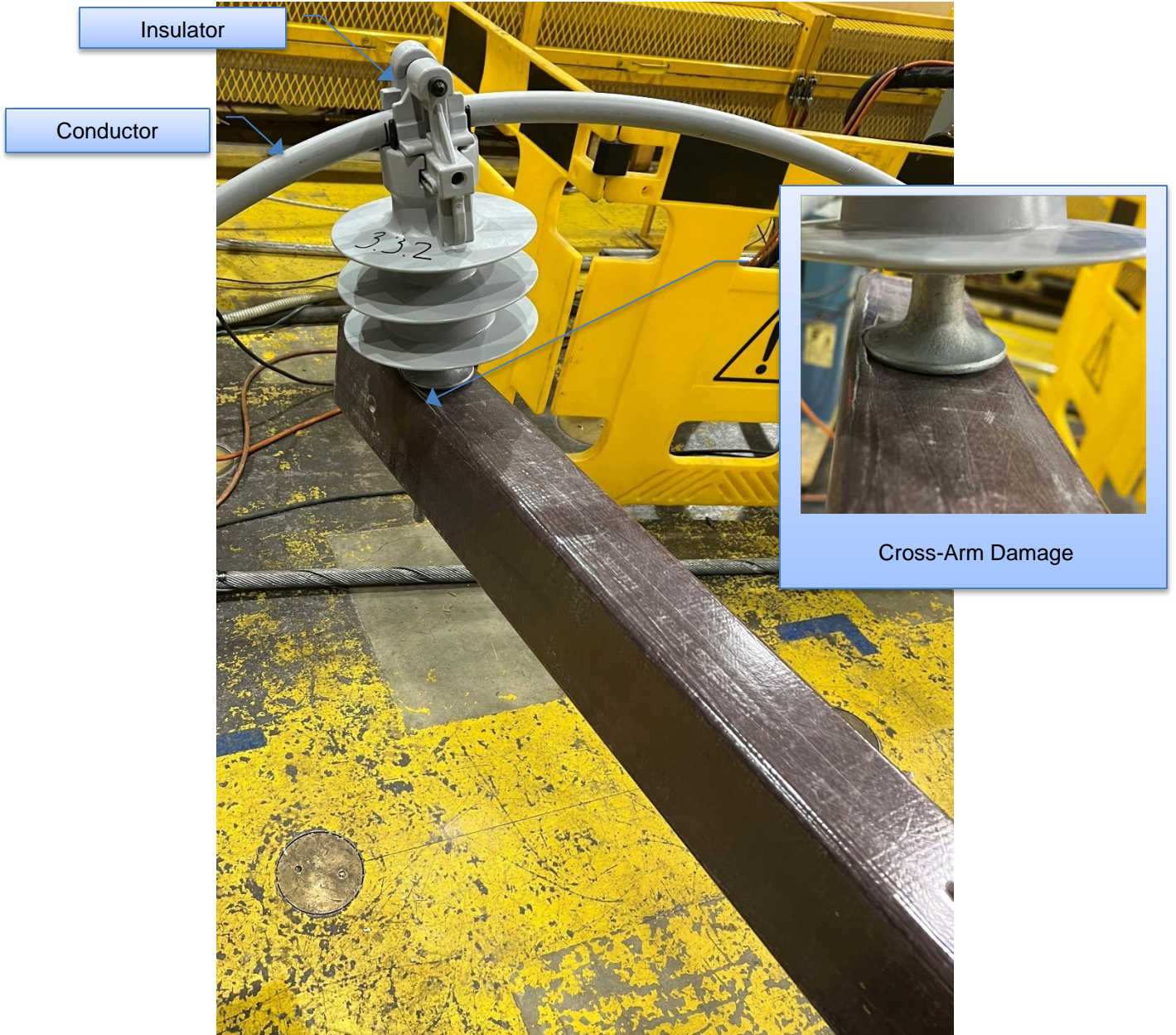


Figure 6-18: Sample 3.3.2 - Insulator and Cross-arm Condition after Test

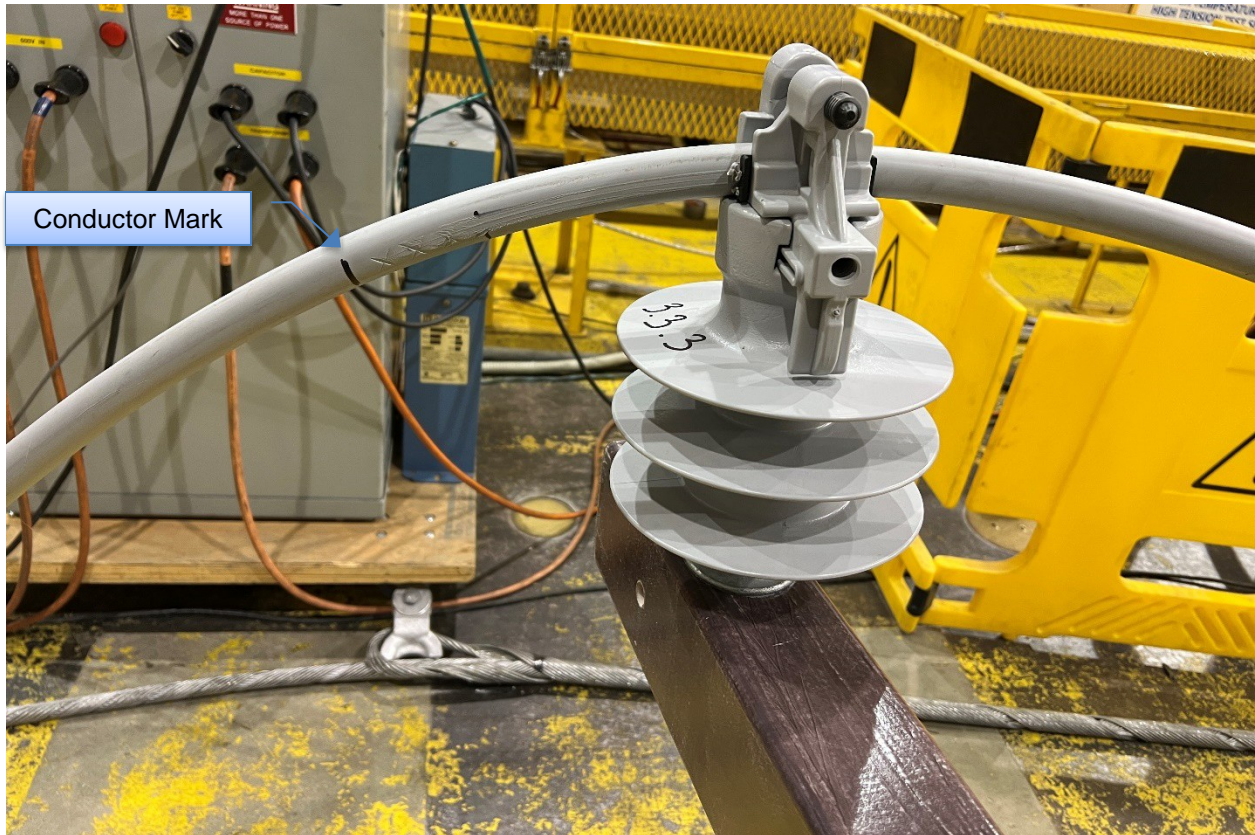


Figure 6-19: Sample 3.3.3 - Insulator and Cross-arm Condition after Test



Figure 6-20: Sample 3.3.3 - 22 kV, 397.5 kcmil AAC Condition after Test

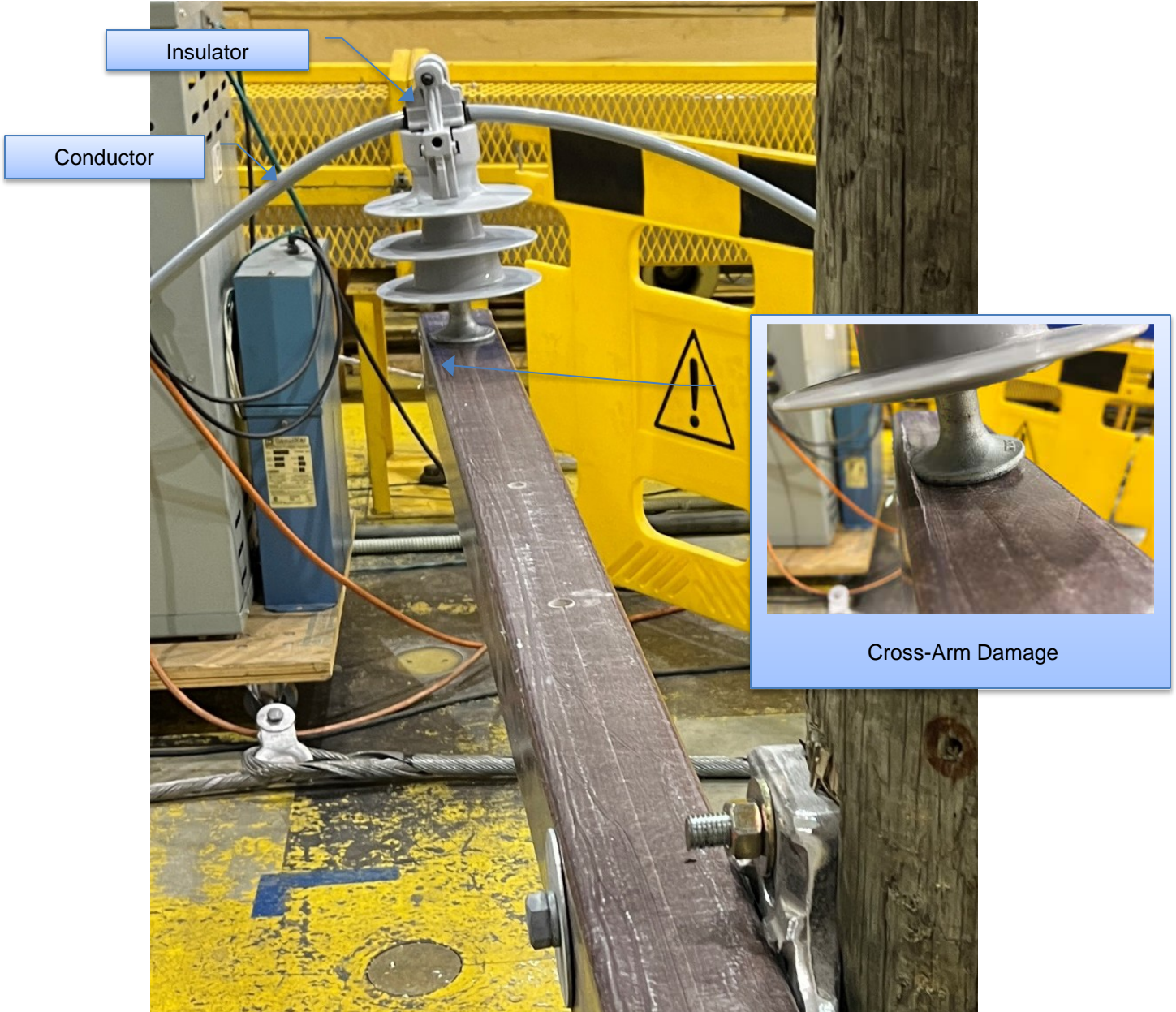


Figure 6-21: Sample 3.4.1 – Insulator and Cross-arm Condition after Test

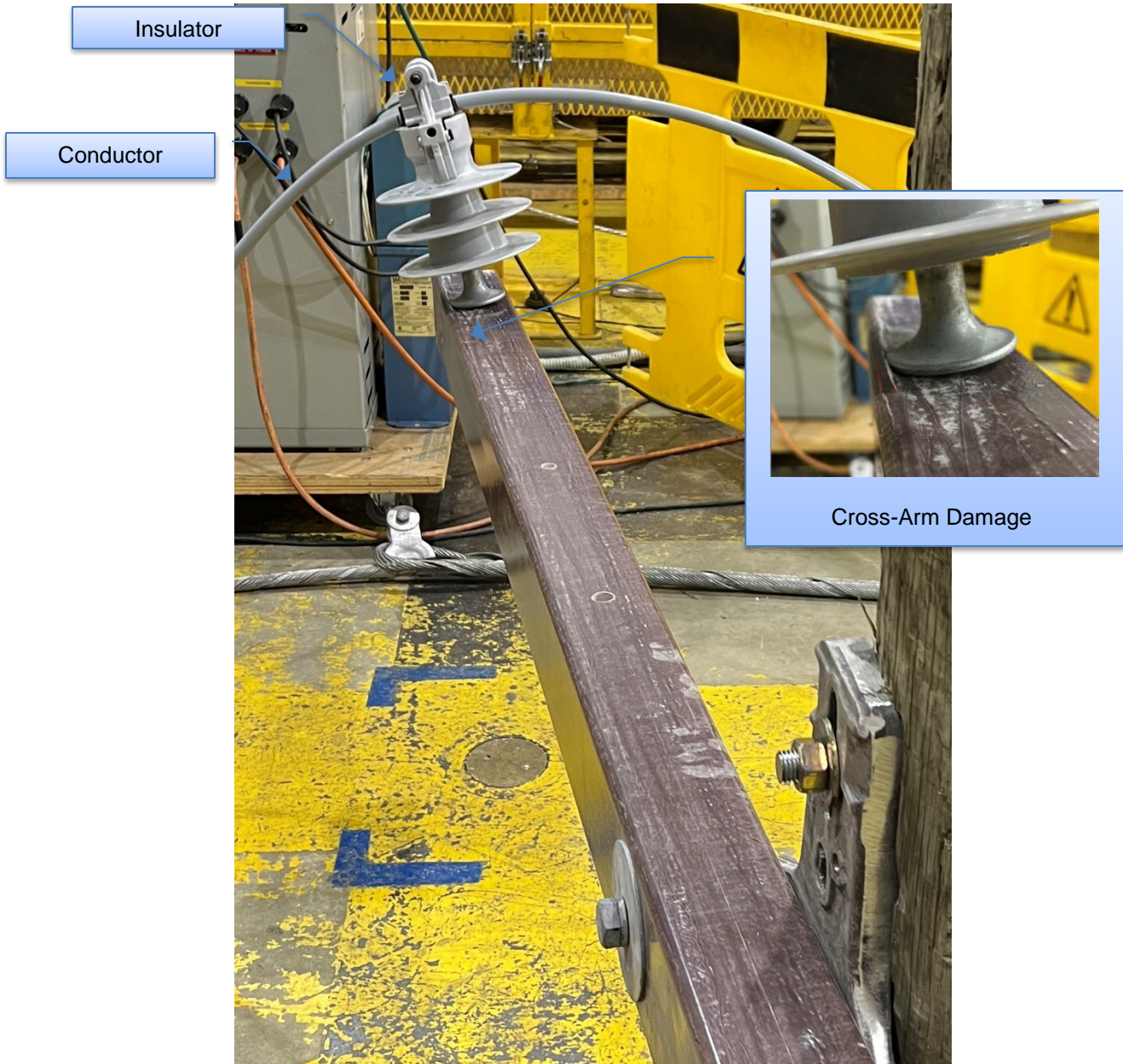


Figure 6-22: Sample 3.4.2 – Insulator and Cross-arm Condition after Test

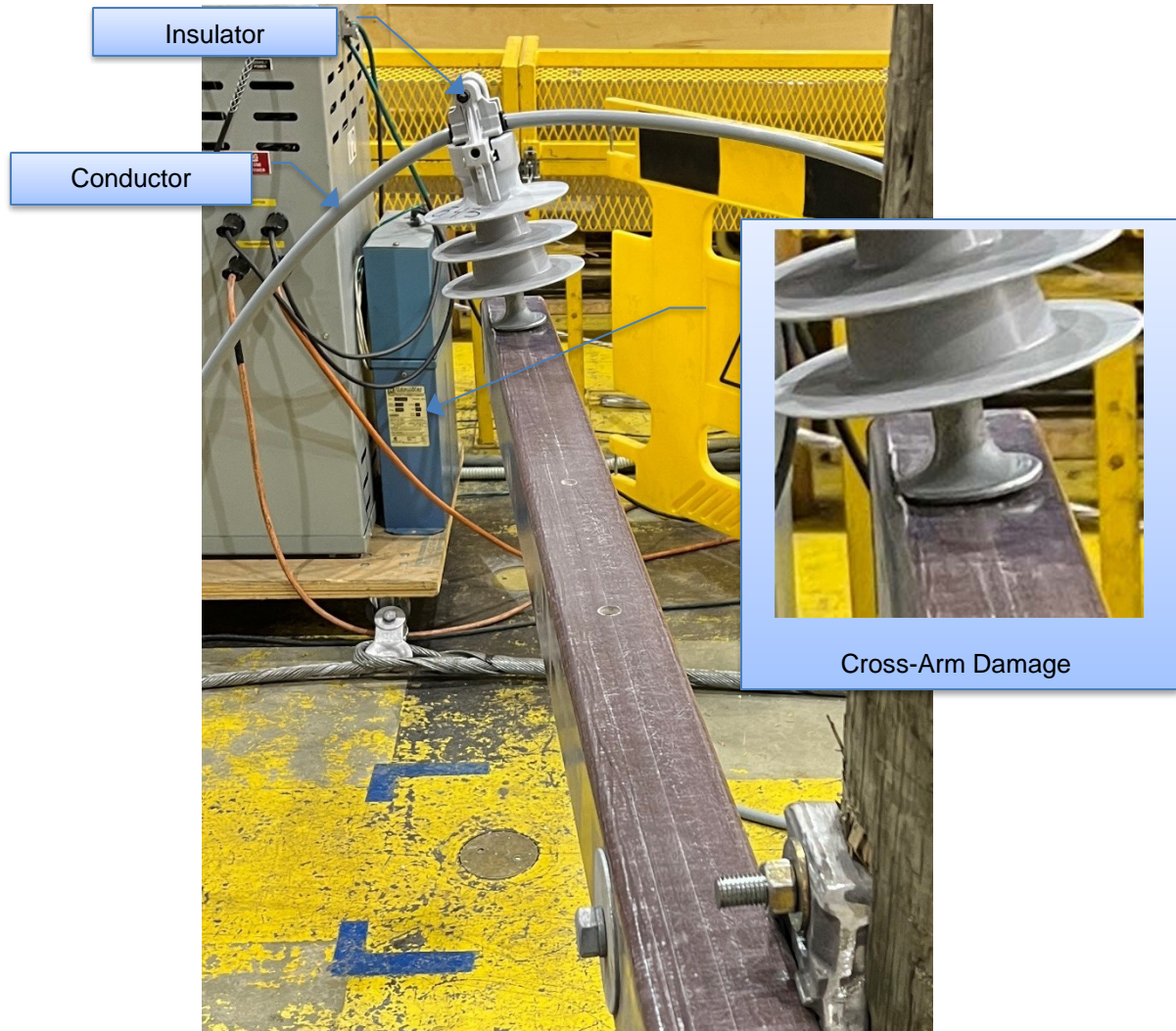


Figure 6-23: Sample 3.4.3 – Insulator and Cross-arm Condition after Test



Figure 6-24: Sample 3.4.3 - 15 kV, 1/0 AWG ACSR Condition after Test



Figure 6-25: Sample 3K.1.1 – Insulator and Cross-arm Condition after Test



Figure 6-26: Sample 3K.1.1 - 17 kV, 1/0 AWG ACSR Condition after Test



Figure 6-27: Sample 3K.1.2 – Insulator and Cross-arm Condition after Test



Figure 6-28: Sample 3K.1.2 - 17 kV, 1/0 AWG ACSR Condition after Test



Figure 6-29: Sample 3K.1. – Insulator and Cross-arm Condition after Test



Figure 6-30: Sample 3K.1.3 - 17 kV, 1/0 AWG ACSR Condition after Test



Figure 6-31: Sample 3K.2.1 – Insulator and Cross-arm Condition after Test



Figure 6-32: Sample 3K.2.2 – Insulator and Cross-arm Condition after Test

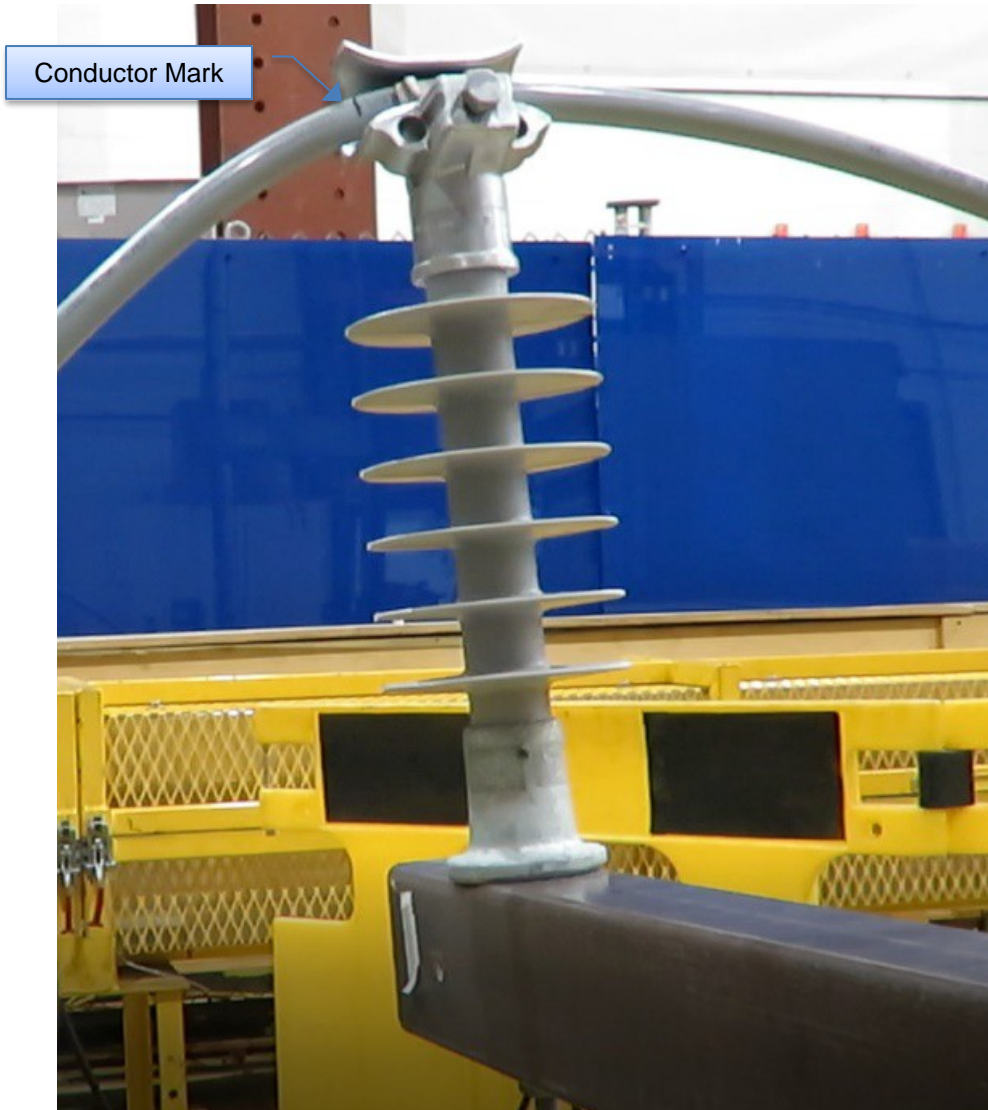


Figure 6-33: Sample 3K.2.3 – Insulator and Cross-arm Condition after Test



Figure 6-34: Sample 3K.1.3 - 17 kV, 1/0 AWG ACSR Condition after Test

7 Acceptance Criteria

There were no acceptance criteria provided by the client for this test. The objective of the Full Mock-up Test was to simulate mechanical loading in the event of a tree falling on the line and evaluate its effect on components (conductor, insulator, cross arm).

8 Conclusion

The test results show that [REDACTED] insulators provided a higher gripping strength on the conductor, as compared to the [REDACTED] clamps top. This translated into a higher slip load which in turn caused the insulator to bend at the pin. Due to the bending process, the shoulder of the pin damaged the cross-arm. In comparison, the [REDACTED] insulators caused the conductor to slip at a lower load which protected the insulator from bending and cross-arm from damage.

[The remainder of this page is intentionally left blank.]



Appendix A Acronyms and Abbreviations

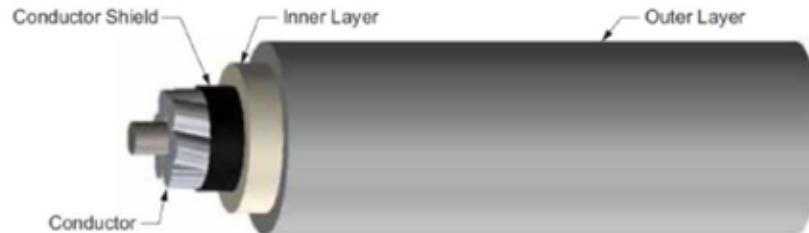
- AAC - All Aluminum Conductor
- ACSR - Aluminum Conductor Steel Reinforced
- ANSI - The American National Standards Institute
- AWG - American Wire Gauge
- ISO - International Organization for Standardization
- RTS - Rated Tensile Strength
- XLPE - Crosslinked Polyethylene

[The remainder of this page is intentionally left blank.]

Appendix B Conductor Data Sheet (as provided by the client)

Covered Conductor Data Sheet

Covered Conductor for 17kV and 35kV



- Conductor:
 - Aluminum Conductor Steel-Reinforced (ACSR) or
 - Hard Drawn Copper (HDCU)
- Conductor Shield: Semiconducting Thermoset Polymer
- Inner Layer: Crosslinked Low Density Polyethylene (XL-LDPE)
- Outer Layer: Crosslinked High Density Polyethylene (XL-HDPE)
 - Track Resistant
 - Abrasion Resistant

Temperature Rating:

Normal Operating Temperature: 90°C

Emergency Operating Temperature: 130°C

Short Circuit Temperature: 250°C

17kV Covered Conductor

ACSR

Conductor Size (AWG)	Conductor Type (Stranding)	Weight (lb/ft)	Conductor Diameter (in)	Conductor Shield Thickness (in)	Inner Layer Thickness (in)	Outer Layer Thickness (in)	Max Nominal Overall Diameter (in)	Maximum Rated Strength (lb.)	Ampacity per Conductor ¹ (Amps)
1/0	ACSR (6x1)	0.289	0.398	0.015 - 0.025	0.075	0.075	0.748	4,160	271
336.4	ACSR (18x1)	0.584	0.684	0.015 - 0.025	0.075	0.075	1.034	8,246	550
336.4	ACSR (30/7)	0.750	0.741	0.015 - 0.025	0.075	0.075	1.091	16,435	561
653.9	ACSR (18x3)	0.998	0.953	0.020 - 0.025	0.080	0.080	1.323	14,060	835

¹ Covered Conductor Cable Normal Operating Rating Criteria:

Ambient Temperature = 40°C

Conductor Temperature = 90°C

Load Factor = 100%

Wind Speed = 4 ft/sec

Coefficient of Emissivity = 0.5

Coefficient of Absorption = 0.5

Latitude = 34°

Elevation of Conductor above Sea Level = 0 ft

Atmosphere = Clear

Local Sun Time = 1:00 pm

Figure C - 1: [REDACTED] 17 kV 1/0 AWG ACSR Conductor Data

35kV Covered Conductor

ACSR

Conductor Size (AWG)	Conductor Type (Stranding)	Weight (lb/ft)	Conductor Diameter (in)	Conductor Shield Thickness (in)	Inner Layer Thickness (in)	Outer Layer Thickness (in)	Max Nominal Overall Diameter (in)	Maximum Rated Strength (lb.)	Ampacity per Conductor ¹ (Amps)
1/0	ACSR (6x1)	0.460	0.398	0.015 - 0.025	0.175	0.125	1.048	4,160	255
336.4	ACSR (18x1)	0.850	0.684	0.015 - 0.025	0.175	0.125	1.334	8,246	518
336.4	ACSR (30x7)	0.981	0.741	0.015 - 0.025	0.175	0.125	1.391	16,435	529
653.9	ACSR (18x3)	1.242	0.953	0.020 - 0.025	0.175	0.125	1.602	14,060	784

¹ Covered Conductor Cable Normal Operating Rating Criteria:

- Ambient Temperature = 40°C
- Conductor Temperature = 90°C
- Load Factor = 100%
- Wind Speed = 4 ft/sec
- Coefficient of Emissivity = 0.5
- Coefficient of Absorption = 0.5
- Latitude = 34°
- Elevation of Conductor above Sea Level = 0 ft
- Atmosphere = Clear
- Local Sun Time = 1:00 pm

Specifications

Must be manufactured to the latest editions of the following standards:

- ASTM B8
- ASTM B232
- ICEA S-121-733

Figure C - 2: XXXXXXXXXX 35 kV 1/0 AWG ACSR Conductor Data

Appendix C Insulator Datasheet

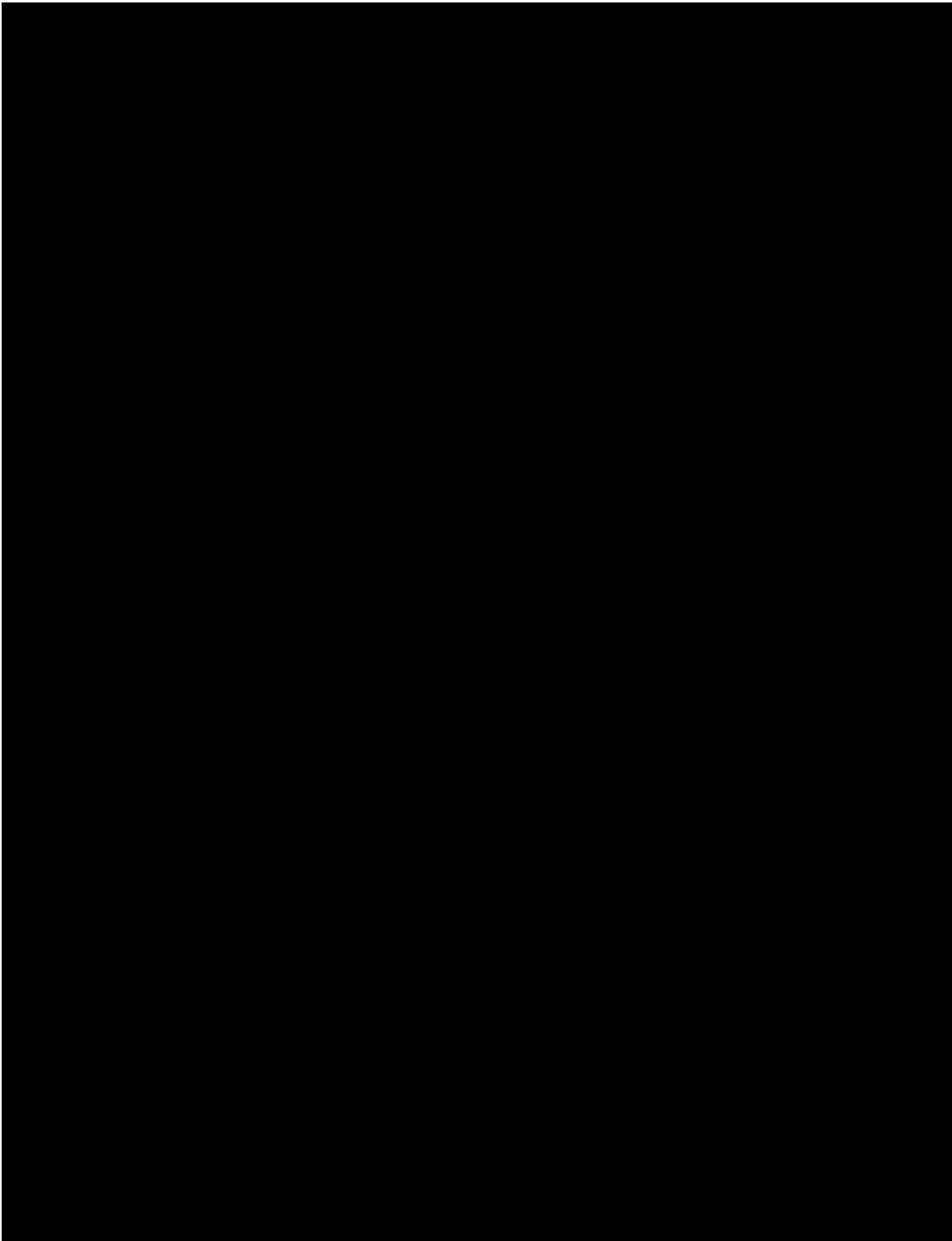


Figure D 1: [REDACTED] 35 kV Insulator [REDACTED]

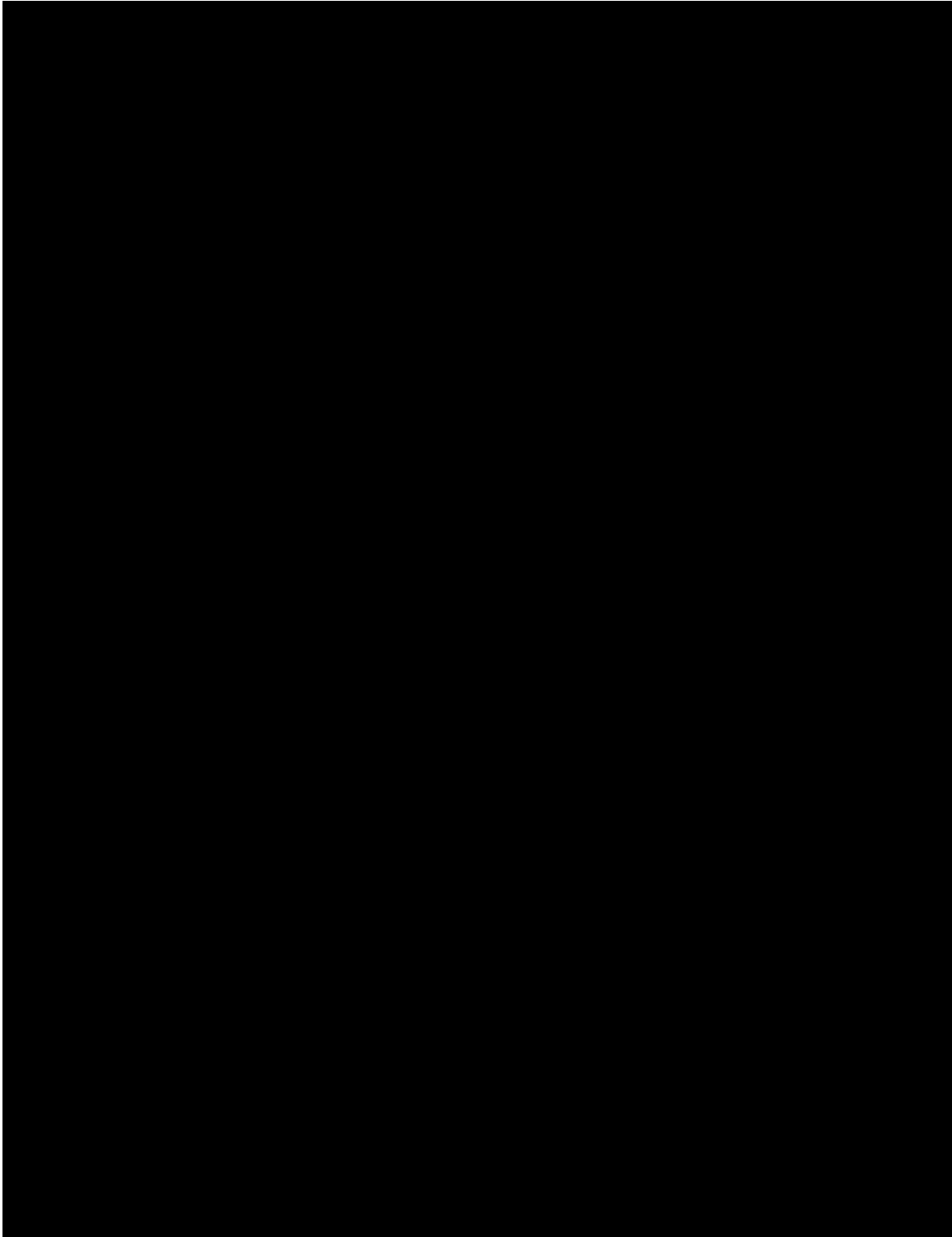


Figure D 2: [REDACTED] Post Insulators [REDACTED] and [REDACTED]

Appendix D Dead-End Bolted Clamps used in the test

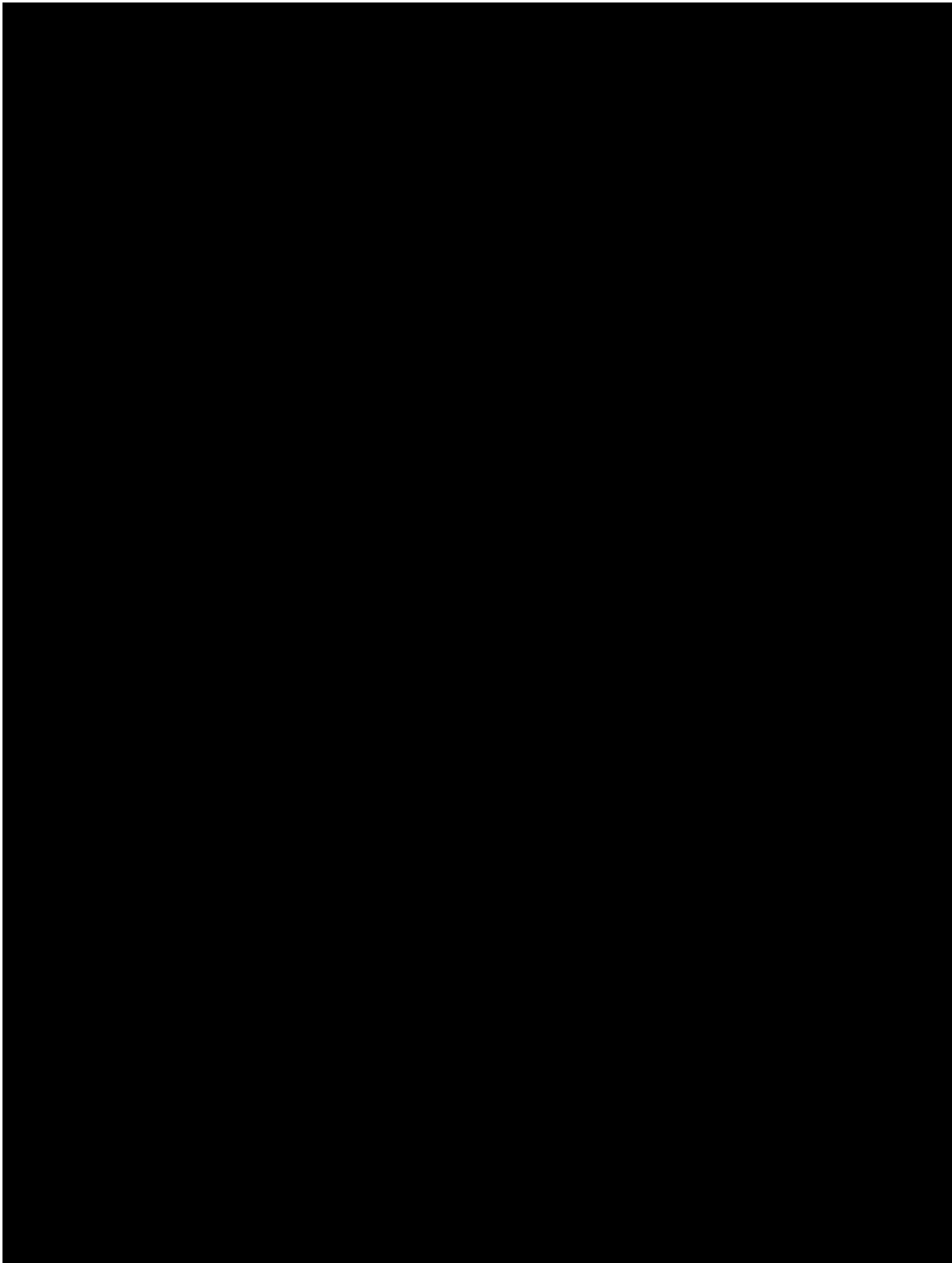


Figure 8-1: [REDACTED] Dead-End Bolted Clamp [REDACTED]

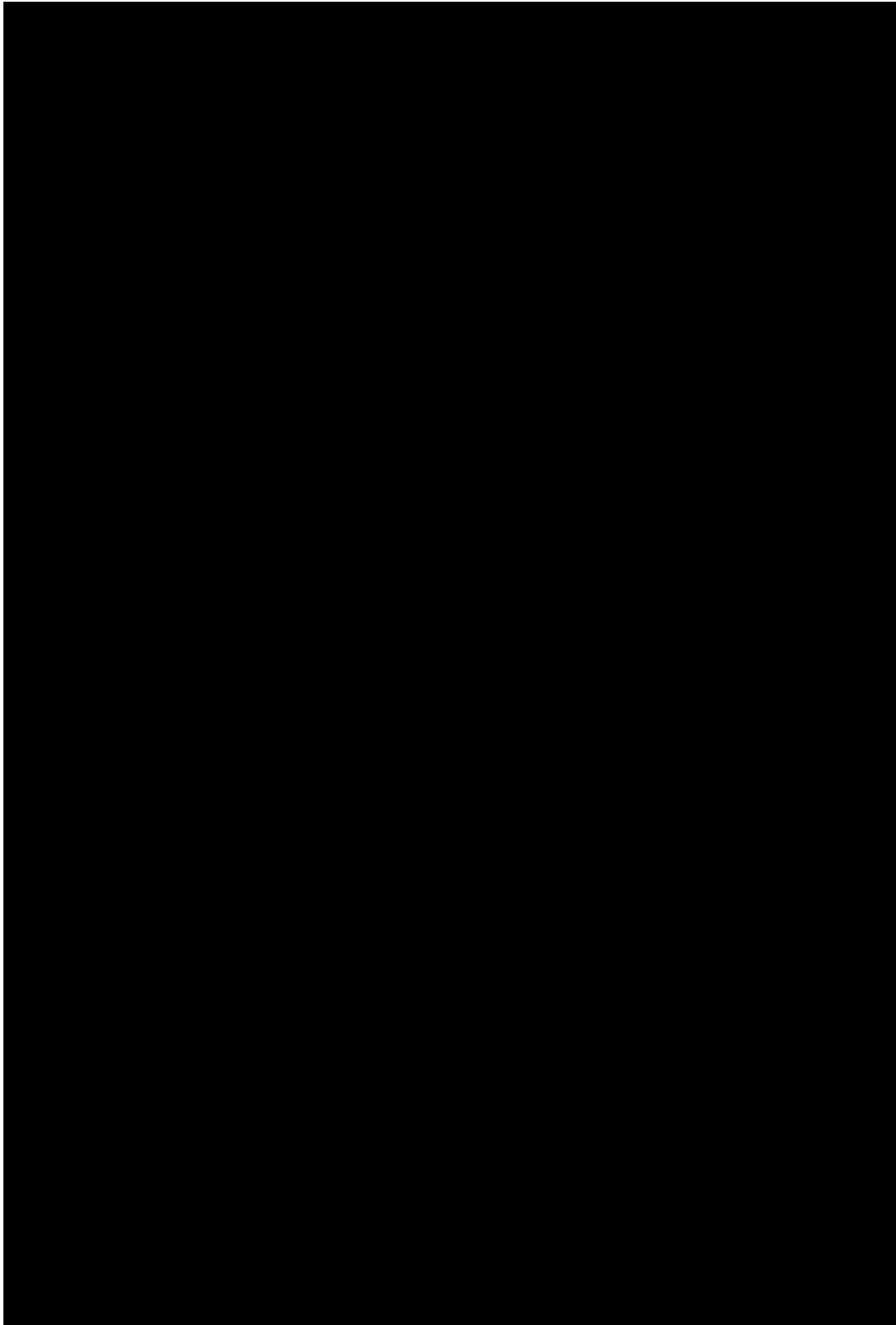


Figure 8-2: [REDACTED] Dead-End Bolted Clamp [REDACTED]



Appendix E Instrument Sheet

EQUIPMENT DESCRIPTION	ASSET No.	ACCURACY CLAIMED	CALIBRATION DATE	CALIBRATION DUE DATE	TEST USE
Data Logger	KIN-01836	±0.1% of Reading	May 27, 2022	May 27, 2023	Data acquisition
Load Cell/ Conditioner	KIN-01725/ KIN-01724	±1% of Reading	October 26, 2021	October 26, 2022	Load
Tape Measure	KIN-06890	< 0.05% of Reading	June 29, 2022	June 29, 2023	Length
Thermocouple/ Transmitter	KIN-00918/ KIN-00919	± 1 °C	October 28, 2021/ October 21, 2021	October 28, 2022/ October 21, 2022	Ambient Temperature

[The remainder of this page is intentionally left blank.]

Appendix F Kinectrics ISO 9001 Certificate of Registration



 **CERTIFICATE OF REGISTRATION**

This is to certify that
Kinectrics Inc.
Kinectrics North America Inc., Kinectrics International Europe ApS or Kinectrics International Inc.
800 Kipling Avenue, Unit 2, Toronto, Ontario M8Z 5G5 Canada

Refer to Attachment to Certificate of Registration dated November 5, 2021 for additional certified sites
operates a
Quality Management System
which complies with the requirements of
ISO 9001:2015
for the following scope of certification
This registration covers the Quality Management System for engineering, consulting, design, testing, project management, research, software development, assessments, operations support, and analysis within our facilities, and at field sites, for customers in the electricity industry and related energy sectors; both nuclear and conventional; as well as processing of radiological and conventional laundry and manufacture, inspection, and repair of personal protection equipment.

Certificate No.:	CERT-0119296	Original Certification Date:	July 7, 1998
File No.:	006555	Certification Effective Date:	May 23, 2021
Issue Date:	November 5, 2021	Certification Expiry Date:	May 22, 2024


Frank Camasta
Global Head of Technical Services
SAI Global Assurance

Registered by:
QM-SAI Canada Limited (SAI Global), 20 Denison Court, Suite 200, Toronto, Ontario M9N 7Y5 Canada. This registration is subject to the SAI Global Terms and Conditions for Certification. While all due care and skill were exercised in carrying out the assessment, SAI Global accepts responsibility only for proven negligence. This certificate remains the property of SAI Global and must be returned to them upon request.
To verify that this certificate is current, please refer to the SAI Global On-Line Certification Register:
https://www.sai-global.com/en-us/assurance/auditing_and_certification/certification_registry/





Appendix G Distribution

Mr. Matt Bowers, Ph.D., P.E.

Exponent
17000 Science Drive, Suite 200
Bowie, Maryland 20715
Email: mowers@exponent.com

Mr. Genti Gorja

Kinectrics AES Inc.
800 Kipling Ave, Unit No.2
Toronto, ON
Canada M8Z 5G5

Email: genti.gorja@kinectrics.com

[The remainder of this page is intentionally left blank.]



NOTE: Component manufacturer information has been redacted from this report.

MECHANICAL TESTING SIMULATING TREE FALLING ON A DEAD END SPAN OF COVERED CONDUCTORS

K-580861-RP-0001 R00

Prepared for

Exponent

Purchase Order No. 00067544

<p>Prepared by</p> <p> Digitally signed by GORJA Genti Date: 2022.11.18 10:27:57 -05'00'</p> <p>Signature & Date</p> <p>Genti Gorja P.Eng. Principal Engineer Line Asset Management</p>	<p>Reviewed by</p> <p> Digitally signed by André Maurice Date: 2022.11.18 11:02:06 -05'00'</p> <p>Signature & Date</p> <p>André Maurice Service Line Manager Line Asset Management</p>	<p>Approved by</p> <p>PETER</p> <p> Digitally signed by PETER Zsolt Date: 2022.11.18 15:53:31 -05'00'</p> <p>Zsolt</p> <p>Signature & Date</p> <p>Zsolt Peter Ph.D. Business Area Director Line Asset Management</p>
--	---	---

Revision History

Rev 00	Description: Original Issue			
	Issue Date: 2022-11-19	Prepared by: Genti Gorja	Reviewed by: André Maurice	Approved by: Zsolt Peter

DISCLAIMER

Kinectrics prepared this report as a work of authorship sponsored by their client. This report has been prepared solely for the benefit of the Client and may not be used or relied upon in whole or in part by any other person or entity without Client permission or without Kinectrics' permission if required by the Contract between Client and Kinectrics Inc . Neither Kinectrics, their client nor any person acting on behalf of them: (a) makes any warranty or representation whatsoever, express or implied, or assumes any legal liability of responsibility for any third party's use, or the results of such use, with respect to (i) the use of any information, apparatus, method, process, or similar item disclosed in this report including the merchantability or fitness for any particular purpose of any information contained in this report or the respective works or services supplied or performed or (ii) that such use does not infringe on or interfere with privately owned rights, including any party's intellectual property; or (b) assumes responsibility for any damages or other liability whatsoever (including any consequential damages resulting from a third party's selection or use of this report or any information, apparatus, method, process, or similar item disclosed).

Copyright © Kinectrics Inc. 2022. All rights reserved.



Table of Contents

1	Executive Summary	4
2	Test Objective and Test Standard.....	5
3	Test Sample.....	5
4	Test Setup	6
5	Test Procedure	8
6	Test Results.....	8
7	Acceptance Criteria.....	33
8	Conclusion	33
Appendix A	Acronyms and Abbreviations	34
Appendix B	Test Components	35
Appendix C	Instrument Sheet.....	39
Appendix D	Kinectrics ISO 9001 Certificate of Registration	40
Appendix E	Distribution	41

1 Executive Summary

This report describes the “Full Mock-Up” tests conducted on covered conductor assemblies to simulate a tree falling onto a dead-end span, as indicated by Exponent.

The tests were performed on various conductor sizes assembled with their respective dead-end clamps and insulators mounted on [REDACTED] composite crossarm. Exponent supplied all materials (test samples and accessories) required for testing. All connectors and conductor assemblies were received in good condition at Kinectrics on August 30, 2022.

The tests were conducted in accordance with client requirements, as outlined in the relevant sections of this document. The test is conducted for information purposes only and there are no acceptance criteria for this test. The test program is summarized in Table 1 1.

Table 1-1: Test Program

Test ID	Conductor	No. Samples Tested	Date Tested	
Full Mock-up	1	17KV #2 AWG CU Conductor	3	November 11, 2022
	2	17kV 2/0 AWG, CU Conductor	3	November 09, 2022
	3	17kV 4/0 AWG, CU Conductor	3	November 11, 2022
	4	17kV 1/0 AWG, 6/1 ACSR Conductor	3	November 10, 2022
	5	17kV 336.4 KCMIL, 18/1 ACSR Conductor	3	November 11, 2022
	6	17kV 336.4 KCMIL, 30/7 ACSR Conductor	3	November 11, 2022
	7	17kV 653.9 KCMIL, 18/3 ACSR Conductor	3	November 10, 2022

The test results show that for smaller size conductors (#2 AWG Cu; 2/0 AWG CU; 4/0 AWG Cu and 1/0 AWG ACSR) the typical failure occurred as a result of conductor slipping out of the dead-end clamp. For larger conductors with higher Rated Tensile Strength (RTS) (336.4 kcmil and 653.9 kcmil) the typical failure point was the composite crossarm. The failure of the crossarm started at the bolts on the mounting plate and propagated to the insulator attachment point. Deformation of the mounting plate on the crossarm occurred in all instances.

The tests were performed by Kinectrics personnel at 800 Kipling Avenue, Toronto, Ontario, M8Z 5G5, Canada. The work was conducted under Exponent Purchase Order No. 00067544 dated January 14, 2022. The tests were performed under Kinectrics’ ISO 9001 Quality Management System. A copy of ISO 9001 Certificate of Registration is included in Appendix D.

2 Test Objective and Test Standard

The Full Mock-up Test is designed to simulate mechanical loading in the event of a tree falling on a dead-end span of the power line and evaluate its effect on components (conductor, insulator, cross arm). The test is performed in general accordance with the procedures requested by Exponent.

3 Test Sample

The test sample consisted of a length of conductor, terminated on both ends with suitable dead-end clamps, as indicated in Table 3-1. The prepared conductor length was tested in combination with an associated dead-end and insulator mounted on the crossarm. All conductors and hardware used in this test program were provided by Exponent.

Table 3-1: Full Mock-up Test: Sample ID and Configuration

Sample ID	Conductor	Dead End	Insulator	Cross Arm
1.1	17KV #2 AWG CU Conductor	[REDACTED]	INSULATOR,15 KV, DEADEND SU	[REDACTED], 10 ft
1.2				
1.3				
2.1	17kV 2/0 AWG, CU Conductor	[REDACTED]	INSULATOR,15 KV, DEADEND SU	[REDACTED], 10 ft
2.2				
2.3				
3.1	17kV 4/0 AWG, CU Conductor	[REDACTED]	INSULATOR,15 KV, DEADEND SU	[REDACTED], 10 ft
3.2				
3.3				
4.1	17kV 1/0 AWG, 6/1 ACSR Conductor	[REDACTED]	INSULATOR,15 KV, DEADEND SU	[REDACTED], 10 ft
4.2				
4.3				
5.1	17kV 336.4 KCMIL, 18/1 ACSR Conductor	[REDACTED]	INSULATOR,15 KV, DEADEND SU	[REDACTED], 10 ft
5.2				
5.3				
6.1	17kV 336.4 KCMIL, 30/7 ACSR Conductor	[REDACTED]	INSULATOR,15 KV, DEADEND SU	[REDACTED], 10 ft
6.2				
6.3				
7.1	17kV 653.9 KCMIL, 18/3 ACSR Conductor	[REDACTED]	INSULATOR,15 KV, DEADEND SU	[REDACTED], 10 ft
7.2				
7.3				

Data sheets for the components (insulators and bolted dead-ends and crossarm) used in this test are shown in Appendix B. The main mechanical characteristics of the conductors used in this test are shown in Table 3-2.

Table 3-2: Test Conductor Main Characteristics

ID	Conductor	Manufacturer	Conductor Diameter [in]	RTS [lb.]
1	17KV #2 AWG, 7 HDCU Conductor	██████	0.292	2,898
2	17kv 2/0 AWG, 19 HDCU Conductor	██████	0.414	5,634
3	17kv 4/0 AWG, 19 HDCU Conductor	██████	0.522	8702
4	17kv 1/0 AWG, 6/1 ACSR Conductor	██████	0.398	4,160
5	17kv 336.4 KCMIL, 18/1 ACSR Conductor	██████	0.684	8,246
6	17kv 336.4 KCMIL, 30/7 ACSR Conductor	██████	0.741	16,435
7	17kv 653.9 KCMIL, 18/3 ACSR Conductor	██████	0.953	13,989

4 Test Setup

The loading was performed using a horizontal test machine. The dead-end span was simulated by attaching one end of the the test sample, as described above, to the pulling cylinder of the horizontal tensile machine and the other end to a dead-end insulator. The insulator was attached to composite crossarm (██████). The cross-arm was mounted on an I-beam frame, which was firmly fixed on the floor. A system of pulleys ensured that the conductor was at an angle coming off the insulator.

A schematic of the test set-up is shown in Figure 4-1 and Figure 4-2. A picture of the actual setup is shown in Figure 4-3.

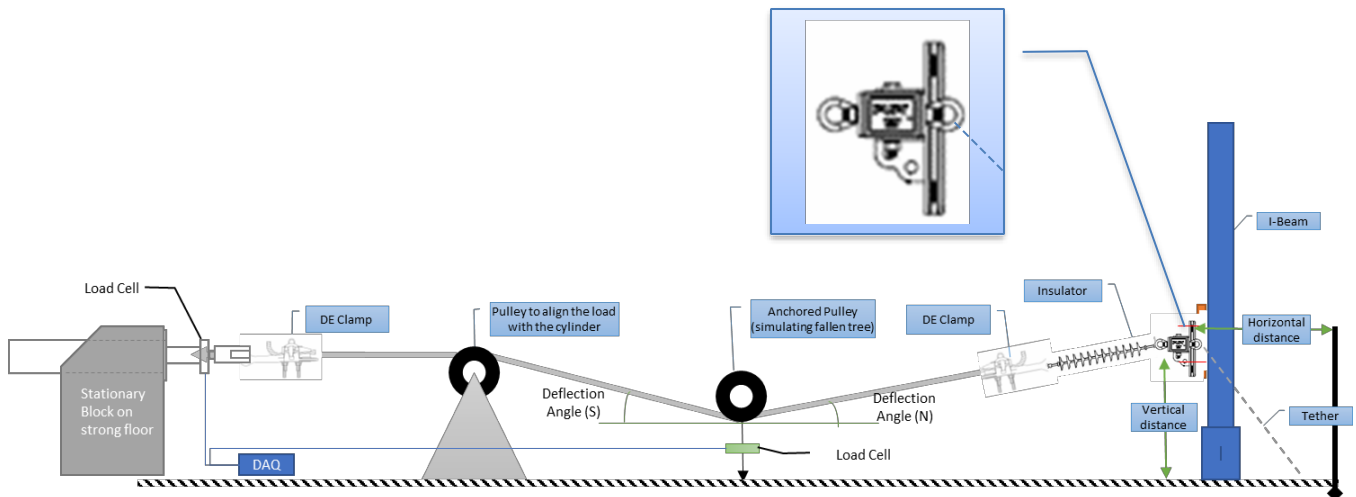


Figure 4-1: Full Mock-up: General View of the Test Setup

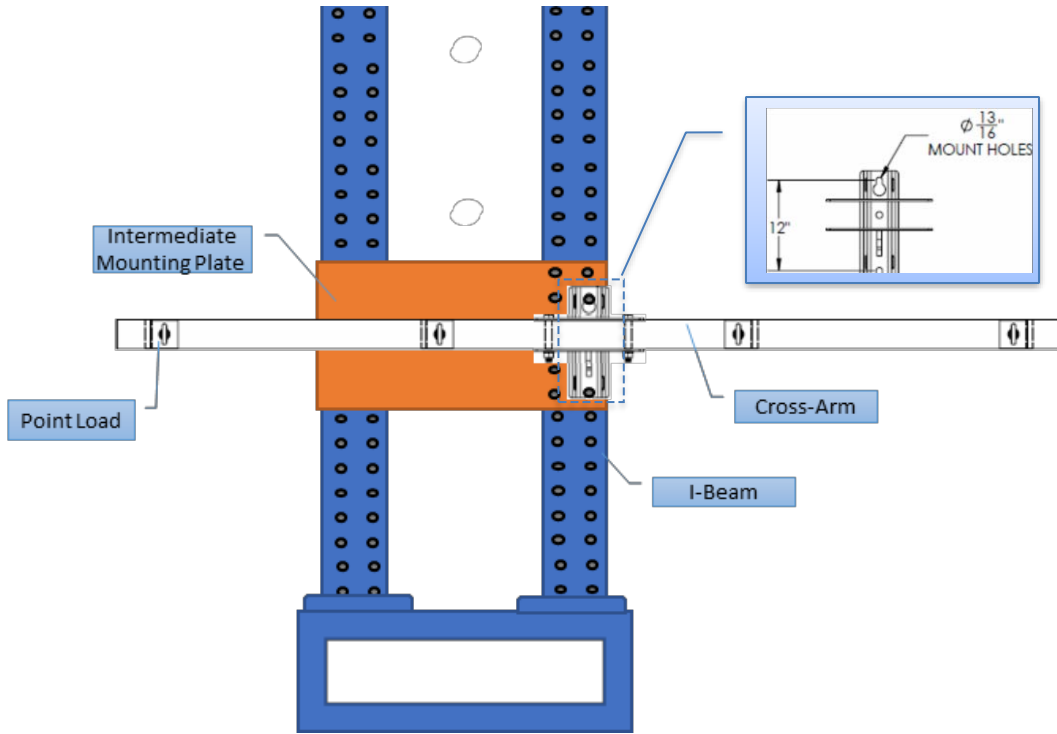


Figure 4-2: Full Mock-up: Front View of the Setup



Figure 4-3: Full Mock-up: Picture of the Setup

The vertical load on the pulley was measured directly by attaching a load cell between the pulley and the floor. The conductor horizontal tension was measured by a load cell located at the hydraulic end of the sample. The controller for the hydraulically activated horizontal test machine recorded the horizontal tension. The data logging rate was every two (2) seconds.

The test was carried out in a temperature-controlled laboratory at $20\text{ }^{\circ}\text{C} \pm 2\text{ }^{\circ}\text{C}$.

5 Test Procedure

Once the setup is complete as shown in Figure 4-2, the test was conducted as follows:

1. A small pretension value was applied with the horizontal piston to remove the slack from the conductor and the conductor was marked at the entry points in the clamp.
2. The conductor tension was increased until the vertical load reached 1,000 lbs on the pulley simulating the fallen tree. The conductor at the insulator clamp was visually monitored for slippage.
3. The horizontal tensile load was then increased continuously at a rate of 1,000 lbs/min until failure occurred (either insulator, cross arm, or the conductor slips out of the insulator).

These steps were repeated for all samples. Pictures of the test samples were taken to document damage after the test. Video recordings of the tests were also provided for Exponent's future reference.

6 Test Results

The load and conductor slippage during the test were monitored and recorded. Test results are summarized in Table 6-1.

Loading profiles for each sample are shown in Figure 6-1 to Figure 6-7. Photos of the slippage and the sample after the test were taken for documentation purposes. Typical pictures of failure location are shown in Figure 6-11 to Figure 6-27. General observations from the test, common for all samples, are provided below:

- The test results show that, for smaller size conductors (#2 AWG Cu; 2/0 AWG CU; 4/0 AWG Cu and 1/0 AWG ACSR), the typical failure occurred as a result of the conductor slipping out of the dead-end clamp.
- For larger conductors with a higher RTS (336.4 kcmil and 653.9 kcmil) the typical failure point was the crossarm. The failure of the crossarm started at the bolts on the mounting plate and propagated to the insulator attachment point.
- Deformation of the mounting plate on the crossarm occurred in all instances.

Table 6-1: Summary of Test Results

Sample ID	Conductor	Dead End	Max Load		Deflection Angle		Failure Mode
			Horizontal (lbs.)	Vertical (lbs.)	South (degree)	North (degree)	
1.1	17kV CU, #2 AWG	[REDACTED]	3021	1443	15.1	12.4	Conductor broke at the South DE; deformed crossarm mounting plate.
1.2			2029	1365	15.3	11.9	Conductor pulled out of South DE; deformed crossarm mounting plate.
1.3			2900	1352	15.7	12.2	Conductor pulled out of South DE; deformed crossarm mounting plate.
2.1	17kV CU, 2/0 AWG	[REDACTED]	1367	567	16.3	15.0	Conductor pulled out of North DE; deformed crossarm mounting plate.
2.2			1570	767	16.0	14.6	Conductor pulled out of South DE; deformed crossarm mounting plate.
2.3			2753	1375	16.9	16.8	Conductor pulled out of South DE; deformed crossarm mounting plate.
3.1	17kV CU, 4/0 AWG	[REDACTED]	1447	693	17.0	12.3	Conductor pulled out of North DE; deformed crossarm mounting plate.
3.2			3257	1503	15.9	11.4	Conductor pulled out of South DE; deformed crossarm mounting plate.
3.3			3030	1509	17.0	16.0	Conductor pulled out of South DE; deformed crossarm mounting plate.
4.1	17kV ACSR 1/0 AWG, 6/1	[REDACTED]	3543	1776	15.8	13.5	Failure at the crossarm (fracture at the center bolt). No conductor slippage at the clamp.
4.2			2973	1410	15.5	13.4	Conductor pulled out of the North DE. deformed crossarm mounting plate.
4.3			2832	1418	16.8	15.6	Conductor pulled out of the South DE. deformed crossarm mounting plate.
5.1	17kV ACSR 336.4 KCMIL, 18/1	[REDACTED]	3683	1739	14.5	16.4	Complete crossarm failure; deformed mounting plate; No conductor slippage at the clamp.
5.2			3709	1771	16.5	12.3	Complete crossarm failure; deformed mounting plate; No conductor slippage at the clamp.
5.3			3607	1720	16.6	12.6	Complete crossarm failure; deformed mounting plate; No conductor slippage at the clamp.
6.1	17kV ACSR 336.4 KCMIL, 30/7	[REDACTED]	3387	1628	16.1	13.2	Complete crossarm failure; deformed mounting plate; No conductor slippage at the clamp.
6.2			3798	1831	15.9	12.4	Complete crossarm failure; deformed mounting plate; No conductor slippage at the clamp.
6.3			3726	1786	16.2	12.0	Complete crossarm failure; deformed mounting plate; No conductor slippage at the clamp.
7.1	17kV ACSR 653.9 KCMIL, 18/3	[REDACTED]	3957	2130	17.1	17.3	Complete crossarm failure; deformed mounting plate; No conductor slippage at the clamp.
7.2			3877	1973	17.2	14.6	Complete crossarm failure; deformed mounting plate; No conductor slippage at the clamp.
7.3			3833	1858	17.3	13.2	Complete crossarm failure; deformed mounting plate; No conductor slippage at the clamp.

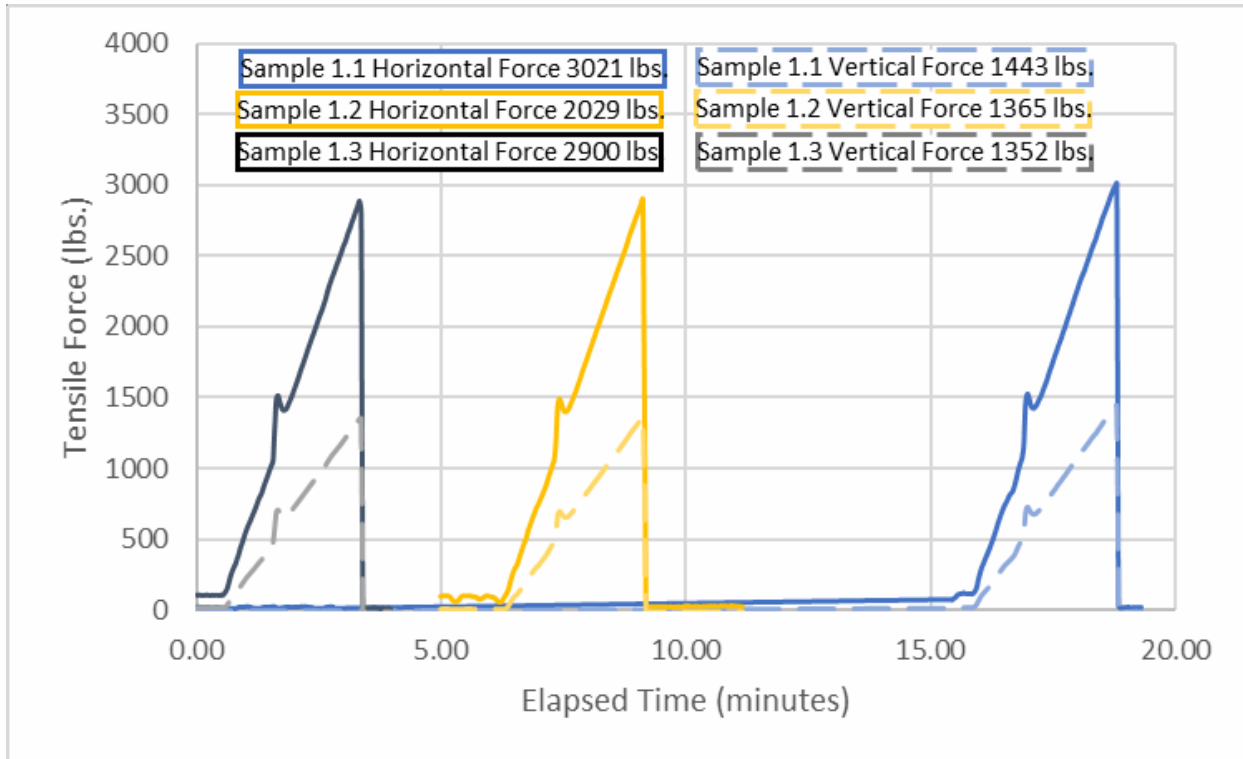


Figure 6-1: Test Load Profile: 17KV #2 AWG, 7 CU Conductor

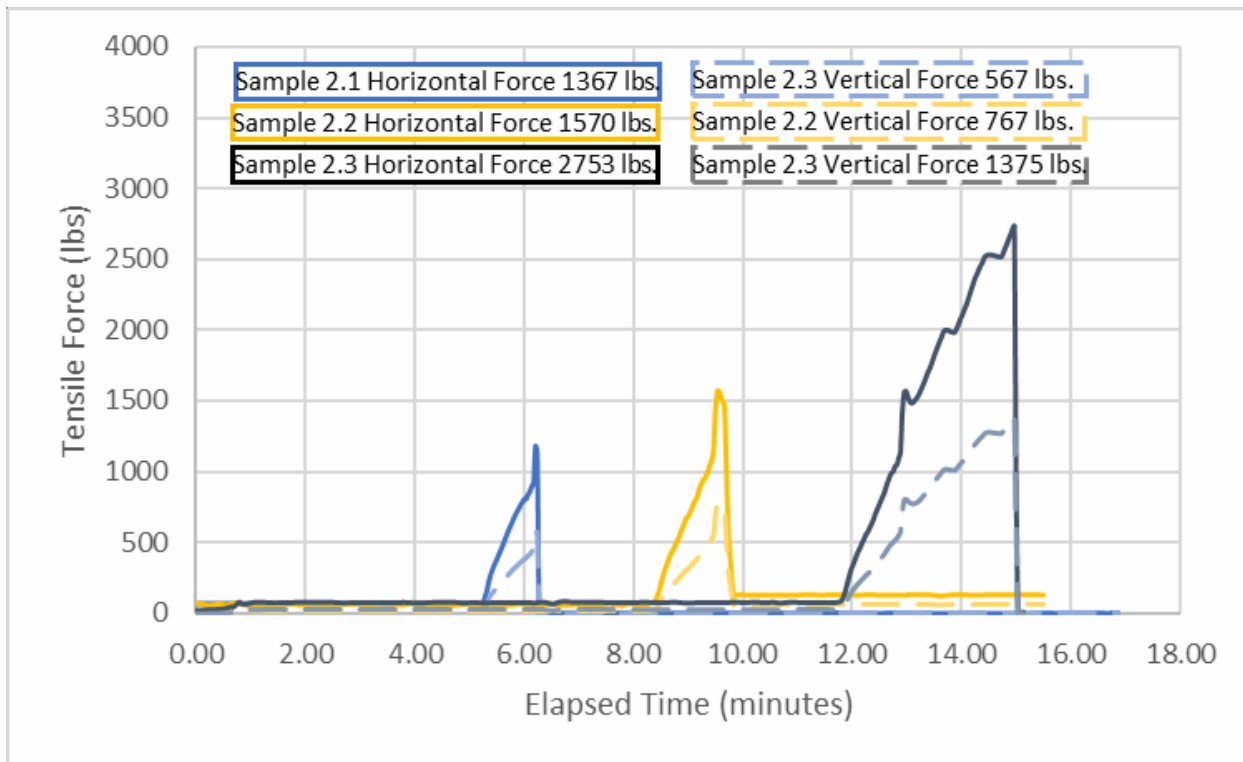


Figure 6-2: Test Load Profile: 17kV 2/0 AWG, 19 CU Conductor

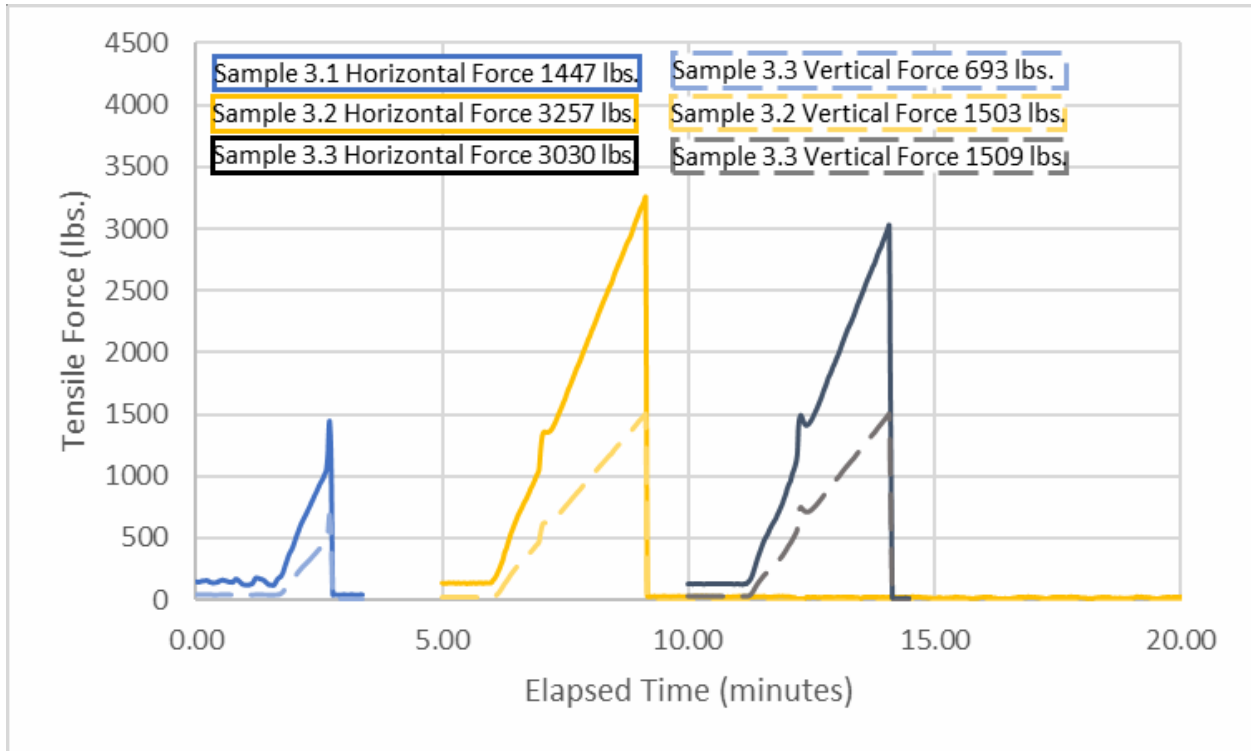


Figure 6-3: Test Load Profile: 17kV 4/0 AWG, 19 CU Conductor

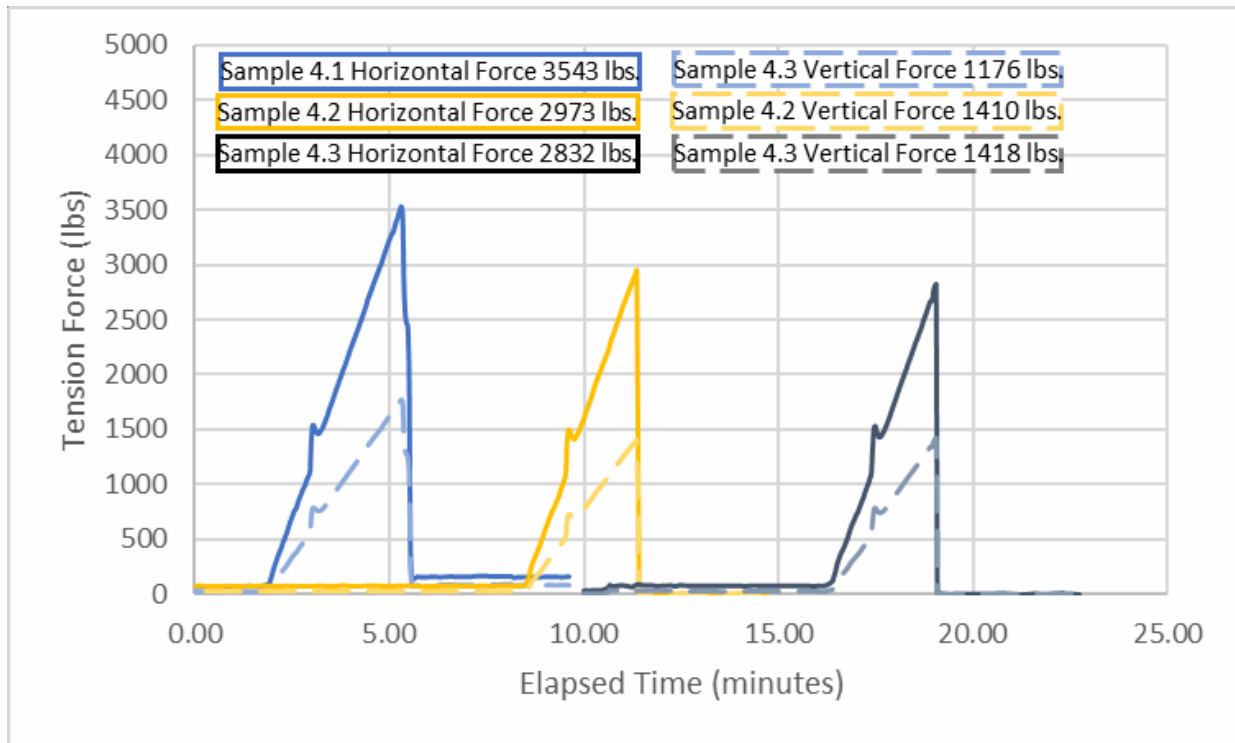


Figure 6-4: Test Load Profile: 17kV 1/0 AWG, 6/1 ACSR Conductor

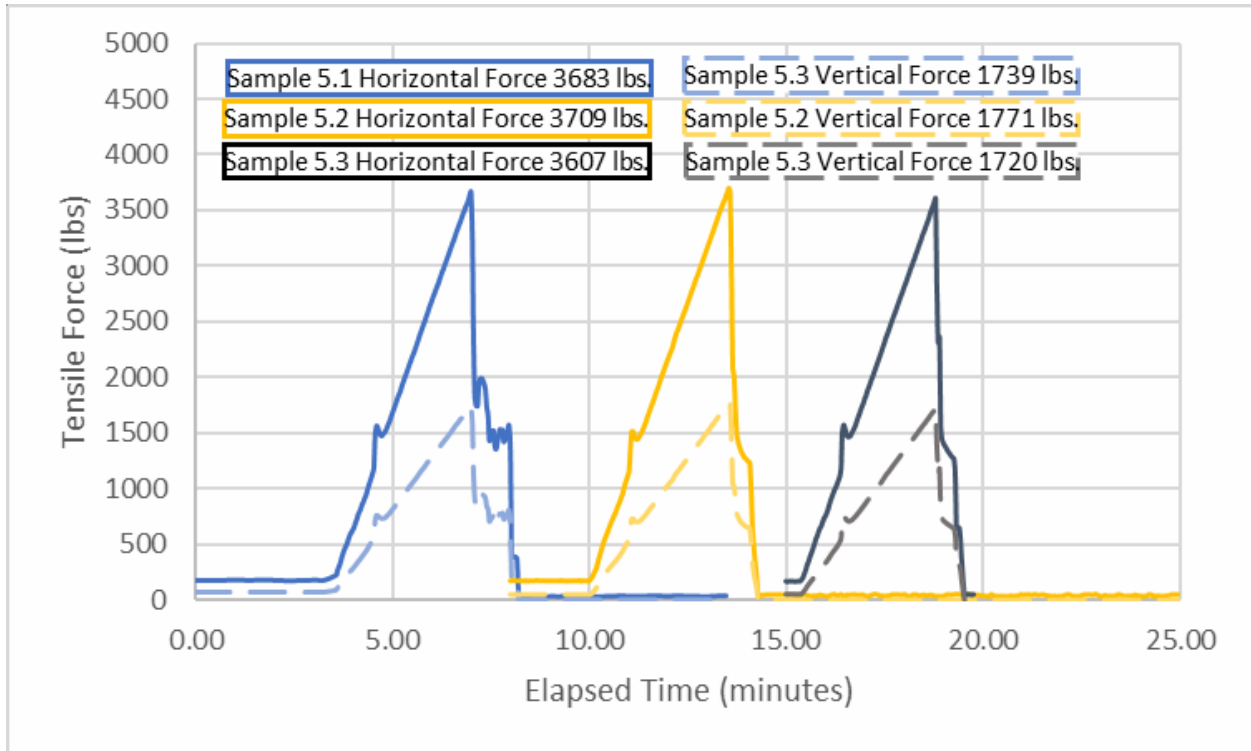


Figure 6-5: Test Load Profile: 17kV 336.4 KCMIL, 18/1 ACSR Conductor

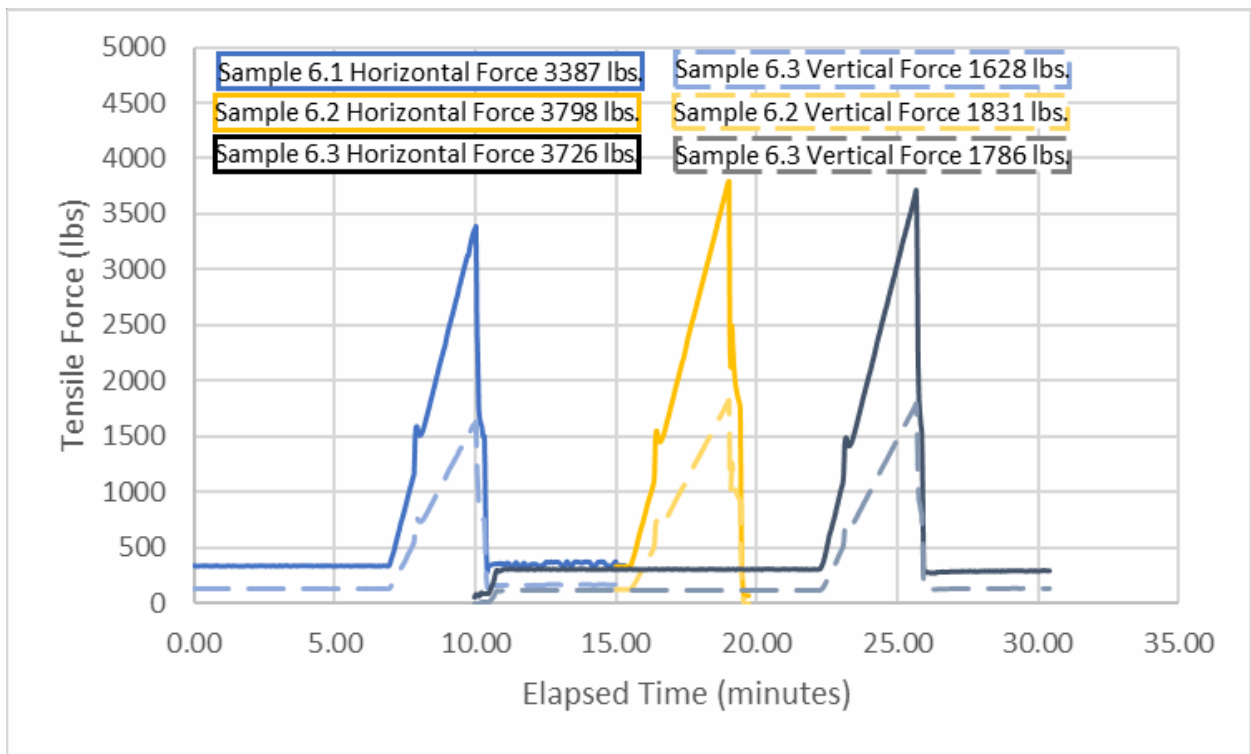


Figure 6-6: Test Load Profile: 17kV 336.4 KCMIL, 30/7 ACSR Conductor

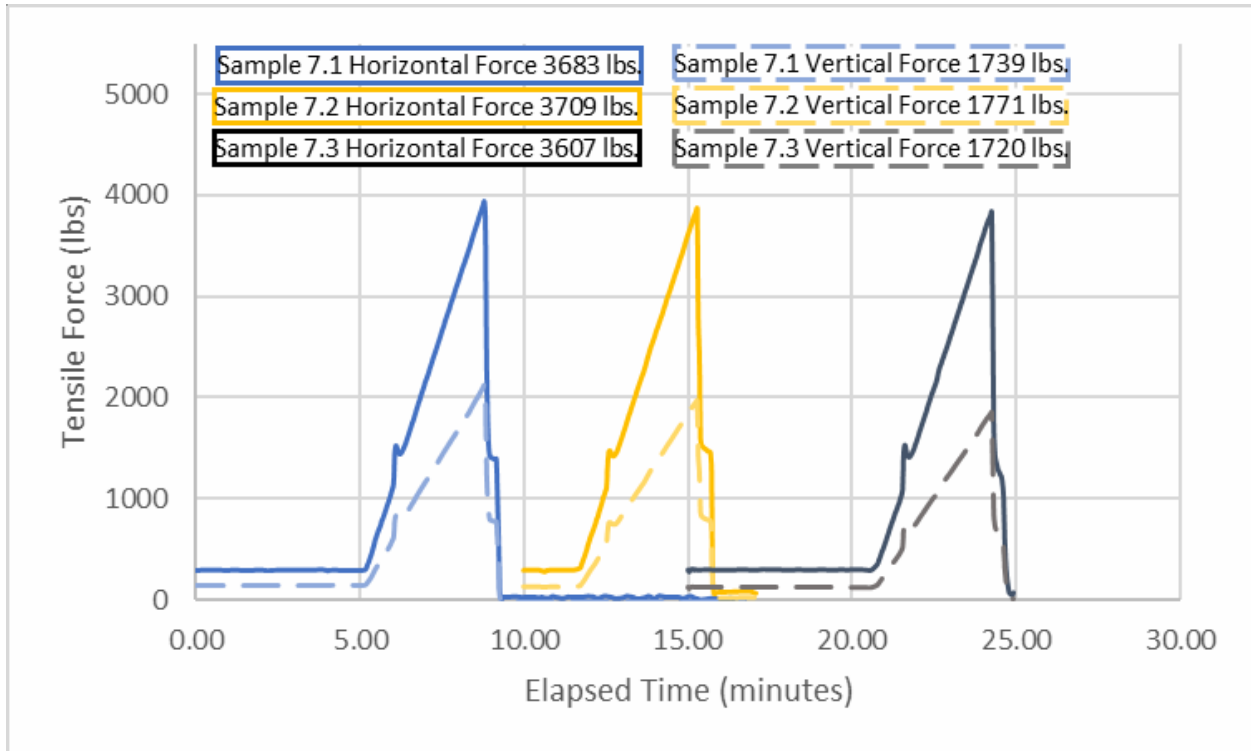


Figure 6-7: Test Load Profile: 17kV 653.9 KCMIL, 18/3 ACSR Conductor

[The remainder of this page is intentionally left blank.]

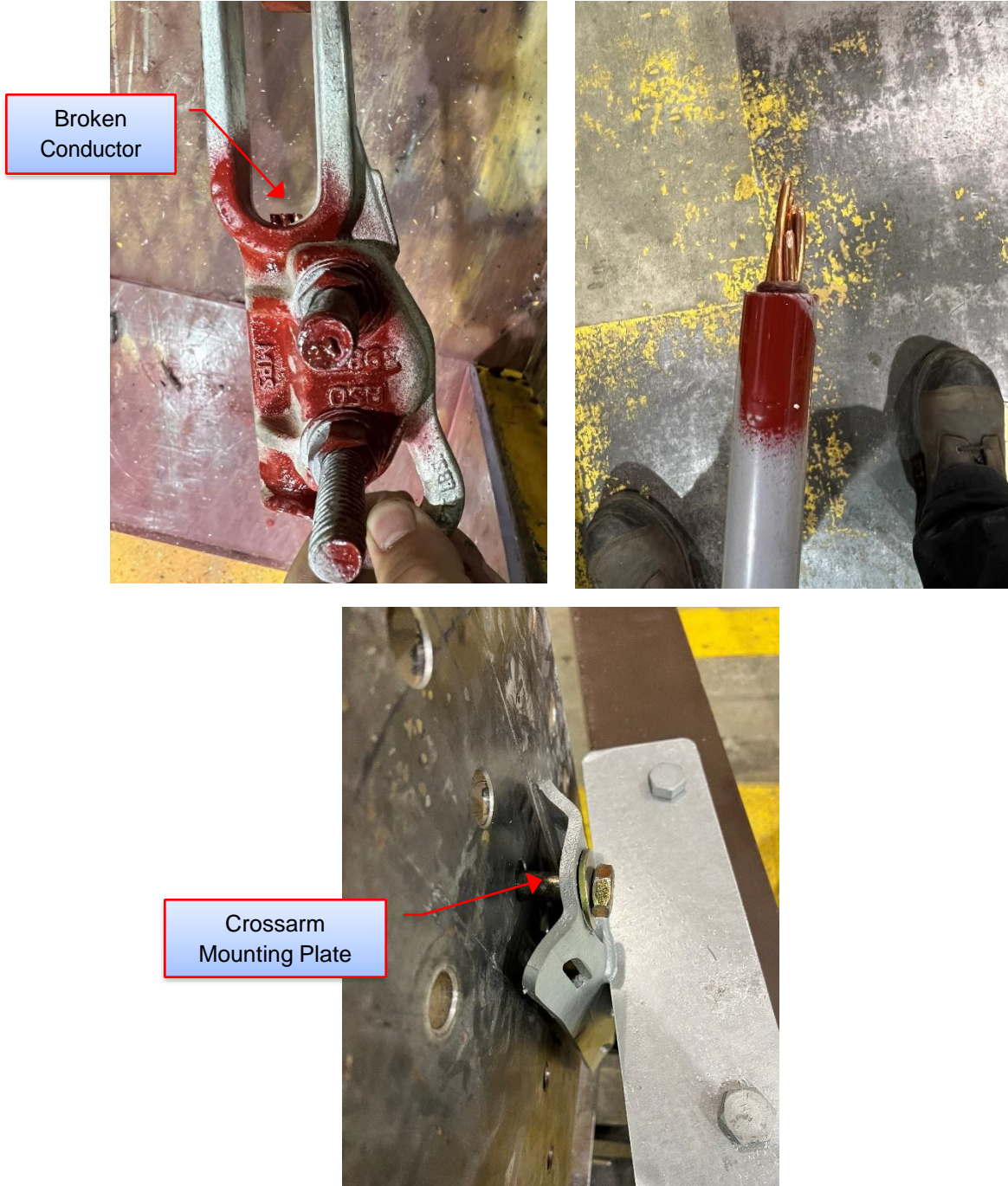


Figure 6-8: Sample 1.1 – Failure Location

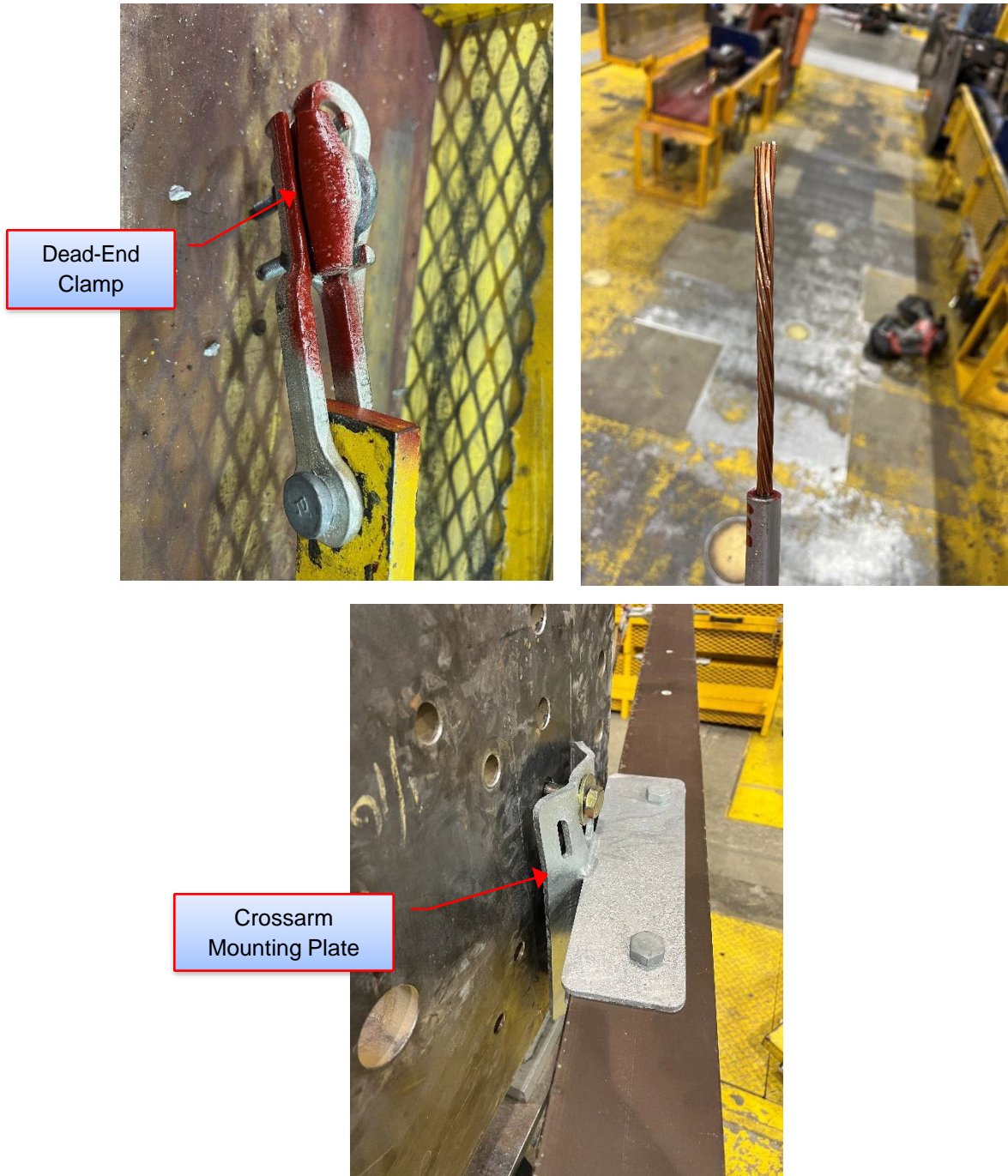


Figure 6-9: Sample 1.2 – Failure Location

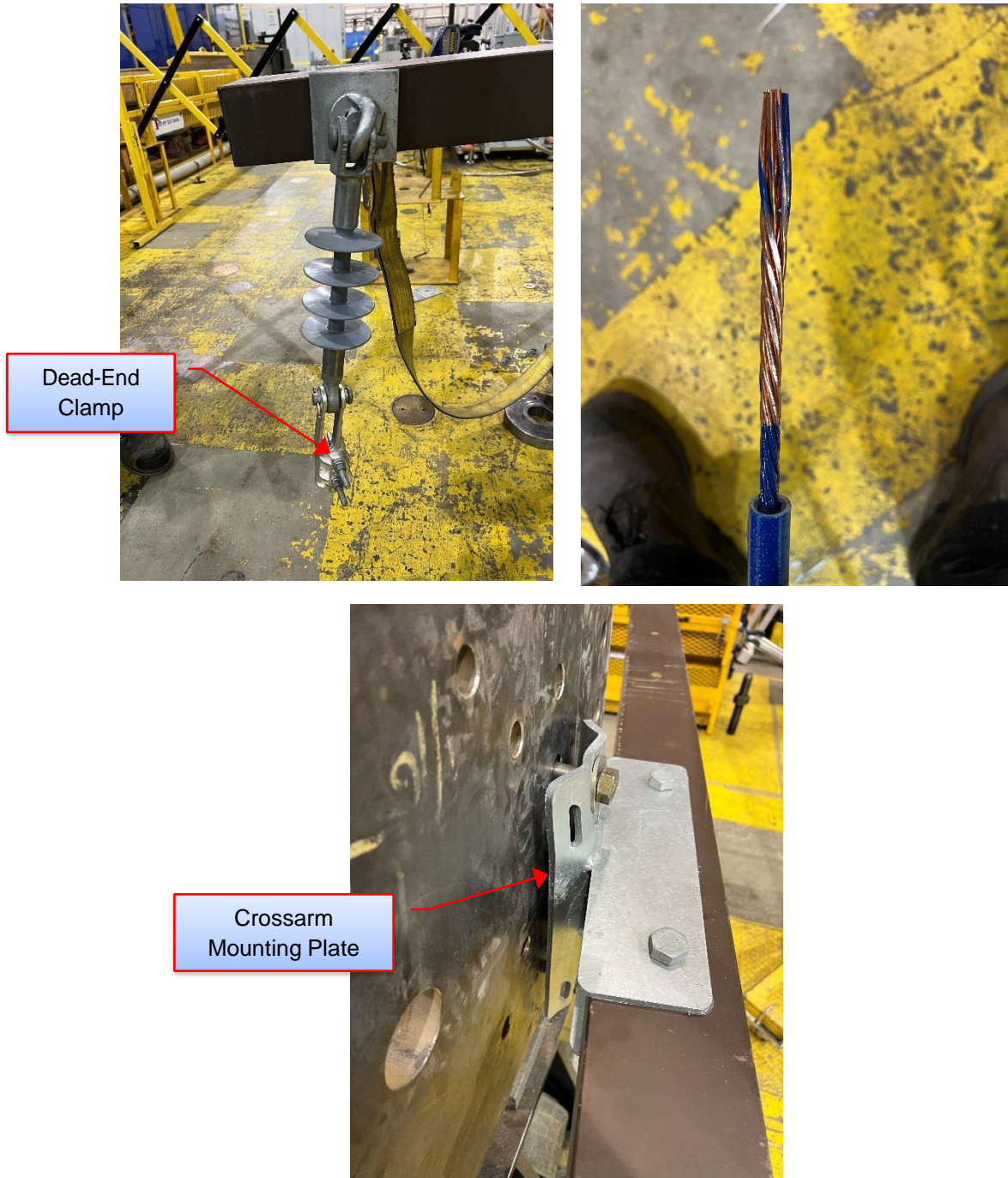


Figure 6-10: Sample 1.3 – Failure Location

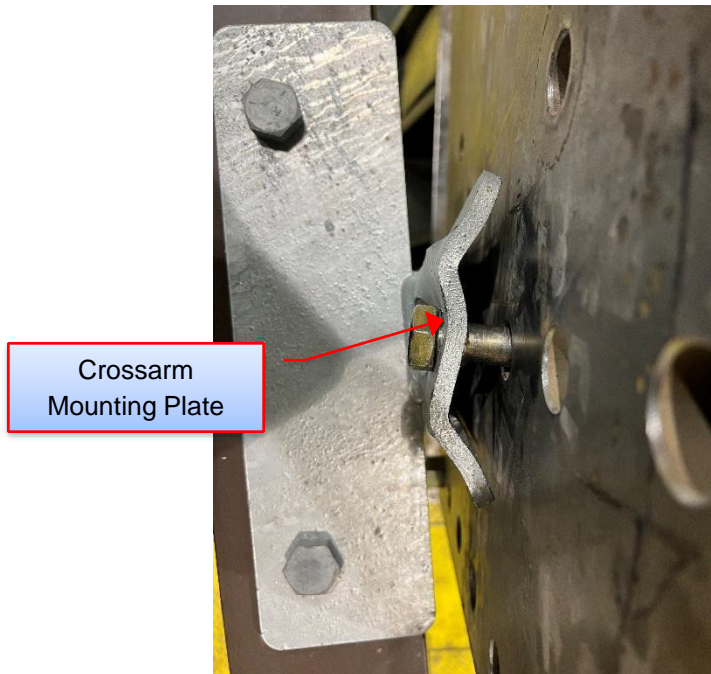


Figure 6-11: Sample 2.1 – Failure Location

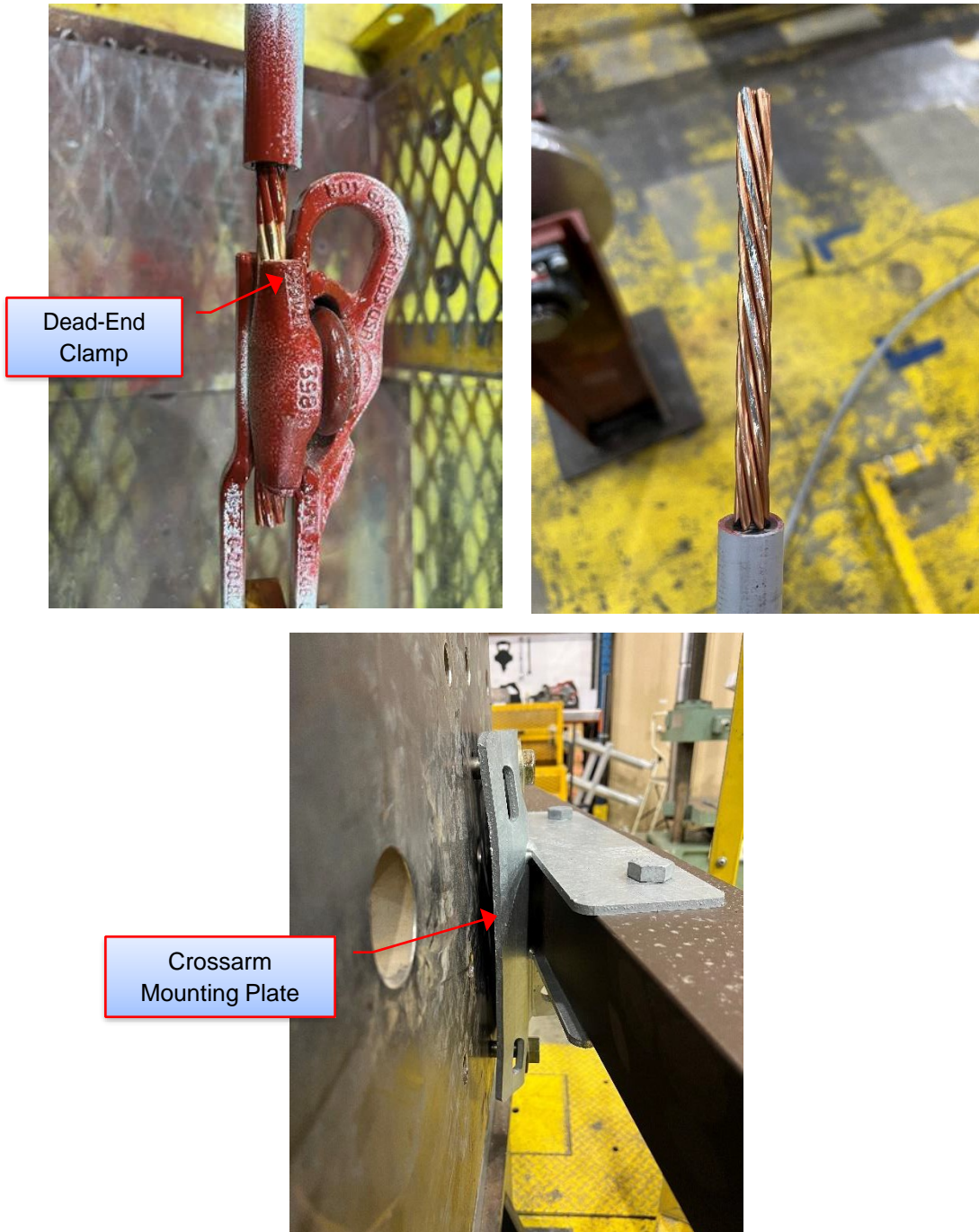


Figure 6-12: Sample 2.2 – Failure Location

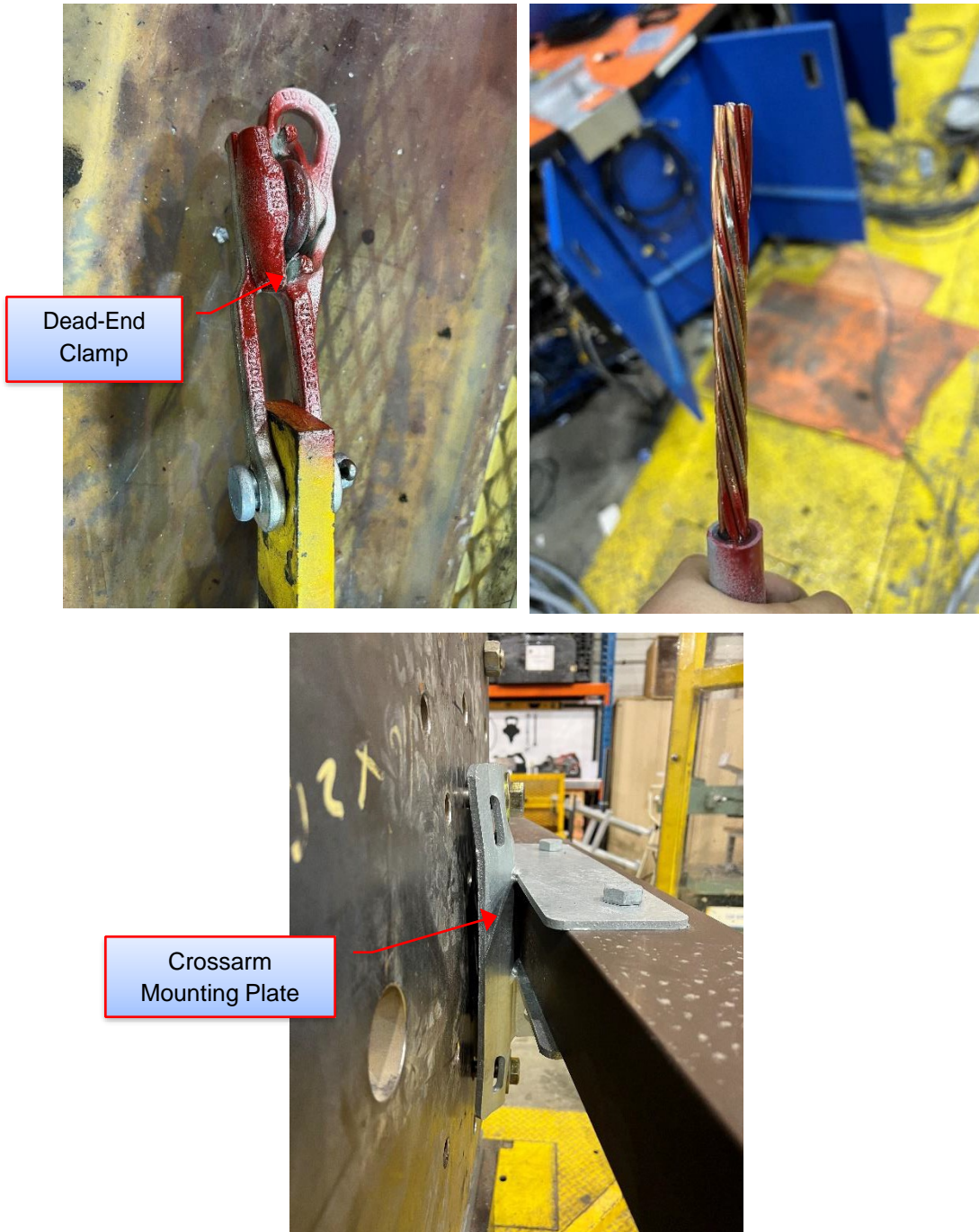


Figure 6-13: Sample 2.3 – Failure Location

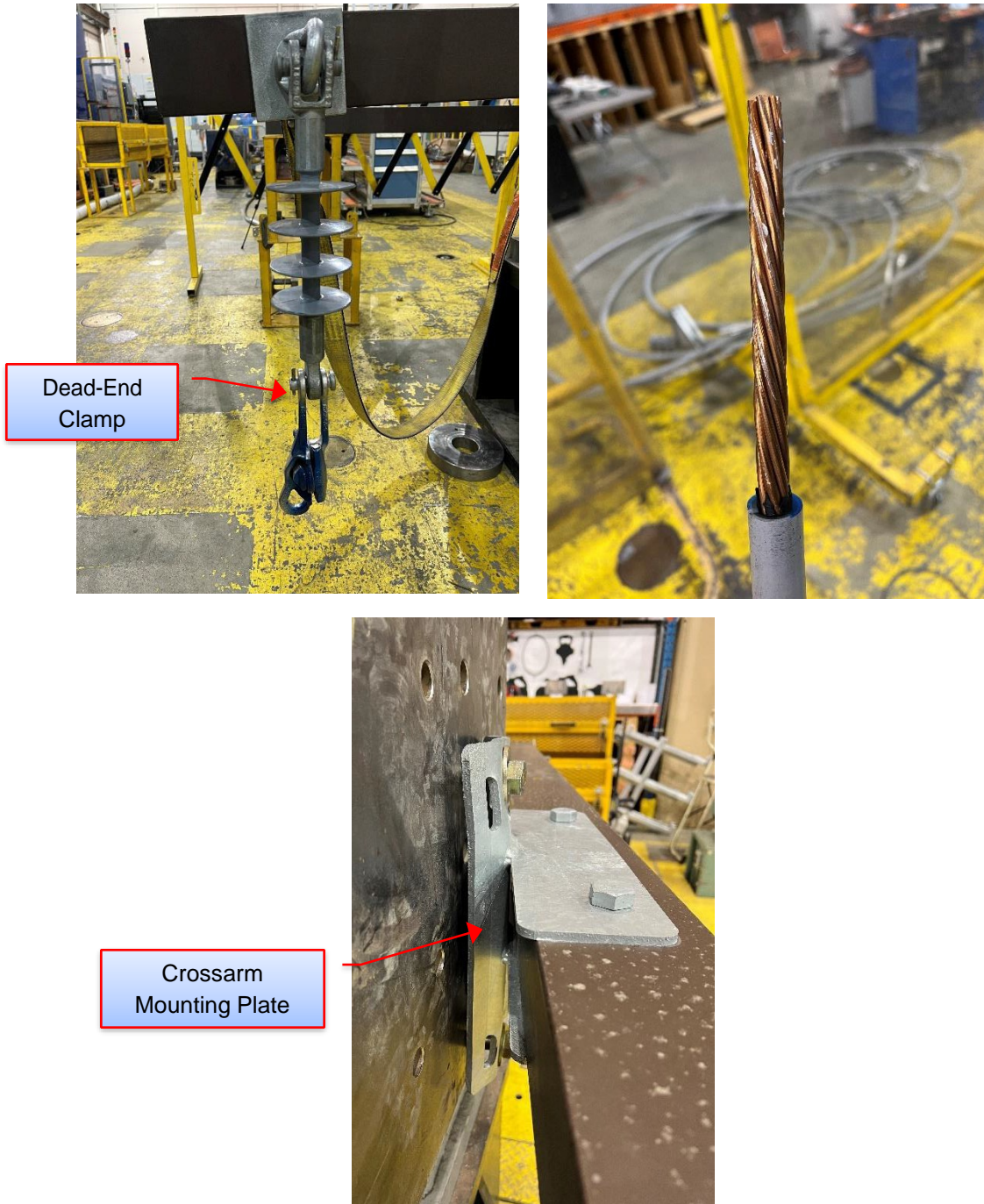


Figure 6-14: Sample 3.1 – Failure Location



Figure 6-15: Sample 3.2 – Failure Location

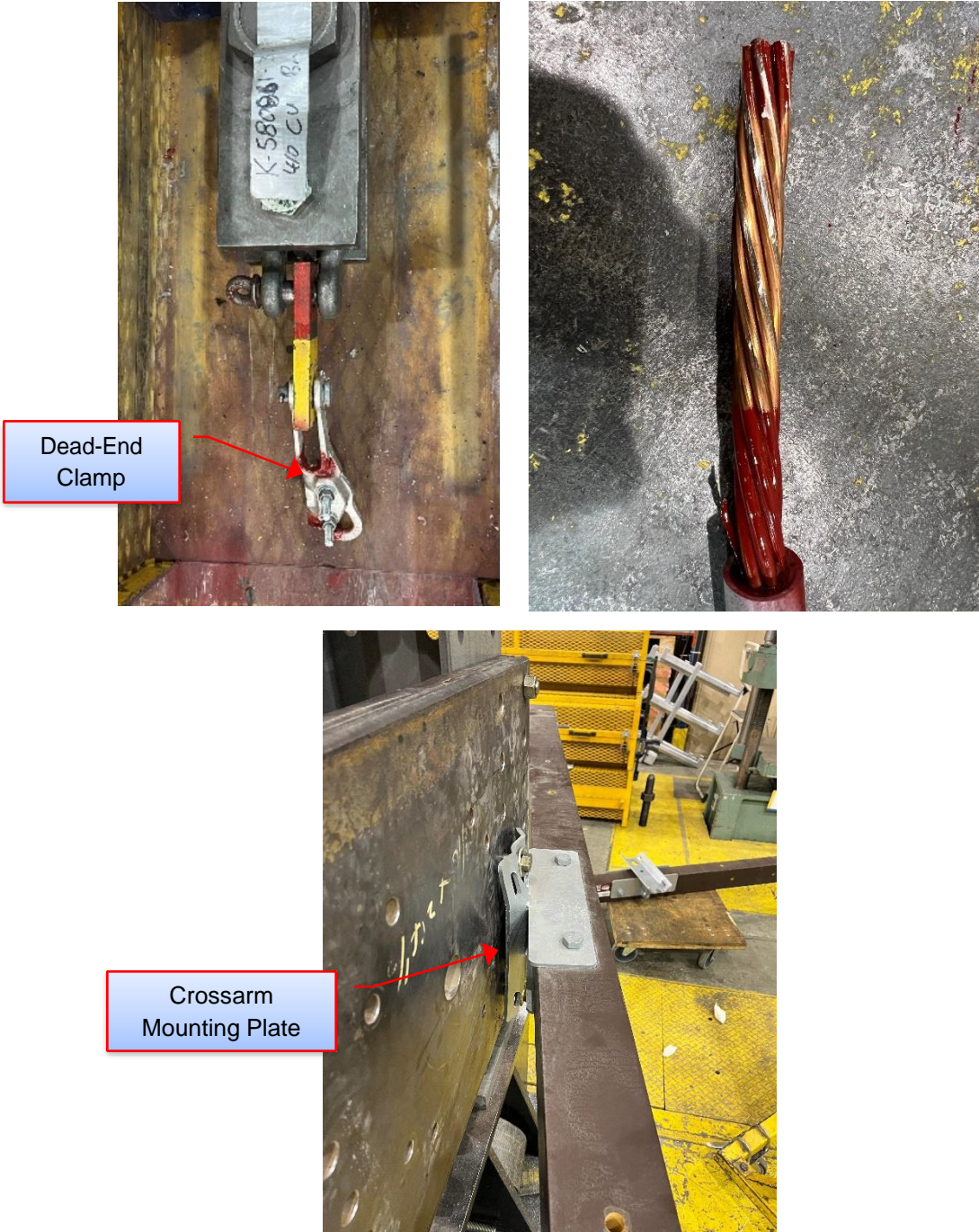


Figure 6-16: Sample 3.3 – Failure Location



Figure 6-17: Sample 4.1 – Failure Location

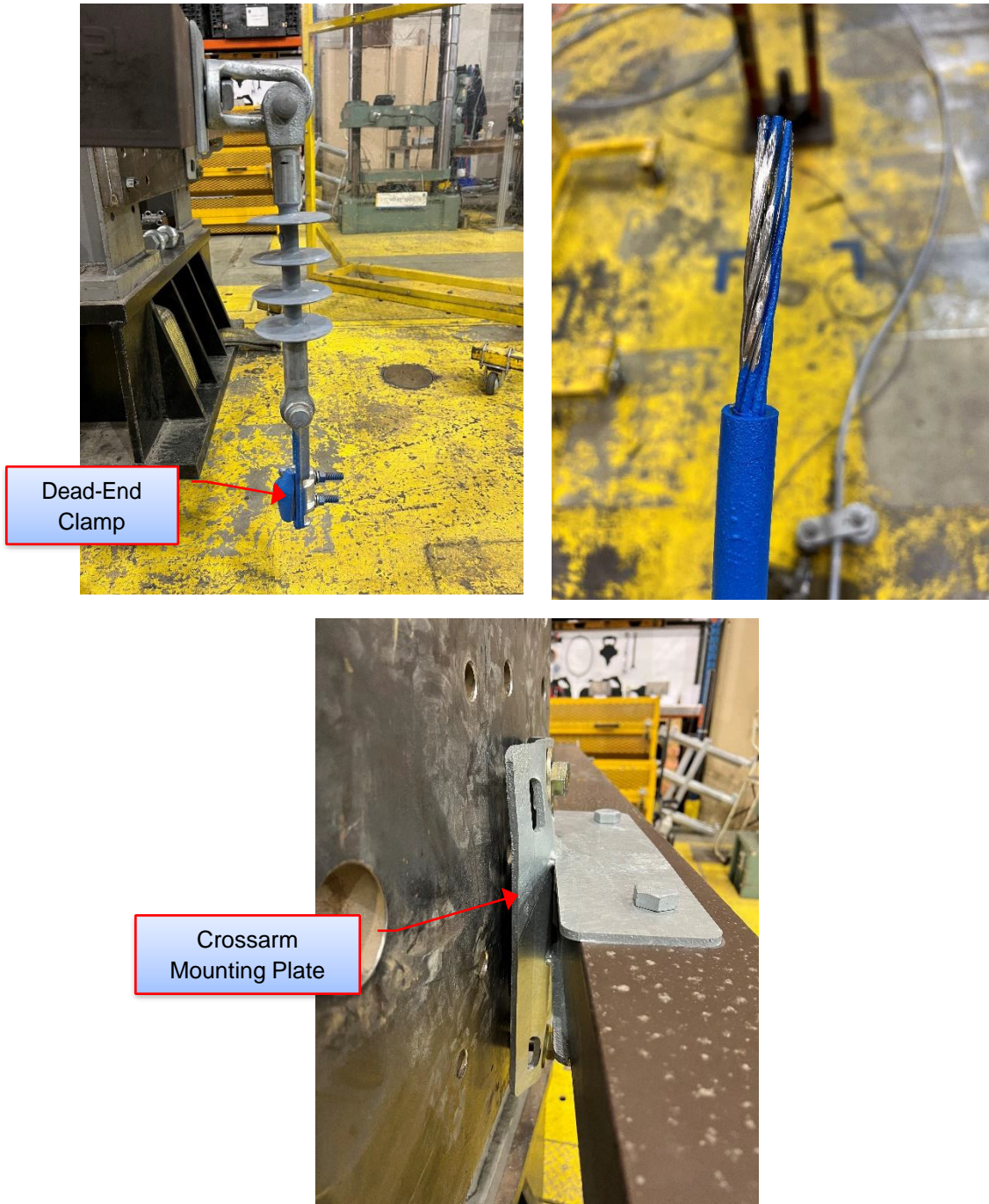


Figure 6-18: Sample 4.2 – Failure Location

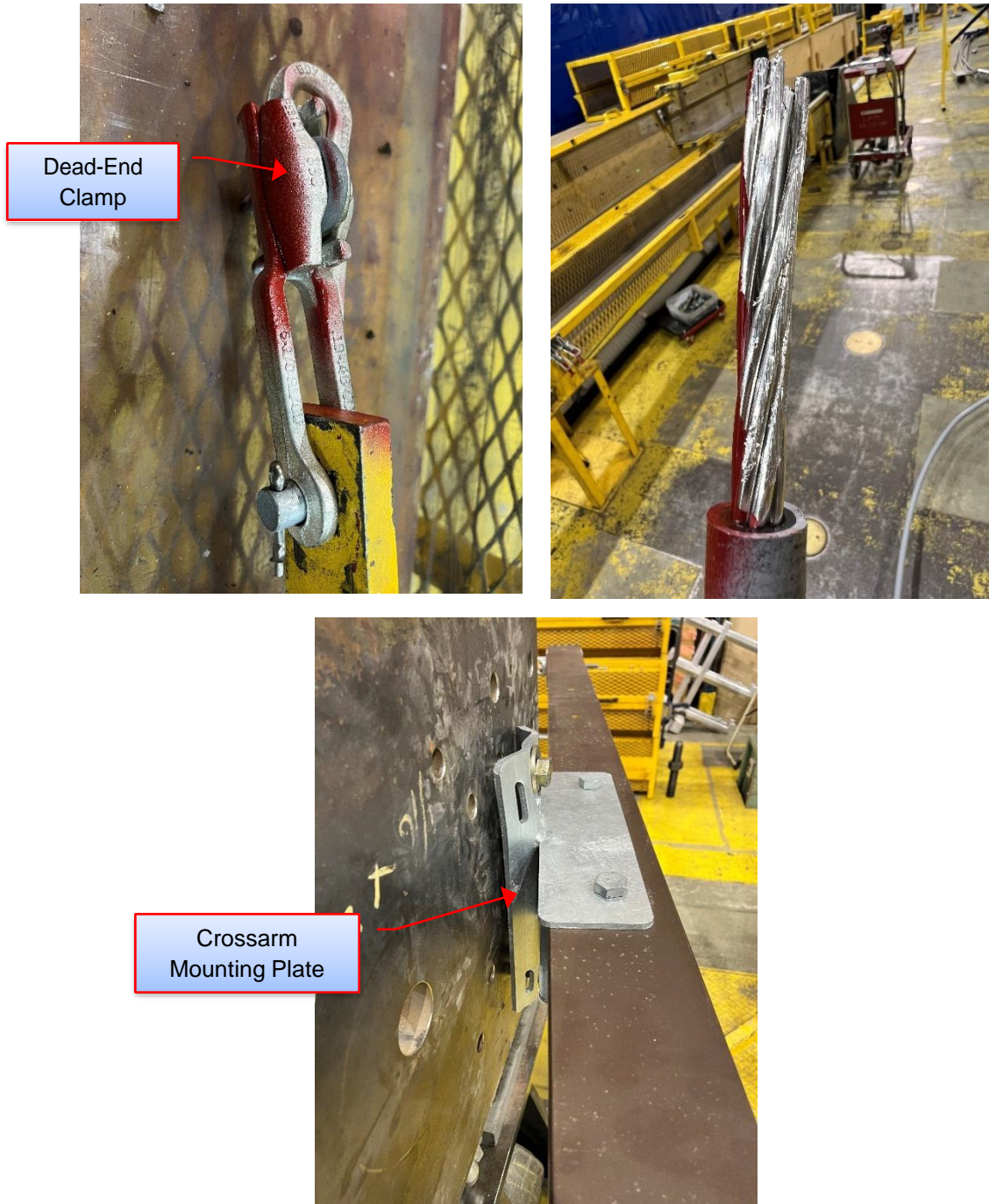


Figure 6-19: Sample 4.3 – Failure Location

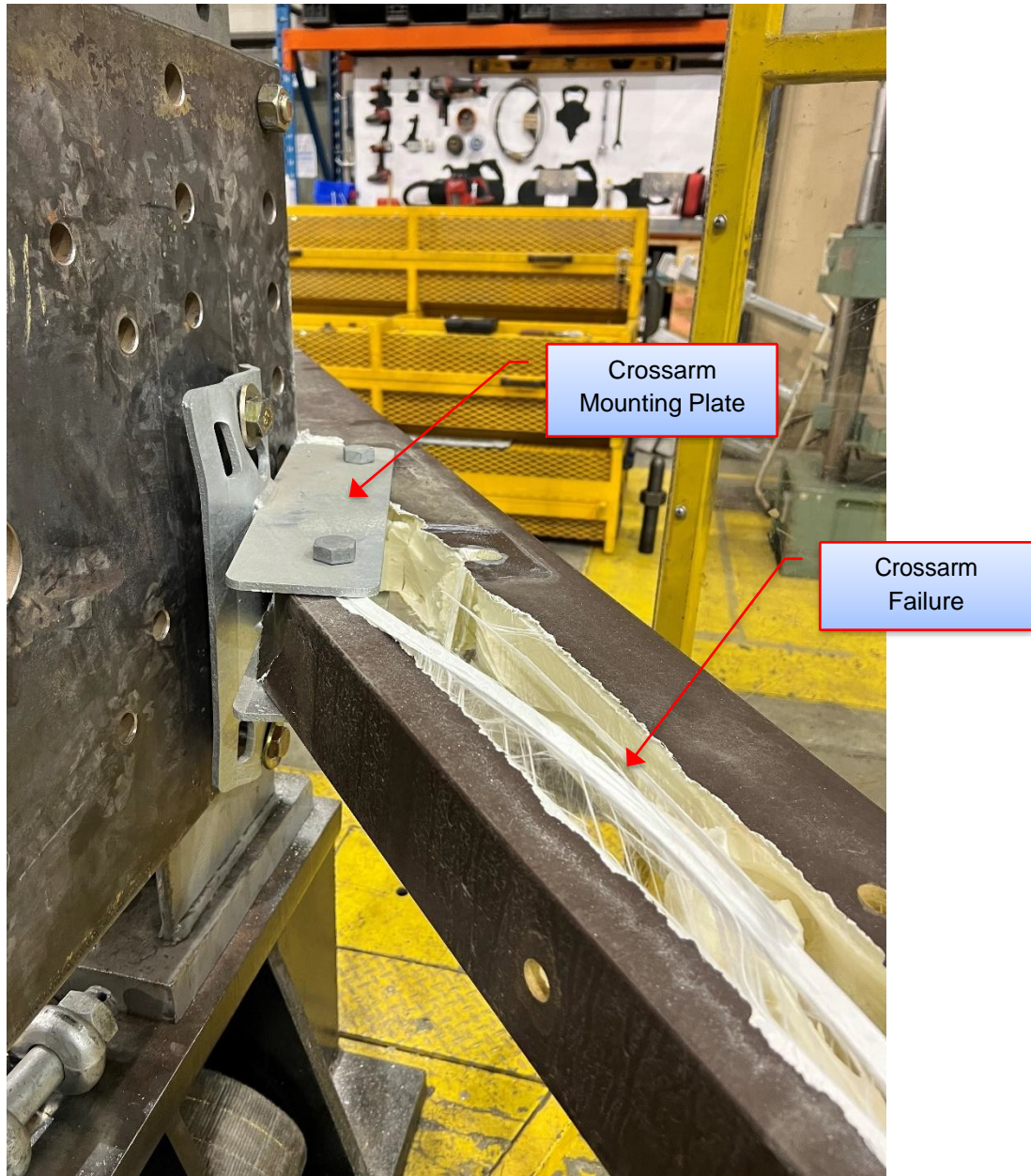


Figure 6-20: Sample 5.1 – Failure Location

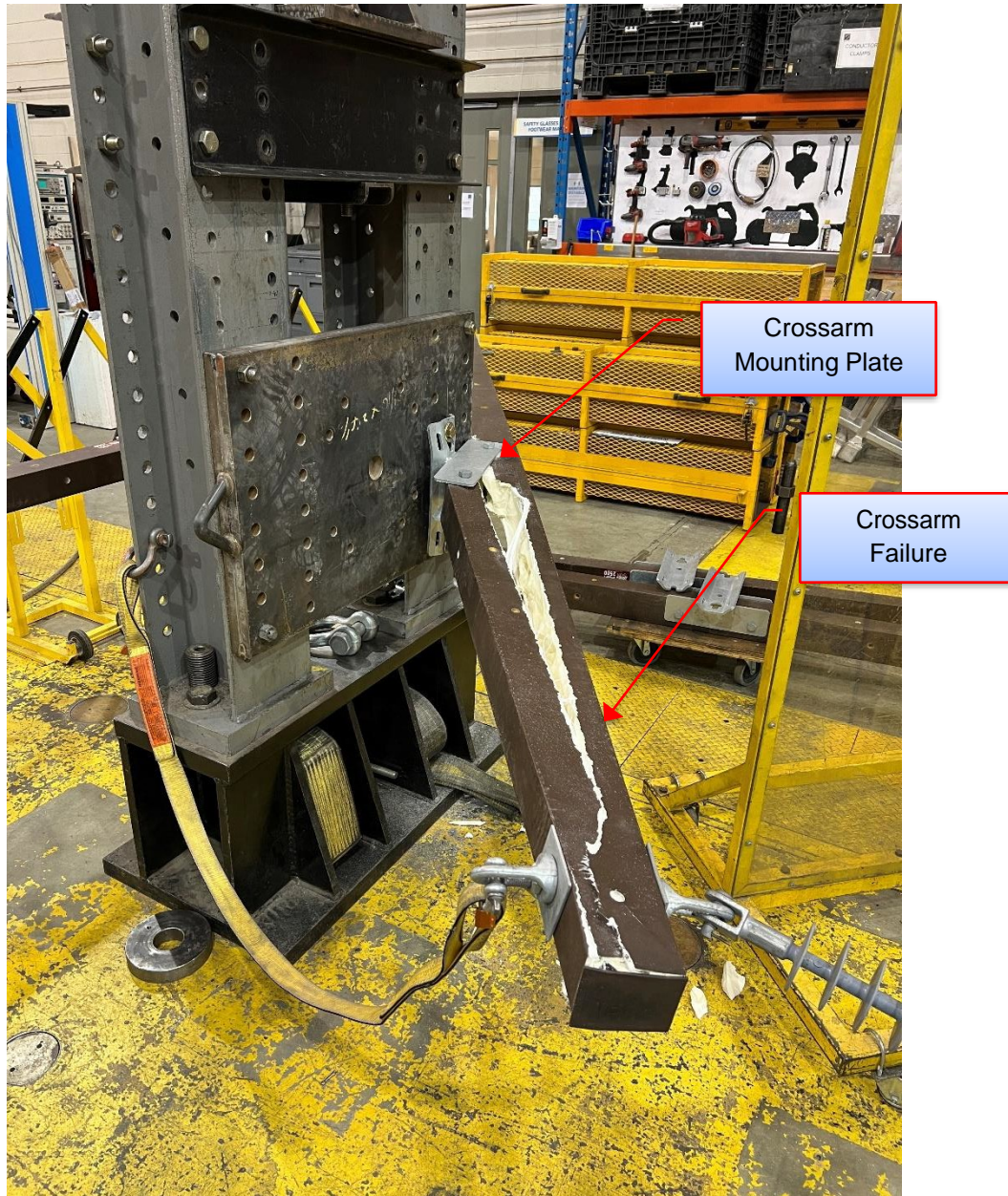


Figure 6-21: Sample 5.3 – Failure Location

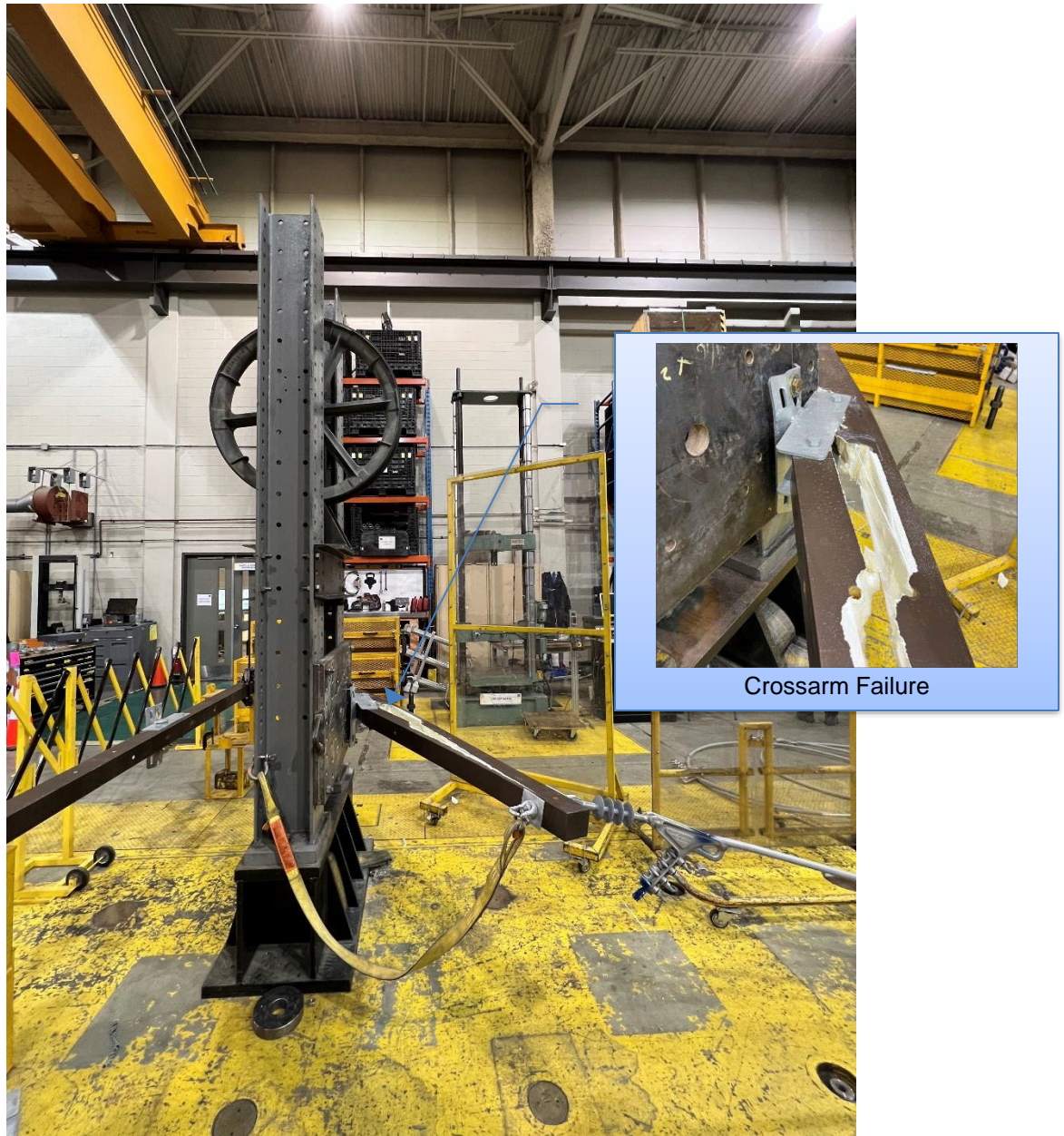


Figure 6-22: Sample 6.1 – Failure Location

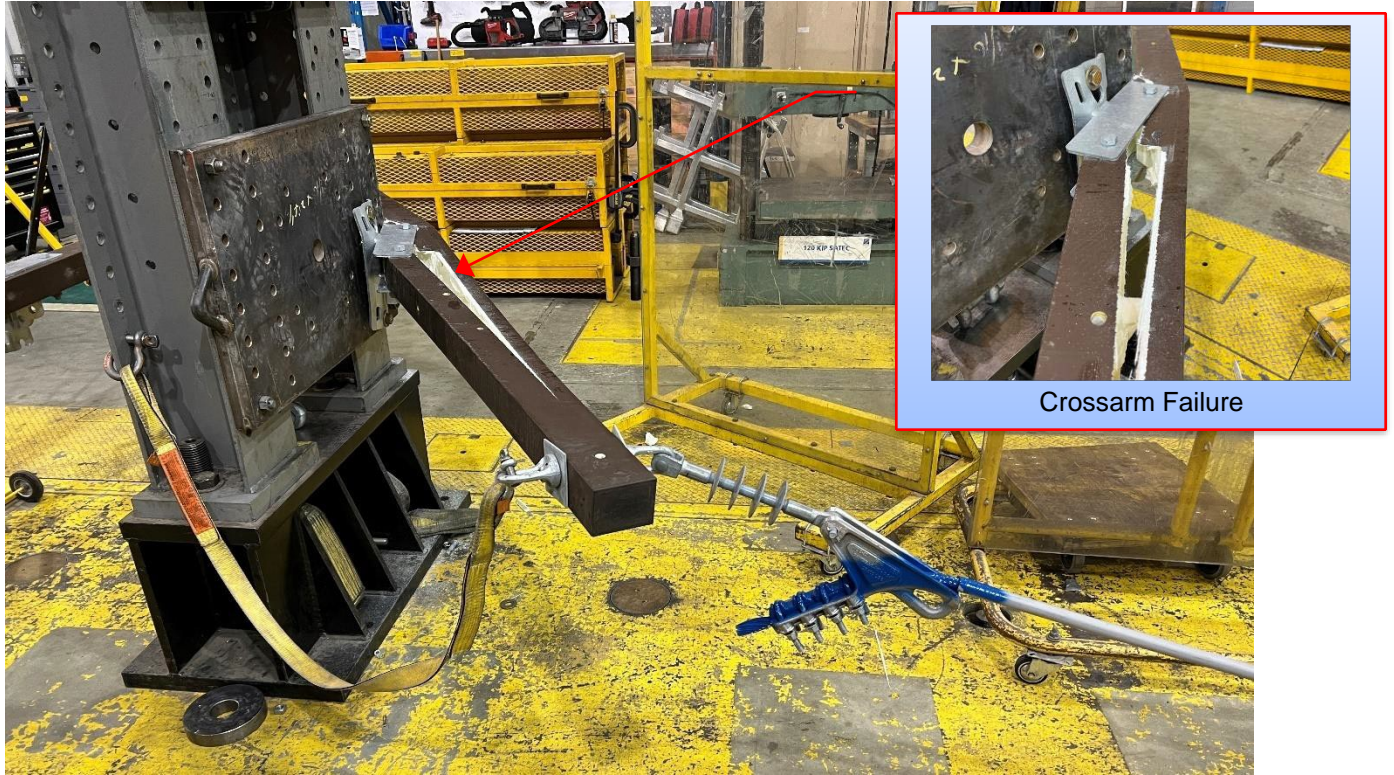


Figure 6-23: Sample 6.2 – Failure Location

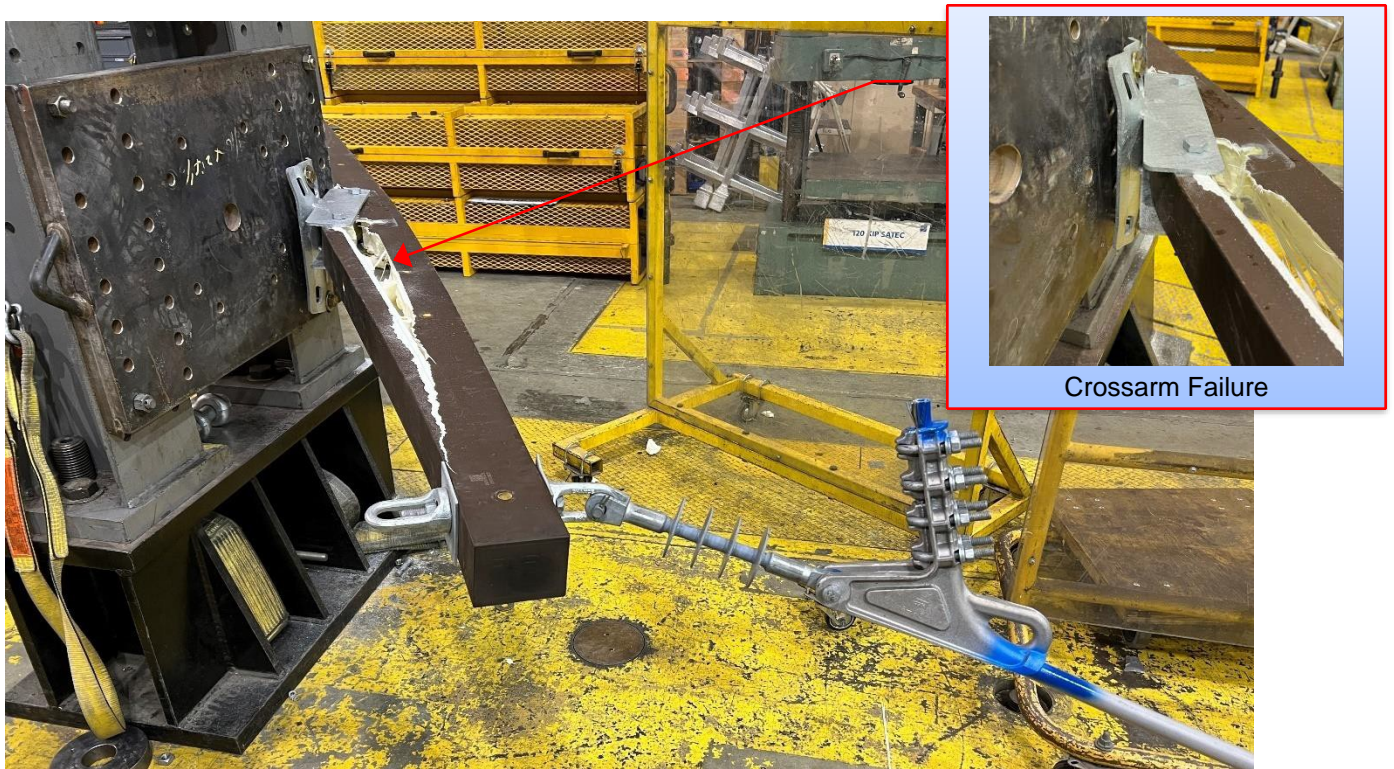


Figure 6-24: Sample 6.3 – Failure Location

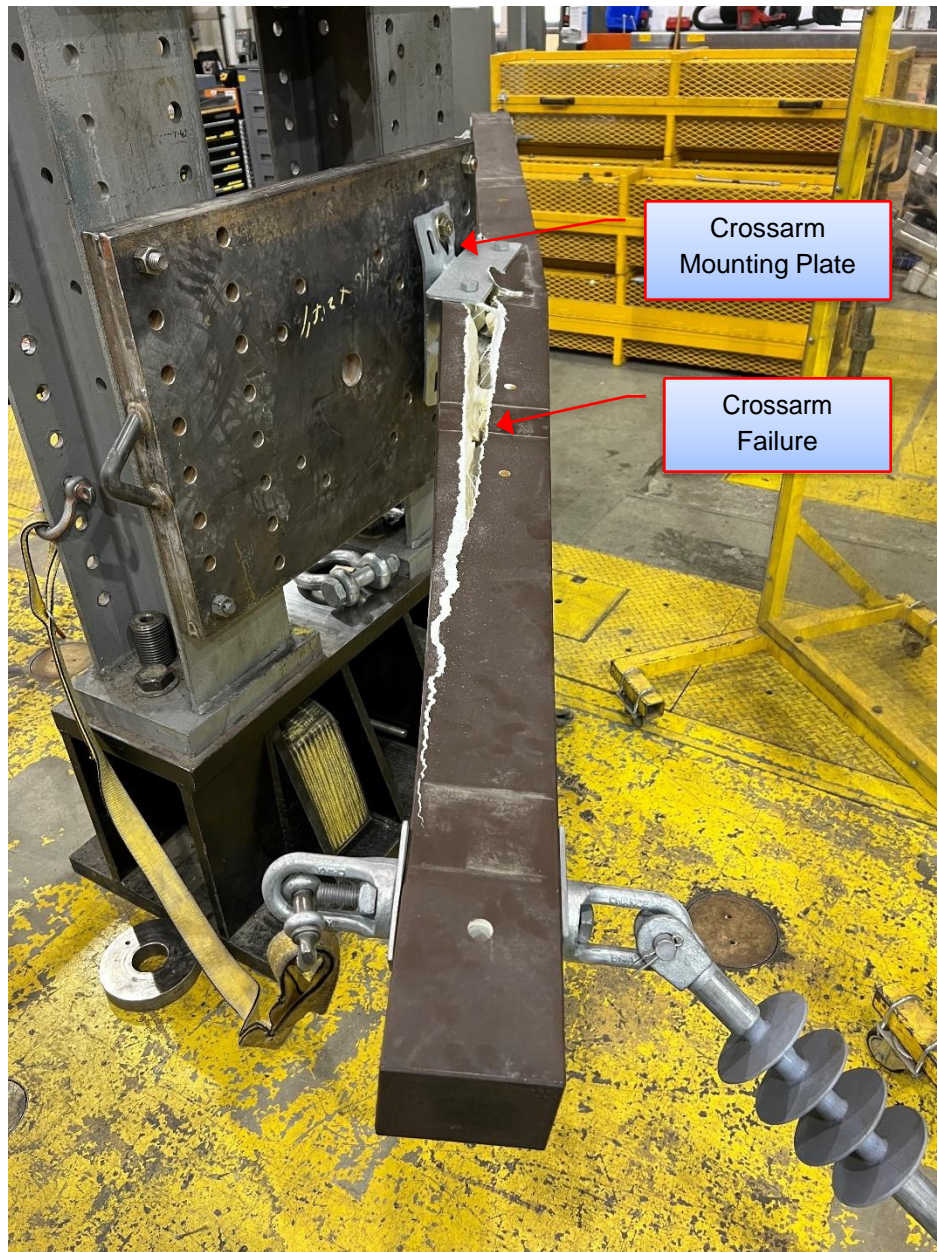


Figure 6-25: Sample 7.1 – Failure Location

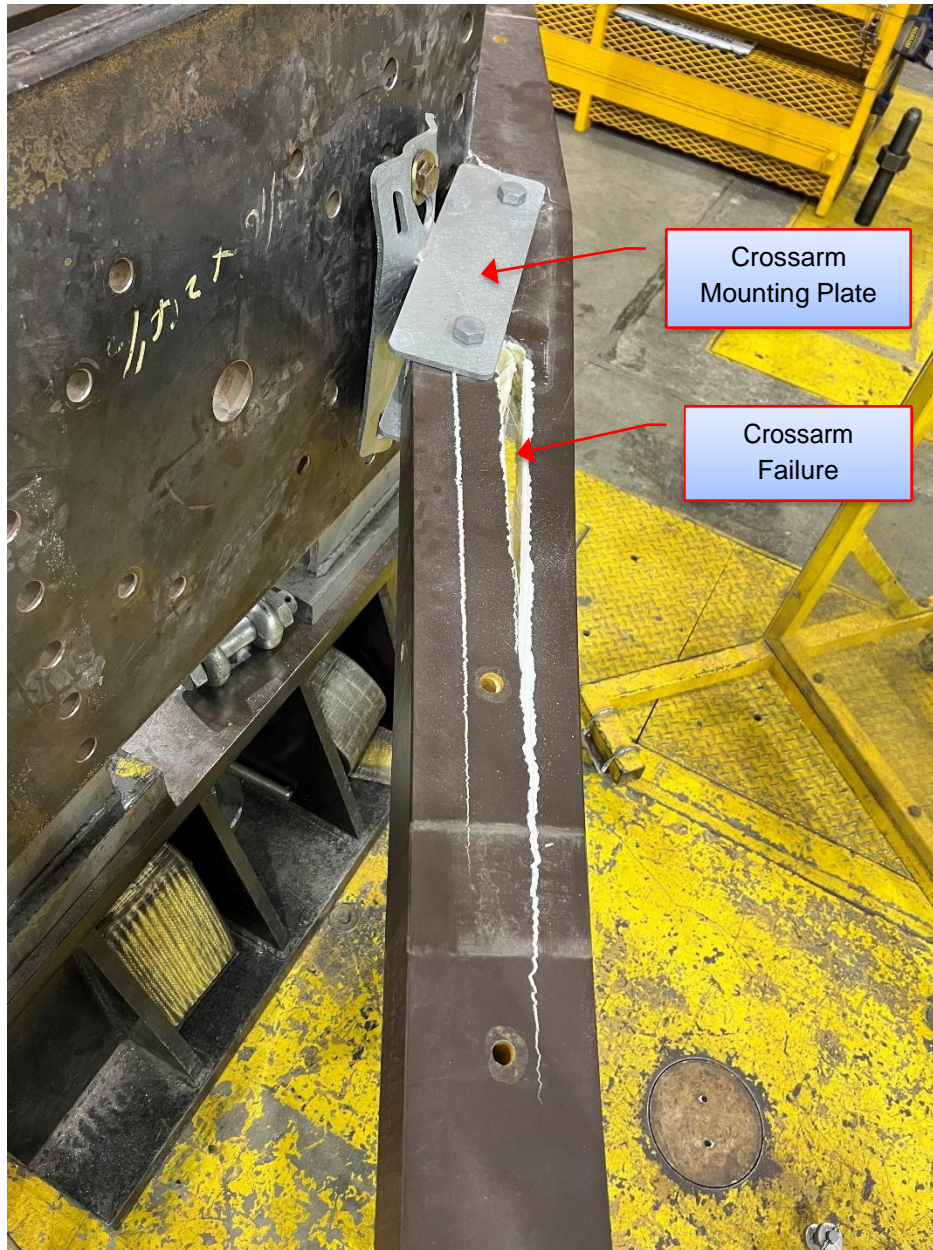


Figure 6-26: Sample 7.2 – Failure Location

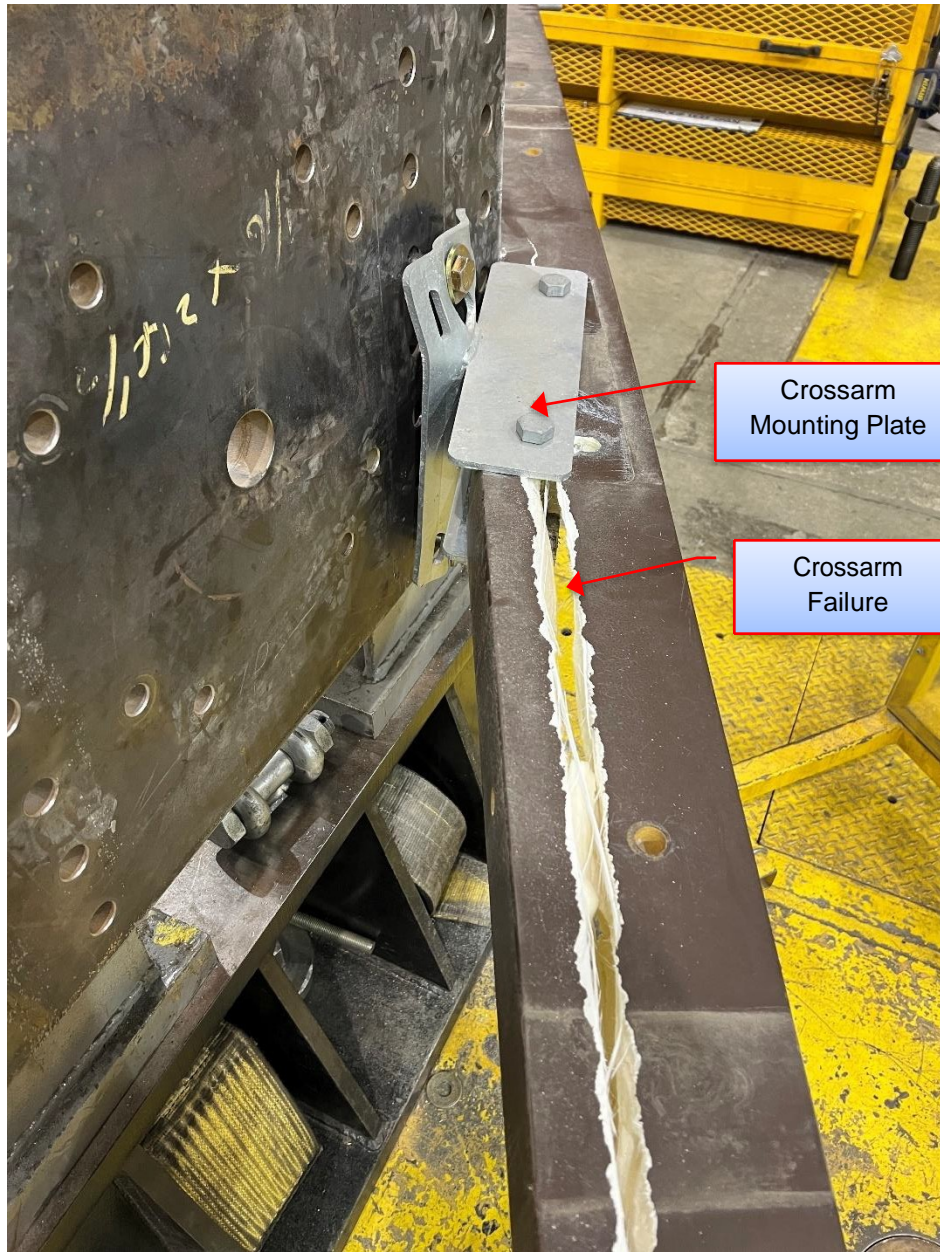


Figure 6-27: Sample 7.3 – Failure Location

7 Acceptance Criteria

There were no acceptance criteria provided by the client for this test. The objective of the Full Mock-up Test was to simulate mechanical loading in the event of a tree falling on the dead-end span of the line and evaluate its effect on components (conductor, insulator, cross arm).

8 Conclusion

The test results show that:

- For smaller size conductors (#2 AWG Cu; 2/0 AWG CU; 4/0 AWG Cu and 1/0 AWG ACSR), the typical failure occurred as a result of conductor slipping out of the dead-end clamp.
- For larger size conductors with higher RTS (336.4 kcmil and 653.9 kcmil) the typical failure point was the crossarm. The failure of the crossarm started at the bolts on the mounting plate and propagated to the insulator attachment point .
- Deformation of the mounting plate on the crossarm occurred in all instances.

[The remainder of this page is intentionally left blank.]



Appendix A Acronyms and Abbreviations

AAC	- All Aluminum Conductor
ACSR	- Aluminum Conductor Steel Reinforced
ANSI	- The American National Standards Institute
AWG	- American Wire Gauge
HDCU	- Hard Drawn Copper
DE	- Dead End
ISO	- International Organization for Standardization
RTS	- Rated Tensile Strength
XLPE	- Crosslinked Polyethylene

[The remainder of this page is intentionally left blank.]

Appendix B Test Components

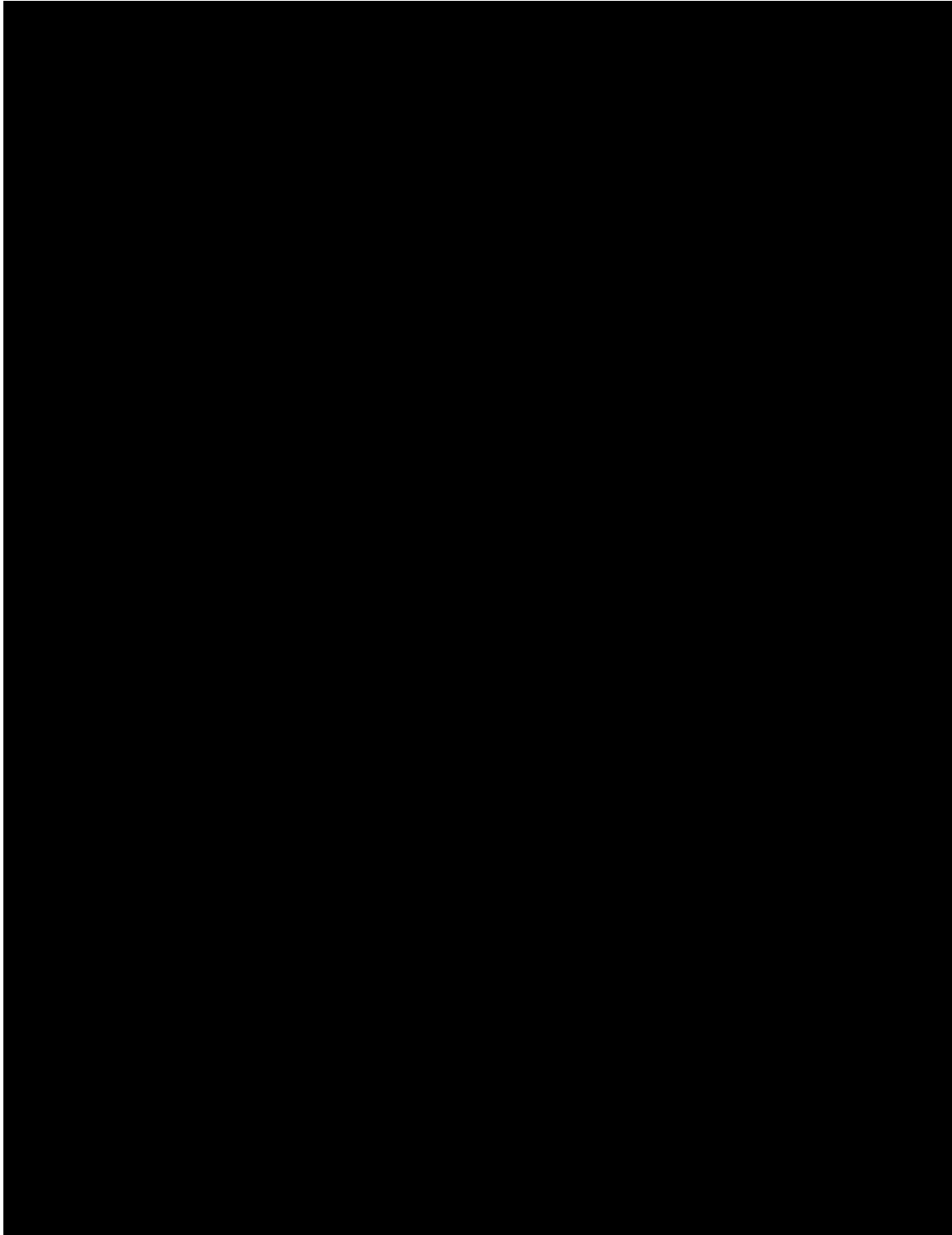


Figure D 1:  15 kV Dead-End Insulator

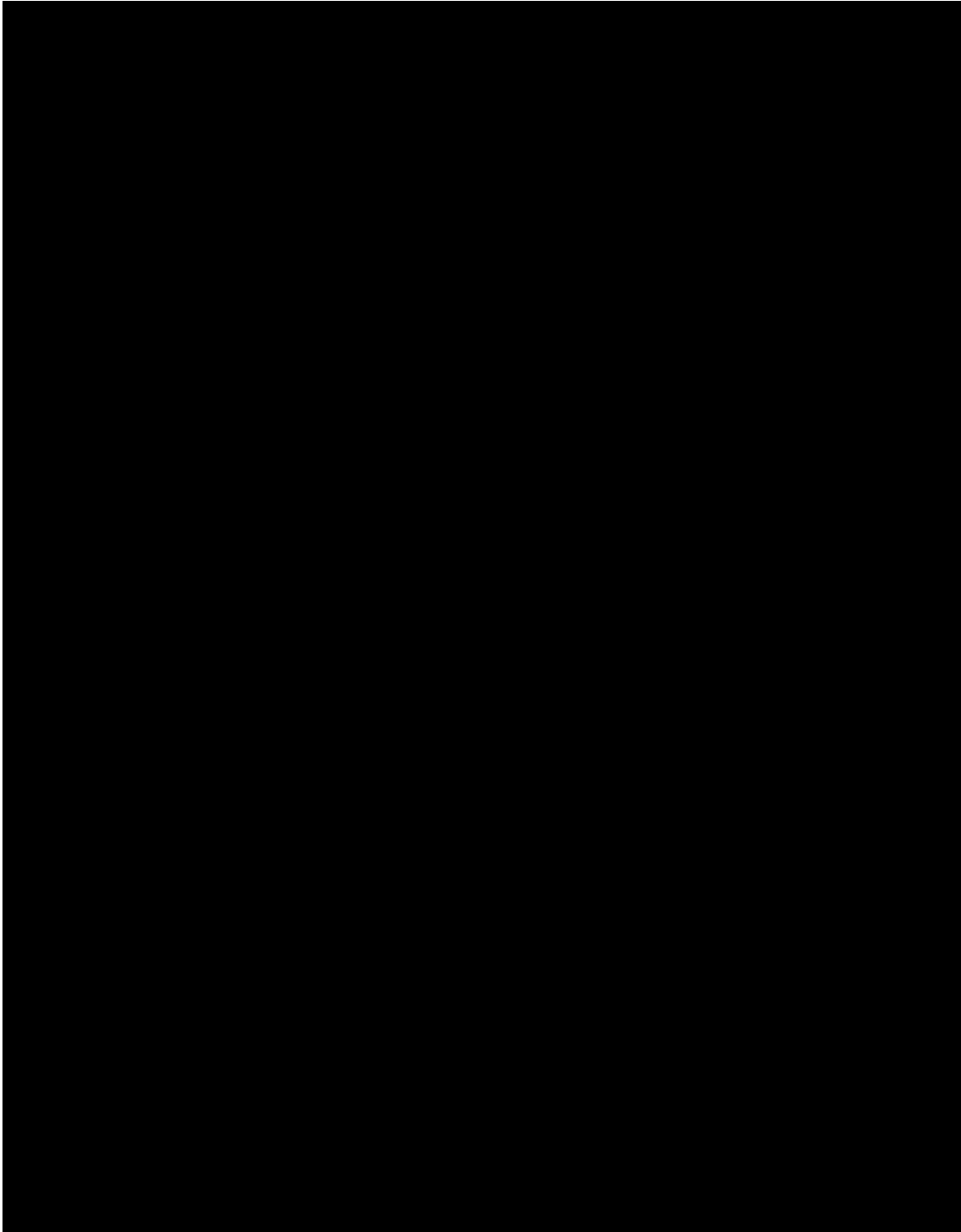


Figure D 2: [REDACTED] Dead-End Bolted Clamp [REDACTED]

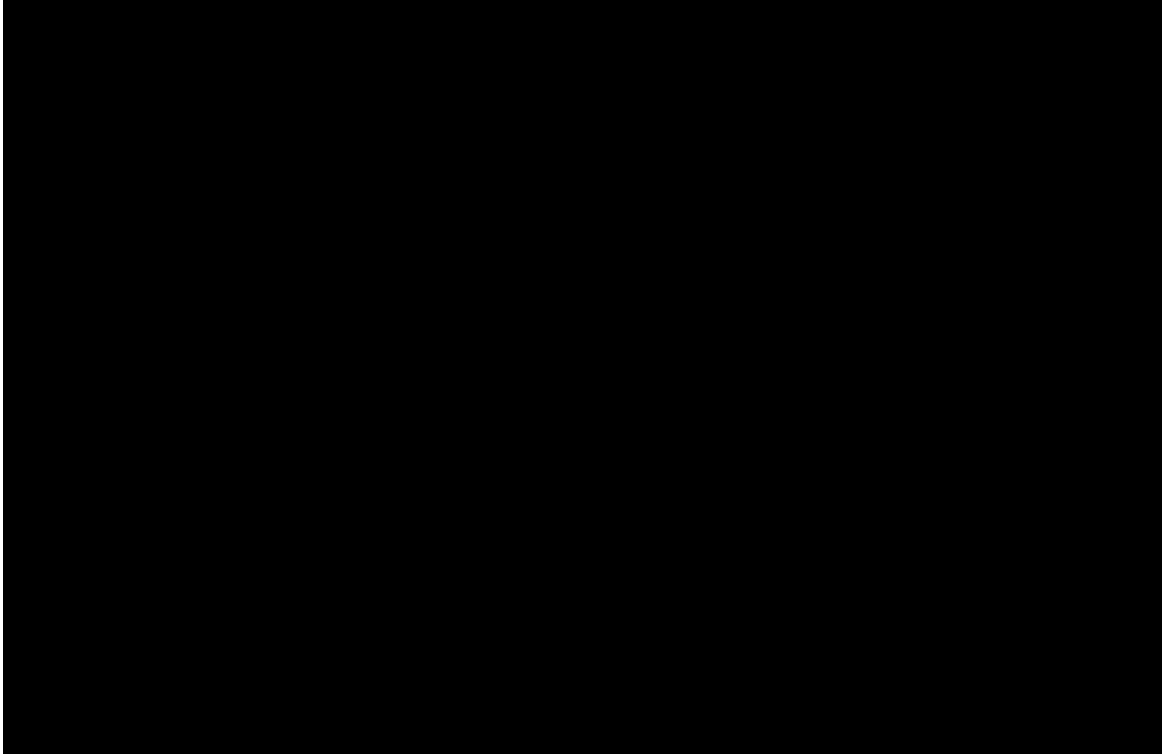


Figure D 3: [REDACTED] Dead-End Bolted Clamp [REDACTED]

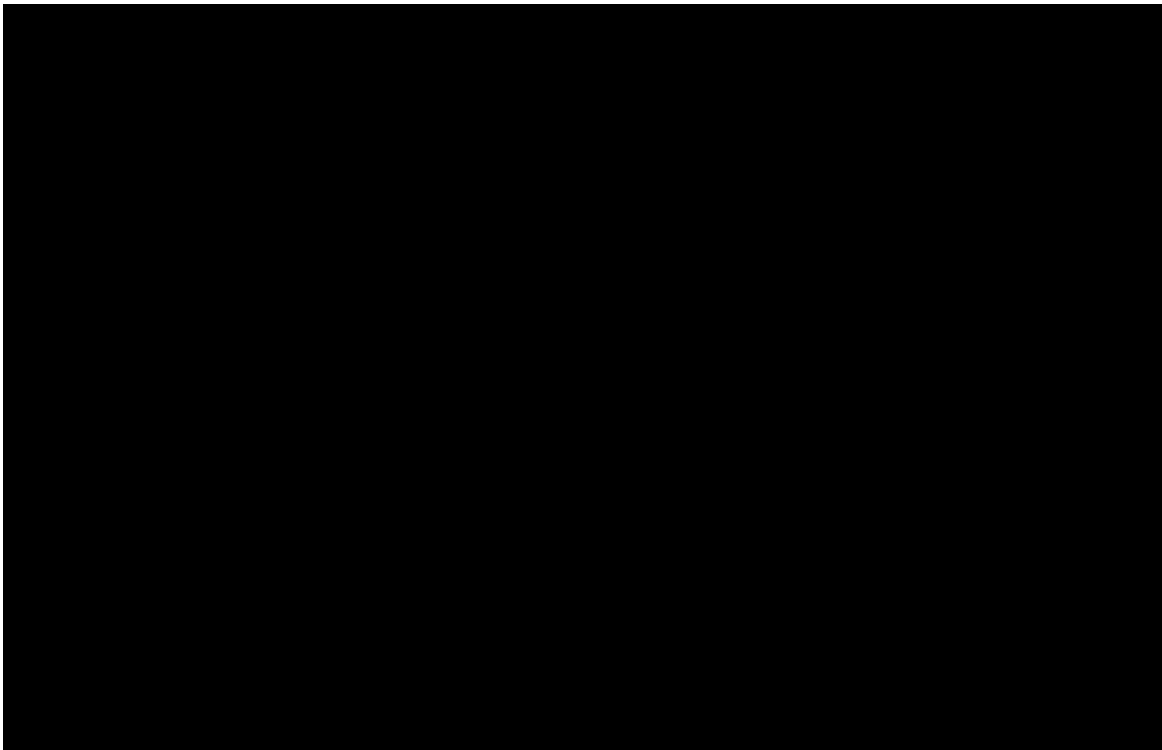


Figure D 4: [REDACTED] Dead-End Bolted Clamp [REDACTED]

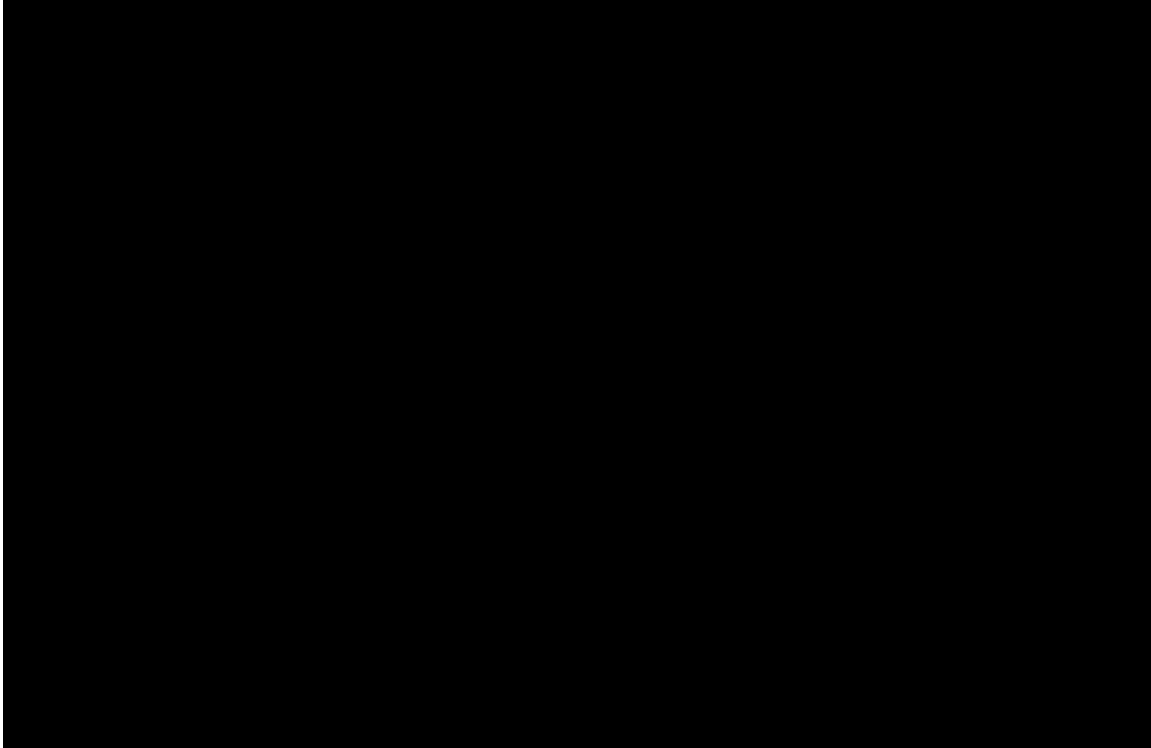


Figure D 5: [REDACTED] Dead-End Bolted Clamp [REDACTED]

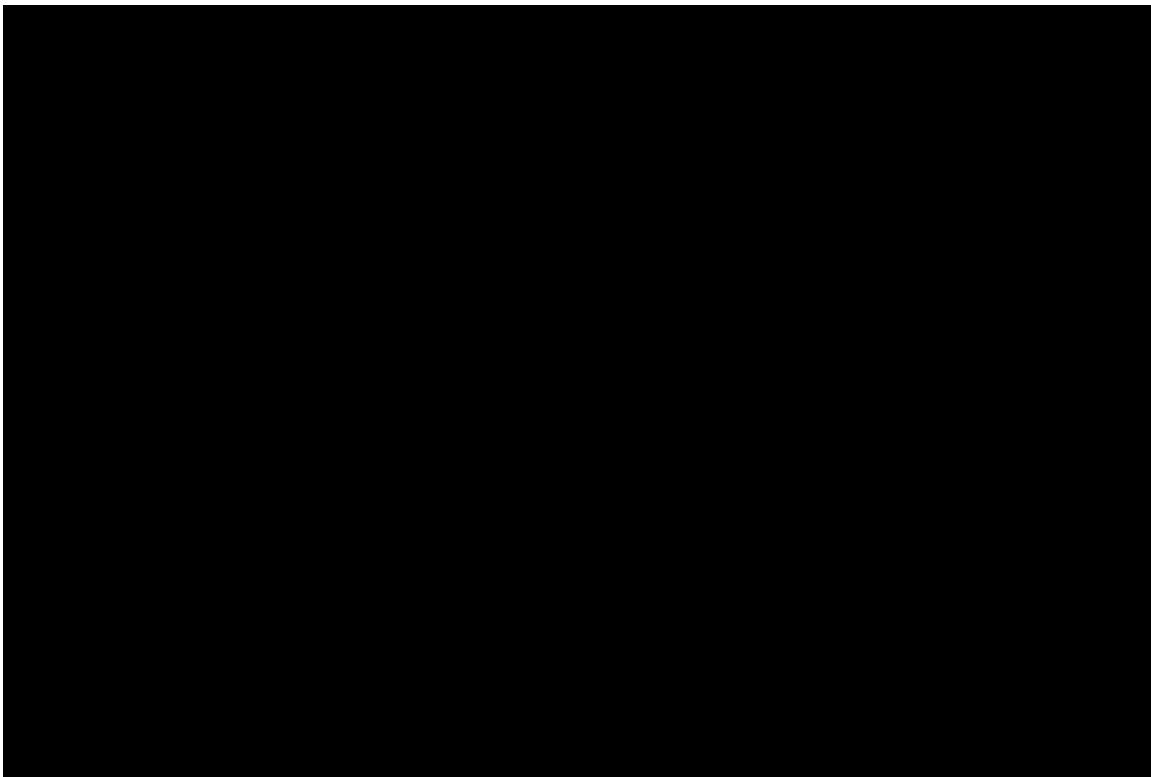


Figure E 1: [REDACTED] Deadened Composite Crossarm



Appendix C Instrument Sheet

EQUIPMENT DESCRIPTION	ASSET No.	ACCURACY CLAIMED	CALIBRATION DATE	CALIBRATION DUE DATE	TEST USE
Data Logger	KIN-01836	$\pm(0.1\% \text{ Rdg})$	May 27, 2022	May 27, 2023	Data acquisition
Load Cell/ Conditioner	KIN-01725/ KIN-01724	$\pm (1\% \text{ Rdg})$	October 26, 2021	November 26, 2022	Horizontal Load
Load Cell/ Conditioner	KIN-06678	$\pm (1\% \text{ Rdg})$	January 27, 2022	January 27, 2023	Vertical Load
Tape Measure	KIN-06890	$< 0.05\% \text{ Rdg}$	June 29, 2022	June 29, 2023	Length
Protractor	KIN-03375	$\pm(0.2^\circ)$	February 7, 2022	February 7, 2023	Angle
Torque Wrench	KIN-03249	$\pm(2\% \text{ Rdg})$	May 6, 2022	May 6, 2023	Installation Torque
Thermocouple/ Transmitter	KIN-00918/ KIN-00919	$\pm (1 \text{ }^\circ\text{C})$	October 28, 2021/ October 21, 2021	October 28, 2022/ October 21, 2022	Ambient Temperature

Appendix D Kinectrics ISO 9001 Certificate of Registration



 **CERTIFICATE OF REGISTRATION**

This is to certify that
Kinectrics Inc.
Kinectrics North America Inc., Kinectrics International Europe ApS or Kinectrics International Inc.
800 Kipling Avenue, Unit 2, Toronto, Ontario M8Z 5G5 Canada

Refer to Attachment to Certificate of Registration dated November 5, 2021 for additional certified sites
operates a
Quality Management System
which complies with the requirements of
ISO 9001:2015
for the following scope of certification
This registration covers the Quality Management System for engineering, consulting, design, testing, project management, research, software development, assessments, operations support, and analysis within our facilities, and at field sites, for customers in the electricity industry and related energy sectors; both nuclear and conventional; as well as processing of radiological and conventional laundry and manufacture, inspection, and repair of personal protection equipment.

Certificate No.:	CERT-0119296	Original Certification Date:	July 7, 1998
File No.:	006555	Certification Effective Date:	May 23, 2021
Issue Date:	November 5, 2021	Certification Expiry Date:	May 22, 2024


Frank Camasta
Global Head of Technical Services
SAI Global Assurance

Registered by:
QMI-SAI Canada Limited (SAI Global), 20 Carlton Court, Suite 200, Toronto, Ontario M5W 7Y5 Canada. This registration is subject to the SAI Global Terms and Conditions for Certification. While all due care and skill was exercised in carrying out this assessment, SAI Global accepts responsibility only for gross negligence. This certificate remains the property of SAI Global and must be returned to them upon request.
To verify that this certificate is current, please refer to the SAI Global On-Line Certification Register:
https://www.sai-global.com/en-us/assurance/auditing_and_certification/certification_register/





Appendix E Distribution

Mr. Matt Bowers, Ph.D., P.E.

Exponent
17000 Science Drive, Suite 200
Bowie, Maryland 20715
Email: mbowers@exponent.com

Mr. Genti Gorja

Kinectrics AES Inc.
800 Kipling Ave, Unit No.2
Toronto, ON
Canada M8Z 5G5

Email: genti.gorja@kinectrics.com

[The remainder of this page is intentionally left blank.]